Universidade do Porto

Faculdade de Engenharia

FEUP

TANNIN RESINS FROM MARITIME PINE BARK AS ADSORBENTS FOR WATER TREATMENT AND RECOVERY OF SUBSTANCES

Thesis submitted in partial fulfilment of the requirements for the degree of Doctor in Philosophy in Chemical and Biological Engineering at the Faculty of Engineering, University of Porto

Supervisor: Sílvia Cristina Rodrigues Santos, Ph.D.
Co-supervisor: Cidália Maria de Sousa Botelho, Ph.D.

LABORATORY OF SEPARATION AND REACTION ENGINEERING
LABORATORY OF CATALYSIS AND MATERIALS

Hugo Alexandre Mendes Bacelo
up201204895@edu.fe.up.pt

Para os meus pais.

ABSTRACT

Pinus pinaster bark is a forest and industrial waste which chemical richness, namely a high tannin content, is commonly ignored. Tannins have been showing to be excellent candidates to produce biosorbents. Tannin-adsorbents have a natural affinity to uptake heavy metals, dyes, surfactants, and pharmaceutical compounds from contaminated waters. Moreover, it is somewhat easy to chemically modify a tannin-adsorbent to enhance its adsorption ability of some substances. However, studies of adsorbents produced through tannins extracted from pine, or of negatively charged adsorbates, i.e., arsenic, antimony, and phosphates, are scarce or absent from the literature. On the other hand, the recovery of precious metals, e.g., gold, by pine bark tannin-adsorbents has not been investigated. Hence, this thesis aimed at contributing to improve knowledge on these topics by producing *P. pinaster* tannin-adsorbents and assessing not only its uptake capacity of arsenic, antimony, phosphates, and gold, but also the potential of recovery through desorption (for antimony, phosphates, and gold). Methods of tannin extraction and polymerization, oxidation and iron and calcium-loading of tannin resins were optimized. At 90 °C and using an alkaline solution, an extraction yield of 24.2 % was achieved and 166 mg of formaldehyde-condensable phenols were extracted per gram of bark used. Polymerization of tannins, under the best conditions, presented an efficiency around 80 %. Oxidation and iron-loading yielded a tannin resin with an iron content of 22 mg g^{-1}. Calcium-loading yielded a tannin resins with a calcium content of 32 mg g^{-1}. None of the adsorbents produced was sufficiently efficient for phosphate uptake. Adsorption assays with As(III) presented negligible results. Equilibrium data obtained for As(V) adsorption by iron-loaded tannin resins showed a maximum adsorption capacity of 0.72 mg g^{-1} (pH 3, 20 °C). Tannin resin (unmodified) presented a good ability to uptake antimony, with maximum adsorption capacities, evaluated in batch mode, of 30-33 mg g^{-1} (Sb(III), pH 6, 20 °C) and 16-47 mg g^{-1} (Sb(V), pH 2, 20 °C). The applicability of the tannin resin on Sb(III) uptake was confirmed in continuous fixed-bed experiments. Breakthrough curves were obtained for different inlet adsorbate concentrations, bed heights, flow rates and aqueous media (distilled water and a simulated mine effluent). The potential of tannin resins to sequester and recover Au(III) from hydrochloric acid and aqua regia solutions was also assessed. Equilibrium isotherms were experimentally determined and maximum adsorption capacities of 343±38 mg g^{-1} and 270±19 mg g^{-1} were found for Au uptake from HCl and HCl/HNO_3 (3:1 v/v) solutions containing 1.0 mol L^{-1} H^+. The work developed here allowed to identify tannin resins as efficient adsorbents for remediation of Sb-contaminated water and for separation, concentration, and recovery of Au from leaching liquors obtained from e-waste.

KEYWORDS: adsorption, pine bark, tannin resins, water remediation, sustainable economy.

RESUMO

A casca de *Pinus pinaster* é um resíduo florestal e industrial cuja riqueza química, nomeadamente um elevado teor de taninos, é habitualmente ignorada. Os taninos têm-se mostrado como excelentes precursores de biosorventes. Os adsorventes tanínicos têm uma afinidade natural para adsorver metais pesados, corantes, surfactantes e compostos farmacêuticos de águas contaminadas. Além disso, é relativamente fácil modificar quimicamente adsorventes tanínicos para aumentar a sua capacidade de adsorção de algumas substâncias. No entanto, estudos de adsorventes produzidos através de taninos extraídos de pinheiro, ou de adsorbatos carregados negativamente, i.e., arsénio, antimónio e fosfatos, são escassos ou ausentes na literatura. Por outro lado, a recuperação de metais preciosos, e.g., ouro, por adsorventes tanínicos de casca do pinheiro ainda não foi investigada. Portanto, esta tese teve como objectivo contribuir para o aprimoramento do conhecimento nestes tópicos ao produzir adsorventes tanínicos de *P. pinaster* e avaliar não apenas a sua capacidade de captação de arsénio, antimónio, fosfatos e ouro, mas também o potencial da sua recuperação por dessorção (para antimónio, fosfatos e ouro). Métodos de extração e polimerização de taninos, oxidação e impregnação de ferro e cálcio foram optimizados. A 90 °C e utilizando uma solução alcalina, um rendimento de extração de 24,2 % foi alcançado e 166 mg de fenóis condensáveis com formaldeído foram extraídos por grama de casca usada. A polimerização dos taninos, nas melhores condições, apresentou uma eficiência em torno de 80 %. A oxidação e a impregnação de ferro produziram uma resina tanínica com um conteúdo de ferro de 22 mg g^{-1}. A impregnação de cálcio produziu uma resina tanínica com conteúdo de cálcio de 32 mg g^{-1}. Nenhum dos adsorventes produzidos foi suficientemente eficiente para captar fosfatos. Os ensaios de adsorção com As(III) apresentaram resultados desprezíveis. Os dados de equilíbrio obtidos para a adsorção de As(V) por resinas oxidadas carregadas com ferro mostraram uma capacidade máxima de adsorção de 0,72 mg g^{-1} (pH 3, 20 °C). A resina tanínica (não modificada) apresentou boa capacidade de captação de antimónio, com capacidades máximas de adsorção, avaliadas em adsorvedor fechado, de 30-33 mg g^{-1} (Sb(III), pH 6, 20 °C) e 16-47 mg g^{-1} (Sb(V), pH 2, 20 °C). A aplicabilidade da resina de tanino na captação de Sb(III) foi confirmada em ensaios contínuos em leito fixo. Curvas de ruptura foram obtidas para diferentes concentrações de adsorbato de entrada, alturas do leito, caudais e meios aquosos (água destilada e um efluente de mina simulado). O potencial das resinas tanínicas para sequestrar e recuperar Au(III) de soluções de ácido clorídrico e aqua regia também foi avaliado. Determinaram-se isotérmicas de equilíbrio e obtiveram-se capacidades máximas de adsorção de 343±38 mg g^{-1} e 270±19 mg g^{-1} em soluções de HCl e HCl/HNO_3 (3:1 v/v) contendo 1,0 mol L^{-1} H^+. O trabalho desenvolvido aqui permitiu identificar as resinas tanínicas como adsorventes eficientes para a remediação de águas contaminadas com Sb e para a separação, concentração e recuperação de Au de licores de lixiviação obtidos a partir de resíduos electrónicos.

PALAVRAS-CHAVE: adsorção, casca de pinheiro, resinas tanínicas, remediação de águas, economia sustentável.

ACKNOWLEDGEMENTS

I would like to thank the Chemical Engineering Department (DEQ) of FEUP and the associated laboratory LSRE-LCM where it was made available for me the space, materials and equipment required for the experimental assays of this thesis.

Particularly, I want to thank Eng. Liliana Pereira (DEQ/FEUP) for the help provided through borrowed equipment and for having contributed to the execution of some assays (DOC, colour leaching, etc.), Eng. Carla Ferreira (DEQ/FEUP) which allowed me to have access to the freeze-dryer equipment, Prof. Fernão Magalhães and Eng. Luís Carlos (DEQ/FEUP) for making possible the use of the particle size analyser, and Prof. Madalena Dias for granting access to the electrophoresis instrument for zeta potential measurements.

Moreover, I leave a special appreciation note for my colleagues of laboratory E404A — Bárbara Vieira, Maria Eduarda Schneider, Jonas Inácio, Maria Beatriz Torrinha, and Andreia Ribeiro — for having helped me carry out some assays which were included in my thesis.

Now a message to my supervisors, Dr. Sílvia Santos and Prof. Cidália Botelho: everything I said in the acknowledgements of my master thesis was confirmed over the last four years. There is nothing more to say other than reinforce my gratitude for your dedication and attention towards helping me in my work and state that without your careful revision this thesis would not be half as good.

On a personal note, I thank my family and friends, especially Marisa Bacelo, Daniel Santos and Pedro Fonseca, for their companionship, solidarity and love, all of which made my journey easier and more joyful.

And lastly, I thank FCT for the research grant (PD/BD/135062/2017).

This work was financially supported by: Base Funding - UIDB/50020/2020 of the Associate Laboratory LSRE-LCM - funded by national funds through FCT/MCTES (PIDDAC).

CONTENTS

LIST OF FIGURES

LIST OF TABLES

ABBREVIATIONS

AAS	Atomic Absorption Spectrometry
AG	*N*-aminoguanidine
APDC	Ammonium pyrrolidinedithiocarbamate
AUR	Adsorbent usage rate
BSN	Bark Stiasny number (mg-precipitate g-bark^{-1})
BTU	Bisthiourea
DEA	Diethylamine
DMA	Dimethylamine
DMTD	2,5-dimercapto-1,3,4-thiadiazole
DOC	Dissolved organic carbon
DW	Distilled water
EBCT	Empty bed contact time
EDA	Ethylenediamine
EDS	Energy Dispersion Spectroscopy
EDTA	Ethylenediaminetetraacetic acid
EFCP	Extracted formaldehyde condensable phenols (mg-GAE g-bark^{-1})
FCPC	Formaldehyde condensable phenolic content (mg-GAE g-extract^{-1})
FTIR	Fourier Transformed Infrared Spectroscopy
GAE	Gallic acid equivalents
HU	Hazen units
IEP	Isoelectric point
LDF	Linear driving force
MA	Methylamine
MAE	Microwave-assisted extraction
ME	Mining tailing waters
MIBK	Methyl isobutyl ketone
MOF	Metal organic frameworks
PB	Pine bark
PWE	Pressurized water extraction
rpm	Rotations per minute
SEM	Scanning Electron Microscopy
SFE	Supercritical fluid extraction
SME	Simulated mining effluent
SN	Stiasny number (g-precipitate g-extract^{-1})
TA	Tannic acid
TE	Tannin extract
TEA	Triethylamine
TEP	Total extracted phenols (mg-GAE g-bark^{-1})
TEPA	Tetraethylenepentamine
TPC	Total phenolic content (mg-GAE g-extract^{-1})
TR	Tannin resin
TR-Ca	Calcium-loaded tannin resin
TR-Fe	Iron-loaded tannin resin
TRO	Oxidized tannin resin
TRO-Ca	Calcium-loaded oxidized tannin resin
TRO-Fe	Iron-loaded oxidized tannin resin
TRp	Tannin resin produced with a precipitated extract
UAE	Ultrasound-assisted extraction
WEEE	Waste electrical and electronic equipment (e-waste)

NOMENCLATURE

a_Y	Yan model parameter
BV_b	Number of bed volumes until breakthrough
C_e	Outlet adsorbate concentration (mg L^{-1})
C_{eq}	Equilibrium concentration of adsorbate (mg L^{-1})
C_f	Final concentration of adsorbate (mg L^{-1})
C_i	Inlet adsorbate concentration (mg L^{-1})
C_{in}	Initial concentration of adsorbate (mg L^{-1})
C_t	Concentration of adsorbate at *t* minutes (mg L^{-1})
D_h	Solid diffusivity coefficients (m^2 s^{-1})
F	Flow rate (mL min^{-1})
k_1	Pseudo first order kinetic constant (min^{-1})
k_2	Pseudo second order kinetic constant (g mg^{-1} min^{-1})
k_{BA}	Bohart-Adams coefficient rate (mL mg^{-1} h^{-1})
K_F	Freundlich equilibrium constant ($mg^{(n-1)/n}$ $L^{1/n}$ g^{-1})
K_L	Langmuir equilibrium constant (mg L^{-1})
k_{LDF}	Linear driving force constant (h^{-1})
k_{Th}	Thomas rate constant (mL mg^{-1} h^{-1})
L	Bed height in column experiments (cm)
n	Freundlich constant related to the adsorption intensity
N_0	Adsorption capacity per unit of bed volume in Bohart-Adams model (mg cm^{-1})
Q	Amount of adsorbate adsorbed per g of adsorbent at saturation in column experiments (mg g^{-1})
$q_{e,m}$	Maximum experimental adsorbed amount (mg g^{-1})
q_{eq}	Amount of adsorbate adsorbed per g of adsorbent at equilibrium (mg g^{-1})
Q_m	Maximum adsorption capacity predicted by Langmuir model (mg g^{-1})
q_t	Amount of adsorbate adsorbed per g of adsorbent at *t* minutes (mg g^{-1})
q_{Th}	Maximum adsorption capacity in Thomas model (mg g^{-1})
q_Y	Maximum adsorption capacity in Yan model (mg g^{-1})
R	Correlation coefficient
R^2	Determination coefficient
S/L	Solid:liquid ratio between adsorbent mass and solution volume (g L^{-1})
SE	Standard error
T	Temperature (ºC)
t_s	Saturation time in column experiments (min)
η_E	Extraction yield (%)
η_{EA}	Extraction yield adjusted (NaCl mass subtracted to extract mass) (%)
η_P	Polymerization yield (%)

CHAPTER I

INTRODUCTION

CHAPTER I INTRODUCTION

1. Motivation and Context

Water is a crucial resource for human activity and subsistence. The production of drinking water requires many times the employment of remediation techniques. Moreover, several industries yield heavily polluted wastewaters which ought to be subjected to treatment before their release into natural water bodies. Hence, water remediation is currently an important research topic. One of the challenges of water remediation is the removal of anionic species, such as those in which arsenic, antimony, and phosphate are usually found in aqueous solutions. The removal of antimony and phosphate should also take into account their recovery due to the many industrial and agricultural applications. In addition, the recovery of precious metals, such as gold, from aqueous solutions would also contribute to a more sustainable economy. Furthermore, the development of environmentally friendly techniques of water remediation and recovery of valuable compounds (characterized by having low energy requirements, using locally available resources, etc.) has been a high priority concern of researchers in the last decades.

Adsorption processes are viewed as relatively simple methods, effective for the removal of various contaminants from aqueous solution. Depending on the water characteristics, adsorption can be applied as an alternative to conventional treatment processes (coagulation/flocculation, biological treatment) or as a final step, at a post-treatment level, in water or industrial wastewater treatment. Commercial adsorbents include mainly activated carbon and activated alumina. The manufacture of these materials involves high energy costs, due to the high temperatures required, which has implications for the acquisition price of the adsorbents and for the environment. In fact, to reduce the environmental impact of adsorption processes, adsorbents should be ideally effective, made of renewable and abundant materials, and should require minimal processing before use.

Biosorption gives a key contribution to reach these goals. It is defined as the property of certain biomolecules, or types of biomass (biosorbents), to bind and concentrate selected ions or molecules from aqueous solutions [1]. The mechanisms of biosorption are generally based on physicochemical interactions between adsorbates and the functional groups present on the biomass surface, such as electrostatic interactions, ion exchange, metal ion chelation or complexation [2]. In the last years, biosorption on marine seaweeds, agricultural wastes, forest residues, and industrial by-products, in native or modified forms, has been indicated as a promising technology for the uptake of heavy metals and organic

contaminants from waters [3-7]. In addition to water remediation, biosorption technology has also recognized applications in the recovery of metals from effluents and hydrometallurgical processes [2, 8, 9]. Adsorbents derived from lignocellulose and tannin materials, seaweeds, and chitosan have shown great potential to selectively uptake precious and critical metals, and to be used in added value applications, such as catalysis [2].

Tannins are natural phenolic polymers found abundantly in bark, wood, leaves, seeds and fruits of a variety of plant species [10]. They are generally classified into condensed and hydrolysable tannins, with condensed tannins representing more than 90 % of the worldwide commercial production [11]. Definitions and chemical classification have been discussed in literature [10-13]. Tannins are soluble in water and viewed as a potential substitute to synthetic phenols. Over time, various applications have been found for tannins. The oldest one is tanning hides for leather manufacturing, but there are many other important uses, such as in wood adhesives, coatings, dyeing, beverages manufacturing, animal nutrition, cosmetics, and pharmaceuticals [12, 14].

In the last years, tannin-derived materials have been extensively investigated as potential adsorbents for water and wastewater treatment and for the recovery of precious metals from liquors. Tannins present numerous adjacent phenolic hydroxyl groups, known to display specific ability to metal chelation [15], which makes them potentially good adsorbents. However, the potential of tannin-adsorbents to uptake toxic metalloids and oxyanions has not been sufficiently assessed.

On the other hand, tannins are of simple extraction and easily modified into tailored adsorbents. Tannins can be obtained from agro-food wastes (e.g., grapeseed, chestnut peels) and from residues of forest exploitation — timber, pulp, and paper mills — which make their use attractive. Some of these materials are frequently incinerated, landfilled, used in horticulture or as energy source, which motivate the search for other ways of valorisation. Even though pine (*Pinus pinaster*) bark is tannin rich, it has rarely been used as a source material to produce tannin-adsorbents.

2. Goals

The goals of this work can be divided into three major sections:

(1) Tannin extraction from pine (*P. pinaster*) bark and optimization of the procedure through characterization of extracts.
(2) Tannin resins production through tannin polymerization and chemical modification procedures (iron- and calcium-loading), and adsorbent characterization.
(3) Assessment of adsorption behaviour of arsenic, antimony, phosphate, and gold by the tannin resins produced.

Tannin extraction is to be optimized in terms of total phenolic content and of formaldehyde-condensable phenols. Also, optimization of the adsorbent production should be undertaken to maximize the amount of adsorbent produced per amount of bark used in the extraction and per amount of extract used in the polymerization. Then, characterization of the adsorbents obtained will serve to correlate some of its properties, i.e., iron or calcium content, with production conditions and adsorption capacities. The applicability of the adsorbents produced in the removal of arsenic, antimony, and phosphates and in the recovery of valuable substances (antimony, phosphates, and gold) should be finally assessed to determine the worth of the pine-tannin resin here produced as an adsorbent.

3. Outline

This thesis contains seven chapters. Chapters II to VI follow the same general structure: (1) literature review about its individual contents; (2) experimental methodology; (3) presentation of results and its discussion and comparison with literature; and (4) major conclusions. Chapter II focuses on tannin extraction from pine bark. Chapter III addresses the preparation and characterization of tannin-adsorbents (in this case, tannin resins) using the extracts described in the previous chapter. Moreover, some preliminary adsorption assays are reported, and the results helped decide which adsorbents and adsorbates were to be studied in the subsequent chapters. Chapter IV is about the removal of arsenic by an iron-loaded oxidized tannin resin. In Chapter V, removal and recovery of antimony by tannin resins is assessed. The topic of Chapter VI is the uptake and recovery of gold by tannin resins. Finally, Chapter VII presents the final remarks: general conclusions are offered, and suggestions for future work are presented.

4. References

[1] Volesky, B., "Biosorption and me," *Water Research,* vol. 41, no. 18, pp. 4017-4029, 2007.

[2] Dodson, J.R., H.L. Parker, A.M. Garcia, A. Hicken, K. Asemave, T.J. Farmer, H. He, J.H. Clark, and A.J. Hunt, "Bio-derived materials as a green route for precious & critical metal recovery and re-use," *Green Chemistry,* vol. 17, no. 4, pp. 1951-1965, 2015.

[3] Fomina, M. and G.M. Gadd, "Biosorption: current perspectives on concept, definition and application," *Bioresource Technology,* vol. 160, pp. 3-14, 2014.

[4] He, J.S. and J.P. Chen, "A comprehensive review on biosorption of heavy metals by algal biomass: Materials, performances, chemistry, and modeling simulation tools," *Bioresource Technology,* vol. 160, pp. 67-78, 2014.

[5] Palma, G., J. Freer, and J. Baeza, "Removal of metal ions by modified *Pinus radiata* bark and tannins from water solutions," *Water Research,* vol. 37, no. 20, pp. 4974-4980, 2003.

[6] Sánchez-Martín, J., M. González-Velasco, J. Beltrán-Heredia, J. Gragera-Carvajal, and J. Salguero-Fernández, "Novel tannin-based adsorbent in removing cationic dye (Methylene Blue) from aqueous solution. Kinetics and equilibrium studies," *Journal of Hazardous Materials,* vol. 174, no. 1-3, pp. 9-16, 2010.

[7] Pavan, F.A., E.S. Camacho, E.C. Lima, G.L. Dotto, V.T.A. Branco, and S.L.P. Dias, "Formosa papaya seed powder (FPSP): Preparation, characterization and application as an alternative adsorbent for the removal of crystal violet from aqueous phase," *Journal of Environmental Chemical Engineering,* vol. 2, no. 1, pp. 230-238, 2014.

[8] Gurung, M., B.B. Adhikari, H. Kawakita, K. Ohto, K. Inoue, and S. Alam, "Recovery of gold and silver from spent mobile phones by means of acidothiourea leaching followed by adsorption using biosorbent prepared from persimmon tannin," *Hydrometallurgy,* vol. 133, pp. 84-93, 2013.

[9] Dittert, I.M., V.J.P. Vilar, E.A.B. da Silva, S.M.A.G.U. de Souza, A.A.U. de Souza, C.M.S. Botelho, and R.A.R. Boaventura, "Adding value to marine macro-algae *Laminaria digitata* through its use in the separation and recovery of trivalent chromium ions from aqueous solution," *Chemical Engineering Journal,* vol. 193, pp. 348-357, 2012.

[10] Khanbabaee, K. and T. van Ree, "Tannins: Classification and Definition," *Natural Product Reports,* vol. 18, no. 6, pp. 641-649, 2001.

[11] Arbenz, A. and L. Averous, "Chemical modification of tannins to elaborate aromatic biobased macromolecular architectures," *Green Chemistry,* vol. 17, no. 5, pp. 2626-2646, 2015.

[12] Pizzi, A., "Tannins: major sources, properties and applications," in *Monomers, Polymers and Composites from Renewable Resources*, M. N. Belgacem and A. Gandini, Eds.: Elsevier, 2008, pp. 179-200.

[13] de Hoyos-Martínez, P.L., J. Merle, J. Labidi, and F. Charrier-El Bouhtoury, "Tannins extraction: A key point for their valorization and cleaner production," *Journal of Cleaner Production,* vol. 206, pp. 1138-1155, 2019.

[14] Shirmohammadli, Y., D. Efhamisisi, and A. Pizzi, "Tannins as a sustainable raw material for green chemistry: A review," *Industrial Crops and Products,* vol. 126, pp. 316-332, 2018.

[15] Slabbert, N., "Complexation of condensed tannins with metal ions," in *Plant Polyphenols*, vol. 59, R. E. Hemingway and P. Laks, Eds. Boston, MA: Springer, 1992, pp. 421-436.

CHAPTER II

TANNIN EXTRACTION

1. Literature Review

Tannins are inexpensive and ubiquitous natural molecules [1], which are polyphenolic secondary metabolites of most higher plants, mainly present in soft tissues (sheets, needles or bark) but also in roots, fruit, and seed [2-5]. After cellulose, hemicellulose, and lignin, tannins are the most abundant compounds extracted from biomass [6]. The reason tannins are so widespread within plants and within tissues of the same plant is their role in the defence against insects, bacteria, and fungi [4]. The most common commercial tannin feedstocks, presently or historically, are wattle or mimosa bark (*Acacia mearnsii* or *mollissima*), quebracho wood (*Schinopsis balansae* or *lorentzii*), oak bark (*Quercus* spp.), chestnut wood (*Castanea sativa*), and mangrove (*Rhizophora* spp.) wood. Nevertheless, multiple trees and shrubs contain significant amounts of tannins [5]. Tannin contents reported in literature for some vegetable sources are presented in Table II.1.

Table II.1 Tannin contents reported for some vegetable materials.

Plant material	**%**	**Reference**
Chestnut (*Castanea*) endodermis/hull	2.50/0.94	[7]
Chestnut (*Castanea*) shell	7-23	[8]
Chestnut (*Castanea*) wood	4-21	[9, 10]
Mangrove (*Rhizophora*) bark	15-42	[9]
Mangrove (*Rhizophora*) leaves	5.2	[11]
Wattle (*Acacia*) bark	15-50	[9]
Hemlock (*Tsuga*) bark	9-20	[9]
Sumac (*Rhus*) leaves	25-32	[9]
Myrobalan (*Terminalia chebula*) nuts	30-40	[9]
Terminalia arjuna bark	20-24	[12]
Quebracho (*Schinopsis* sp.) wood	20-43	[9, 10]
Chestnut oak (*Quercus montana*)	10-14	[9]
Black oak (*Quercus velutina*)	8-12	[9]
Myrica rubra bark	17	[13]
Pinus pinaster bark	22.5	[14]
Pinus oocarpa bark	16-36[a]	[15]
Eucalyptus spp. bark	1-40	[16-18]
Grey and black alder (*Alnus* sp.)	12.6[a]	[19]

a – Only condensed tannins.

Tannins are important commercial substances, traditionally used as tanning agents in the leather industry, allowing the transformation of hide into leather. Other uses include wood adhesives (as phenol substitutes in the formulations), pharmaceutical and food industry applications, ore flotation agents, cement superplasticizers, fireproof and insulating

foams, coagulants/flocculants, and precipitation of polluting materials by complexation with heavy metals, adsorbents for proteins and antibiotics and for metal ions recovery, among others [3-5, 20, 21].

Historically, tannins have been loosely classified into two classes of phenolic molecules: hydrolysable tannins and condensed or polyflavonoid tannins. Hydrolysable tannins are of nonpolymeric nature and can be fractionated into simple components by treatment with hot water or by enzymes [3]. Condensed tannins are non-hydrolysable oligomeric and polymeric proanthocyanidins, made up of flavonoid units (flavan-3-ols and flavan-3,4-diols) [22], with a degree of polymerization between two and greater than fifty [3]. Even though both classes of tannins present a significant reactivity towards formaldehyde (and, to a lesser extent, other aldehydes) due to their phenolic nature, several reasons, such as lack of macromolecular structure, low phenol substitution and low nucleophilicity, make hydrolysable tannins of less chemical and economical interest for the production of resins and adhesives, and other applications apart from leather tanning [5]. Condensed tannins have also the advantage of being present in considerable amounts in the wood and bark of several trees [5]. Thus, condensed tannins are more suitable building blocks for resin production.

Fig. II.1 presents the structures of a flavonoid unit and a condensed tannin [5]. The presence of phenolic groups in tannins clearly indicates its anionic nature [23]. Phenolic groups act as weak acids, therefore can deprotonate, being good hydrogen donors, to form phenoxide ion which is resonance-stabilized.

Condensed tannins are soluble in water but, through a step-growth polymerization reaction between tannins and formaldehyde (cross-linking agent), an insoluble non-linear polymer can be produced. This polymer has the potential to be a somewhat stable material that presents properties of interest for use as a biosorbent, such as the presence of many hydroxyl groups and the potential to be chemically modified to increase its efficiency or to grant it affinity to a compound or element which otherwise would not have. Tannin-adsorbents produced from different sources (*Acacia*, *Schinopsis*, *Pinus*, *Diospyros*) have been studied not only for the removal of heavy metals and organics [24-30] but also for the recovery of precious metals [31-36].

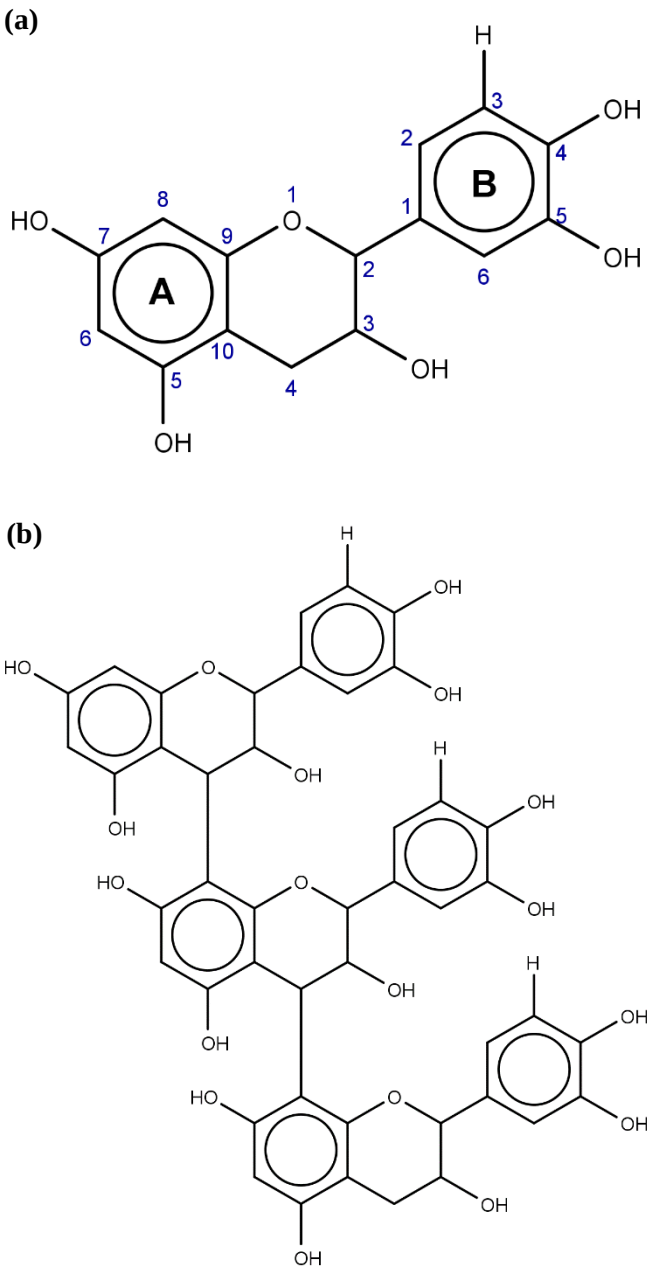

Fig. II.1 Structures of (a) a flavonoid monomer unit and of (b) a pine condensed tannin (i.e., a procyanidin) (adapted from [5]).

Although no longer the most common tree in mainland Portugal, *Pinus pinaster* (maritime pine) continues to be widespread in the Portuguese forest. In Fig. II.2, the variation between 1995 and 2015 of the occupied forest areas by the five most common trees in mainland Portugal is presented. In that 20-year period, maritime pine saw its area shrink 265 thousand hectares mainly due to fires and parasite-induced diseases [37]. However, the decrease of *P. pinaster* area between 2005 and 2015 was notoriously less accentuated than the one registered in the previous ten years (Fig. II.2). Moreover, the most recent data (2015) indicates that *P. pinaster* represents roughly a fifth (22.1±1.1 %, 713 300 ha)

of all forest area in mainland Portugal, sharing the second-place of most common trees with cork oak (22.3±1.1 %, 719 900 ha) behind eucalyptus (26.2±1.0 %, 845 000 ha) [37]. Besides that, the other two species that make up the top-five remain remarkably less common than maritime pine. Hence, its higher abundance than most other trees in Portugal is expected to remain a reality in the, at least short-term, future.

Since it represents 10-20 % of the tree trunk [38], pine bark is a common forest waste, appearing also as a residue from timber industry, which is commonly incinerated, landfilled, used in horticulture or as energy source. However, its use for heat/power generation has operational, economic, and environmental limitations [39]; in addition, these options despise the valuable chemical content of this biomass. Indeed, the bark of maritime pine is particularly rich in condensed tannins, mainly procyanidins (Fig. II.1b) [40, 41]. In pine tannins, the flavonoid unit is repeated up to 30 times with an average degree of polymerization of 6-7 [42], while in mimosa and quebracho tannins it is repeated 2-11 times and polymerization degree averages around 4-5 [22, 43]. For this reason, pine tannins are more suitable than mimosa or quebracho tannins to produce formaldehyde-resins. Thus, pine bark, as a forest waste, is an easily obtained low-cost source-material for condensed tannin extraction. The extraction of tannins from vegetable residues such as pine bark constitutes then an important contribution for their reuse and valorisation, and for tannins sustainable production.

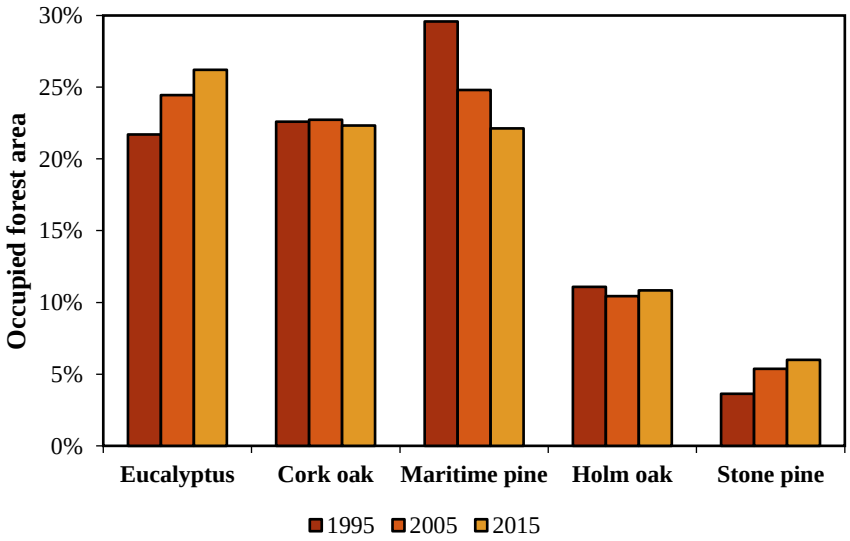

Fig. II.2 Variation of occupied forest area by the five most common trees in mainland Portugal between 1995 and 2015. Plot drawn using data reported in the 6th National Forest Inventory [37].

There are no universal conditions for extracting tannins from vegetable sources [6, 44]. Tannin content can vary greatly depending on species and on plant tissue [45], in addition to being sensible to seasonal and environmental factors (water availability, temperature, light intensity, soil quality, etc.) [44, 46]. Thus, the extraction procedure should be optimized in a case-specific basis. Extraction yield and the composition of extracts depends on type of solvent, extraction time, temperature, solid-liquid ratio, and preparation of the sample, which is commonly milled, used in fresh, frozen, or dried state.

The polar nature of water makes it a possible extraction solvent for many compounds [47]. The traditional industrial method for tannin extraction from vegetable matter is exactly based on hot/boiling water, with temperatures ranging from 50 °C to 110 °C, using autoclaves working in counter-current, contact times of several hours (6-10 h) and tannin-containing material/water ratios equal to 0.4-0.5 in mass. Tannins are then concentrated, by evaporation under vacuum, to limit the oxidation [6, 48].

Aqueous extraction is the simplest procedure, generating environmentally-benign residues and high yields, with the high amount of solvent required as the sole disadvantage [49, 50]. However, if the goal is to extract condensed tannins, an alkaline solution may be more appropriate since water has more affinity towards hydrolysable tannins [49, 51]. In the literature, regardless of the tannin source, there are many reports of extractions with sodium hydroxide solutions [16, 40, 51-54]. The concentration of the alkaline solution has been shown to have a positive correlation with the extraction yield as it avoids self-condensation reactions of tannins which are promoted at acidic conditions. However, its indiscriminate increase may be undesirable since it can increase the amount of impurities found in the extract [44, 53] and thus using moderate amounts of base is recommended [15, 51]. Moreover, the alkaline solution may be spiked with Na_2SO_3 and $NaHSO_3$ [55] or only Na_2SO_3 [56] to reduce the high viscosity of extraction solutions, which is also a consequence of tannin self-condensation, and, consequently, to increase the reactivity towards formaldehyde of the tannins present in the resulting extract. Finally, the application of sodium salt solutions containing $NaHSO_3$ and $NaHCO_3$ [41] or Na_2SO_3 and Na_2CO_3 [57] to extract pine tannins has also been reported. Extraction procedures commonly followed by researchers to obtain tannins from *P. pinaster* bark are aligned with this general trend: use of alkaline solutions, containing sodium hydroxide, with or without salts [40, 54-56, 58].

Some authors have reported extractions using organic solvents, such as methanol, acetone, and hexane [56, 59-67]. However, the principles of green extractions are important to consider and one of them advocates for the "use of alternative solvents and principally water or agro-solvents" [47]. The use of petrochemical solvents should be avoided, considering the related negative environmental effects, and flammability and toxicity risks [49].

Furthermore, new extraction methods have been developed in the last years, such as supercritical fluid extraction (SFE) [68-75], microwave-assisted extraction (MAE) [63, 76-82], ultrasound-assisted extraction (UAE) [63, 83-91], and pressurized water extraction (PWE) [91-93]. The most common solvents for MAE and UAE are organic: ethanol, methanol, and acetone [44, 49, 94, 95]. Even though SFE is most commonly undertaken with carbon dioxide (CO_2) as the extraction fluid, many times an organic co-solvent is applied to ameliorate the low extraction capability of CO_2 due to its non-polarity nature [44]. In general, these methods present the following advantages [44, 49, 94, 95]: (1) short extraction times; (2) low solvent amount; (3) the ability to selectively extract specific phenolic compounds, yielding extracts more pure in the desired compound; (4) low toxicity (SFE and PWE); and (5) requirement of low or mild temperatures, in the case of SFE and UAE. On the other hand, there are some drawbacks [44, 49, 94, 95]: (a) high investment costs, except for UAE; and (b) high temperatures and the consequently possibility of thermal degradation (PWE and MAE).

These methods are mostly used to yield extracts to be applied as food supplements, and in the pharmaceutical industry due to the high amount of antioxidant compounds [49, 95]. Nonetheless, for the preparation of biosorbents such methods are not the most appropriate due to its complexity and expensiveness and since a thorough extract purification is not required. Although sugar, organic acids or other plant components are known to occur as impurities in tannin extracts [6], the presence of polyphenolic compounds, other than tannins, can sometimes even improve the adsorption ability, as suggested by the results of Palma et al. [96]. Moreover, a low final cost is assured by selecting a simple process for extraction and subsequent procedures.

2. Methodology

2.1. Pine bark

P. pinaster bark (Fig. II.3) was collected from the coastal North region of Portugal, milled in a regular coffee mill, dried in an oven at 65 °C and used in this work. Particle size distribution (obtained after sieving and weighing of each fraction) of the milled bark was as follows: <0.15 mm = 40±1 %, 0.15-0.50 mm = 24±3 %, 0.50-1.00 mm = 30±1 %, >1.00 mm = 6.8±0.1 %. Initially, some assays were done with bark broken up to small pieces (1-2 cm), instead of milled bark, to facilitate filtration. However, higher extractions yields were attained with milled bark and, consequently, every extraction assay after that was done with milled bark.

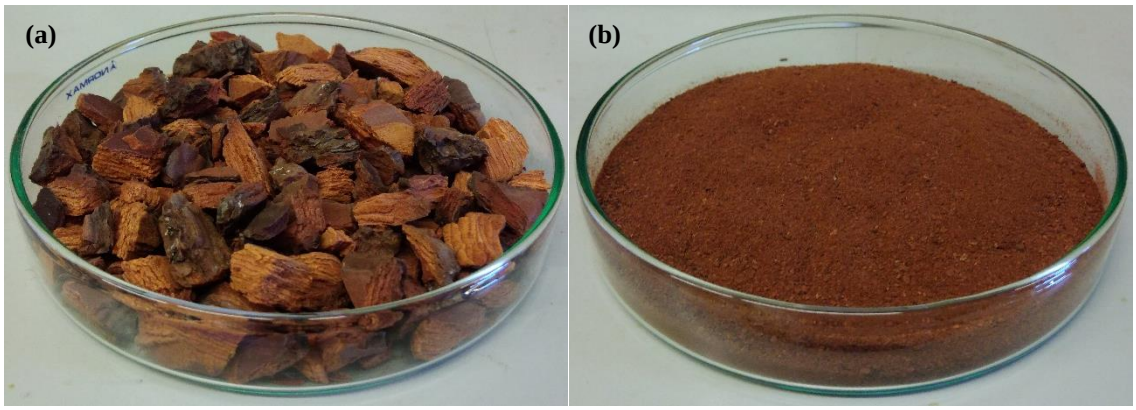

Fig. II.3 *Pinus pinaster* bark (a) broken up to pieces and (b) milled.

2.2. Aqueous vs. organic extraction

Tannin extraction was carried out by two procedures for comparison purposes: (1) alkaline aqueous batch extraction and (2) alcoholic Soxhlet extraction. The alkaline batch procedure was reported by Pepino et al. [40] and by Sánchez-Martín et al. [24] and it was applied here with the following amounts: 50 g of dried bark, 300 mL of tap water (i.e., using a solid:liquid ratio of 1:6) and NaOH 5 % (w/w, in respect to the bark). The mixture was kept at 80 °C and 600 rpm for 90 min, in a heating plaque/magnetic stirrer (*Heidolph* MR 3001). Subsequently, the solids were separated from the liquid by filtration (*Whatman* qualitative paper filter) and the liquid was neutralized using a 2 mol L^{-1} HCl solution, prepared from 37 % (w/w) analytical grade commercial solution (*Valente e Ribeiro, Lda*)

[40]. For the alcoholic extraction, milled bark was subjected to 20 cycles with ethanol 70 % (v/v) and a solid:liquid ratio of 1:12. The Soxhlet apparatus was subjected to heating, maintaining the solvent at boiling point (≈80 °C) to guarantee its reflux.

The water of the resulting extraction solution from both procedures was evaporated using a heating plaque and a glass crystallizer and, finally, the humid precipitate was dried in an oven at 65 °C. The resultant material was considered the tannin extract (TE).

2.3. Aqueous alkaline extraction

The alkaline method was then further optimized. Temperature (70 °C, 80 °C, and 90 °C) and contact time (60 min and 90 min), as well as the amount of NaOH (2.5-10 w/w %, in respect to the bark), were varied to find an optimal set of conditions. Moreover, the procedure described in Section 2.2 of this Chapter was subjected to two modifications: (1) a heating plaque with temperature control was used (*Velp Scientifica* Arex Digital Pro); and (2) extract production from the extraction solution was done through freeze-drying (*Labconco* FreeZone 2.5 Plus) instead of evaporation of the liquid fraction. The freeze-dried solid material was considered the tannin extract (TE, Fig. II.4).

Fig. II.4 Freeze-dried tannin extract (TE).

2.4. Extraction parameters

The extraction yield and the extract characteristics provided by the studied methods were determined and compared. Extraction yield (η_E) denotes the ratio between the amounts (in mass) of extract produced and dry bark initially used.

Extract characteristics were assessed by the determination of total polyphenolic content (TPC), Stiasny number (SN), and formaldehyde-condensable phenolic content (FCPC). TPC was determined using the Folin-Ciocalteu method [97] and adapted from Lazar et al. [83]. For each analysis, 1.00 mL of extract solution (25 mg of tannin extract dissolved in 50.0 mL of distilled water) was mixed with 0.50 mL of Folin-Ciocalteu reagent (*Panreac*), 2.0 mL of 100 g L^{-1} Na_2CO_3 (analytical grade, *Merck*) and 5.0 mL of distilled water. In order to avoid precipitate formation, sodium carbonate solution was added last [98]. The mixture was kept in the dark at room temperature for 90 min. The absorbance of each solution was measured by an UV-vis spectrophotometer (*VWR* UV-6300PC Double Beam Spectrophotometer) at a wavelength of 765 nm. TPC values were calculated considering a predetermined calibration curve obtained using gallic acid standard solutions (15-100 mg L^{-1}) and expressed as mg of gallic acid equivalents (GAE) per gram of tannin extract.

The procedure carried out to estimate the amount of formaldehyde-condensable phenols was adapted from the one described by Hoong et al. [99]. For each analysis, 50 mL of extract solution (250 mg of extract dissolved in 50 mL of distilled water) were added to 5 mL of formaldehyde (36 %, analytical grade, *Labsolve*) and 5 mL of 10 mol L^{-1} HCl, and the mixture was kept at 80 °C for 30 min under reflux in a heating digester (*Velp Scientifica* DK6). The reaction mixture was filtrated under vacuum using membrane filters with 0.45 µm porosity. The precipitate was then dried in an oven at 65 °C up to constant weight. The quantification of the formaldehyde-condensable phenolic material was then performed in two ways [40]: (i) Stiasny number (SN), defined as the ratio between mass of the precipitate obtained and mass of the total dissolved extract, expressed here as g-precipitate per g-extract; (ii) FCPC which was calculated by the difference between the phenolic content of the solution, determined by the Folin-Ciocalteu method, before and after reaction with formaldehyde and expressed as mg of gallic acid equivalents per gram of tannin extract.

Furthermore, using extract properties and extraction yield obtained, the following extracted quantities per amount of starting material were calculated: total extracted phenols (TEP), denoting the total phenols (mg-GAE) extracted per gram of bark; bark Stiasny number (BSN) defined in this work as the mass in mg of polymerized product (precipitate) obtained per gram of bark; and extracted formaldehyde condensable phenols (EFCP), representing the amount of formaldehyde condensable phenols (measured in mg-GAE) extracted per gram of bark.

3. Results and Discussion

3.1. Aqueous vs. organic extraction

Extraction results for alkaline and alcoholic extractions are presented in Table II.2. The yield found in this work for the organic extraction (3.2±0.4 %, Soxhlet, ethanol 70 % v/v) does not fare well against what is reported in the literature for *Pinus radiata* or *P. pinaster* extractions with ethanol. For example, Bocalandro et al. [100] achieved a slightly higher extraction yield from *P. radiata* bark (4.7±0.2 %) using ethanol 75 % in a bench-scale reactor at 120 ºC and a solid:liquid of 1:20. Ethanol solutions were also tested by Ramos et al. [67] as solvents for tannin extraction from *P. radiata* bark at different temperatures in a reactor with a solid:liquid ratio of 1:20 and using a concentration (75 %) similar to the one used here (70 %) the yield reported was ≈1.2 % and ≈6 % for 40 ºC and 120 ºC, respectively. In these works, a lower solid:liquid ratio and a higher or lower temperature was used; hence comparisons must be made carefully, especially in the case in which temperatures higher than the solvent boiling point are used because that requires pressures above atmospheric. Even so, since *P. radiata* bark is consistently reported as being less tannin-rich than *P. pinaster* bark regardless of extraction conditions, the considerably higher yields obtained by Bocalandro et al. [100] and Ramos et al. [67] suggest the operational apparatus and parameters for alcoholic extraction used here may not be optimal.

Table II.2 Extraction results obtained by organic extraction (Soxhlet apparatus) with ethanol and by batch alkaline mode. Values represent average from duplicates ± maximum deviation.

	Extraction in ethanol	**Alkaline extraction**
η_E (%)	3.2±0.4	15±1
Extract properties (expressed per gram of extract):		
TPC (mg g^{-1})	482±37	378±24
SN (g g^{-1})	0.66±0.02	0.67±0.02
FCPC (mg g^{-1})	389±34	352±26
% FCPC	81±2	93±1
Extracted quantities (expressed per gram of bark):		
TEP (mg g^{-1})	16±3	57±8
BSN (mg g^{-1})	21±2	100±10
EFCP (mg g^{-1})	13±4	53±8

On the other hand, for pine (*P. pinaster*) bark, with a microwave assisted extraction, ethanol 80 % as solvent and a solid:liquid ratio of 1:10, Chupin et al. [81] achieved the highest yield found in the literature (9.2±0.1 %). The agitation caused by the microwave irradiation which can ameliorate the mass transfer phenomenon [44] may help explain, at least partially, the significantly higher yield. In contrast, a direct comparison could be made with the results obtained by Pepino et al. [40] who achieved an extraction yield of 8.9 % using also a Soxhlet apparatus at solvent boiling point and after 52 cycles. However, which solvent concentration and solid:liquid ratio was used is not made clear in their paper, thus drawing conclusions is not prudent. Finally, Seabra et al. [56] performed extractions in a round-bottom flask without stirring and under solvent mixture reflux at boiling point with three ethanol concentrations (5 %, 10 % and 15 %) and a fixed solid:liquid ratio of 1:10; the yield reported was ≈6-7 %. Since the solvent concentration used was much lower and the yield obtained was twice as much, the Soxhlet apparatus may indeed not be optimal for tannin extraction from pine bark. The reason for this is perhaps an easier solvent circulation in a round-bottom flask than in a Soxhlet which in turn facilitates the contact between solvent and solid.

However, none of those yields were higher than the one obtained in the alkaline extraction of this work (Table II.2). Such results indicate that ethanol may not be the best solvent to extract tannins. Indeed, the yield for the alkaline extraction (15±1 %) was considerably higher than for the alcoholic one (3.2±0.4 %). Higher extraction yields with aqueous conditions than with organic solvents from *Pinus* bark were also reported by Pepino et al. [40] and by Ramos et al. [67].

Regarding aqueous extractions, the yield obtained depends on the alkaline solution concentration, temperature, time, solid:liquid ratio, degree of agitation, and particle size of the bark. More aggressive conditions, such as higher NaOH concentration and/or higher temperature, seem to favour the extraction yield [54-56, 63]. Literature reports extraction yields from *P. pinaster* varying roughly between 21 % and 50 %, obtained using alkali concentrations between 1 % and 5 % and temperatures in the range 80-100 ºC [54-56, 58]. The value here obtained (15±1 %), even though it is about five times higher than the alcoholic extraction yield, is somewhat below that range suggesting that further optimization of the extraction procedure might be possible. Beyond extraction conditions, the

age of the tree and its exposure to sunlight [101], among other factors [46], can also influence the amount of phenols contained in its bark and subsequently the extracted amount.

Looking at the extract characteristics (Table II.2), TPC of the alcoholic extract is higher than of the alkaline one. This indicates that ethanol, even though it granted lower extraction yields, has a higher specificity to phenolics than the alkaline solution and this is also in line with results reported by Pepino et al. [40] and by Ramos et al. [67]. Regarding SN and FCPC values, both methods generated extracts with similar properties (no statistically significant difference was observed between values). Thus, even though the alcoholic extract was richer in phenolic content, it was not richer in formaldehyde-condensable material, which is a more important property, than the alkaline extract. Moreover, in the alkaline extract 93 % of phenols were found to be condensable with formaldehyde, a higher percentage than that of the organic extract (84 %).

Alkaline extraction led to higher amounts of total extracted phenols (57±8 mg-GAE g^{-1} vs. 16±3 mg-GAE g^{-1}). In addition, alkaline extraction also generated higher BSN and EFCP values (about 3 and 2.5 times higher, respectively) in comparison to the organic extraction. These two parameters, BSN and EFCP, are of great importance for this work since they directly reflect the amount of tannin resin that is possible to obtain per gram of *P. pinaster* bark. Thus, the alkaline method was found to be overall better suited for this work.

3.2. Aqueous alkaline extraction

The effect of operational variables (temperature, contact time, and NaOH amount) of the alkaline extraction procedure was studied. Extraction yields and extract properties results, obtained for each set of temperature and contact time conditions and 5 % NaOH, are presented in Table II.3. As it can be observed, a longer contact time did not present advantages in any property nor in the yield, suggesting that 60 min is enough. Within a contact time of 60 min, an increase of temperature conferred a very slight increase in extraction yield at 90 °C. However, temperature appears to have no significant impact on the extract properties, as well as on the extracted quantities. The only exception is the BSN, for which a slight increase is observed. Given the importance of this property, since

it is a direct indicator of the amount of adsorbent that can be obtained, 90 °C was considered the optimal temperature for tannin extraction. Nonetheless, 70 °C would have been a good choice given that the yield is not drastically affected (only a 15 % decrease is observed) and, hence, the procedure would have granted almost the same amount of extract with lower energy costs.

The extraction yield obtained under the optimal conditions was still considerably lower than values reported on the literature. For example, using the same conditions except of contact time (30 min), Vázquez et al. [54] achieved a yield of 30.7 %, which is 1.6 times higher than the value here reported (18.4 %, Table II.3). Moreover, the SN here obtained was 0.75 g g^{-1} while those authors reported a considerable higher value (0.88 g g^{-1}). Of note, their extract was obtained through spray-drying which, together with bark properties, may explain these differences.

Table II.3 Extraction results obtained by batch alkaline mode with 5 % w/w NaOH at different temperature and contact time. Values represent average from duplicates ± maximum deviation.

Experimental conditions	Contact time = 60 min			Contact time = 90 min		
	T = 70 °C	T = 80 °C	T = 90 °C	T = 70 °C	T = 80 °C	T = 90 °C
η_E (%)	16±1	16±1	18.4±0.4	17±1	17.3±0.1	19±2
Extract properties (expressed per gram of extract):						
TPC (mg g^{-1})	621±30	585±33	610±26	504±66	624±13	619±20
SN (g g^{-1})	0.73±0.03	0.75±0.03	0.75±0.01	0.75±0.02	0.74±0.02	0.74±0.03
FCPC (mg g^{-1})	606±31	568±33	586±26	490±66	605±12	598±17
% FCPC	97.6±0.3	97.1±0.2	96.1±0.2	97.1±0.5	97.0±0.2	96.5±0.3
Extracted quantities (expressed per gram of bark):						
TEP (mg g^{-1})	100±9	96±9	113±8	85±15	108±2	115±11
BSN (mg g^{-1})	116.6±0.4	124±4	138±4	125±8	129±4	136±2
EFCP (mg g^{-1})	98±9	93±9	108±7	82±15	105±2	111±10

Lastly, an optimization of the NaOH amount was performed. The more alkaline the medium is, the higher is the extraction yield (Table II.4), as it is also reported in the literature under similar conditions [54-56, 63], which is explained by the hampering of tannin self-condensation reactions. Indeed, extraction yield increased from 11.3 % to 31.1 % when the NaOH amount was increased from 2.5 % to 10 %, a three-fold increase. However, these values are influenced by the amount of NaCl generated when the extraction solution is neutralized with HCl. The presence of this salt in the extracts makes the results inconclusive: the increase in yield could be entirely justified by the salt mass increase. To circumvent this problem, the mass of NaCl was estimated through molar calculations and

subtracted from the extract mass. Hence, adjusted values for extraction yields were obtained (η_{EA}, Table II.4). The yield still increased when the extraction is done with more NaOH but at a slower rate: from 2.5 % to 10 % NaOH the extraction yield doubled, from 7.7 % to 16.4 %.

In Fig. II.5, the influence of NaOH amount on extract properties and extracted quantities is presented. The extract properties decline with an increase of NaOH amount (Fig. II.5a), which suggests molecules other than phenols are being extracted from the bark, making the extraction less selective. In line with this, Chupin et al. [55] also reported a decrease of SN, from 0.49 g g^{-1} to 0.18 g g^{-1}, when the amount of NaOH was increased from 1 % to 5 %. In contrast, the extracted quantities, which are expressed per mass unit of the starting material, increase with an increase of the NaOH amount (Fig. II.5b), which means that indeed an higher amount of phenols is being extracted from the bark even though the extract becomes less concentrated in these compounds. Vázquez et al. [54] reported a decrease in SN from 0.94 g g^{-1} to 0.88 g g^{-1} with the increase of NaOH amount from 2.5 % to 5 %, while BSN increased from 250 mg g^{-1} to 270 mg g^{-1}, corroborating the results obtained here. Moreover, Seabra et al. [56] performed an alkaline extraction under reflux at the solvent boiling point and the results were parallel to those reported here: both the extraction yield and the TEP increased with the increase of NaOH in the solution from 0.5 % to 1.5 %.

Although better results were achieved with NaOH 10 %, we decided to use just 7.5 % due to the slowing down of the increase in extracted quantities along with increasing NaOH amount. For example, BSN increased 55 % and 20 % with the increase of NaOH amount from 2.5 % to 5 % and from 5 % to 7.5 %, respectively. The last increase of NaOH amount only granted a 14 % increase in BSN. Such slight improvement does not provide justification to use more reagents in the procedure, namely NaOH for the extraction and HCl for the pH neutralization of the extraction solution.

Table II.4 Extraction yields obtained by batch alkaline mode with different amounts of NaOH. Values represent average from duplicates ± maximum deviation. Experimental conditions: T = 90 °C, t = 60min.

	Amount of NaOH in % (w/w, in respect to the bark)			
	2.5	**5.0**	**7.5**	**10.0**
η_E (%)	11.3±0.2	18.4±0.4	24.2±0.1	31.1±0.1
η_{EA} (%)	7.7±0.2	11.1±0.4	13.2±0.1	16.4±0.1

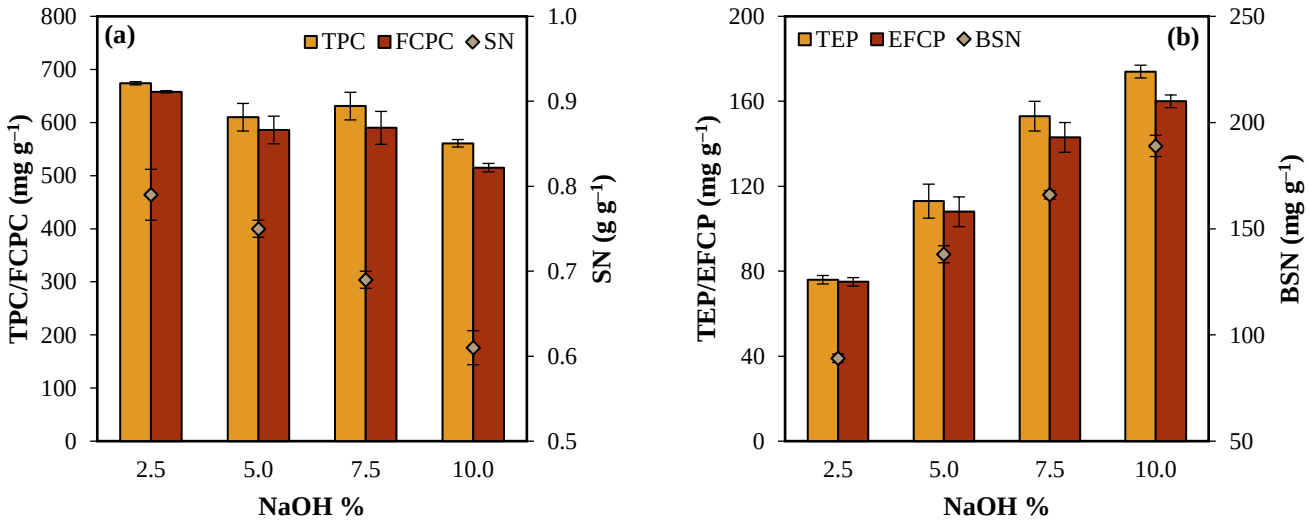

Fig. II.5 Extract properties (a) and extracted quantities (b) obtained by batch alkaline mode with different amounts of NaOH. Error bars represent maximum deviation of duplicate average. Experimental conditions: T = 90 °C, t = 60min.

Freeze-drying was shown to be a more advantageous procedure to obtain the tannin extract than the evaporation one. Comparing the extraction results obtained, under the same conditions (80 °C, 90 min, NaOH 5%), through evaporation (Table II.2) and through freeze-dying (Table II.3), the latter procedure granted better values. Indeed, the extraction yield is slightly higher (17.3±0.1 % vs. 15±1 %). On the other hand, total phenols and formaldehyde-condensable phenols present in the freeze-dried extract were about twice as much as in the evaporated one (TCP and EFCP, Table II.2 and Table II.3). Since extraction yields were similar, the same variation — i.e., a roughly two-fold increase — is also observable for TEP and EFCP values. However, SN and BSN values were not remarkably higher. For example, freeze-drying led to an increase of BSN only of 29 % (129±4 mg g^{-1} vs. 100±10 mg g^{-1}). Freeze-drying yielded higher quality extracts due to its ability to preserve the native structures of condensed tannins [6] since the drying temperature is kept very low, avoiding molecule thermal degradation.

Table II.5 presents a summary of the extraction yields and the amounts of total phenols and of formaldehyde-condensable phenols that can be obtained per gram of bark of three *Pinus* species, calculated with values reported in literature.

Table II.5 Extraction yield of *Pinus* bark reported in the literature. Total extracted phenols and amounts of condensable tannins that can be obtained per gram of pine bark: calculated values from literature results. Extractions listed in this table, unless otherwise stated, were made in batch mode.

Solvent	S:L	T (°C)	Time (min)	η_E (%)	TEP (mg g^{-1})	BSN (mg g^{-1})	Ref.
Pinus oocarpa							
[a] Water	1:15	–	120	24.8	–	163	[15]
[a] Na_2CO_3 5 %	1:15	–	120	35.7	–	321	
Pinus radiata							
Water	1:50	100	60	23.2	–	–	[102]
Water	1:20	120	120	≈12	≈21	–	[67]
Acetone 25 %	1:20	120	120	≈11	≈33	–	
Ethanol 25 %	1:20	120	120	≈10	≈30	–	
Ethanol 75 %	1:20	120	120	≈6	≈24	–	
Acetone 70 %	1:10	20	180	8.7	–	–	[63]
Ethanol 75 %	1:20	120	120	4.7	26	–	[100]
Pinus pinaster							
[b] Ethanol 80 %	1:10	–	3	9.2	28	45	[81]
Water	1:6	90	90	6.3	43	–	[57]
Na_2SO_3 2 % + Na_2CO_3 0.5 %	1:5	75	60	9.8	88	–	
Water	1:8	80	30	6.4	–	60	[54]
NaOH 2.5 %	1:6	90	30	26.4	–	250	
NaOH 5 %	1:6	90	30	30.7	–	270	
NaOH 2 %	1:10	100	30	33.6	–	–	[58]
[c] NaOH 1 %	1:9	80	120	22	62	110	[55]
[c] NaOH 5 %	1:9	80	120	31	22	60	
[a] NaOH 0.5 %	1:10	–	120	≈22	≈70	–	[56]
[a] NaOH 1.5 %	1:10	–	120	≈38	≈89	–	
[a,d] NaOH 1.5 %	1:10	–	120	≈50	≈102	–	
[a] Ethanol 15 %	1:10	–	120	≈7	≈24	–	
[a,d] Ethanol 15 %	1:10	–	120	≈17	≈52	–	
NaOH 1 %	1:5	90	30	27.7	114	159	[40]
[e,f] Ethanol 70 %	1:12	–	–	3.2	16	21	This work
[f] NaOH 5 %	1:6	80	90	15	57	100	
[g] NaOH 5 %	1:6	90	60	18.4	113	138	
[g] NaOH 7.5 %	1:6	90	60	24.2	153	166	

a – Extraction under reflux at the solvent boiling point; b – Microwave assisted extraction (100 W); c – Solvent also contains Na_2SO_3 0.25 % + $NaHSO_3$ 0.25 %; d – Solvent also contains Na_2SO_3 1 %; e – Extraction performed in a Soxhlet (20 cycles); f – Extract obtained by evaporation of liquid fraction; g – Extract obtained by freeze-drying.

Under the optimal conditions here determined (90 °C, 60 min, 7.5 % NaOH), the extraction yield obtained (24.2±0.1 %) is at the low end of the range of values reported in the literature for alkaline extractions of *P. pinaster* bark, which ranges from 21 % to 50 % (Table II.5); however, it is higher than any value reported for *P. radiata* (4.7-12 %). Extraction yields comparison ought to be done with some caution since yield is a parameter which may be calculated differently by different authors: in some cases, as is this work

an example, yield is considered the ratio between the extract mass obtained and the bark mass used, while in others the bark mass differential before and after the extraction is considered the yield. Moreover, in some papers it is not made explicitly clear how the yield was calculated. Hence, there may be some variation in the values, at least partially, due to the way the yield was calculated and not because of experimental conditions.

The extracted quantities, obtained here under optimal conditions, fare better against what is reported in the literature than the extraction yield does (Table II.5). Indeed, the TEP is higher than any value found for extractions from *Pinus* species bark and BSN is one of the highest values. Such observations suggest that the extraction procedure can hardly be further optimized.

4. Conclusions

Alkaline extraction was optimized in terms of temperature, contact time and NaOH amount, with the extract being obtained through freeze-drying. A higher contact time (90 min) was proven not to be advantageous when compared with 60 min. Extraction yield was slightly higher when performed at the highest temperature tested (90 °C); however, extract properties did not improve with the increase of temperature except for the amount of biosorbent produced per gram of bark used where a considerable difference is observed. In terms of NaOH amount, it was clear that the more alkaline the solution was the better results were obtained. However, to minimize the amount of basic solution used, it was decided not to use the highest NaOH amount tested but the second highest. Thus, the optimal conditions here considered are: T = 90 °C, t = 60 min, and NaOH 7.5 %. Of note, however, tannin extracts might be obtained using lower temperatures than 90 °C without considerable negative changes in the extraction yield or in the relevant extract properties or extracted quantities. The tannin extract obtained with the optimal conditions has a phenolic content of 631±30 mg of gallic acid equivalents per g of extract which in turn grants the production of 166±2 mg of polymerized material per g of bark used in the extraction.

5. References

[1] Hemingway, R.W., "Structural variations in proanthocyanidins and their derivatives," in *Chemistry and Significance of Condensed Tannins*: Springer, 1989, pp. 83-107.

[2] Haslam, E., *Plant Polyphenols: Vegetable Tannins Revisited*. Cambridge: Cambridge University Press, 1989.

[3] Khanbabaee, K. and T. van Ree, "Tannins: Classification and Definition," *Natural Product Reports*, vol. 18, no. 6, pp. 641-649, 2001.

[4] Pizzi, A., "Tannins: Prospectives and Actual Industrial Applications," *Biomolecules*, vol. 9, no. 8, 2019.

[5] Pizzi, A., "Tannins: major sources, properties and applications," in *Monomers, Polymers and Composites from Renewable Resources*, M. N. Belgacem and A. Gandini, Eds.: Elsevier, 2008, pp. 179-200.

[6] Arbenz, A. and L. Averous, "Chemical modification of tannins to elaborate aromatic biobased macromolecular architectures," *Green Chemistry*, vol. 17, no. 5, pp. 2626-2646, 2015.

[7] Lee, H.J., I.H. Choi, D.H. Kim, S.M. Amanullah, and S.C. Kim, "Nutritional characterization of tannin rich chestnut (*Castanea*) and its meal for pig," *Journal of applied animal research*, vol. 44, no. 1, pp. 258-262, 2016.

[8] Vázquez, G., J. González-Alvarez, J. Santos, M.S. Freire, and G. Antorrena, "Evaluation of potential applications for chestnut (*Castanea sativa*) shell and eucalyptus (*Eucalyptus globulus*) bark extracts," *Industrial Crops and Products*, vol. 29, no. 2, pp. 364-370, 2009.

[9] Young, R.A., "Wood and Wood Products," in *Kent and Riegel's Handbook of Industrial Chemistry and Biotechnology*, J. A. Kent, Ed. Boston, MA: Springer US, 2007, pp. 1234-1293.

[10] Panzella, L., F. Moccia, M. Toscanesi, M. Trifuoggi, S. Giovando, and A. Napolitano, "Exhausted Woods from Tannin Extraction as an Unexplored Waste Biomass: Evaluation of the Antioxidant and Pollutant Adsorption Properties and Activating Effects of Hydrolytic Treatments," *Antioxidants (Basel)*, vol. 8, no. 4, 2019.

[11] Hernes, P.J. and J.I. Hedges, "Tannin signatures of barks, needles, leaves, cones, and wood at the molecular level," *Geochimica Et Cosmochimica Acta*, vol. 68, no. 6, pp. 1293-1307, 2004.

[12] Patnaik, T., R.K. Dey, and P. Gouda, "Isolation of triterpenoid glycoside from bark of *Terminalia arjuna* using chromatographic technique and investigation of pharmacological behavior upon muscle tissues," *Journal of Chemistry*, vol. 4, no. 4, pp. 474-479, 2007.

[13] Ma, H.W., X.P. Liao, X. Liu, and B. Shi, "Recovery of platinum(IV) and palladium(II) by bayberry tannin immobilized collagen fiber membrane from water solution," *Journal of Membrane Science*, vol. 278, no. 1-2, pp. 373-380, 2006.

[14] Jorge, F.C., P. Brito, L. Pepino, A. Portugal, H. Gil, and R.P. da Costa, "Métodos de extracção de taninos e de preparação de adesivos para derivados de madeira: uma revisão," *Silva Lusitana*, vol. 10, no. 1, pp. 101-109, 2002.

[15] Vieira, M.C., R.C.C. Lelis, B.C. da Silva, and G.D.L. Oliveira, "Tannin extraction from the bark of *Pinus oocarpa* var. *oocarpa* with sodium carbonate and sodium bisulfite," *Floresta e Ambiente*, vol. 18, no. 1, pp. 1-8, 2011.

[16] Pinto, P.C.R., G. Sousa, F. Crispim, A.J.D. Silvestre, and C.P. Neto, "*Eucalyptus globulus* bark as source of tannin extracts for application in leather industry," *ACS Sustainable Chemistry & Engineering*, vol. 1, no. 8, pp. 950-955, 2013.

[17] Trugilho, P.F., F. Mori Akira, J. Lima Tarcísio, and D. Cardoso Pereira, "Determinação do teor de taninos na casca de *Eucalyptus spp*," *Cerne*, vol. 9, no. 2, 2003.

[18] Sartori, C.J., G.S. Mota, I. Miranda, F.A. Mori, and H. Pereira, "Tannin extraction and characterization of polar extracts from the barks of two *Eucalyptus urophylla* hybrids," *BioResources*, vol. 13, no. 3, pp. 4820-4831, 2018.

[19] Janceva, S., T. Dizhbite, G. Telisheva, U. Spulle, L. Klavinsh, and M. Dzenis, "Tannins of deciduous trees bark as a potential source for obtaining ecologically safe wood adhesives," *Environment, Technology, Resources*, vol. 1, pp. 265-270, 2011.

[20] Shirmohammadli, Y., D. Efhamisisi, and A. Pizzi, "Tannins as a sustainable raw material for green chemistry: A review," *Industrial Crops and Products*, vol. 126, pp. 316-332, 2018.

[21] Singh, A.P. and S. Kumar, "Applications of Tannins in Industry," in *Tannins-Structural Properties, Biological Properties and Current Knowledge*: IntechOpen, 2019.

[22] Pizzi, A., "Tannin-Based Wood Adhesives," in *Wood Adhesives: Chemistry and Technology*, A. Pizzi, Ed. New York: Marel Dekker Inc., 1983, pp. 177-248.

[23] Yin, C.Y., "Emerging usage of plant-based coagulants for water and wastewater treatment," *Process Biochemistry*, vol. 45, no. 9, pp. 1437-1444, 2010.

[24] Sánchez-Martín, J., J. Beltrán-Heredia, and P. Gibello-Pérez, "Adsorbent biopolymers from tannin extracts for water treatment," *Chemical Engineering Journal*, vol. 168, no. 3, pp. 1241-1247, 2011.

[25] Beltrán-Heredia, J., P. Palo, J. Sánchez-Martín, J.R. Domínguez, and T. González, "Natural adsorbents derived from tannin extracts for pharmaceutical removal in water," *Industrial & Engineering Chemistry Research*, vol. 52, pp. 50-57, 2012.

[26] Huang, L., Q. Shuai, and S. Hu, "Tannin-based magnetic porous organic polymers as robust scavengers for methylene blue and lead ions," *Journal of Cleaner Production*, vol. 215, pp. 280-289, 2019.

[27] Inoue, K., H. Paudyal, H. Nakagawa, H. Kawakita, and K. Ohto, "Selective adsorption of chromium(VI) from zinc(II) and other metal ions using persimmon waste gel," *Hydrometallurgy*, vol. 104, no. 2, pp. 123-128, 2010.

[28] Li, X., Z. Wang, J. Ning, M. Gao, W. Jiang, Z. Zhou, and G. Li, "Preparation and characterization of a novel polyethyleneimine cation-modified persimmon tannin bioadsorbent for anionic dye adsorption," *Journal of Environmental Management*, vol. 217, pp. 305-314, 2018.

[29] Ogata, T., S. Morisada, Y. Oinuma, Y. Seida, and Y. Nakano, "Preparation of adsorbent for phosphate recovery from aqueous solutions based on condensed tannin gel," *Journal of Hazardous Materials*, vol. 192, no. 2, pp. 698-703, 2011.

[30] Xu, Q., Y. Wang, L. Jin, Y. Wang, and M. Qin, "Adsorption of Cu(II), Pb(II) and Cr(VI) from aqueous solutions using black wattle tannin-immobilized nanocellulose," *Journal of Hazardous Materials*, vol. 339, pp. 91-99, 2017.

[31] Fan, R.Y., F. Xie, X.L. Guan, Q.L. Zhang, and Z.R. Luo, "Selective adsorption and recovery of Au(III) from three kinds of acidic systems by persimmon residual based bio-sorbent: A method for gold recycling from e-wastes," *Bioresource Technology*, vol. 163, pp. 167-171, 2014.

[32] Gurung, M., B.B. Adhikari, S. Alam, H. Kawakita, K. Ohto, and K. Inoue, "Persimmon tannin-based new sorption material for resource recycling and recovery of precious metals," *Chemical Engineering Journal*, vol. 228, pp. 405-414, 2013.

[33] Kim, Y.H., M.N. Alam, Y. Marutani, T. Ogata, S. Morisada, and Y. Nakano, "Improvement of Pd(II) Adsorption Performance of Condensed-tannin Gel by Amine Modification," *Chemistry Letters*, vol. 38, no. 10, pp. 956-957, 2009.

[34] Liao, X., M. Zhang, and B. Shi, "Collagen-fiber-immobilized tannins and their adsorption of Au(III)," *Industrial & Engineering Chemistry Research*, vol. 43, pp. 2222-2227, 2004.

[35] Xie, F., Z.J. Fan, Q.L. Zhang, and Z.R. Luo, "Selective Adsorption of Au^{3+} from Aqueous Solutions Using Persimmon Powder-Formaldehyde Resin," *Journal of Applied Polymer Science*, vol. 130, no. 6, pp. 3937-3946, 2013.

[36] Liu, F.L., S.Y. Wang, and S.X. Chen, "Adsorption behavior of Au(III) and Pd(II) on persimmon tannin functionalized viscose fiber and the mechanism," *International Journal of Biological Macromolecules*, vol. 152, pp. 1242-1251, 2020.

[37] ICNF, "6º Inventário Florestal Nacional (IFN6) – Relatório Final," Instituto da Conservação da Natureza e das Florestas. Portugal. 2015.

[38] Vieito, C., P. Pires, and M.V. Velho, "*Pinus Pinaster* Bark Composition and Applications," in *Novel Technologies and Systems for Food Preservation* (Practice, Progress, and Proficiency in Sustainability). 2019, pp. 174-189.

[39] Feng, S.H., S.N. Cheng, Z.S. Yuan, M. Leitch, and C.B. Xu, "Valorization of bark for chemicals and materials: A review," *Renewable & Sustainable Energy Reviews,* vol. 26, pp. 560-578, 2013.

[40] Pepino, L., P. Brito, F.C. Jorge, R.P. da Costa, M.H. Gil, and A. Portugal, "Comparison of Quantification Methods for the Condensed Tannin Content of Extracts of *Pinus Pinaster* Bark," in *Biorelated Polymers: Sustainable Polymer Science and Technology*, E. Chiellini, H. Gil, G. Braunegg, J. Buchert, P. Gatenholm, and M. Van Der Zee, Eds. Boston, US: Springer 2001.

[41] Navarrete, P., A. Pizzi, H. Pasch, K. Rode, and L. Delmotte, "MALDI-TOF and ^{13}C NMR characterization of maritime pine industrial tannin extract," *Industrial Crops and Products,* vol. 32, no. 2, pp. 105-110, 2010.

[42] Pizzi, A., *Advanced Wood Adhesives Technology*. New York: Marcel Dekker Inc., 1994.

[43] Pasch, H., A. Pizzi, and K. Rode, "MALDI–TOF mass spectrometry of polyflavonoid tannins," *Polymer,* vol. 42, no. 18, pp. 7531-7539, 2001.

[44] de Hoyos-Martínez, P.L., J. Merle, J. Labidi, and F. Charrier-El Bouhtoury, "Tannins extraction: A key point for their valorization and cleaner production," *Journal of Cleaner Production,* vol. 206, pp. 1138-1155, 2019.

[45] Bele, A.A., V.M. Jadhav, and V.J. Kadam, "Potential of tannins: A review," *Asian Journal of Plant Sciences,* vol. 9, no. 4, p. 209, 2010.

[46] Frutos, P., G. Hervas, F.J. Giráldez, and A.R. Mantecón, "Tannins and ruminant nutrition," *Spanish Journal of Agricultural Research,* vol. 2, no. 2, pp. 191-202, 2004.

[47] Chemat, F., M.A. Vian, and G. Cravotto, "Green Extraction of Natural Products: Concept and Principles," *International Journal of Molecular Sciences,* vol. 13, no. 7, pp. 8615-8627, 2012.

[48] Matturro, G., P. Danesi, A. Festuccia, and C. Mustacchi, "Process and plant to extract and concentrate tannins from wood and from other natural products," 2006.

[49] Fraga-Corral, M., P. García-Oliveira, A.G. Pereira, C. Lourenço-Lopes, C. Jimenez-Lopez, M.A. Prieto, and J. Simal-Gandara, "Technological Application of Tannin-Based Extracts," *Molecules,* vol. 25, no. 3, 2020.

[50] Cuong, D.X., N.X. Hoan, D.H. Dong, N. Van Thanh, H.T. Ha, D.T.T. Tuyen, and D.X. Chinh, "Tannins: Extraction from Plants," in *Tannins-Structural Properties, Biological Properties and Current Knowledge*: IntechOpen, 2019.

[51] Aires, A., R. Carvalho, and M.J. Saavedra, "Valorization of solid wastes from chestnut industry processing: Extraction and optimization of polyphenols, tannins and ellagitannins and its potential for adhesives, cosmetic and pharmaceutical industry," *Waste Management,* vol. 48, pp. 457-464, 2016.

[52] Kunnambath, P.M. and S. Thirumalaisamy, "Characterization and Utilization of Tannin Extract for the Selective Adsorption of Ni(II) Ions from Water," *Journal of Chemistry,* 2015.

[53] Ping, L., N. Brosse, L. Chrusciel, P. Navarrete, and A. Pizzi, "Extraction of condensed tannins from grape pomace for use as wood adhesives," *Industrial Crops and Products,* vol. 33, no. 1, pp. 253-257, 2011.

[54] Vázquez, G., J. González-Alvarez, S. Freire, F. López-Suevos, and G. Antorrena, "Characteristics of *Pinus pinaster* bark extracts obtained under various extraction conditions," *Holz Als Roh-Und Werkstoff,* vol. 59, no. 6, pp. 451-456, 2001.

[55] Chupin, L., C. Motillon, F. Charrier-El Bouhtoury, A. Pizzi, and B. Charrier, "Characterisation of maritime pine (*Pinus pinaster*) bark tannins extracted under different conditions by spectroscopic methods, FTIR and HPLC," *Industrial Crops and Products,* vol. 49, pp. 897-903, 2013.

[56] Seabra, I.J., R.B. Chim, P. Salgueiro, M.E.M. Braga, and H.C. de Sousa, "Influence of solvent additives on the aqueous extraction of tannins from pine bark: potential extracts for leather tanning," *Journal of Chemical Technology & Biotechnology,* vol. 93, no. 4, pp. 1169-1182, 2018.

[57] Sanchez-Sanchez, A., M.T. Izquierdo, S. Mathieu, J. González-Álvarez, A. Celzard, and V. Fierro, "Outstanding electrochemical performance of highly N-and O-doped carbons derived from pine tannin," *Green Chemistry,* vol. 19, no. 11, pp. 2653-2665, 2017.

[58] Fradinho, D.M., C.P. Neto, D. Evtuguin, F.C. Jorge, M.A. Irle, M.H. Gil, and J.P. de Jesus, "Chemical characterisation of bark and of alkaline bark extracts from maritime pine grown in Portugal," *Industrial Crops and Products,* vol. 16, no. 1, pp. 23-32, 2002.

[59] Arasaretnam, S. and L. Karunanayake, "Synthesis, Characterization, and Metal Adsorption Properties of Tannin-Phenol-Formaldehyde Resins Produced Using Tannin from Dried Fruit of *Terminalia chebula* (Aralu)," *Journal of Applied Polymer Science,* vol. 115, no. 2, pp. 1081-1088, 2010.

[60] Onem, E., G. Gulumser, S. Akay, and O. Yesil-Celiktas, "Optimization of tannin isolation from acorn and application in leather processing," *Industrial Crops and Products,* vol. 53, pp. 16-22, 2014.

[61] Prior, R.L., S.A. Lazarus, G.H. Cao, H. Muccitelli, and J.F. Hammerstone, "Identification of procyanidins and anthocyanins in blueberries and cranberries (*Vaccinium spp.*) using high-performance liquid chromatography/mass spectrometry," *Journal of Agricultural and Food Chemistry,* vol. 49, no. 3, pp. 1270-1276, 2001.

[62] Liao, X.P., L. Li, and B. Shi, "Adsorption recovery of thorium(IV) by *Myrica rubra* tannin and larch tannin immobilized onto collagen fibres," *Journal of Radioanalytical and Nuclear Chemistry,* vol. 260, no. 3, pp. 619-625, 2004.

[63] Aspé, E. and K. Fernández, "The effect of different extraction techniques on extraction yield, total phenolic, and anti-radical capacity of extracts from *Pinus radiata* bark," *Industrial Crops and Products,* vol. 34, no. 1, pp. 838-844, 2011.

[64] Bikoro Bi Athomo, A., S.P. Engozogho Anris, R. Safou-Tchiama, F.J. Santiago-Medina, T. Cabaret, A. Pizzi, and B. Charrier, "Chemical composition of African mahogany (*K. ivorensis A. Chev*) extractive and tannin structures of the bark by MALDI-TOF," *Industrial Crops and Products,* vol. 113, pp. 167-78, 2018.

[65] Engozogho Anris, S.P., A.B. Bi Athomo, R. Safou Tchiama, F.J. Santiago-Medina, T. Cabaret, A. Pizzi, and B. Charrier, "The condensed tannins of Okoume (*Aucoumea klaineana* Pierre): A molecular structure and thermal stability study," *Scientific Reports,* vol. 10, no. 1, pp. 1-14, 2020.

[66] Karaseva, V., A. Bergeret, C. Lacoste, L. Ferry, and H. Fulcrand, "Influence of extraction conditions on chemical composition and thermal properties of chestnut wood extracts as tannin feedstock," *ACS Sustainable Chemistry & Engineering,* vol. 7, no. 20, pp. 17047-17054, 2019.

[67] Ramos, V., C. Bocalandro, S. Riquelme, V. Sanhueza, E. Aspé, M. Roeckel, and K. Fernández, "Effect of the bench scale extraction conditions on *Pinus radiata* bark extract yield, antioxidant properties and composition," *Maderas. Ciencia y tecnología,* vol. 15, no. 1, pp. 31-44, 2013.

[68] Murga, R., R. Ruiz, S. Beltrán, and J.L. Cabezas, "Extraction of natural complex phenols and tannins from grape seeds by using supercritical mixtures of carbon dioxide and alcohol," *Journal of Agricultural and Food Chemistry,* vol. 48, no. 8, pp. 3408-3412, 2000.

[69] Yesil-Celiktas, O., F. Otto, S. Gruener, and H. Parlar, "Determination of extractability of pine bark using supercritical CO_2 extraction and different solvents: optimization and prediction," *Journal of Agricultural and Food Chemistry,* vol. 57, no. 2, pp. 341-347, 2009.

[70] Braga, M.E.M., R.M.S. Santos, I.J. Seabra, R. Facanali, M.O.M. Marques, and H.C. de Sousa, "Fractioned SFE of antioxidants from maritime pine bark," *The Journal of Supercritical Fluids,* vol. 47, no. 1, pp. 37-48, 2008.

[71] Seabra, I.J., A.M.A. Dias, M.E.M. Braga, and H.C. De Sousa, "High pressure solvent extraction of maritime pine bark: Study of fractionation, solvent flow rate and solvent composition," *The Journal of Supercritical Fluids,* vol. 62, pp. 135-148, 2012.

[72] Conde, E., J. Hemming, A. Smeds, B.D. Reinoso, A. Moure, S. Willför, H. Domínguez, and J.C. Parajó, "Extraction of low-molar-mass phenolics and lipophilic compounds from *Pinus pinaster* wood with compressed CO_2," *The Journal of Supercritical Fluids,* vol. 81, pp. 193-199, 2013.

[73] Richter, B.E., B.A. Jones, J.L. Ezzell, N.L. Porter, N. Avdalovic, and C. Pohl, "Accelerated solvent extraction: A technique for sample preparation," *Analytical Chemistry,* vol. 68, no. 6, pp. 1033-1039, 1996.

[74] Ju, Z.Y. and L.R. Howard, "Effects of solvent and temperature on pressurized liquid extraction of anthocyanins and total phenolics from dried red grape skin," *Journal of Agricultural and Food Chemistry,* vol. 51, no. 18, pp. 5207-5213, 2003.

[75] Ferrentino, G., N. Haman, K. Morozova, G. Tonon, and M. Scampicchio, "Phenolic compounds extracted from spruce (*Picea abies*) by supercritical carbon dioxide as antimicrobial agents against gram-positive bacteria assessed by isothermal calorimetry," *Journal of Thermal Analysis and Calorimetry,* pp. 1-11, 2020.

[76] Liazid, A., M. Palma, J. Brigui, and C.G. Barroso, "Investigation on phenolic compounds stability during microwave-assisted extraction," *Journal of Chromatography A,* vol. 1140, no. 1-2, pp. 29-34, 2007.

[77] Garofulić, I.E., V. Dragović-Uzelac, A.R. Jambrak, and M. Jukić, "The effect of microwave assisted extraction on the isolation of anthocyanins and phenolic acids from sour cherry Marasca (*Prunus cerasus* var. Marasca)," *Journal of Food Engineering,* vol. 117, no. 4, pp. 437-442, 2013.

[78] Routray, W. and V. Orsat, "Microwave-assisted extraction of flavonoids: a review," *Food and Bioprocess Technology,* vol. 5, no. 2, pp. 409-424, 2012.

[79] Spigno, G. and D.M. De Faveri, "Microwave-assisted extraction of tea phenols: a phenomenological study," *Journal of Food Engineering,* vol. 93, no. 2, pp. 210-217, 2009.

[80] Pan, X., G. Niu, and H. Liu, "Microwave-assisted extraction of tea polyphenols and tea caffeine from green tea leaves," *Chemical Engineering and Processing: Process Intensification,* vol. 42, no. 2, pp. 129-133, 2003.

[81] Chupin, L., S.L. Maunu, S. Reynaud, A. Pizzi, B. Charrier, and F. Charrier-El Bouhtoury, "Microwave assisted extraction of maritime pine (*Pinus pinaster*) bark: Impact of particle size and characterization," *Industrial Crops and Products,* vol. 65, pp. 142-149, 2015.

[82] Mellouk, H., A. Meullemiestre, Z. Maache-Rezzoug, B. Bejjani, A. Dani, and S.-A. Rezzoug, "Valorization of industrial wastes from French maritime pine bark by solvent free microwave extraction of volatiles," *Journal of Cleaner Production,* vol. 112, pp. 4398-4405, 2016.

[83] Lazar, L., A.I. Talmaciu, I. Volf, and V.I. Popa, "Kinetic modeling of the ultrasound-assisted extraction of polyphenols from *Picea abies* bark," *Ultrasonics Sonochemistry,* vol. 32, pp. 191-197, 2016.

[84] Liu, M., J. Wang, K. Yang, Y. Qi, J. Zhang, M. Fan, and X. Wei, "Optimization of ultrasonic-assisted extraction of antioxidant tannin from young astringent persimmon (*Diospyros kaki* L.) using response surface methodology," *Journal of Food Processing and Preservation,* vol. 42, no. 7, 2018.

[85] Zhou, Z., Y. Huang, J. Liang, M. Ou, J. Chen, and G. Li, "Extraction, purification and anti-radiation activity of persimmon tannin from *Diospyros kaki* L.f.," *Journal of Environmental Radioactivity,* vol. 162-163, pp. 182-188, 2016.

[86] Toma, M., M. Vinatoru, L. Paniwnyk, and T.J. Mason, "Investigation of the effects of ultrasound on vegetal tissues during solvent extraction," *Ultrasonics Sonochemistry,* vol. 8, no. 2, pp. 137-142, 2001.

[87] Herrera, M.C. and M.D. Luque de Castro, "Ultrasound-assisted extraction for the analysis of phenolic compounds in strawberries," *Analytical and Bioanalytical Chemistry,* vol. 379, no. 7-8, pp. 1106-1112, 2004.

[88] Ghafoor, K., Y.H. Choi, J.Y. Jeon, and I.H. Jo, "Optimization of ultrasound-assisted extraction of phenolic compounds, antioxidants, and anthocyanins from grape (*Vitis vinifera*) seeds," *Journal of Agricultural and Food Chemistry,* vol. 57, no. 11, pp. 4988-4994, 2009.

[89] Proestos, C. and M. Komaitis, "Ultrasonically assisted extraction of phenolic compounds from aromatic plants: comparison with conventional extraction technics," *Journal of Food Quality,* vol. 29, no. 5, pp. 567-582, 2006.

[90] Meullemiestre, A., E. Petitcolas, Z. Maache-Rezzoug, F. Chemat, and S.A. Rezzoug, "Impact of ultrasound on solid–liquid extraction of phenolic compounds from maritime pine sawdust waste.

Kinetics, optimization and large scale experiments," *Ultrasonics Sonochemistry*, vol. 28, pp. 230-239, 2016.

[91] Liazid, A., M. Schwarz, R.M. Varela, M. Palma, D.A. Guillén, J. Brigui, F.A. Macías, and C.G. Barroso, "Evaluation of various extraction techniques for obtaining bioactive extracts from pine seeds," *Food and Bioproducts Processing*, vol. 88, no. 2-3, pp. 247-252, 2010.

[92] García-Marino, M., J.C. Rivas-Gonzalo, E. Ibáñez, and C. García-Moreno, "Recovery of catechins and proanthocyanidins from winery by-products using subcritical water extraction," *Analytica Chimica Acta*, vol. 563, no. 1-2, pp. 44-50, 2006.

[93] Ju, Z.Y. and L.R. Howard, "Subcritical water and sulfured water extraction of anthocyanins and other phenolics from dried red grape skin," *Journal of Food Science*, vol. 70, no. 4, pp. S270-S276, 2005.

[94] Panzella, L., F. Moccia, R. Nasti, S. Marzorati, L. Verotta, and A. Napolitano, "Bioactive phenolic compounds from agri-food wastes: An update on green and sustainable extraction methodologies," *Frontiers in Nutrition*, vol. 7, 2020.

[95] Ferreira-Santos, P., E. Zanuso, Z. Genisheva, C.M.R. Rocha, and J.A. Teixeira, "Green and sustainable valorization of bioactive phenolic compounds from *Pinus* by-products," *Molecules*, vol. 25, no. 12, p. 2931, 2020.

[96] Palma, G., J. Freer, and J. Baeza, "Removal of metal ions by modified *Pinus radiata* bark and tannins from water solutions," *Water Research*, vol. 37, no. 20, pp. 4974-4980, 2003.

[97] Singleton, V.L. and J.A. Rossi, "Colorimetry of total phenolics with phosphomolybdic-phosphotungstic acid reagents," *American journal of Enology and Viticulture*, vol. 16, pp. 144-158, 1965.

[98] Cicco, N. and V. Lattanzio, "The Influence of Initial Carbonate Concentration on the Folin-Ciocalteu Micro-Method for the Determination of Phenolics with Low Concentration in the Presence of Methanol: A Comparative Study of Real-Time Monitored Reactions," *American Journal of Analytical Chemistry*, vol. 2, pp. 840-848, 2011.

[99] Hoong, Y.B., M.T. Paridah, C.A. Luqman, M.P. Koh, and Y.F. Loh, "Fortification of sulfited tannin from the bark of *Acacia mangium* with phenol-formaldehyde for use as plywood adhesive," *Industrial Crops and Products*, vol. 30, no. 3, pp. 416-421, 2009.

[100] Bocalandro, C., V. Sanhueza, A.M. Gomez-Caravaca, J. Gonzalez-Alvarez, K. Fernandez, M. Roeckel, and M.T. Rodriguez-Estrada, "Comparison of the composition of *Pinus radiata* bark extracts obtained at bench- and pilot-scales," *Industrial Crops and Products*, vol. 38, pp. 21-26, 2012.

[101] Alonso-Amelot, M.E., A. Oliveros-Bastidas, and M.P. Calcagno-Pisarelli, "Phenolics and condensed tannins of high altitude *Pteridium arachnoideum* in relation to sunlight exposure, elevation, and rain regime," *Biochemical Systematics and Ecology*, vol. 35, no. 1, pp. 1-10, 2007.

[102] Ku, C.S., J.P. Jang, and S.P. Mun, "Exploitation of polyphenol-rich pine barks for potent antioxidant activity," *Journal of Wood Science*, vol. 53, no. 6, pp. 524-528, 2007.

CHAPTER III

PREPARATION AND CHARACTERIZATION OF TANNIN-ADSORBENTS

1. Literature review

Since tannins are water-soluble compounds, their use as adsorbents requires a conversion into insoluble solid matrices, which can be done by polymerization (autocondensation or cross-linking reaction) or by immobilization in solid supports. Different procedures have been successfully performed, under a few different sets of conditions, yielding different products here generally termed as tannin-adsorbents. Additionally, some authors went beyond that and further chemically modified the tannin-adsorbents to enhance adsorptive properties or to provide easier solid/liquid separations.

According to *Scopus* (keywords: "tannin" and "adsorbent", "tannin" and "adsorption"; accessed on May 19th, 2021), a collection of 178 scientific papers published between 2010 and 2021 about tannin-adsorbents was extracted. Those papers were organized in terms of tannin source-materials (Fig. III.1a) and adsorbates (Fig. III.1b). The procedure to prepare tannin-adsorbents most commonly involves a vegetable source-material, predominantly persimmon (*Diospyros*) waste [1, 2]. However, extracts from tree barks (or woods) are also frequently used, with trees from the *Acacia* (also named wattle or mimosa) and the *Myrica* (bayberry) genera being the most common ones. Moreover, oak, quebracho, and chestnut trees (*Quercus* spp., *Schinopsis* spp., and *Castanea* spp., respectively) were also used as tannin sources but far less commonly (Fig. III.1a). Finally, the use of a tannin solution prepared from tannic acid is a different approach reported by many authors.

Water remediation has been one of the research focuses of tannin-adsorbents, mainly to remove toxic heavy metals, such as chromium and lead, from contaminated waters (Fig. III.1b). Due to their commercial and industrial importance, some of those adsorbates are removed with the second purpose of being recovered and reused. Furthermore, the ability of tannin-adsorbents to uptake organic pollutants, such as dyes, pharmaceuticals, surfactants, and detergents, has also been assessed. Among these, dyes have received the most attention, with methylene blue (cationic dye) more commonly reported. On the other hand, recovery of valuable and precious metals (e.g., copper, gold, palladium), and, to a lesser extent, of rare earth metals, by tannin-adsorbents has been widely investigated. Of note, reports on the removal of toxic metalloids, such as arsenic and antimony, as well as other oxyanions (e.g., phosphate), are scarce or non-existent.

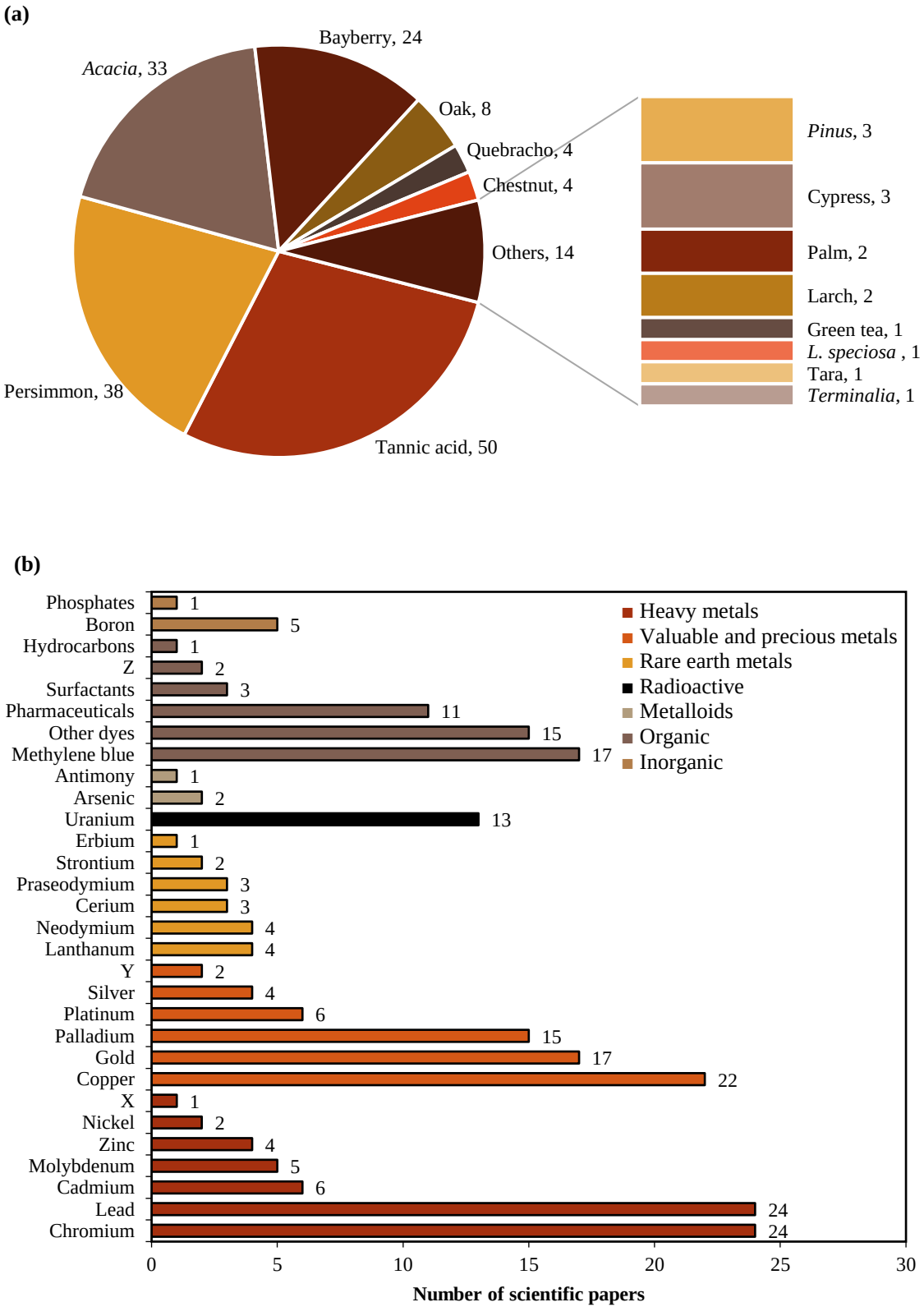

Fig. III.1 Number of scientific papers which report the production of tannin-adsorbents (a) from a specific source-material and (b) to uptake a specific adsorbate. Collection of 178 papers published between 2010 and 2021. X = aluminium, manganese, or vanadium; Y = mercury, germanium, indium, rhodium, or gallium; Z = detergents, caffeine, or toxins.

1.1. Tannin Resins

Insolubilization of tannins can be achieved through a step-growth polymerization reaction with formaldehyde (or other aldehyde) that can be either acid- or base-catalysed [3, 4]. Tannins reactivity towards aldehydes is explained by their high nucleophilic reactivity created by the hydroxyl groups linked to the aromatic rings, making these molecules undergo electrophilic aromatic substitutions [4]. In such reaction, an aldehyde compound establishes methylene bridge linkages between the tannin monomers at C8 or C6 reactive positions of the A-ring (Fig. II.1), depending on the tannin type [3, 4]. Thus, a tannin non-linear insoluble polymer, known as tannin resin or tannin gel, is synthesized, which can be directly employed as an adsorbent or still be subjected to further chemical modifications.

The experimental procedure in basic medium generally involves the dissolution of tannin extract in sodium hydroxide solution, addition of formaldehyde, polymerization reaction conducted at high temperature and, finally, washing, drying, and sieving. Successful insolubilization of tannins has been attained with formaldehyde amounts ranging from 0.2 mL to 2.0 mL per g of dried tannin extract, at 80 °C and for 3-18 h [5-28]. A summary of experimental conditions (NaOH solution concentration, amounts of alkaline solution and of crosslinking agent per amount of extract, and contact time) reported in the literature is presented in Table III.1. Usually, polymerization is conducted using dried tannin extracts, but the aqueous extract obtained from a vegetable material can be also directly used for formaldehyde crosslinking, skipping the evaporation/freeze-drying step. Fayemiwo et al. [29] followed this procedure and obtained successful polymerization in alkaline solution at 50 °C, for 1 h using 3 mL of formaldehyde per g of vegetable starting material (green tea leaves). Moreover, even though alkaline medium is more commonly yielded with sodium hydroxide, successful tannin polymerization has been also achieved in ammonia solutions [30-35].

Tannin-formaldehyde resins may be also obtained in media other than alkaline. For example, polymerization has been performed in acidic medium with HCl [36-41], with H_2SO_4 [42, 43], and with HNO_3 [44]. Moreover, some researchers have further improved the polymerization by employing a second crosslinking reaction, this time with glutaraldehyde in alkaline medium, obtaining a material that they identified as polytannin glutaraldehyde resin [45, 46].

Table III.1 Collection of operational parameters reported in the literature for polymerization reactions achieved in alkaline (NaOH) medium with an aldehyde as a crosslinking agent at 80 °C. Formaldehyde used was from a commercial solution (36-37 % wt).

Extract		NaOH solution		Crosslinking agent	Reaction time (h)	Ref.
Species	Tissue	C (mol L^{-1})	V (mL g^{-1})	V (mL g^{-1})		
Formaldehyde						
A. mearnsii	Bark	0.065	12.4	0.10	8	[7, 8]
A. mearnsii	Bark	0.065	12.4	0.37	8	[7, 8]
A. mearnsii	–	0.225	1.8	0.21	12	[13, 14]
A. mearnsii	–	0.250	1.9	0.30	12	[18]
A. mearnsii	–	0.250	1.6	0.21	12	[23-27]
A. nilotica	Leaves	0.065	8.9	0.29	12	[9]
C. sempervivens	Bark	0.065	12.4	0.37	8	[7, 8]
D. kaki	Feed material	0.225	3.9	0.39	12	[12]
D. kaki	–	0.250	1.8	0.21	12	[15]
D. kaki	Feed material	0.225	3.6	0.43	12	[17]
D. kaki	Waste	0.250	2.2	0.20	12	[19-21]
P. pinaster	Bark	0.065	12.4	0.10	8	[7, 8]
P. pinaster	Bark	0.065	12.4	0.37	8	[7, 8]
P. pinaster	Bark	0.065	12.4	0.40	8	[10]
R. apiculata	Bark	0.225	1.8	0.50	3	[16]
S. balansae	Bark	0.065	12.4	0.43	8[a]	[6]
S. balansae	Bark	0.065	12.4	0.10	8	[7, 8]
S. balansae	Bark	0.065	12.4	0.37	8	[7, 8]
S. balansae	Bark	0.065	12.4	0.40	8	[11]
S. balansae	–	0.250	0.5	2.00	8	[22]
Acetaldehyde						
A. mearnsii	Bark	0.065	12.4	0.06	8	[7, 8]
A. nilotica	Leaves	0.065	12.4	0.40	8	[9]
Formaldehyde and acetaldehyde						
A. nilotica	Leaves	0.065	5.6	0.44:0.44	16	[9]
A. nilotica	Leaves	0.065	5.6	0.55:0.55	18	[9]

a – 75 °C

Formaldehyde is commonly used because it provides faster reaction kinetics compared to other aldehydes [4], but polymerization has also been achieved in some cases with acetaldehyde [7-9, 37], glutaraldehyde [37, 47], or benzaldehyde [48]. Tannin resins may also be obtained in the absence of aldehydes, through self-condensation reaction between hydroxyl groups of polyphenols and/or polysaccharides, which commonly coexist in the extract or tannin-rich waste, a reaction catalysed by concentrated sulfuric acid at high temperature [49-57], a procedure that has been mostly explored for persimmon tannins.

Regardless of polymerization procedure, its optimization is important. The quantities of reagent and of catalyst, reaction time, and tannin source are important factors which influence polymerization yield as well as the chemical properties of the resulting resins. For example, Sánchez-Martín et al. [7] evaluated the impact of the formaldehyde amount added to the tannin solution, from four vegetable sources, and reported no polymerization in some cases. This is the result of either insufficient cross-linking agent amount or non-adequate tannin chemistry of the source used. Furthermore, the effect of resin preparation conditions on adsorption capacity should also be assessed. Indeed, Kamel et al. [46] reported differences in adsorption capacity caused by varying experimental conditions of the polymerization procedure.

The stability of tannin resins in aqueous solution is an important factor to make sure the solid is sufficiently insolubilized and an adsorbent should not leach its components to the water causing secondary pollution. This factor can be assessed by measuring dissolved organic carbon (DOC) in water after stirring with the solid at different pH. For example, Gurung et al. [49] compared DOC levels leached by the starting material (persimmon tannin powder) with DOC levels leached by the adsorbent (crosslinked persimmon tannin gel) in HCl solutions of concentrations up to 6.0 mol L^{-1}. The adsorbent was shown to be practically insoluble in strongly acidic solutions (HCl >0.5 mol L^{-1}) while the starting material generated DOC levels above 150 mg-C L^{-1}. However, the assessment of the stability of tannin resins is still uncommonly reported in the literature reviewed.

Tannin resins are characterized by negligible surface areas, ranging from 0.2 m^2 g^{-1} to 14 m^2 g^{-1}, and by nonporous texture [6-8, 10]. In fact, their potential as adsorbents lies on the chemical wealth of their surface. In addition to the phenolic groups, which abound in tannin resins, other functional groups may also be present in significant amounts, such as carboxylic groups, lactonic groups, and carbonyl groups [39, 40], thus tannin resins commonly present an acidic surface. On the other hand, the measurements of the zeta potentials at several pH values characterized the resins in terms of their surface charge. The results allowed to find out at which pH does the isoelectric point (IEP) occurs. The surface charge and the IEP are important parameters to predict and understand the influence of pH on adsorption. Most isoelectric points of tannin resins have been identified at very low pH values, roughly 2 [19-22, 35, 38] or below 3 [27, 28]. This confirms the anionic nature of the tannin resins surface, predicted by the high prevalence of phenolic groups, in a wide pH range and its ability to interact with positively charged adsorbates

by electrostatic attraction. In contrast, unless tannin resins are subjected to further chemical treatment, its electrostatic affinity for anions will be practically negligible.

1.2. Chemically Modified Tannin Resins

1.2.1. Introduction of Amino Groups

Compared to hydroxyls, amino groups have higher affinity and selectivity for soft metal ions, as the nitrogen atom is a stronger electron donor than oxygen. Thus, chemical modification of tannin resins has been performed by anchoring nitrogen containing functional groups on the adsorbent surface to improve its affinity to soft metal acids. Fig. III.2 presents schematically several ways to obtain amine-modified tannin resins.

The replacement of some –OH by $–NH_2$ groups in tannin resins, polymerized with formaldehyde in alkaline medium, can be achieved by reaction with ammonia at high temperature (60 °C) for 12 h [25-28]. Elemental analysis confirmed that the ammonia treatment introduced nitrogen groups into the resins: up to 3 % of nitrogen was identified in the ammonia-modified forms while the tannin source-material presents just 0.5 % of this element [25, 26]. The reaction with ammonia caused the zeta potential of the unmodified resin, at pH 3, to increase from -7.1 mV to 5.7 mV which means the isoelectric point of the adsorbent also increased [27].

Tertiary and quaternary-amine type tannin resins were obtained by the introduction of ligands after chloromethylation. This is achieved by heating the mixture of tannin resin with paraformaldehyde and concentrated HCl for several hours. Ligands such as NH_3 (ammonia) [58], *N*-aminoguanidine (AG) [17], bisthiourea (BTU) [53], tetraethylenepentamine (TEPA) [59], diethylamine (DEA) and triethylamine (TEA) [60], ethylenediamine (EDA) and methylamine (MA) [57], dimethylamine (DMA) [55], and 2,5-dimercapto-1,3,4-thiadiazole (DMTD) [61, 62] have been successfully anchored. Alternatively, amine ligands can also be successfully anchored by simultaneous chloromethylation and contact with ethylenediamine (EDA) [15]. DMA-modified resins, in a particular work, have been subjected to further treatment by contact with a solution containing methyl iodide, sodium iodide and sodium carbonate and the resulting product was termed quaternary amine persimmon tannin gel [63].

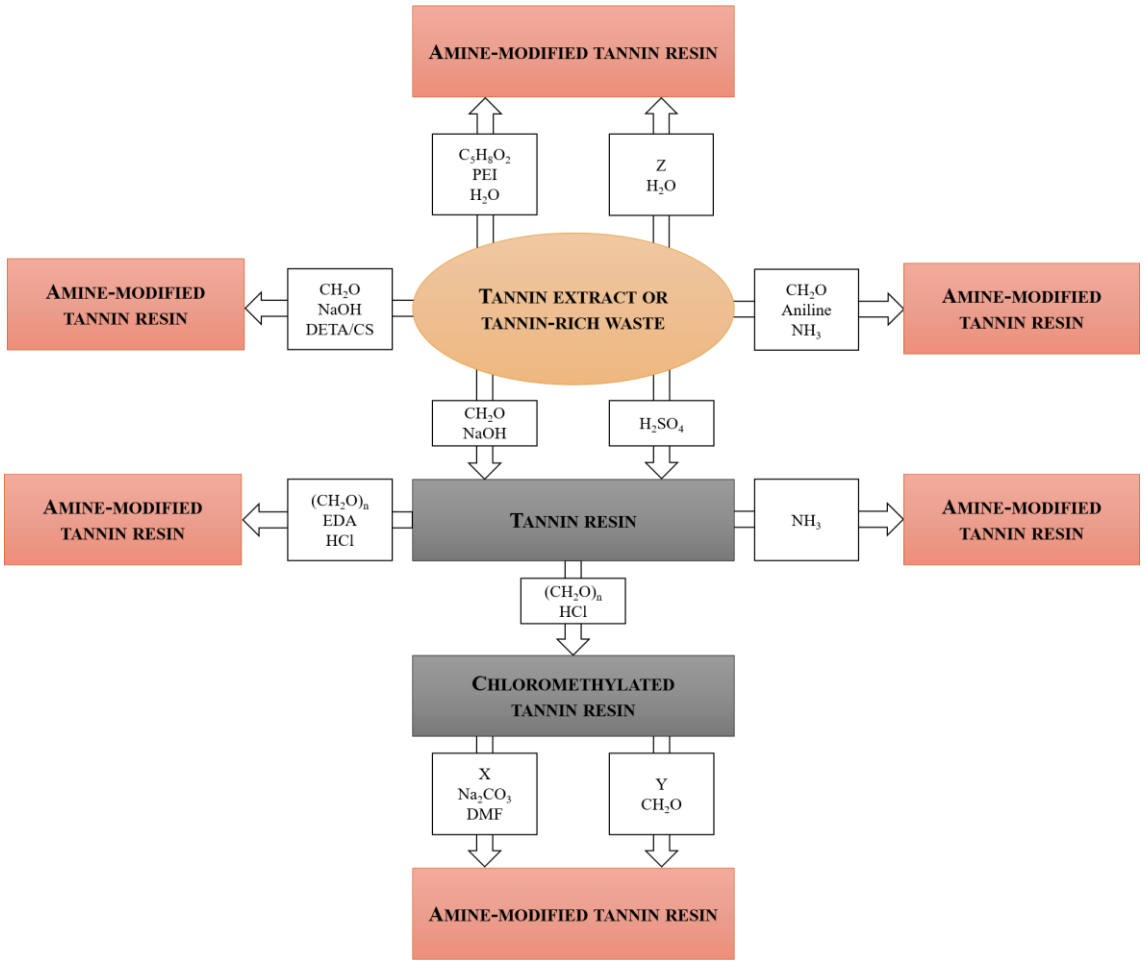

Fig. III.2 Schematization of the production methods for different types of amine-modified tannin resins. CH_2O – formaldehyde; $(CH_2O)_n$ – paraformaldehyde; $C_5H_8O_2$ – glutaraldehyde; PEI – polyethylene-imine; DETA – diethylenetriamine; CS – carbon disulphide; EDA – ethylenediamine; DMF – dimethyl-formamide; HA – hexamethylendiamine; X = BTU, AG or TEPA; Y = DMA, DEA or TEA; Z=PEI or HA.

Unmodified tannin resins usually present a negative charge in practically any pH (IEPs at pH 2-3, see Subsection 1.1). Shan et al. [60] reported a point of zero charge for TEA-modified tannin resin at pH 7.7, indicating that the amine-treatment led a positive charge in the adsorbent surface when pH is below 7.7. Moreover, the points of zero charge of EDA- and MA-modified resins, produced by Wang et al. [57], were also reported to be higher than most unmodified resins (6.1 and 6.3, respectively).

Bayberry tannin has been used to obtain diethylenetriamine (DETA) modified resins through the reaction between tannins, formaldehyde and carbon sulphide in an ammonia solution [64]. Measurements of zeta potentials at different pH have shown that IEP occurs close to pH 4, slightly lower than most amine-modified tannin resins. Patil-Shinde et al. [33] and Mulani et al. [34] produced tannin-aniline-formaldehyde resins by mixing commercial tannin powder with formaldehyde and aniline in a solution of ammonia.

Tannin resins enhanced with polyethyleneimine (PEI) have been yielded by submitting persimmon tannin powder to an aqueous solution containing glutaraldehyde and the amine compound [47]. The zeta potential of PEI-modified tannin resin at pH 7 was very high, almost 40 mV, corroborating other findings that showed an increase of isoelectric points by introducing amino groups into resins. Other synthesis procedures of tannin-polyethyleneimine adsorbents which eliminate the need of cross-linking agents, such as aldehydes, have been also recently proposed as more simple and eco-friendly alternatives [65, 66]. In a different approach, Liu et al. [67] proposed poly(tannin-hexamethylendiamine), which can be simply synthetized by stirring tannins with hexamethylendiamine (HA) under one-step reaction and mild conditions.

1.2.2. Iron-loading

Iron-based adsorbents have been capturing the interest of researchers, owing to their efficiency on contaminants' uptake, nontoxicity, and low cost, and natural abundance of iron. Iron materials are known to be suitable adsorbents for many metal oxyanions [68] and phosphates [69]. However, the difficulty to handle with very fine particles of iron oxides has dictated the exploitation of iron-based adsorbents, requiring the use of different support media, such as activated carbon [70], activated alumina [71], graphene oxide sheets [72], seaweeds [73], or cork granulates [74-77]. The incorporation of iron is expected to shift the point of zero charge of the adsorbent to higher values, facilitating electrostatic interaction between the adsorbent surface and anionic adsorbates, and provide specific adsorption sites. Tannin resins have also been loaded with iron, yielding an iron-loaded tannin resin, as has been reported by Ogata et al. [14] and Shilowa et al. [48].

Tannin resins, polymerized with formaldehyde in alkaline medium, were subjected to oxidation by nitric acid, followed by iron adsorption from a stirred Fe(III) solution. The results presented by Ogata et al. [14] showed the importance of performing the oxidation step with HNO_3, where hydroxyl groups of the tannin resins were partially oxidized to carbonyl ones, which have a higher affinity to adsorb iron. Moreover, the importance of optimizing the oxidation time and the nitric acid concentration, to avoid excessive oxidation and decomposition of the gel, was also demonstrated. Thus, iron was successfully loaded into tannin resins, achieving a content of ≈80 mg-Fe per g^{-1} after contact for 48 h with a 1 mol-Fe(III) L^{-1} solution, and this modification favoured phosphate adsorption.

In contrast, Shilowa et al. [48] submitted tannin resins yielded by polymerization with benzaldehyde in ammonia solution to iron-grafting, which involves introducing the resin to an ammonia solution containing Fe(II) and Fe(III). They named the resulting product an iron-doped tannin resin which was successfully applied for lead and nickel uptake from water, presenting adsorption capacities substantially higher than those of unmodified resins.

Overall, though, iron-loading of tannin resins for adsorption applications have been scarcely reported. Furthermore, loading of other metals, such as calcium, has yet to be investigated. Calcium could be a potentially better alternative to iron because, on the one hand, it is also low cost and it has affinity towards the same compounds and, on the other, it is more environmentally innocuous. Iron- or calcium-loaded tannin resins, if found to be efficient for phosphate uptake, could then be directly applied as a fertilizer. For example, Ogata et al. [14] proposed submitting their P-saturated iron-loaded adsorbent into soils as an alternative to elution for the recovery of phosphates.

1.2.3. Other Modifications

Xie et al. [20] employed an alkaline treatment (contact with 0.5 mol L^{-1} NaOH, 25 °C) to activate persimmon powder-formaldehyde resin. Infrared spectra showed that main functional groups remained practically unchanged after the modification, as well as the isoelectric point (pH ≈2). Nevertheless, results of textural properties seem to indicate that the alkaline treatment improved surface morphological features of the material, namely porosity and stability.

A black wattle tannin gel has been xanthated by Sun et al. [38] to enhance its performance for Cu(II) uptake. This modification was achieved by reacting the tannin gel with carbon disulphide in the presence of sodium hydroxide. Sulphur has a high affinity to most heavy metal ions, being able to efficiently form stable chelating complexes. Hence, the introduction of sulphur chelating moieties into the adsorbents is expected to considerably increase the adsorption capacity of metals. Elemental analysis confirmed the introduction of sulphurs into the adsorbent. In addition, zeta potential measurements revealed that the surface of the modified gel became more negatively charged than that of the unmodified one. The authors argued this difference contributed to improving copper adsorption by the xanthated tannin gel.

1.3. Composites

Immobilization of tannins in porous and solid materials has been another approach to overcome the solubility of tannins. A strong bond between tannins and the supporting matrix should be achieved to avoid leakage of tannin during the adsorption.

1.3.1. Immobilization Biomaterials

Several biomaterials have been used to immobilize tannins, such as collagen. This natural biomass is abundant (obtained from skins of domestic animals), exhibits excellent mechanical strength and has several functional groups that can react with many other chemicals, tannins included. In addition to creating a water-insoluble matrix, the process gives unique fibrous structure and hydrophilicity properties to the adsorbent [78]. Tannins from barks of *Myrica* genus trees (bayberry) [78-85], commercial persimmon tannin powder [86-88] and black wattle tannins [89, 90] have been immobilized onto collagen. Tannins are usually first mixed with collagen or collagen fibres, allowing interactions based on hydrogen bonds and hydrophobic associations, and are further covalently immobilized by a crosslinking agent, typically oxazolidine [78-83, 89, 90] or glutaraldehyde [84, 86-88].

An immobilization biomaterial alternative to collagen is cellulose, with which tannin-adsorbents have been produced. For example, Xu et al. [91] proposed the immobilization of black wattle tannin onto dialdehyde nanocellulose, previously obtained by oxidation of nanocrystalline cellulose. The authors argued that the use of dialdehyde nanocellulose, which acts as both the matrix and crosslinker, makes the preparation route greener, as it avoids the use of additional crosslinking agents, such as oxazolidine and glutaraldehyde. Recent studies have been focused on tannin immobilization on regenerated cellulose, under the form of microspheres [92-94], hydrogels [95, 96] and aerogels [97], which were produced by homogeneous reaction. Later, the immobilization of tannins on microfibrillated cellulose was proposed, using glutaraldehyde as immobilization agent [98]. The reactions taking place involve tannin immobilization on cellulose and self-crosslinking of cellulose and tannins. The resultant material exhibited an entangled network structure, which is probably advantageous for adsorption, and a negative zeta potential in the pH range 2-10 [92].

Others immobilization biomaterials include chitosan [99-105], gelatine [106-108], and alginates [109, 110]. Persimmon and bayberry tannins have been frequently anchored in chitosan by a cross-linking reaction with glutaraldehyde in water or ethylic acid solution. Alternatively, tannin-chitosan adsorbents can also be produced by reacting tannic acid with chitosan [103]. Literature has shown these adsorbents to be efficient towards heavy and precious metals, rare earth elements, as well as some dyes. On the other hand, bayberry tannins were successfully fixed onto electrospun fibres of poly vinyl alcohol (PVA) in gelatine [106, 107]. The resulting adsorbents seem to have affinity towards uranyl ions even at trace levels. Moreover, there are reports of the use of alginate microspheres to synthesise tannin-adsorbents. Finally, tannins have also been successfully immobilized on corn starch [111] and jute fibre [112] and the resulting tannin-adsorbents were evaluated for recovery of gold and for removal of colour from textile effluents, respectively.

1.3.2. Mesoporous Silica

Mesoporous silica has also been proposed in literature as a supporting matrix for tannins immobilization [113-117]. Mesoporous silicate materials, besides presenting a high surface area, show excellent swelling resistance in different solvents and a good mechanical, thermal and chemical stability.

Tannins extracted from bayberry tree barks have been successfully immobilized in silica beads [113, 114]. Silica beads were aminated and were subsequently mixed with tannins and glutaraldehyde (cross-linking agent), which reacts with the amino group of mesoporous matrix establishing covalent bonds [114]. Binaeian et al. [115] used a similar procedure but with oak gall tannins and hexagonal mesoporous silicate.

Other researchers [116] prepared hybrid materials by mixing mimosa (*Acacia*) tannins with APTES (3-aminopropyltriethoxysilane). Textural characterization of the solid showed that tannin was efficiently encapsulated, probably through covalent bond between the silyl derivative and the hydroxyl groups of the tannin. Moreover, Huang et al. [117] anchored simultaneously tannins and polyethyleneimine in alkaline medium, yielding a tannin-adsorbent in the absence of aldehydes.

1.3.3. Carbon-based Materials

Composites of tannins and carbon-based materials have also been proposed as adsorbents. For example, Luzardo et al. [36] prepared composites of carbon nanotubes and formaldehyde resins prepared from resorcinol mimosa (*Acacia*) tannins. On the other hand, Wang et al. [118], [119] and Zhang et al. [120] mixed persimmon tannin powder with a dispersion of graphene oxide and further reacted with glutaraldehyde, producing persimmon tannin/graphene oxide (PT/GO) composites. Functionalization of tannin with graphene oxide was then achieved by the phenolic condensation reactions, π–π interaction, and hydrogen bonding (between hydroxyl group of persimmon tannin and graphene oxide). The resultant material was reported to have a good stability in strong acidic solution (50 % HCl) [118].

Furthermore, some authors were able to produce tannin-adsorbents of this kind in the absence of aldehydes by mixing tannic acid (TA) with graphene oxide (GO), yielding a TA-GO nanocomposites [121] or aerogels [122]. Finally, tannin-based carbon-iron oxide nanocomposites have been produced and applied for arsenic uptake from water [123]. This material was obtained after adding quebracho tannins to an iron chloride solution, collecting and drying the filtrate and submitting it to pyrolysis.

1.3.4. Magnetic Nanostructured Materials

Attention has been recently focused on tannins immobilization in magnetic nanostructured materials to improve solid/liquid separation and recycling properties of the adsorbents. The magnetism is afforded by a magnetic iron oxide core. A silica shell protects the magnetic core and provides ease of functionalization, physical/chemical stability, and biocompatibility.

Gao et al. [124], [125] prepared magnetic graphene oxide decorated with persimmon tannin (Fe_3O_4/PT/GO) nanocomposites, which presented good magnetic properties under the action of an external magnetic field, before and after being used as an adsorbent. Additionally, Fan et al. [126] proposed magnetic microspheres obtained by amino modification with 3-aminopropyl triethylsilane of Fe_3O_4@SiO_2 nanoparticles, followed by the grafting of persimmon tannin through the crosslinking with glutaraldehyde, between C6

of A-rings and the amino group of the particles. The resultant material is referred to be stable, and no iron was detected in acid solutions.

Tannic acid has also been used to prepare magnetic tannin-adsorbents. Luo et al. [127] immobilized tannins from tannic acid in Fe_3O_4 nanoparticles and the resulting adsorbent was shown to be effective to uptake lead and mercury. Generally, zeta potentials of the modified iron nanoparticles were lower across the pH range studied, and the isoelectric point dropped from ≈5 to ≈3. A similar approach was assessed by Wang et al. [128], functionalizing nickel-iron nanoparticles with tannic acid. At pH 3-5, adsorption capacities of the tannin-adsorbent were between twice and thrice as much as that of the unmodified nickel-iron nanoparticles, confirming the beneficial effect of tannins on lead adsorption. Qian et al. [129] endeavoured in a more complex approach to yield a tannin-adsorbent efficient for cationic dye uptake. The procedure consists of synthesising tannic acid-iron oxide nanoparticles and subsequently coating them, first with polyethyleneimine and, second with titanium oxide nanoparticles.

The work conducted by Huang et al. [130] opens doors to the research in tannin-based magnetic porous organic polymers. Tannin acid was chemically linked by 4,4′-diaminobiphenyl through azo-coupling reactions, without sacrificing phenolic –OH groups, to form a porous structure. The Fe_3O_4@SiO_2 magnetic nanoparticles were integrated into the porous structure during the polymerization. The values of magnetic saturation of these materials can be easily tailored by altering the number of magnetic nanoparticles.

1.4. Tannin Rigid Foams

Tannin rigid foams are known for a long time, but their possible application as another type of tannin-adsorbent was only recently exploited [131-135]. The procedure of preparation of tannin foams consists of three of steps: mixing of reagents, the expansion step catalysed by a strong acid, and finally, a curing (aging) step to harden and stabilize the network [131]. Optimization of the variables involved in the process can be performed to reduce the cost of the synthesis. Sánchez-Martín et al. [132] optimized the amounts of reagents involved in the foaming process of mimosa (*Acacia*) tannin foams, considering the resultant sorption properties of the biosorbent. Tannin foams, such as tannin resins, usually present a very low surface area.

Pine tannins, on the other side, are known to have a very high reactivity with formaldehyde under acidic conditions [133], causing significant difficulties in the foaming process. The preparation of pine tannin foams was however made possible by Lacoste et al. [133], [134], which were later evaluated as adsorbents for chromium [135]. A different approach was taken by Issaoui et al. [136] who produced a phenolic foam based on *Acacia* condensed tannins, oak and chestnut hydrolysable tannins, and *P. pinaster* lignins, yielding an adsorbent efficient for heavy metals, such as lead and copper.

2. Methodology

The polymerization procedure selected for this work was based on the cross-linking reaction between tannins and formaldehyde, which results in a tannin resin, due to its simplicity and low cost. The local availability of pine bark and the chemical properties of its phenolic content, together with the scarcity of studies about pine bark tannin-adsorbents, justify the decision to use this biomass as a tannin source-material. According to the literature review, the potential of metal-loaded tannin resins has not been sufficiently assessed. Thus, the resins here produced were loaded with iron and calcium to evaluate the resulting materials as adsorbents.

2.1. Polymerization

The tannin-adsorbent produced in this work was a tannin resin yielded by polymerization through a reaction with formaldehyde in basic medium, following a procedure adapted from Sánchez-Martín et al. [7] and Xie et al. [19]. The tannin extract, obtained either by evaporation or freeze-drying (Chapter II), was dissolved in a 0.25 mol L^{-1} NaOH solution at room temperature, followed by the addition of formaldehyde (36 % wt, analytical grade, *Labsolve*) to function as a crosslinking reagent. After polymerization at 80 °C for 8 h, the precipitate was dried at 65 °C, milled, washed successively with 0.05 mol L^{-1} HNO_3 solution and distilled water to remove unreacted substances. Finally, the obtained solid was once more dried at 65 °C. The resultant product was considered the tannin resin (Fig. III.3), abbreviated as TR or TRp if the extract used was freeze-dried or precipitated, respectively. This resin either was directly applied as an adsorbent or was subjected to chemical modifications before adsorption application.

To optimize the polymerization reaction, the effect of two experimental conditions was studied at different levels: (1) the volume of NaOH solution (studied in the range of 4-12 mL per gram of extract); and (2) formaldehyde amount (studied in the range of 0.05-0.80 mL per gram of extract). These ranges of values were chosen based on literature (Table III.1). The influence of temperature and contact time on yield was not assessed since most of the authors report using the values chosen here (80 °C and 8 h, Table III.1). The polymerization yield (denoted as η_P), defined as the ratio between the mass of polymer-

ized product and the mass of dissolved extract, was considered the response to be maximized. The optimal conditions were used to produce resins to be tested as an adsorbent and to be also subjected to oxidation and iron-loading.

Fig. III.3 Tannin resin (TR).

2.2. Iron-loading

The iron-loading procedure was based on Ogata et al. [14], involving an oxidation step before the contact with the iron solution. The authors have optimized an iron-loading procedure for a wattle tannin resin considering oxidation time and nitric acid concentration as variables. A similar procedure was optimized to load iron into resins made by pine tannins in the present work. Considering the conclusions of the researchers, which point to better results with shorter reaction times and lower acid concentrations, the oxidation periods tested were limited to 120 min and the highest HNO_3 concentration considered was 2 mol L^{-1}. Additionally, temperature was considered a variable due to the expected influence on the oxidation degree, its importance for the energy requirements of the process, and the subsequent cost of the adsorbent. The following oxidation step variables were studied: nitric acid concentration (1 mol L^{-1} and 2 mol L^{-1}), temperature (40 ºC, 50 ºC, and 60 ºC), and time of oxidation (15-120 minutes).

One gram of TR was added to 100 mL of nitric acid solution, representing a solid:liquid ratio of 10 g L^{-1}, and the mixture was kept stirring in a heating plaque/magnetic stirrer with automatic temperature control (*Velp Scientifica* Arex Digital Pro) at the desired temperature and for the desired time. Next, the solid was washed with water to remove the

remaining HNO_3 from the particles and dried in an oven at 65 ºC. The resultant product was considered the oxidized tannin resin (TRO).

Iron-loading was carried out by adding 0.5 g of TRO to 100 mL of a 200 mg L^{-1} Fe(III) solution, representing a solid:liquid ratio of 5 g L^{-1}, prepared from ferric chloride ($FeCl_3 \cdot 6H_2O$), at initial pH 2 (adjusted with HNO_3). The mixture was kept under stirring in an orbital shaker (*Biosan* PSU-10i) at room temperature for 24 h, followed by washing the solid with water to remove unreacted species. Finally, the solid was dried in an oven at 65 ºC. The resultant product was considered the iron-loaded oxidized tannin resin (TRO-Fe). The non-oxidized resin was also subjected to the same iron treatment, to prove the positive effect of oxidation on iron uptake, yielding an iron-loaded tannin resin (TR-Fe).

The oxidation conditions that yielded the best results both in terms of mass loss (after contact with nitric acid solution) and iron content (after contact with Fe(III) solution) were considered optimal. Subsequently, the concentration of the iron solution was varied between 50 mg-Fe L^{-1} and 2000 mg-Fe L^{-1} to define the optimal value for iron uptake. Iron-loaded tannin resin was then produced in the optimal conditions found and used in the adsorption assays. The resin was separated by particle size and the fractions <0.15 mm and 0.15-0.50 mm were selected, which represent 17 % and 61 % of total sample weight, respectively.

Iron content of the metal-loaded resins, expressed as mg of iron per g of solid, was determined by digesting 0.25 g of resin in glass tubes at 150 ºC for 2 h with 5.0 mL of distilled water, 12.0 mL of HCl and 4.0 mL of HNO_3 (concentrated acids, 37 % wt and 65 % wt, respectively) [137], which were placed in a heating digester (*Velp Scientifica* DK6). Samples were digested in duplicate, and a blank digestion was also performed. After digestion, solutions were filtered through cellulose acetate membrane filters (0.45 µm porosity). Iron content of samples, before and after particle size separation, were determined. Iron concentrations were measured by atomic absorption spectrometry (AAS) in air-acetylene flame (*GBC* 932 Plus spectrometer), using a single-element cathode lamp and the following instrumental conditions: wavelength of 248.3 nm, slit width of 0.2 nm, and three replicates. Calibration curves were obtained and accepted for a determination coefficient (R^2) higher than 0.995.

2.3. Calcium-loading

As mentioned in Subsection 1.2.2, calcium-loading of tannin resins has never been assessed. In addition, several calcium-loaded adsorbents have been reported in the literature as being efficient towards phosphate. Thus, the potential of a calcium-loaded tannin resin for phosphate uptake was here evaluated, with the subsequent goal of directly applying the adsorbent loaded with calcium and phosphate as a fertilizer.

Calcium-loading was carried out adding 0.25 g of TR or TRO (obtained in optimized conditions for iron-loading) to 50 mL of a Ca solution, representing a solid:liquid ratio of 5.0 g L^{-1}, with concentrations ranging from 10 mg-Ca L^{-1} to 1500 mg-Ca L^{-1} prepared from calcium chloride ($CaCl_2 \cdot 2H_2O$), at initial pH 6. The mixture was kept under stirring in an orbital shaker (*Biosan* PSU-10i) at room temperature for 24 h, followed by washing the solid with distilled water to remove unreacted species. Finally, the solid was dried in an oven at 50 ºC. The resultant products were considered the calcium-loaded tannin resin (TR-Ca) and the calcium-loaded oxidized tannin resin (TRO-Ca).

Calcium content of resins, expressed as mg of calcium per g of solid resin, was determined following the acid digestion procedure used for iron content determination. Calcium content was also estimated by mass balance, measuring calcium concentrations of the solution prior and after contact with resins. Calcium concentrations were measured by AAS in air-acetylene flame (*GBC* 932 Plus spectrometer), using a single-element cathode lamp and the following instrumental conditions: wavelength of 422.7 nm, slit width of 0.5 nm, and three replicates. Calibration curves were obtained and accepted for a determination coefficient (R^2) higher than 0.995.

2.4. Characterization of Tannin Resins

Infrared spectra of tannin extracts and tannin resins were obtained by FTIR (Fourier Transform Infrared Spectroscopy) in a *Shimadzu* IRAffinity spectrometer, with a wavenumber range from 400 cm^{-1} to 4000 cm^{-1}, through 50 scans and with a resolution of 8.0 cm^{-1}.

Scanning Electron Microscopy (SEM) and Energy Dispersion Spectroscopy (EDS) were used to obtain images and chemical composition of tannin resins. The SEM/EDS assay

was performed at CEMUP-LMEV (Materials Centre of the University of Porto, Laboratory for Scanning Electron Microscopy and X-Ray Microanalysis) using a high resolution (Schottky) Environmental Scanning Electron Microscope with X-Ray Microanalysis and Electron Backscattered Diffraction analysis: *Quanta* 400 FEG ESEM/EDAX Genesis X4M. Samples were coated with a gold/palladium thin film, by sputtering, using the SPI Module Sputter Coater equipment.

Granulometric distribution of resins was determined by laser diffraction spectroscopy (*Coulter* LS 230) using water as the dispersion medium.

The zeta potentials of TR, TRO, and TRO-Fe at different pH values (ranging from 2 to 8) were determined in NaCl 0.001 mol L^{-1} suspensions, prepared with a solid:liquid ratio of 0.5 g L^{-1}, and using an electrophoresis instrument *Malvern* Zetaziser Nano ZS90. The sample was put in a folded capillary Zeta cell, and the measurement of the zeta potential was carried out at 25 °C. The analysis was performed in triplicate for each sample, and the data is expressed as average ± standard deviation.

The dissolved organic carbon (DOC) values represent the organic matter leaching and thus indicate the resin stability. Moreover, in the case of iron-loaded resins, iron leaching is also an indicator of resin stability. With that in mind, the following stability assay was carried out. TR, TRO, and TRO-Fe were individually submitted to distilled water solutions at different pH (in the range 2-9, adjusted by small additions of NaOH or HCl solutions) with a solid:liquid ratio of 2.0 g L^{-1} and the mixture was kept under agitation for 24 h. DOC values of the samples were measured by catalytic oxidation at 680 °C, in a *Shimadzu* TOC-L CSH analyser. Iron concentrations in solution after contact with TRO-Fe were determined as described in section 2.2.

Moreover, an assay to evaluate the stability of TR (range of particle sizes: 0.15-0.50 mm) in terms of DOC and colour leaching, was undertaken by adding a resin sample in distilled water at a certain pH within the range 2-7 with a solid:liquid ratio of 0.5 g L^{-1} for 24 h at 20 °C. After filtration (cellulose membrane filters,0.45 µm porosity), colour of the liquid phase was determined by absorbance measurement at 400 nm by a spectrophotometer (*Thermo Scientific* Genesys 10S UV-Vis), according to a standard procedure [138], and results were expressed in Hazen units (HU).

2.5. Adsorbate/Adsorbent Screening

2.5.1. Adsorption Batch Assays

Preliminary adsorption assays were done to assess the affinity of each produced resin towards arsenic, antimony, and phosphate. Some resins were however not submitted to adsorption assays, such as TR-Fe due to its low iron content. Experimental conditions of these assays are presented in Table III.2. Adsorption experiments were carried out by adding a certain mass of resin to a certain volume of adsorbate solution with the desired initial concentration and suspensions were kept at constant pH and stirring for 20-24 h at 20 °C. After that, solutions were filtered through cellulose acetate membrane filters (0.45 µm porosity) and adsorbate concentration in the liquid phase was measured. The amount of adsorbate adsorbed per gram of adsorbent (q_{eq}) was calculated by Eq. III.1, where C_{in} and C_{eq} are the initial and equilibrium adsorbate concentrations, respectively, and S/L is the solid:liquid ratio.

$$q_{eq} = \frac{(C_{in} - C_{eq})}{S/L} \qquad \textbf{Eq. III.1}$$

Table III.2 Experimental conditions of preliminary adsorption assays (T = 20 °C, t = 20-24h).

Adsorbent	C_{in} (mg L^{-1})	pH	S/L (g L^{-1})
Arsenic – As(III) or As(V)			
TR [a]	5	4	10
TRO [a]	5	4	10
TRO-Fe [a]	5	4	10
TR-Ca [b]	0.5	4	10
Antimony – Sb(III) or Sb(V)			
TR [b]	20	4	0.5
TRO [b]	20	4	0.5
TRO-Fe [b]	20	4	0.5
Phosphate – PO_4			
TR-Ca [b]	5	2-7	10
TRO [b]	5	4	10
TRO-Ca [b]	5	4	10
TRO-Fe 0 [b]	5	2, 4, 7	10

a – without granulometric separation; b – 0.15-0.50 mm.

2.5.2. Adsorbates Solutions

As(III) and As(V) solutions were prepared by diluting lab-made standards prepared with As_2O_3 (1000±10 mg-As L^{-1}, 2-5 % HCl) and with $HAsNa_2O_4{\cdot}7H_2O$ (994±10 mg-As L^{-1}, 2 % HCl), respectively. Sb(III) solutions were prepared by dilution of a commercial standard solution, containing 1000 mg-Sb L^{-1} in a tartaric acid matrix (*SCP Science*, 1 % tartaric acid). Sb(V) solutions were prepared from dissolution of potassium hexahydroxo-antimonate(V) salt (analytical grade). Phosphate solutions were prepared by dissolution of potassium dihydrogen phosphate (KH_2PO_4, for analysis, *Sigma-Aldrich*) in distilled water.

2.5.3. Analytical Methods

Arsenic concentrations were measured by atomic absorption spectrometry (AAS) with electrothermal atomization in a graphite furnace (*GBC* GF 3000 SenAA Dual spectrometer), using a single-element cathode lamp and the following instrumental conditions: wavelength of 197.3 nm, slit width of 1.0 nm, lamp currents of 5 mA, and four replicates. Antimony concentrations were measured by AAS in air-acetylene flame (*GBC* 932 Plus spectrometer) or with electrothermal atomization in a graphite furnace (*GBC* GF 3000 SenAA Dual spectrometer), using a single-element cathode lamp and the following instrumental conditions: wavelength of 217.6 nm, slit width of 0.2 nm, lamp current of 10 mA, and three replicates. In the cases of TRO-Fe, iron leaching was evaluated through iron concentrations measurement by AAS (as described in Subsection 2.2 of this Chapter). Calibration curves were obtained and accepted for a determination coefficient (R^2) higher than 0.995. Dissolved phosphate in solutions was determined by the colorimetric ascorbic acid method (Standard Methods 4500-P E [139]), with a working range of 0.05-0.75 mg-P L^{-1}.

3. Results and Discussion

3.1. Polymerization

Tannin resins were obtained through polymerization of extracts in alkaline medium and using formaldehyde as a cross-linking agent. Two tannin extracts were used: (1) precipitated tannin extract, obtained by evaporation of the extract solution (Chapter II, Section 2.2); and (2) freeze-dried extract, obtained in the optimized conditions determined in Section 3.2 of Chapter II. In Fig. III.4, the results of the influence by solvent and catalyst amounts (expressed per gram of precipitated tannin extract) on the polymerization yield (η_P) are presented. As shown (Fig. III.4b), an increase in the amount of formaldehyde added to the reaction generally increases the polymerization yield. Such behaviour was somewhat predictable since formaldehyde is the crosslinking reagent of the reaction. Using 4.0 mL of NaOH 0.25 mol L^{-1} solution per g of extract, yield consistently increased until reaching a maximum for 0.80 mL of formaldehyde per g of extract (Fig. III.4b). Alternatively, using 6.0 mL of NaOH 0.25 mol L^{-1} per g of extract the yield increased until a maximum of 0.40 mL g^{-1}, evening out above that value. This indicates that amount of formaldehyde (0.40 mL per gram of extract) is enough to react with total dissolved tannins. To achieve the best yield and, simultaneously, to use the minimum amount of formaldehyde, it was decided that the best conditions, within those assessed in this assay, are 6.0 mL of NaOH 0.25 mol L^{-1} and 0.40 mL of formaldehyde per g of extract.

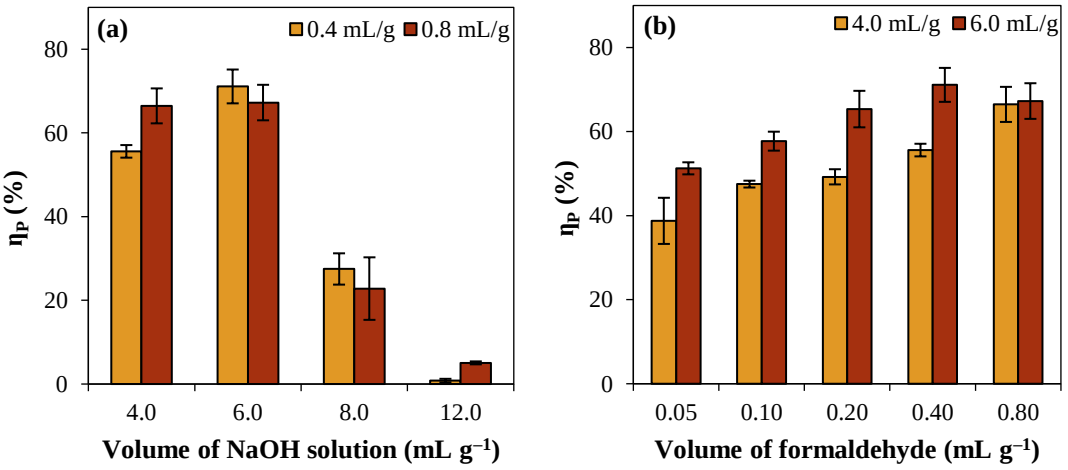

Fig. III.4 Influence on polymerization yield of precipitated extracts, by: (a) the volume of sodium hydroxide solution, at different formaldehyde amounts; (b) the amount of formaldehyde used in the reaction, at different volumes of NaOH solution. Assays were done in triplicate and error bars represent maximum absolute deviations from the average.

Additionally, higher amounts of NaOH solution, given fixed amounts of formaldehyde (0.4 mL g^{-1} and 0.8 mL g^{-1}), were tested (Fig. III.4a). Although yield may initially increase with the amount of NaOH solution, it decreases rapidly, independently of the amount of formaldehyde used, as can be observed in Fig. III.4a. This can be explained by the higher amount of solvent that keeps tannins dissolved, decreasing the driving force to polymerization. Then, it was considered that 6.0 mL of NaOH 0.25 mol L^{-1} solution per g of extract was the optimal volume for a given amount of formaldehyde, upholding the conclusion of the formaldehyde assay. At optimal conditions — 6.0 mL NaOH 0.25 mol L^{-1} and 0.4 mL formaldehyde (36 % solution) per g of precipitated tannin extract — polymerization yield was 71±4 %.

The polymerization yield was also studied under different conditions of NaOH and formaldehyde amounts using the freeze-dried tannin extract and the results are presented in Fig. III.5. The freeze-dried extract was unmistakeably easier to dissolve than the precipitated extract, presenting thus a practical advantage over the evaporation method. The amount of NaOH solution, in the range studied, did not affect polymerization yield (Fig. III.5a). However, it was observed that the extract was easier to dissolve with 4 mL of NaOH than with 2 mL of NaOH per g of extract. For that practical reason, 4 mL of NaOH 0.25 mol L^{-1} solution per g of extract was chosen for the formaldehyde assay. In Fig. III.5b, a trend is evident: increasing the amount of formaldehyde increases the polymerization yield, reaching a plateau at 0.2 mL of formaldehyde per g of extract. Hence, that amount was determined to be the optimal for the fixed amount of NaOH solution used.

The expected polymerization yield, using those amounts of solvent and reagent (4.0 mL NaOH 0.25 mol L^{-1} and 0.2 mL formaldehyde (36 % solution) per g of freeze-dried tannin extract), is ≈80 %. This is an improvement in relation to the precipitated extract, for which higher amounts of solvent and catalyst lead to lower polymerization yields. Therefore, the freeze-dried extract was shown to be better fitted for this work.

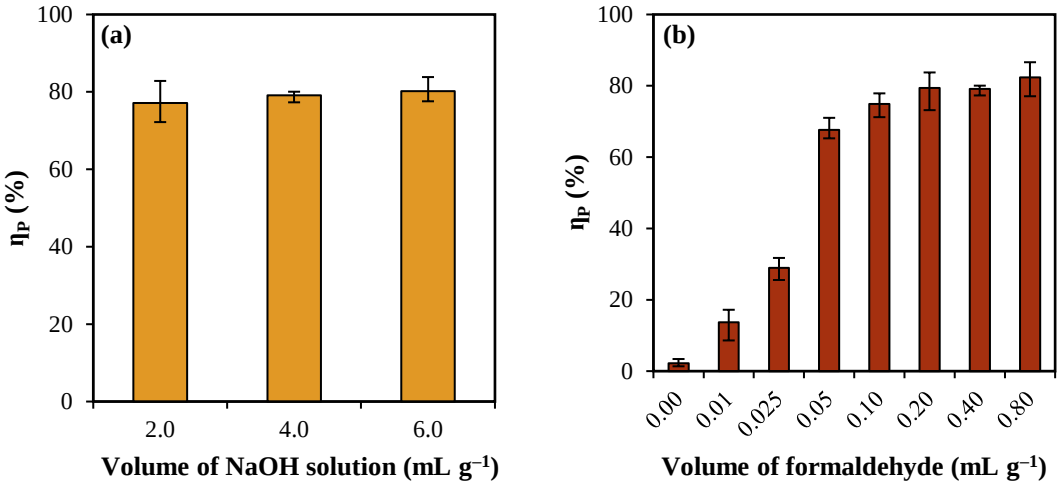

Fig. III.5 Influence on polymerization yield of freeze-dried extracts, by: (a) the volume of sodium hydroxide solution, using 0.4 mL of formaldehyde per g of extract; (b) the amount of formaldehyde used in the reaction, with 4 mL of NaOH 0.25 mol L^{-1} per g of extract. Assays were done in triplicate and error bars represent maximum absolute deviations from the average.

3.2. Iron-loading

Fig. III.6 presents the influence of oxidation variables on the amount of iron loaded into oxidized tannin resins. Oxidation with HNO_3 2 mol L^{-1} at 60 °C (evaluated for oxidation times of 15 and 30 min) yielded resins with the highest iron uptake capacities (Fig. III.6a). However, even with just 15 min of contact time, the resin was visibly different suggesting its polymerization state may be compromised. The higher colour leaching during the iron-loading assays with those resin samples corroborates such observation. After 60 min of contact, the mass loss observed after oxidation was too high (27±5 %) and, thus, the resin oxidized in those conditions was not subjected to iron-loading. Similarly, oxidation with this acid concentration was not attempted for 90 min since mass losses were expected to be also too high. With the same acid concentration and at 40 °C, the iron uptake was considerably lower even when prolonging the contact time until 90 min.

On the other hand, oxidation with HNO_3 1 mol L^{-1} at 40 °C granted the resin an even lower uptake capacity. On the other hand, oxidation at 60 °C for 90 min of contact time caused high mass losses (37±13 %) and the yielded resin was not subjected to iron-loading as well as a contact time of 120 min at this temperature was not assessed. Such results suggest that oxidation at these conditions (HNO_3 1 mol L^{-1} at 40 °C for any contact time or at 60 °C for contact times higher than 60 min) are suboptimal (Fig. III.6b). At that acid

concentration, every other set of conditions caused very little mass loss (≤7 %) and, generally, increasing the contact time as well as the temperature led to higher iron uptake. The optimal results, in terms of iron content and mass losses, were obtained with a resin oxidized with a solution of HNO_3 1 mol L^{-1} at 50 °C for 90 min.

TR was also subjected to iron-loading under the same experimental conditions. Iron-loading of TR yielded a low metal content (8.0±0.2 mg-Fe g^{-1}) in comparison to most TRO materials, which achieved iron contents up to three times higher. This is similar to what Ogata et al. [14] reported and, thus, the importance of the oxidation step was confirmed.

After finding the optimal oxidation conditions, the initial iron concentration was varied to assess its influence on iron uptake and find an optimal value, and the results are presented in Fig. III.7. Clearly, iron uptake increases with increasing initial metal concentration but only until ≈1250 mg-Fe L^{-1}, after which iron content in the solid does not increase much farther than 20 mg g^{-1}. Consequently, TRO-Fe samples used in adsorption assays were obtained by submitting TRO (oxidized at optimal conditions) to iron-loading from a 1250 mg-Fe L^{-1} solution. Using those conditions, an iron-loaded oxidized tannin resin with an iron content of 22±2 mg g^{-1} is obtained.

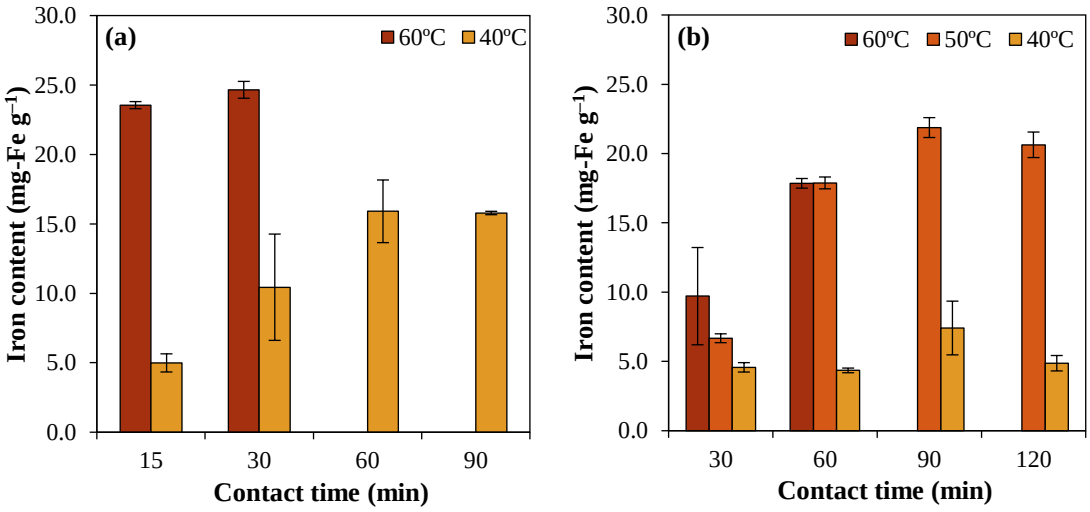

Fig. III.6 Influence on iron uptake by oxidation time, temperature, and HNO_3 concentration, using a solution of 200 mg-Fe L^{-1} at initial pH 2 and room temperature. (a) HNO_3 2 mol L^{-1}; (b) HNO_3 1 mol L^{-1}. Every assay was done in duplicate and error bars represent absolute deviations.

Particle size separation was conducted, and two granulometric fractions were selected: 0.15-0.50 mm, with an iron content of 13±1 mg g^{-1}, and <0.15 mm, with an iron content of 31±4 mg g^{-1}. The difference in iron contents is explained by different surface areas:

smaller particles have a higher surface area which exposes a higher number of functional groups able to uptake iron ions.

Ogata et al. [14] managed to yield an iron-loaded wattle tannin resin with an iron content of 85 mg-Fe g^{-1}. Of note, with a non-oxidized resin the maximum iron content was of 37 mg-Fe g^{-1}. The oxidation of the resin was performed with HNO_3 2 mol L^{-1} for 120 min and iron treatment with a 1 mol L^{-1} solution of Fe(III) at initial pH 2 for 5 days. The concentration used was substantially higher than the one used here (≈55 g-Fe L^{-1} vs. 1.25 g-Fe L^{-1}). Moreover, the tannin used in that study was a commercially available powder obtained from wattle (*Acacia*), that may contain different characteristics, namely a high purity (e.g., higher content of polyphenols).

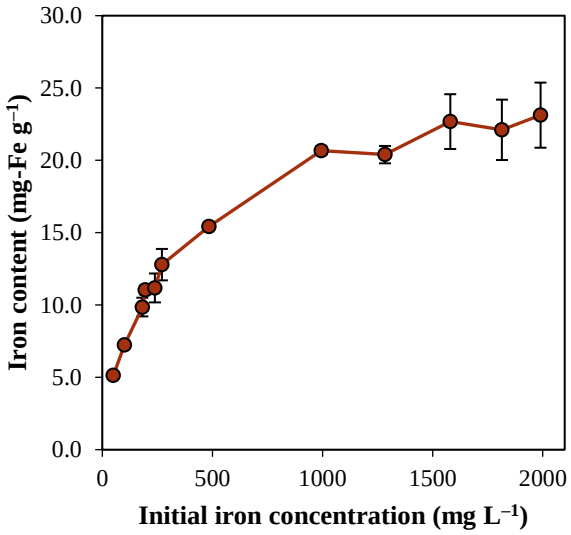

Fig. III.7 Influence on iron uptake by initial Fe(III) concentration at initial pH 2 and room temperature using a tannin resin oxidized with HNO_3 1 mol L^{-1} at 50 °C for 90 min. Every assay was done in duplicate and error bars represent absolute deviations.

Other biomass-derived adsorbents have been subjected to iron-loading. For example, Pintor et al. [74] submitted cork granulates to iron precipitation under different conditions (0.05-0.1 mol-Fe L^{-1}, 10-20 g L^{-1}, pH 5-7) which yielded adsorbents with iron contents within a range (4.1-24.0 mg-Fe g^{-1}) similar to that obtained here. On the other hand, Vieira et al. [73] prepared iron-coated seaweeds (*Sargassum muticum*) and an iron content of 55±2 mg-Fe g^{-1} was achieved. Even though seaweeds were loaded with twice as much iron as tannin resins were, comparisons ought to be done with precaution since experimental conditions were noticeably different, with an iron concentration and a solid:liquid ratio five and two times higher, respectively.

3.3. Calcium-loading

Samples of TR and TRO were submitted to calcium-loading. The TRO used was obtained under the experimental conditions found to be optimal for iron uptake. Calcium content of both resins, prior to calcium-loading, was measured: 9.6 mg g^{-1} (TR) and 0.4 mg g^{-1} (TRO). The results of the influence by initial calcium concentration on uptake by each resin are presented in Fig. III.8. The amount of calcium retained by the solid was evaluated by two methods, acid digestion of the solid and mass balance applied in the liquid phase, and different results were obtained.

Calcium removal from the solution by TRO is highly dependent on Ca concentration, reaching 89 mg-Ca g^{-1} (Fig. III.8b). However, after separation from the liquid, the solid was washed which possibily caused the retained calcium to leach out partially. Probably only the calcium ions which were stably bound to the solid remained. This explains the much lower calcium contents measured in the solid by acid digestion, limited to ≈25 mg-Ca g^{-1} (Fig. III.8a).

Regarding TR, the difference between the amount of calcium retained in the solid calculated by the two methods seems to be less significant (Fig. III.8a and Fig. III.8b). This may be an indication of the establishment of more stable bonds between Ca and TR. In this case, the maximum uptake (calculated by acid digestion) was 22 mg g^{-1}, which occurs for Ca concentrations higher than 215 mg L^{-1} (Fig. III.8a). The procedure generates an adsorbent containing 32 mg-Ca g^{-1} (original content plus calcium retained from the solution) in these conditions.

Tannin resins usually present a great chelating ability towards cationic metals, due to the abundance of adjacent phenolic hydroxyl groups [3, 140], explaining the considerable calcium uptake. The partial oxidation has not decreased calcium uptake, but lead to the dissolution of the metal initially present in the solid which, ultimately, led to a lower calcium content. Therefore, TR was found to be better suited for calcium-loading and adsorbent application since it requires fewer production steps than the TRO and yields a solid material with similar calcium content.

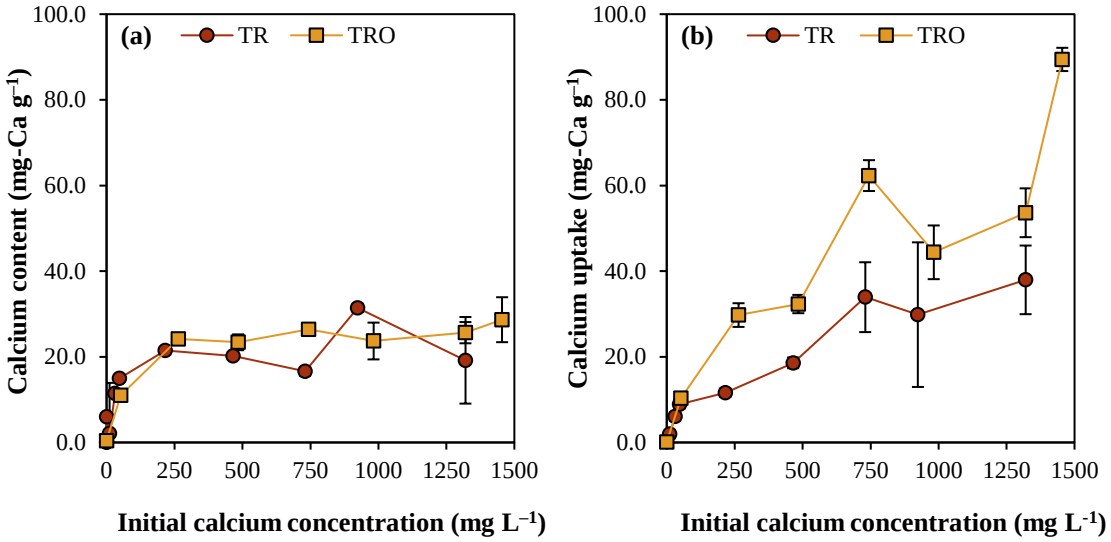

Fig. III.8 Influence on calcium uptake by initial Ca concentration at initial pH 6 and room temperature using TR or TRO: results from (a) acid digestion and (b) mass balance in the liquid phase. Every assay was done in duplicate and error bars represent absolute deviations.

3.4. Characterization of Tannin Resins

Fig. III.9 displays the IR spectra obtained for the tannin extracts and tannin resins. A broad band was observed between 3200 and 3800 cm^{-1}, as expected for materials with many –OH groups [141, 142]. Indeed, a particularly intense peak can be observed in that range in the freeze-dried tannin extract spectrum (Fig. III.9a). A peak of less intensity is observed in the precipitated tannin extract spectrum possibly due to the oxidation of –OH groups during the evaporation of the extraction solution. The tannin resin spectrum (Fig. III.9b) also presents a peak characteristic of the OH stretching vibration, but its height is about one fourth of the peak observed for the extract spectrum, explained by the considerably higher degree of resin polymerization (Fig. III.9b). The small peak observed at 2905 cm^{-1} for the tannin extract is due to aromatic C-H stretching [141, 143]. A similar peak is not observed in the spectrum of tannin resin possibly because the particle size of the resin is noticeably larger and thus the equipment does not detect such a small peak. Finally, the spectrum of the extract presents a broad peak, starting roughly at 1800 cm^{-1}, which indicates the presence of carbonyl groups (1630-1820 cm^{-1}) and aromatic rings (1450-1600 cm^{-1}) [142]. For the resin, this peak is reduced both in range as in height.

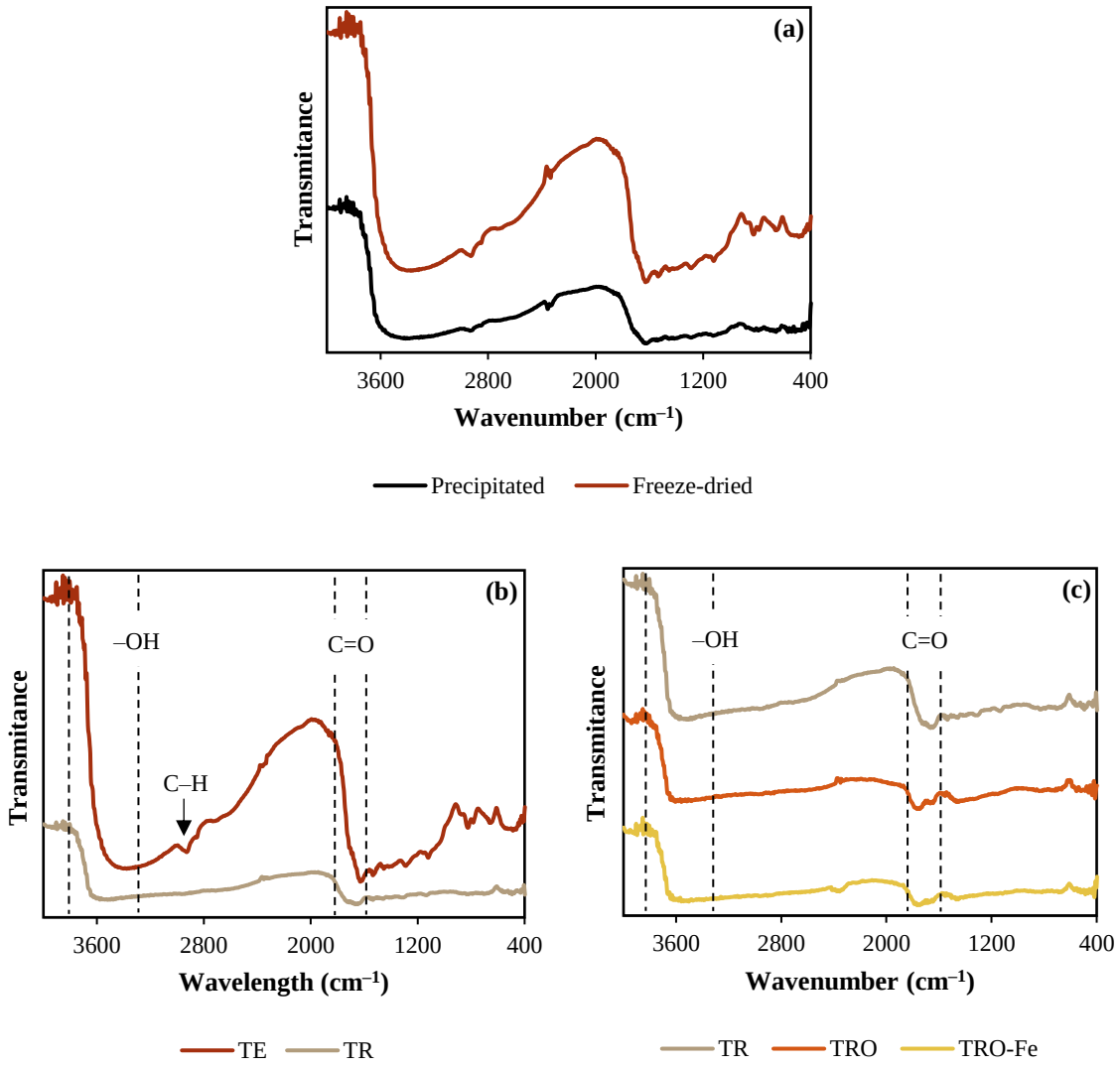

Fig. III.9 Infrared spectra of (a) precipitated and freeze-dried extracts, (b) freeze-dried tannin extract and tannin resin, (c) tannin resin, oxidized tannin resin, and iron-loaded oxidized tannin resin.

After oxidation, the resin was expected to present a smaller O-H peak and a higher C=O peak, due to the oxidation of hydroxyl groups into carbonyl ones during the contact with HNO_3 solution [14]. There is indeed a reduction of the O-H peak height from TR to TRO, and an almost complete flattening of the C=O peak was observed (Fig. III.9c). The spectrum reported by Ogata et al. [14] for the non-oxidized resin did not present a C=O peak at all, which was only present in the oxidized resins spectra. Such observation indicates that the TR produced in this work was considerably oxidized before contact with a nitric acid solution. Comparing TRO and TRO-Fe spectra, slight differences were observed in the region of C=O band, corroborating the iron ability to interact particularly with these groups [14], but no other detectable changes were observed.

Fig. III.10 presents SEM images obtained for the precipitated and the freeze-dried tannin extracts and of the resins produced by both. The precipitated extract particles have in general a rough surface (Fig. III.10a) and some non-uniform agglomerates of NaCl (probably resultant from the pH neutralization of the extraction solution with HCl) are observable in the particles' surface. The freeze-dried extract presents a completely different aspect: it is composed mainly by thin-sliced particles with well-defined crystals of NaCl in its surface (Fig. III.10b). This difference in physical configurations helps explain the improved solubility of the freeze-dried extract when compared to the precipitated one.

On the other hand, both resins present particles with smooth surfaces with some deformities and do not appear to be porous (Fig. III.10c and Fig. III.10d). Porosity is developed by high temperature activation procedures, which was not applied here, hence the observation of low porosity was expectable. Sánchez-Martín et al. [7] obtained SEM images for cypress, quebracho, wattle, and pine tannin resins and observed smooth-surface non-porous particles as well. Moreover, tannin resins do not significantly differ before and after oxidation. Finally, iron- and calcium-loaded resins (Fig. III.10e and Fig. III.10f, respectively) do not present any major morphological difference comparatively with the unmodified tannin resin. Nevertheless, EDS spectra of TRO-Fe and TR-Ca, obtained for particles observed in Fig. III.10e and Fig. III.10f, respectively, confirmed that iron- and calcium-loading was successful (Fig. III.11). The highest peaks are those of C and O, which is expected for biomass-derived materials. EDS spectra of TR merely presented peaks corresponding to C and O (data not shown).

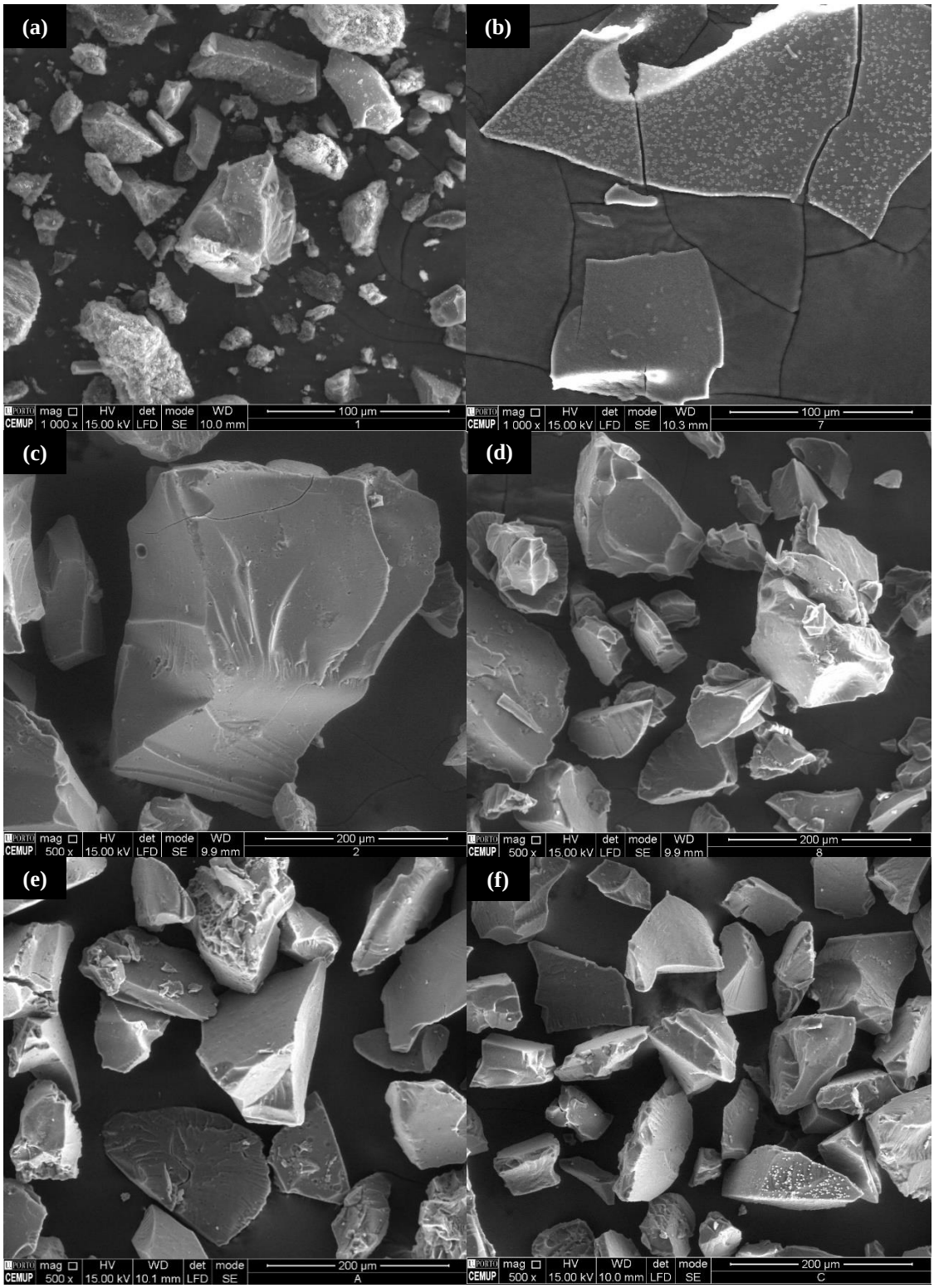

Fig. III.10 SEM images of (a) the precipitated tannin extract, (b) the freeze-dried tannin extract, the tannin resin produced with (c) a precipitated extract and (d) a freeze-dried extract, (e) an oxidized iron-loaded tannin resin (< 0.15 mm), and (f) a calcium-loaded tannin resin.

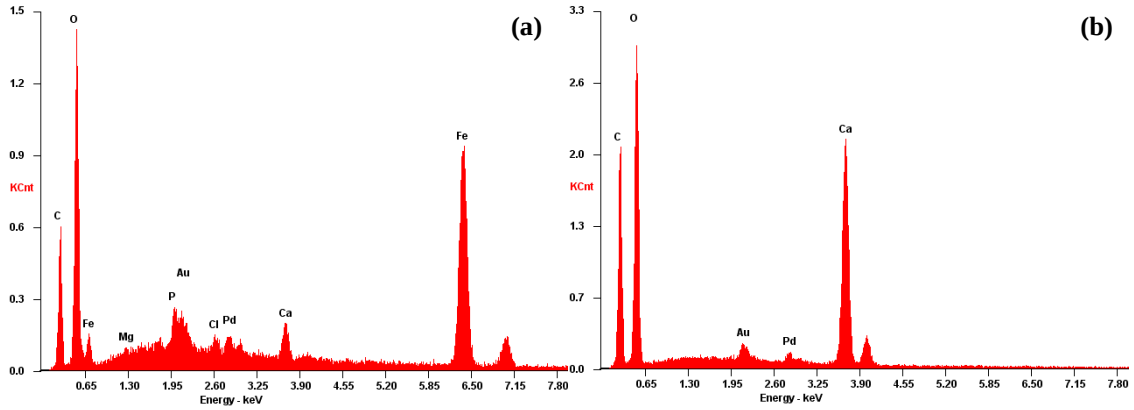

Fig. III.11 EDS spectra obtained from (a) TRO-Fe and (b) TR-Ca.

Granulometric distributions of TR, TRO, and TRO-Fe is presented in Fig. III.12 and in Table III.3. Almost half of TR particles have diameters ranging from 0.15 mm to 0.50 mm, while particles with diameters below 0.15 mm and above 0.50 mm represent roughly a third and a quarter, respectively, of the total sample. The distribution of TRO and TRO-Fe particle sizes was found to be similar to that of TR. However, oxidation and iron-loading lead to a decrease of finer particles (<0.15 mm). Furthermore, median diameters of the TR particles in the fractions <0.15 mm, 0.15-0.50 mm and 1-2 mm were calculated as 0.083 mm, 0.265 mm, and 1.3 mm, respectively. TRO and TRO-Fe fractions (0.15-0.50 mm) presented median particle sizes of 0.257 mm and 0.260 mm, respectively.

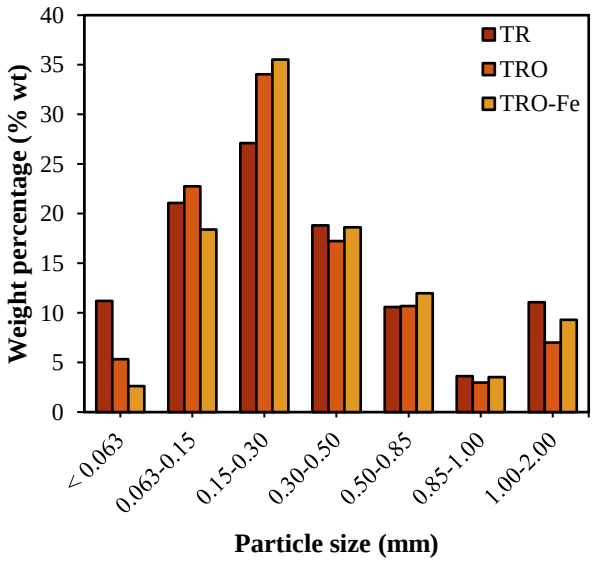

Fig. III.12 Granulometric distribution of TR, TRO, and TRO-Fe.

Table III.3 Granulometric distribution of the fraction <0.15 mm of TR, the fractions 0.15-0.30 mm of TR, TRO, and TRO-Fe, and the fraction 1.00-2.00 mm of TR.

Fraction	**Weight percentage (% wt)**		
<0.15 mm	**<0.05 mm**	**0.05-0.10 mm**	**0.10-0.15 mm**
TR	24	34	42
0.15-0.30 mm	**0.15-0.25 mm**	**0.25-0.35 mm**	**0.35-0.50 mm**
TR	39	33	28
TRO	41	17	42
TRO-Fe	40	17	43
1.00-2.00 mm	**1.00-1.25 mm**	**1.25-1.50 mm**	**1.50-2.00 mm**
TR	45	28	26

Fig. III.13 presents zeta potential measurements for TR, TRO and TRO-Fe. Within the pH range studied, negative potentials were observed for the three resins, which is attributed to the anionic nature of phenolic hydroxyl groups. Values gradually decreased with increasing pH, due to the higher ionization degree of these groups. The isoelectric points of TR, TRO, and TRO-Fe were estimated by extrapolation as 2.1, 1.8, and 1.4, respectively. This means that the surface charge of the resins is only positive at extreme acidic pH conditions.

The IEP obtained for TR agrees with values reported in the literature for tannin resins prepared from other vegetable sources, such as quebracho (IEP at pH 2.17) [22], black wattle (IEP at pH 1.6) [38], and persimmon (IEP at pH 2.21) [19, 20]. The results also show that the oxidation of the tannin resin and subsequent iron loading did not cause significant variation in the adsorbents' surface charge since the zeta potential patterns are virtually identical to TR. In the oxidation of TR to generate TRO, part of the catecholic hydroxy groups located in B-ring is oxidized by nitric acid to carbonyl groups, giving rise to o-quinone compounds [14]. The hydroxyl groups that remained in the original form (A- and B-rings) are then supposed to rule the surface charge of TRO, which explains the similarity observed between TR and TRO.

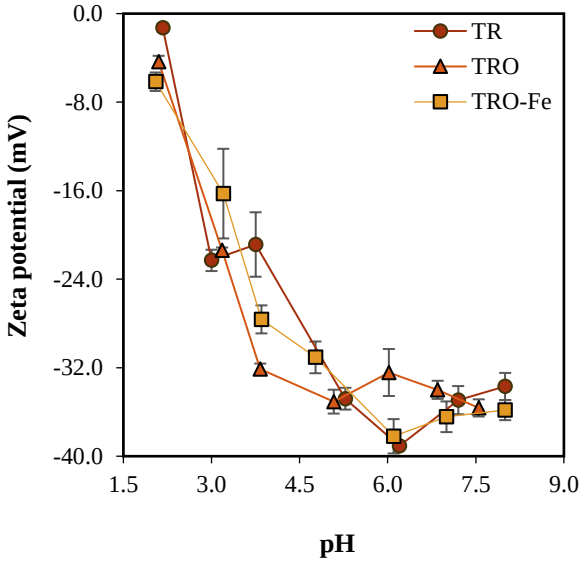

Fig. III.13 Zeta potential of tannin resin, oxidized tannin resin and iron-loaded oxidized tannin at different pH (electrolyte: NaCl 0.001 mol L^{-1}).

Tannins form stable complexes with iron(III), in stoichiometries depending on the pH [140, 144, 145]. Moreover, previous studies [14] showed that carbonyl groups, obtained by the oxidation of tannin resins, have a higher affinity to iron ions than hydroxy groups. Tannin-iron complexes include positively charged mono-complexes, expected to be formed at pH below 2, and negatively charged complexes, including bis-complexes (pH of 3-6) and tris-complexes (pH of above 7) [140, 144, 145]. Considering the pH at which the iron-loading proceeded, a mixture of mono (positively charged) and bis-complexes (negatively charged) is expected to be present in TRO-Fe. In certain pH conditions, the surface charge of TRO-Fe is less negative than TRO, but overall, the surface zeta potentials did not significantly differ from those of TR and TRO (Fig. III.13). This can be attributed to the limited Fe content of TRO-Fe (13 mg g^{-1}) and the predominance of anionic hydroxyl groups. The results here obtained for TRO-Fe are in line with Hao et al. [146], who also presented negative zeta potentials in the whole pH range for a tannin foam with immobilized Fe(III).

The stability of an adsorbent is an important factor which must be assessed and considered together with its adsorption capacity. Leaching of organic material and colour are example markers of chemical stability. Fig. III.14 presents DOC and colour values obtained in leaching experiments conducted with TR (fraction 0.15-0.50 mm) suspensions at different pH. DOC levels were below 7 mg-C L^{-1} for pH values up to 6. Only a very slight increase to 9 mg-C L^{-1} was observed at pH 7.

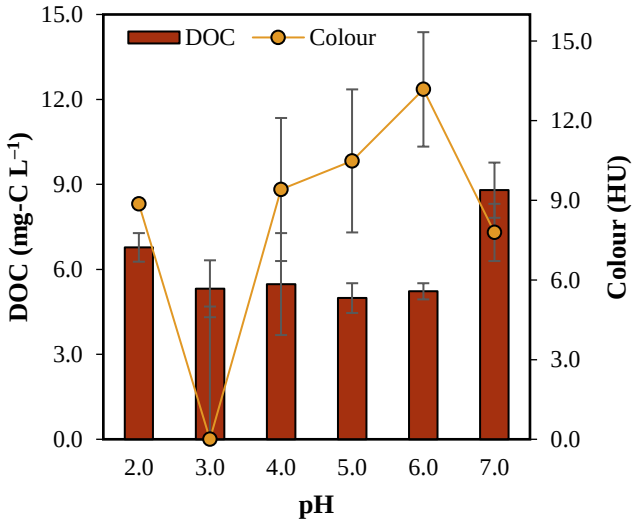

Fig. III.14 Results of leaching experiments: dissolved organic carbon (DOC) and colour obtained for TR granulometric fraction of 0.15-0.50 mm with a solid:liquid ratio of 0.5 g L^{-1}.

DOC leaching was also assessed using a greater solid:liquid ratio, not only by TR but also by TRO and TRO-Fe (Fig. III.15). TR caused higher leaching of organic material than in the last assay due to the greater solid:liquid ratio. In general, DOC concentrations for solutions that were in contact with TR and TRO increased with pH, even though that TR led to a steeper increase (Fig. III.15). Indeed, at pH 2 both resins lead to similar values but at pH 4 DOC values increased thrice and twice higher for TR and TRO, respectively. Moreover, DOC values increased further with the increase of pH with TR, reaching a maximum of 17.3±0.7 mg-C L^{-1} at pH 9, while for TRO it remained below 11 mg-C L^{-1}. Finally, for TRO-Fe at pH 2 the DOC value was even lower, and it was never higher than 5 mg-C L^{-1}. The lower DOC values observed for TRO and TRO-Fe may be due to the additional treatments these resins were subjected to, which must have caused leaching of organic matter, leading to more stable solids. In any case, these values are considerably low and suggest that the application of these resins will not cause significant secondary pollution in terms of organic matter.

Colour measurements are all below 13 HU (maximum value recorded at pH 6, Fig. III.14). At pH 3, colour is even below the limit of detection (5 HU). To give an idea about the non-significance of the recorded values, 20 HU is the parametric value for colour in drinking water (Portuguese legislation [147]). The results obtained for DOC and colour indicate high chemical stability of TR.

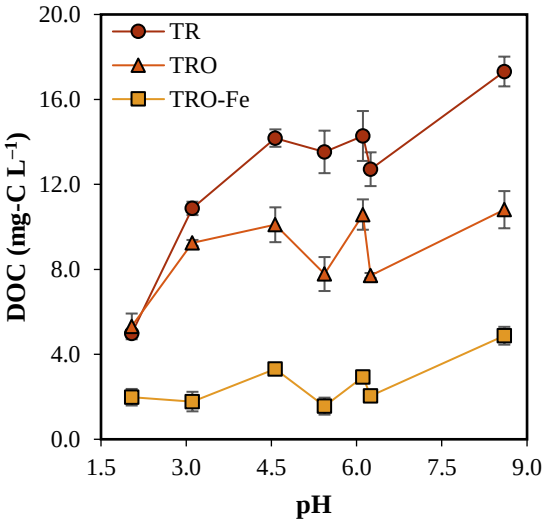

Fig. III.15 Dissolved organic carbon (DOC) leached by TR, TRO, and TRO-Fe at different pH with a solid:liquid ratio of 2 g L^{-1} at 20 °C for 24 h.

Regarding TRO-Fe, significant leaching of the iron was observed at pH 2 and 3, with dissolved levels attaining 17±1 mg-Fe L^{-1} and 5.6±0.2 mg-Fe L^{-1}, respectively, corresponding to 47±2 % and 17±1 % of the initial metal content of the adsorbent. This means that TRO-Fe application in strongly acidic conditions is not advised or will require a further step for iron removal (e.g., precipitation). At moderately acidic and neutral conditions, TRO-Fe is relatively stable, with iron leaching limited to 1-3.5 % of its metal content.

3.5. Adsorbate/Adsorbent Screening

3.5.1. Arsenic

Preliminary adsorption assays with TR, TRO, TRO-Fe, and TR-Ca were done with solutions of As(III) and As(V) at pH 4. Results showed that only TRO-Fe has the ability to uptake arsenic (Fig. III.16). Nearly null results (As removals below 10 % and uptake <0.03 mg g^{-1}, for both oxidation states) were obtained for TR and TRO, while TRO-Fe adsorbed 0.24±0.3 mg g^{-1} and 0.155±0.003 mg g^{-1} (42±5 % and 28.8±0.1 % removal from solution) of As(III) and As(V), respectively.

On the other hand, calcium-loading granted a slight improvement on adsorption capacity, with TR-Ca removing 10±2 % and 4±1 % of As(III) and As(V), respectively (Fig. III.16).

Nevertheless, arsenic uptake by TR-Ca was still low, indicating calcium-loading does not yield a resin with affinity towards arsenic. Calcium content of TR-Ca was higher than iron content of TRO-Fe (32±1 mg-Ca g^{-1} vs. 22±2 mg-Fe g^{-1}; 1.25±0.03 mmol-Ca g^{-1} vs. 0.39±0.04 mmol-Fe g^{-1}) therefore the lack of adsorption capacity by TR-Ca means that the introduction of iron creates specific adsorption sites for arsenic in the resin.

These results confirm the necessity of loading iron into the resin so it can have affinity towards arsenic. Thus, uptake of arsenic was only further evaluated with TRO-Fe. Chapter IV presents a more in-depth assessment of arsenic adsorption by the iron-loaded oxidized tannin resin.

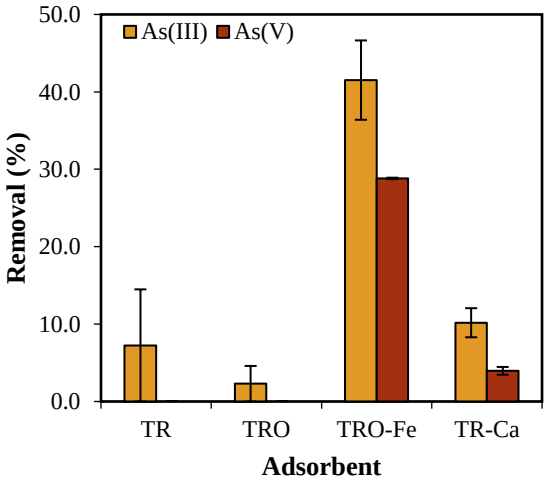

Fig. III.16 Adsorption assays using different adsorbents in arsenic solutions (C_{in} = 5 mg L^{-1} for TR, TRO, and TRO-Fe; C_{in} = 0.5 mg L^{-1} for TR-Ca) at pH 4 and a solid:liquid ratio of 10 g L^{-1}.

3.5.2. Antimony

Fig. III.17 presents antimony adsorbed amounts by TR, TRO and TRO-Fe at pH 4. Highest removals for both adsorbates were achieved by TR: 17±1 % for Sb(III) and 33±6 % for Sb(V). TRO presented removals <10 % of both oxidation states, representing the second-best performance. This was expected considering that the oxidation was only conducted as an intermediate step to obtain the iron-loaded adsorbent, and that TR partial oxidation causes loss of hydroxyl groups, decreasing the available sites for complexation.

TRO-Fe also performed worse than TR, with removals of <3 %. A wide variety of materials have been modified with iron, bearing in mind the specific affinity between Fe-O

bonds and Sb (e.g., [75, 148]). In this case, however, iron-loading did not enhance adsorptive properties of TR, which indicate a higher affinity of Sb to the polyol groups of TR, than to the iron complexes in TRO-Fe.

In conclusion, TR is more suitable to adsorb antimony in both oxidation states than the oxidized and iron-loaded forms. TR was hence selected to be used in the subsequent antimony adsorption experiments, which is the focus of Chapter V. From an operational and environmental point of view, TR is advantageous over TRO-Fe, considering its simpler preparation, easier pH control and absence of secondary pollution generated by iron leaching. Nevertheless, the removals by TRO and TRO-Fe were still significant and the adsorption capacity of antimony by those resins was further explored and this study is also presented in Chapter V.

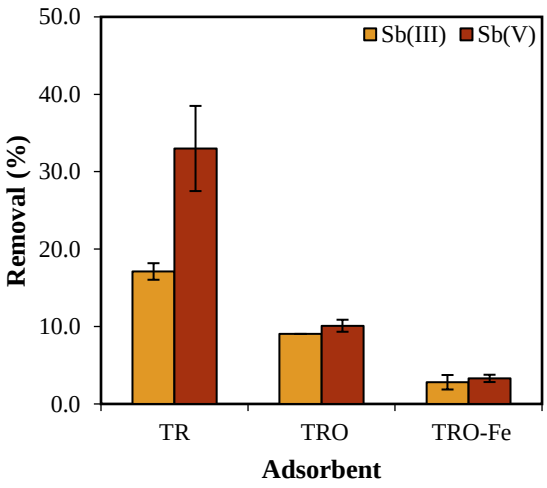

Fig. III.17 Adsorption assays using different adsorbents in antimony solutions (C_{in} = 20 mg L^{-1}) at pH 4 and a solid:liquid ratio of 0.5 g L^{-1}.

3.5.3. Phosphate

Phosphate uptake by different resins was assessed by different adsorbents and in Fig. III.18 the results obtained at pH 4 are presented. Calcium and iron present a high affinity towards phosphate, which explains the effective phosphate adsorption that literature shows by calcium-rich materials [149-152] and by iron-loaded adsorbents [14, 77, 153, 154]. For that reason, and also due to the unfavourable surface charge properties, TR which contain low calcium and/or iron contents poorly adsorbed phosphate. Only metal-loaded resins presented some ability to adsorb phosphate (Fig. III.18). However, calcium-

and iron-loading of the tannin resins did not yield an adsorbent sufficiently effective for phosphate uptake. Phosphate removal by TR-Ca did not surpass 11 % at pH 2-4 and was null at pH 5-7 while TRO-Ca was only able to remove 2.5±0.9 % at pH 4. These results contrast with the efficient calcium-rich adsorbents reported in the literature, which may be due to great differences in calcium content (32 mg-Ca g^{-1} vs. 61.5-78.5 mg-Ca g^{-1} [151] and 229.1-361.4 mg-Ca g^{-1} [150]).

Uptake capacity of TRO-Fe at pH 4 was similar to that of TR-Ca, with a removal of 10.6±0.3 %. The results obtained by Ogata et al. [14] using an iron-loaded *Acacia* tannin resin were not possible to replicate here, which, once again, may be due to differences in metal content. The poor adsorption results here observed led to phosphate being abandoned as a target adsorbate and the topic was not further assessed.

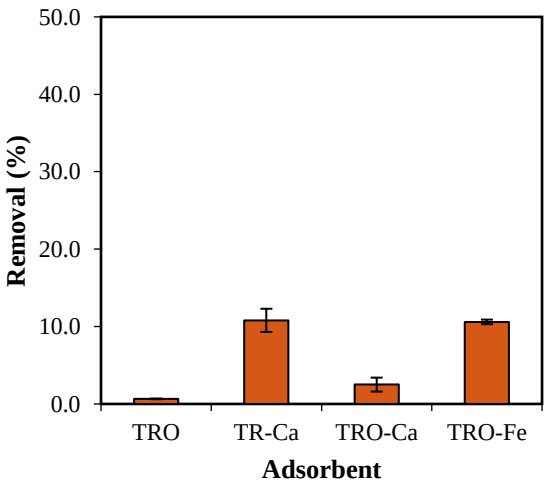

Fig. III.18 Adsorption assays using different adsorbents in phosphate solutions (C_{in} = 5 mg L^{-1}) at pH 4 and a solid:liquid ratio of 10 g L^{-1}.

4. Conclusions

Precipitated tannin extracts were converted into resins (insoluble matrices) by polymerization. The amounts of solvent/catalyst (NaOH) and reagent (formaldehyde) were optimized to maximize gelification yield while minimizing chemicals use. Optimal conditions were found when extracts were dissolved in 6.0 mL of NaOH 0.25 mol L^{-1} per g of extract and when 0.40 mL of formaldehyde per g of extract was added. Better results were achieved using a freeze-dried extract. In addition of granting a higher solubility to the extract, freeze-drying allowed to obtain higher polymerization efficiencies using lower amounts of NaOH and formaldehyde (4.0 and 0.20 mL per g of extract, respectively), with an expected yield of tannin resin of 80 %.

Optimum conditions for the oxidation were identified at a temperature of 50 °C, HNO_3 concentration of 1 mol L^{-1} and a contact time of 90 min, giving a maximum iron content of 22±2 mg per g of tannin resin after contact with a 1250 mg-Fe L^{-1} solution. On the other hand, calcium-loading was best with a non-oxidized tannin resin and a solution with a concentration of 215 mg-Ca L^{-1} was found to be sufficient to achieve saturation. In these conditions, a resin with a calcium content of 32±1 mg per g of tannin resin is expected to be obtained.

The stability of adsorbents is of great importance due to the risk of secondary pollution; higher the stability, lower the risk. Results obtained hitherto seem to suggest that tannin resins here produced are stable in solution, which does not usually happen with many of the low-cost materials reported in literature. Furthermore, tannin resin can be produced in varied particle sizes, which is important for application at full-scale, and are believed to be economically competitive with conventional adsorbents, due to the observed efficiency and the relatively simple production.

In preliminary assays, unmodified tannin resins presented the best performance for antimony adsorption while only iron-loaded oxidized tannin resins were able to significantly uptake arsenic. In contrast, none of the adsorbents tested for phosphate removal from water was effective.

5. References

[1] Ampiaw, R.E. and W. Lee, "Persimmon tannins as biosorbents for precious and heavy metal adsorption in wastewater: a review," *International Journal of Environmental Science and Technology*, 2020.

[2] Inoue, K., M. Gurung, Y. Xiong, H. Kawakita, K. Oht, and S. Alam, "Hydrometallurgical recovery of precious metals and removal of hazardous metals using persimmon tannin and persimmon wastes," *Metals*, Review vol. 5, no. 4, pp. 1921-1956, 2015, Art. no. A13.

[3] Pizzi, A., "Tannins: major sources, properties and applications," in *Monomers, Polymers and Composites from Renewable Resources*, M. N. Belgacem and A. Gandini, Eds.: Elsevier, 2008, pp. 179-200.

[4] Arbenz, A. and L. Averous, "Chemical modification of tannins to elaborate aromatic biobased macromolecular architectures," *Green Chemistry*, vol. 17, no. 5, pp. 2626-2646, 2015.

[5] Nakano, Y., K. Takeshita, and T. Tsutsumi, "Adsorption mechanism of hexavalent chromium by redox within condensed-tannin gel," *Water Research*, vol. 35, no. 2, pp. 496-500, 2001.

[6] Sánchez-Martín, J., J. Beltrán-Heredia, and C. Carmona-Murillo, "Adsorbents from *Schinopsis balansae*: Optimisation of significant variables," *Industrial Crops and Products*, vol. 33, no. 2, pp. 409-417, 2011.

[7] Sánchez-Martín, J., J. Beltrán-Heredia, and P. Gibello-Pérez, "Adsorbent biopolymers from tannin extracts for water treatment," *Chemical Engineering Journal*, vol. 168, no. 3, pp. 1241-1247, 2011.

[8] Beltrán-Heredia, J., P. Palo, J. Sánchez-Martín, J.R. Domínguez, and T. González, "Natural adsorbents derived from tannin extracts for pharmaceutical removal in water," *Industrial & Engineering Chemistry Research*, vol. 52, pp. 50-57, 2012.

[9] Kunnambath, P.M. and S. Thirumalaisamy, "Characterization and Utilization of Tannin Extract for the Selective Adsorption of Ni(II) Ions from Water," *Journal of Chemistry*, 2015.

[10] Sánchez-Martín, J., J. Beltrán-Heredia, I.J. Seabra, M.E.M. Braga, and H.C. De Sousa, "Adsorbent derived from *Pinus pinaster* tannin for cationic surfactant removal," *Journal of Wood Chemistry and Technology*, vol. 32, no. 1, pp. 28-50, 2012.

[11] Sánchez-Martín, J., M. González-Velasco, J. Beltrán-Heredia, J. Gragera-Carvajal, and J. Salguero-Fernández, "Novel tannin-based adsorbent in removing cationic dye (Methylene Blue) from aqueous solution. Kinetics and equilibrium studies," *Journal of Hazardous Materials*, vol. 174, no. 1-3, pp. 9-16, 2010.

[12] Xiong, Y., H.T. Wang, Z.N. Lou, W.J. Shan, Z.Q. Xing, G.C. Deng, D.B. Wu, D.W. Fang, and B.K. Biswas, "Selective adsorption of molybdenum(VI) from Mo-Re bearing effluent by chemically modified astringent persimmon," *Journal of Hazardous Materials*, vol. 186, no. 2-3, pp. 1855-1861, 2011.

[13] Ogata, T. and Y. Nakano, "Mechanisms of gold recovery from aqueous solutions using a novel tannin gel adsorbent synthesized from natural condensed tannin," *Water Research*, vol. 39, no. 18, pp. 4281-4286, 2005.

[14] Ogata, T., S. Morisada, Y. Oinuma, Y. Seida, and Y. Nakano, "Preparation of adsorbent for phosphate recovery from aqueous solutions based on condensed tannin gel," *Journal of Hazardous Materials*, vol. 192, no. 2, pp. 698-703, 2011.

[15] Yi, Q., R. Fan, F. Xie, H. Min, Q. Zhang, and Z. Luo, "Selective Recovery of Au(III) and Pd(II) from Waste PCBs Using Ethylenediamine Modified Persimmon Tannin Adsorbent," *Procedia Environmental Sciences*, vol. 31, pp. 185-194, 2016.

[16] Oo, C.-W., M.J. Kassim, and A. Pizzi, "Characterization and performance of *Rhizophora apiculata* mangrove polyflavonoid tannins in the adsorption of copper (II) and lead (II)," *Industrial Crops and Products*, vol. 30, no. 1, pp. 152-161, 2009.

[17] Gurung, M., B.B. Adhikari, S. Morisada, H. Kawakita, K. Ohto, K. Inoue, and S. Alam, "*N*-aminoguanidine modified persimmon tannin: A new sustainable material for selective adsorption,

preconcentration and recovery of precious metals from acidic chloride solution," *Bioresource Technology*, vol. 129, pp. 108-117, 2013.

[18] Maria Rahman, M., N. Akter, M. Razaul Karim, N. Ahmad, M.M. Rhaman, I.A. Siddiquey, N. Mohammad Bahadur, and M.A. Hasnat, "Optimization, kinetic and thermodynamic studies for removal of Brilliant Red (X-3B) using Tannin gel," *Journal of Environmental Chemical Engineering*, vol. 2, pp. 76-83, 2014.

[19] Xie, F., Z.J. Fan, Q.L. Zhang, and Z.R. Luo, "Selective Adsorption of Au^{3+} from Aqueous Solutions Using Persimmon Powder-Formaldehyde Resin," *Journal of Applied Polymer Science*, vol. 130, no. 6, pp. 3937-3946, 2013.

[20] Xie, F., R. Fan, Q. Yi, Q. Zhang, and Z. Luo, "NaOH Modification of Persimmon Powder-formaldehyde Resin to Enhance Cu^{2+} and Pb^{2+} Removal from Aqueous Solution," *Procedia Environmental Sciences*, vol. 31, pp. 817-826, 2016.

[21] Xie, F., R. Fan, Q. Yi, Z. Fan, Q. Zhang, and Z. Luo, "Adsorption recovery of Pd(II) from aqueous solutions by persimmon residual based bio-sorbent," *Hydrometallurgy*, vol. 165, pp. 323-328, 2016.

[22] Yurtsever, M. and İ.A. Şengil, "Biosorption of Pb(II) ions by modified quebracho tannin resin," *Journal of Hazardous Materials*, vol. 163, no. 1, pp. 58-64, 2009.

[23] Kim, Y.H. and Y. Nakano, "Adsorption mechanism of palladium by redox within condensed-tannin gel," *Water Research*, vol. 39, no. 7, pp. 1324-1330, 2005.

[24] Kim, Y.H., T. Ogata, and Y. Nakano, "Kinetic analysis of palladium(II) adsorption process on condensed-tannin gel based on redox reaction models," *Water Research*, vol. 41, no. 14, pp. 3043-3050, 2007.

[25] Kim, Y.H., M.N. Alam, Y. Marutani, T. Ogata, S. Morisada, and Y. Nakano, "Improvement of Pd(II) Adsorption Performance of Condensed-tannin Gel by Amine Modification," *Chemistry Letters*, vol. 38, no. 10, pp. 956-957, 2009.

[26] Morisada, S., Y.H. Kim, T. Ogata, Y. Marutani, and Y. Nakano, "Improved Adsorption Behaviors of Amine-Modified Tannin Gel for Palladium and Platinum Ions in Acidic Chloride Solutions," *Industrial & Engineering Chemistry Research*, vol. 50, no. 4, pp. 1875-1880, 2011.

[27] Morisada, S., T. Rin, T. Ogata, Y.H. Kim, and Y. Nakano, "Adsorption removal of boron in aqueous solutions by amine-modified tannin gel," *Water Research*, vol. 45, no. 13, pp. 4028-4034, 2011.

[28] Akter, N., M.A. Hossain, M.J. Hassan, M.K. Amin, M. Elias, M.M. Rahman, A.M. Asiri, I.A. Siddiquey, and M.A. Hasnat, "Amine modified tannin gel for adsorptive removal of Brilliant Green dye," *Journal of Environmental Chemical Engineering*, vol. 4, no. 1, pp. 1231-1241, 2016.

[29] Fayemiwo, O.M., M.O. Daramola, and K. Moothi, "Tannin-based adsorbents from green tea for removal of monoaromatic hydrocarbons in water: Preliminary investigations," *Chemical Engineering Communications*, vol. 205, no. 4, pp. 549-556, 2018.

[30] Şengil, İ.A. and M. Özacar, "Biosorption of Cu(II) from aqueous solutions by mimosa tannin gel," *Journal of Hazardous Materials*, vol. 157, no. 2-3, pp. 277-285, 2008.

[31] Şengil, İ.A. and M. Özacar, "Competitive biosorption of Pb^{2+} Cu^{2+} and Zn^{2+} ions from aqueous solutions onto valonia tannin resin," *Journal of Hazardous Materials*, vol. 166, no. 2-3, pp. 1488-1494, 2009.

[32] Can, M., E. Bulut, A. Ornek, and M. Ozacar, "Synthesis and characterization of valonea tannin resin and its interaction with palladium (II), rhodium (III) chloro complexes," *Chemical Engineering Journal*, vol. 221, pp. 146-158, 2013.

[33] Patil-Shinde, V., K.B. Mulani, K. Donde, N.N. Chavan, S. Ponrathnam, and S.S. Tambe, "The Removal of arsenite [As(III)] and arsenate [As(V)] ions from wastewater using TFA and TAFA resins: Computational intelligence based reaction modeling and optimization," *Journal of Environmental Chemical Engineering*, vol. 4, no. 4, pp. 4275-4286, 2016.

[34] Mulani, K., S. Daniels, K. Rajdeo, S. Tambe, and N. Chavan, "Tannin-aniline-formaldehyde resole resins for arsenic removal from contaminated water," *Canadian Chemical Transactions*, vol. 2, no. 4, p. 450, 2014.

[35] Yurtsever, M. and A. Şengil, "Adsorption and desorption behavior of silver ions onto valonia tannin resin," *Transactions of Nonferrous Metals Society of China*, vol. 22, no. 11, pp. 2846-2854, 2012.

[36] Luzardo, F.H.M., F.G. Velasco, I.K.S. Correia, P.M.S. Silva, and L.C. Salay, "Removal of lead ions from water using a resin of mimosa tannin and carbon nanotubes," *Environmental Technology & Innovation*, vol. 7, no. Supplement C, pp. 219-228, 2017.

[37] García, D.E., W.G. Glasser, A. Pizzi, C. Lacoste, and M.-P. Laborie, "Polyphenolic resins prepared with maritime pine bark tannin and bulky-aldehydes," *Industrial Crops and Products*, vol. 62, pp. 84-93, 2014.

[38] Sun, X., J. Zhang, and Y. You, "Enhancement of Cu(II) removal by carbon disulfide modified black wattle tannin gel," *Colloids and Surfaces A: Physicochemical and Engineering Aspects*, vol. 608, p. 125594, 2021.

[39] Alvares Rodrigues, L., K. Koibuchi Sakane, E. Alves Nunes Simonetti, and G. Patrocínio Thim, "Cr total removal in aqueous solution by PHENOTAN AP based tannin gel (TFC)," *Journal of Environmental Chemical Engineering*, vol. 3, no. 2, pp. 725-733, 2015.

[40] Alvares Rodrigues, L., J. Parmentier, J.B. Parra, and G. Patrocínio Thim, "Preparation of nodular carbon cryogel from simple and inexpensive polycondensation reaction of commercial modified black wattle tannin," *Journal of Sol-Gel Science and Technology*, vol. 67, no. 3, pp. 519-526, 2013.

[41] Gong, Q.Q., X.Y. Guo, S. Liang, C. Wang, and Q.H. Tian, "Study on the adsorption behavior of modified persimmon powder biosorbent on Pt(IV)," *International Journal of Environmental Science and Technology*, vol. 13, no. 1, pp. 47-54, 2016.

[42] Vázquez, G., G. Antorrena, J. Gonzalez, and M.D. Doval, "Adsorption of heavy metal ions by chemically modified *Pinus pinaster* bark," *Bioresource Technology*, vol. 48, no. 3, pp. 251-255, 1994.

[43] Vázquez, G., J. González-Álvarez, S. Freire, M. López-Lorenzo, and G. Antorrena, "Removal of cadmium and mercury ions from aqueous solution by sorption on treated *Pinus pinaster* bark: kinetics and isotherms," *Bioresource Technology*, vol. 82, no. 3, pp. 247-251, 2002.

[44] Palma, G., J. Freer, and J. Baeza, "Removal of metal ions by modified *Pinus radiata* bark and tannins from water solutions," *Water Research*, vol. 37, no. 20, pp. 4974-4980, 2003.

[45] Alhumaimess, M.S., I.H. Alsohaimi, A.A. Alqadami, M.A. Khan, M.M. Kamel, O. Aldosari, M.R. Siddiqui, and A.E. Hamedelniel, "Recyclable glutaraldehyde cross-linked polymeric tannin to sequester hexavalent uranium from aqueous solution," *Journal of Molecular Liquids*, 2019.

[46] Kamel, M.M., A.M. Abd El-Mgeed, and M.A. El-Hewaihy, "Synthesis of a novel tannin–formaldehyde resin from Acacia nilotica fruit extract and its viability for adsorption of manganese from ground water," *Water Science and Technology: Water Supply*, vol. 13, no. 5, pp. 1236-1248, 2013.

[47] Li, X., Z. Wang, J. Ning, M. Gao, W. Jiang, Z. Zhou, and G. Li, "Preparation and characterization of a novel polyethyleneimine cation-modified persimmon tannin bioadsorbent for anionic dye adsorption," *Journal of Environmental Management*, vol. 217, pp. 305-314, 2018.

[48] Shilowa, P.M., B.J. Okoli, O.T. Olaniyan, J.S. Modise, and F. Mtunzi, "Immobilised Tannin: Efficient Trap for Nickel and Lead Ions in Aqueous Solution," *Environmental Challenges*, p. 100058, 2021.

[49] Gurung, M., B.B. Adhikari, H. Kawakita, K. Ohto, K. Inoue, and S. Alam, "Recovery of Au(III) by using low cost adsorbent prepared from persimmon tannin extract," *Chemical Engineering Journal*, vol. 174, no. 2-3, pp. 556-563, 2011.

[50] Inoue, K., H. Paudyal, H. Nakagawa, H. Kawakita, and K. Ohto, "Selective adsorption of chromium(VI) from zinc(II) and other metal ions using persimmon waste gel," *Hydrometallurgy*, vol. 104, no. 2, pp. 123-128, 2010.

[51] Gurung, M., B.B. Adhikari, H. Kawakita, K. Ohto, K. Inoue, and S. Alam, "Recovery of gold and silver from spent mobile phones by means of acidothiourea leaching followed by adsorption using biosorbent prepared from persimmon tannin," *Hydrometallurgy*, vol. 133, pp. 84-93, 2013.

[52] Laksmi, M.P., D.A. Nurani, and D.U.C. Rahayu, "Polymerization of the tannin extract from the leave of *Acacia mangium* and its application as an adsorbent for the removal of lead," in *Basic and*

Applied Sciences Interdisciplinary Conference 2017, 18-19 Aug. 2017, UK, 2020, vol. 1442, p. 012058 (6 pp.): IOP Publishing.

[53] Gurung, M., B.B. Adhikari, H. Kawakita, K. Ohto, K. Inoue, and S. Alam, "Selective Recovery of Precious Metals from Acidic Leach Liquor of Circuit Boards of Spent Mobile Phones Using Chemically Modified Persimmon Tannin Gel," *Industrial & Engineering Chemistry Research*, vol. 51, no. 37, pp. 11901-11913, 2012.

[54] Parajuli, D., H. Kawakita, K. Inoue, K. Ohto, and K. Kajiyama, "Persimmon peel gel for the selective recovery of gold," *Hydrometallurgy*, vol. 87, no. 3-4, pp. 133-139, 2007.

[55] Xiong, Y., C.R. Adhikari, H. Kawakita, K. Ohto, K. Inoue, and H. Harada, "Selective recovery of precious metals by persimmon waste chemically modified with dimethylamine," *Bioresource Technology*, vol. 100, no. 18, pp. 4083-4089, 2009.

[56] Xiong, Y., C.B. Chen, X.J. Gu, B.K. Biswas, W.J. Shan, Z.N. Lou, D.W. Fang, and S.L. Zang, "Investigation on the removal of Mo(VI) from Mo-Re containing wastewater by chemically modified persimmon residua," *Bioresource Technology*, vol. 102, no. 13, pp. 6857-6862, 2011.

[57] Wang, Y., F. Ren, Z. Lou, W. Shan, Y. Wang, and Y. Xiong, "Hydroxyl-assisted nitrogen-containing group modified persimmon tannin with enhanced recovery capacity for Mo(VI) in aqueous solution," *Journal of Chemical Technology & Biotechnology*, vol. 96, no. 1, pp. 188-198, 2021.

[58] Lou, Z.-N., Y.-X. Li, F.-Q. Ren, Q. Zhang, L. Wan, Z.-Q. Xing, S.-L. Zang, and Y. Xiong, "Selectivity recovery of molybdenum(VI) from rhenium(VII) by amine-modified persimmon waste," *Rare Metals*, vol. 35, no. 6, pp. 502-508, 2016.

[59] Gurung, M., B.B. Adhikari, S. Alam, H. Kawakita, K. Ohto, and K. Inoue, "Persimmon tannin-based new sorption material for resource recycling and recovery of precious metals," *Chemical Engineering Journal*, vol. 228, pp. 405-414, 2013.

[60] Shan, W.J., F.Q. Ren, Q. Zhang, L. Wan, Z.Q. Xing, Z.N. Lou, and Y. Xiong, "Enhanced adsorption capacity and selectivity towards molybdenum in wastewater by a persimmon tannin waste based new adsorbent," *Journal of Chemical Technology and Biotechnology*, vol. 90, no. 5, pp. 888-895, 2015.

[61] Zhang, S., Y. Ji, F. Ao, Y. Wang, J. Zhao, and S. Chen, "Selective adsorption of Au^{III} from aqueous solution using 2,5-Dimercapto-1,3,4-thiadiazole modified persimmon tannin," *Journal of the Brazilian Chemical Society*, vol. 29, no. 7, pp. 1487-1498, 2018.

[62] Zhang, S., J. Dang, J. Lin, M. Liu, M. Zhang, and S. Chen, "Selective enrichment and separation of Ag(I) from electronic waste leachate by chemically modified persimmon tannin," *Journal of Environmental Chemical Engineering*, vol. 9, no. 1, p. 104994, 2021.

[63] Gurung, M., B.B. Adhikari, K. Khunathai, H. Kawakita, K. Ohto, H. Harada, and K. Inoue, "Quaternary Amine Modified Persimmon Tannin Gel: An Efficient Adsorbent for the Recovery of Precious Metals from Hydrochloric Acid Media," *Separation Science and Technology*, vol. 46, no. 14, pp. 2250-2259, 2011.

[64] Zhao, C., H. Zheng, Y. Sun, B. Liu, Y. Zhou, Y. Liu, and X. Zheng, "Fabrication of tannin-based dithiocarbamate biosorbent and its application for Ni(II) ion removal," *Water, Air, & Soil Pollution*, vol. 228, no. 11, p. 409, 2017.

[65] Jiang, W., Y. Xing, T. Wang, J. Liao, J. He, W. Chen, J. Wang, and L. Mo, "Green Synthesis of Tannin-Polyethylenimine Adsorbent for Removal of Cu(II) from Aqueous Solution," *Journal of Chemical & Engineering Data*, vol. 65, no. 11, pp. 5593-5605, 2020.

[66] Shang, Y., G. Zhu, D. Yan, Q. Liu, T. Gao, and G. Zhou, "Tannin cross-linked polyethyleneimine for highly efficient removal of hexavalent chromium," *Journal of the Taiwan Institute of Chemical Engineers*, vol. 119, pp. 52-59, 2021.

[67] Liu, Q., Q. Liu, B. Liu, T. Hu, W. Liu, and J. Yao, "Green synthesis of tannin-hexamethylendiamine based adsorbents for efficient removal of Cr(VI)," *Journal of Hazardous Materials*, vol. 352, pp. 27-35, 2018.

[68] Benjamin, M.M., R.S. Sletten, R.P. Bailey, and T. Bennett, "Sorption and filtration of metals using iron-oxide-coated sand," *Water Research*, vol. 30, no. 11, pp. 2609-2620, 1996.

[69] Bacelo, H., A.M.A. Pintor, S.C.R. Santos, R.A.R. Boaventura, and C.M.S. Botelho, "Performance and prospects of different adsorbents for phosphorus uptake and recovery from water," *Chemical Engineering Journal*, vol. 381, 2020.

[70] Arcibar-Orozco, J.A., D.B. Josue, J.C. Rios-Hurtado, and J.R. Rangel-Mendez, "Influence of iron content, surface area and charge distribution in the arsenic removal by activated carbons," *Chemical Engineering Journal*, vol. 249, pp. 201-209, 2014.

[71] Das, B., R.R. Devi, I.M. Umlong, K. Borah, S. Banerjee, and A.K. Talukdar, "Arsenic(III) adsorption on iron acetate coated activated alumina: thermodynamic, kinetics and equilibrium approach," *Journal of Environmental Health Science and Engineering*, vol. 11, 2013.

[72] Fu, Y., J.Y. Wang, Q.X. Liu, and H.B. Zeng, "Water-dispersible magnetic nanoparticle-graphene oxide composites for selenium removal," *Carbon*, vol. 77, pp. 710-721, 2014.

[73] Vieira, B.R.C., A.M.A. Pintor, R.A.R. Boaventura, C.M.S. Botelho, and S.C.R. Santos, "Arsenic removal from water using iron-coated seaweeds," *Journal of Environmental Management*, vol. 192, pp. 224-233, 2017.

[74] Pintor, A.M.A., B.R.C. Vieira, S.C.R. Santos, R.A.R. Boaventura, and C.M.S. Botelho, "Arsenate and arsenite adsorption onto iron-coated cork granulates," *Science of the Total Environment*, vol. 642, pp. 1075-1089, 2018.

[75] Pintor, A.M.A., B.R.C. Vieira, R.A.R. Boaventura, and C.M.S. Botelho, "Removal of antimony from water by iron-coated cork granulates," *Separation and Purification Technology*, vol. 233, p. 116020, 2020.

[76] Pintor, A.M.A., C.C. Brandão, R.A.R. Boaventura, and C.M.S. Botelho, "Multicomponent adsorption of pentavalent As, Sb and P onto iron-coated cork granulates," *Journal of Hazardous Materials*, p. 124339, 2020.

[77] Pintor, A.M.A., B.R.C. Vieira, C.C. Brandão, R.A.R. Boaventura, and C.M.S. Botelho, "Complexation mechanisms in arsenic and phosphorus adsorption onto iron-coated cork granulates," *Journal of Environmental Chemical Engineering*, vol. 8, no. 5, p. 104184, 2020.

[78] Huang, X., X.P. Liao, and B. Shi, "Hg(II) removal from aqueous solution by bayberry tannin-immobilized collagen fiber," *Journal of Hazardous Materials*, vol. 170, no. 2-3, pp. 1141-1148, 2009.

[79] Liao, X., M. Zhang, and B. Shi, "Collagen-fiber-immobilized tannins and their adsorption of Au(III)," *Industrial & Engineering Chemistry Research*, vol. 43, pp. 2222-2227, 2004.

[80] Ma, H.W., X.P. Liao, X. Liu, and B. Shi, "Recovery of platinum(IV) and palladium(II) by bayberry tannin immobilized collagen fiber membrane from water solution," *Journal of Membrane Science*, vol. 278, no. 1-2, pp. 373-380, 2006.

[81] Wang, R., X. Liao, and B. Shi, "Adsorption Behaviors of Pt(II) and Pd(II) on Collagen Fiber Immobilized Bayberry Tannin," *Industrial & Engineering Chemistry Research*, vol. 44, no. 12, pp. 4221-4226, 2005.

[82] Liao, X., Z. Lu, X. Du, X. Liu, and B. Shi, "Collagen Fiber Immobilized *Myrica rubra* Tannin and Its Adsorption to UO_2^{2+}," *Environmental Science & Technology*, vol. 38, no. 1, pp. 324-328, 2004.

[83] Liao, X., Z. Lu, M. Zhang, X. Liu, and B. Shi, "Adsorption of Cu(II) from aqueous solutions by tannins immobilized on collagen," *Journal of Chemical Technology & Biotechnology*, vol. 79, no. 4, pp. 335-342, 2004.

[84] Liao, X.P., L. Li, and B. Shi, "Adsorption recovery of thorium(IV) by *Myrica rubra* tannin and larch tannin immobilized onto collagen fibres," *Journal of Radioanalytical and Nuclear Chemistry*, vol. 260, no. 3, pp. 619-625, 2004.

[85] Liao, H., J. Yu, W. Zhu, M. Kuang, T. Duan, Y. Zhang, X. Lin, X. Luo, and J. Zhou, "Nano-zero-valent Fe/Ni particles loaded on collagen fibers immobilized by bayberry tannin as an effective reductant for uranyl in aqueous solutions," *Applied Surface Science*, Article vol. 507, 2020, Art. no. 145075.

[86] Cui, J., Z.M. Wang, F.L. Liu, P.B. Dai, R. Chen, and H.Y. Zhou, "Preparation of persimmon tannins immobilized on collagen adsorbent and research on its adsorption to Cr(VI)," in *Materials Science Forum*, 2013, vol. 743, pp. 523-530: Trans Tech Publications.

[87] Liu, F.L., Z.M. Wang, H.G. Zhang, G.Y. Li, and H.Y. Zhou, "Adsorption of In^{3+} from aqueous solutions by persimmon tannins-immobilized collagen fiber," in *Advanced Materials Research*, 2013, vol. 788, pp. 114-118: Trans Tech Publications.

[88] Liu, F., Z. Wang, and G. Li, "Adsorption of Ag^{+} by persimmon tannins immobilized on collagen fiber," *Desalination and Water Treatment*, vol. 52, no. 37-39, pp. 7172-7179, 2014.

[89] Zeng, Y.H., X.P. Liao, Q. He, and B. Shi, "Recovery of Th(IV) from aqueous solution by reassembled collagen-tannin fiber adsorbent," *Journal of Radioanalytical and Nuclear Chemistry*, vol. 280, no. 1, pp. 91-98, 2009.

[90] Sun, X., X. Huang, X.P. Liao, and B. Shi, "Adsorptive removal of Cu(II) from aqueous solutions using collagen-tannin resin," *Journal of Hazardous Materials*, vol. 186, no. 2-3, pp. 1058-63, 2011.

[91] Xu, Q., Y. Wang, L. Jin, Y. Wang, and M. Qin, "Adsorption of Cu(II), Pb(II) and Cr(VI) from aqueous solutions using black wattle tannin-immobilized nanocellulose," *Journal of Hazardous Materials*, vol. 339, pp. 91-99, 2017.

[92] Pei, Y., X. Wu, G. Xu, Z. Sun, X. Zheng, J. Liu, and K. Tang, "Tannin-immobilized cellulose microspheres as effective adsorbents for removing cationic dye (Methylene Blue) from aqueous solution," *Journal of Chemical Technology and Biotechnology*, vol. 92, no. 6, pp. 1276-84, 2017.

[93] Pei, Y., G. Xu, X. Wu, K. Tang, and G. Wang, "Removing Pb(II) Ions from Aqueous Solution by a Promising Absorbent of Tannin-Immobilized Cellulose Microspheres," *Polymers*, vol. 11, no. 3, 2019.

[94] Liu, J., Z. Yu, Q. Li, Y. Lv, C. Lin, J. Huang, Y. Liu, and M. Liu, "Adsorption behavior of gardenia yellow pigment on embedded spherical cellulose adsorbent," *RSC Advances*, vol. 11, no. 8, pp. 4407-4416, 2021.

[95] Pei, Y., S. Chu, Y. Chen, Z. Li, J. Zhao, S. Liu, X. Wu, J. Liu, X. Zheng, and K. Tang, "Tannin-immobilized cellulose hydrogel fabricated by a homogeneous reaction as a potential adsorbent for removing cationic organic dye from aqueous solution," *International Journal of Biological Macromolecules*, vol. 103, pp. 254-260, 2017.

[96] Ning, F., J. Zhang, M. Kang, C. Ma, H. Li, and Z. Qiu, "Hydroxyethyl cellulose hydrogel modified with tannic acid as methylene blue adsorbent," *Journal of Applied Polymer Science*, vol. 138, no. 8, p. 49880, 2021.

[97] Ji, Y., Y. Wen, Z. Wang, S. Zhang, and M. Guo, "Eco-friendly fabrication of a cost-effective cellulose nanofiber-based aerogel for multifunctional applications in Cu(II) and organic pollutants removal," *Journal of Cleaner Production*, Article vol. 255, 2020, Art. no. 120276.

[98] Wang, G., Y. Chen, G. Xu, and Y. Pei, "Effective removing of methylene blue from aqueous solution by tannins immobilized on cellulose microfibers," *International Journal of Biological Macromolecules*, vol. 129, pp. 198-206, 2019.

[99] Qiu, X., Y. Shen, R. Yang, H. Zhang, and S. Zhao, "Adsorption of RE^{3+} from aqueous solutions by bayberry tannin immobilized on chitosan," *Environmental Technology*, vol. 40, no. 2, pp. 202-209, 2019.

[100] Sun, H., N. Xia, Z. Liu, F. Kong, and S. Wang, "Removal of copper and cadmium ions from alkaline solutions using chitosan-tannin functional paper materials as adsorbent," *Chemosphere*, vol. 236, p. 124370, 2019.

[101] Jing, Y., Y. Chen, X. Wang, and L. Nengzi, "Adsorption of La^{3+}, Ce^{3+} from Aqueous Solutions by Bayberry Tannin Grafted Chitosan," in *IOP Conference Series: Earth and Environmental Science*, 2018, vol. 153.

[102] Li, X., Z. Wang, H. Liang, J. Ning, G. Li, and Z. Zhou, "Chitosan modification persimmon tannin bioadsorbent for highly efficient removal of Pb(II) from aqueous environment: the adsorption equilibrium, kinetics and thermodynamics," *Environmental Technology (United Kingdom)*, Article vol. 40, no. 1, pp. 112-124, 2019.

[103] Badawi, M.A., N.A. Negm, M.T.H. Abou Kana, H.H. Hefni, and M.M. Abdel Moneem, "Adsorption of aluminum and lead from wastewater by chitosan-tannic acid modified biopolymers: Isotherms, kinetics, thermodynamics and process mechanism," *International Journal of Biological Macromolecules*, Article vol. 99, pp. 465-476, 2017.

[104] Peng, Y., H. Huang, Y. Wu, S. Jia, F. Wang, J. Ma, Y. Liao, and H. Mao, "Plant tannin modified chitosan microfibers for efficient adsorptive removal of Pb^{2+} at low concentration," *Industrial Crops and Products,* Article vol. 168, 2021, Art. no. 113608.

[105] Wang, Z., J. Ning, C. Yang, X. Li, M. Gao, G. Li, and Z. Zhou, "Functionalization of persimmon tannin with chitosan for the removal of cationic and anionic dyes from aqueous solutions," *Desalination and Water Treatment,* Article vol. 150, pp. 339-347, 2019.

[106] Meng, J., X. Lin, H. Li, Y. Zhang, J. Zhou, Y. Chen, R. Shang, and X. Luo, "Adsorption capacity of kelp-like electrospun nanofibers immobilized with bayberry tannin for uranium(VI) extraction from seawater," *RSC Advances,* vol. 9, no. 14, pp. 8091-8103, 2019.

[107] Meng, J., X. Lin, J. Zhou, R. Zhang, Y. Chen, X. Long, R. Shang, and X. Luo, "Preparation of tannin-immobilized gelatin/PVA nanofiber band for extraction of uranium (VI) from simulated seawater," *Ecotoxicology and Environmental Safety,* vol. 170, pp. 9-17, 2019.

[108] Hassoune, J., S. Tahiri, M. El Krati, M. Luisa Cervera, and M. De La Guardia, "Removal of Hexavalent Chromium from Aqueous Solutions Using Biopolymers," *Journal of Environmental Engineering (United States),* Article vol. 144, no. 8, 2018, Art. no. 04018060.

[109] Zhang, X., X. Lin, Y. He, and X. Luo, "Phenolic hydroxyl derived copper alginate microspheres as superior adsorbent for effective adsorption of tetracycline," *International Journal of Biological Macromolecules,* vol. 136, pp. 445-459, 2019.

[110] Sun, X., J. Zhang, G. Ding, and Y. You, "Tannin-based biosorbent encapsulated into calcium alginate beads for Cr(VI) removal," *Water Science and Technology,* vol. 81, no. 5, pp. 936-948, 2020.

[111] Liu, F., G. Peng, T. Li, G. Yu, and S. Deng, "Au(III) adsorption and reduction to gold particles on cost-effective tannin acid immobilized dialdehyde corn starch," *Chemical Engineering Journal,* vol. 370, pp. 228-236, 2019.

[112] Roy, A., "Removal of color from real textile dyeing effluent utilizing tannin immobilized jute fiber as biosorbent: optimization with response surface methodology," *Environmental Science and Pollution Research,* vol. 28, no. 10, pp. 12011-12025, 2021.

[113] Huang, X., X.P. Liao, and B. Shi, "Tannin-immobilized mesoporous silica bead (BT-SiO_2) as an effective adsorbent of Cr(III) in aqueous solutions," *Journal of Hazardous Materials,* vol. 173, no. 1-3, pp. 33-39, 2010.

[114] Huang, X., Y.P. Wang, X.P. Liao, and B. Shi, "Adsorptive recovery of Au^{3+} from aqueous solutions using bayberry tannin-immobilized mesoporous silica," *Journal of Hazardous Materials,* vol. 183, no. 1-3, pp. 793-798, 2010.

[115] Binaeian, E., N. Seghatoleslami, and M.J. Chaichi, "Synthesis of oak gall tannin-immobilized hexagonal mesoporous silicate (OGT-HMS) as a new super adsorbent for the removal of anionic dye from aqueous solution," *Desalination and Water Treatment,* vol. 57, no. 18, pp. 8420-8436, 2016.

[116] Leite, A.J.B., E.C. Lima, G.S. dos Reis, P.S. Thue, C. Saucier, F.S. Rodembusch, S.L.P. Dias, C.S. Umpierres, and G.L. Dotto, "Hybrid adsorbents of tannin and APTES (3-aminopropyltriethoxysilane) and their application for the highly efficient removal of acid red 1 dye from aqueous solutions," *Journal of Environmental Chemical Engineering,* vol. 5, no. 5, pp. 4307-4318, 2017.

[117] Huang, Q., M. Liu, J. Zhao, J. Chen, G. Zeng, H. Huang, J. Tian, Y. Wen, X. Zhang, and Y. Wei, "Facile preparation of polyethylenimine-tannins coated SiO_2 hybrid materials for Cu^{2+} removal," *Applied Surface Science,* vol. 427, pp. 535-544, 2018.

[118] Wang, Z., X. Li, H. Liang, J. Ning, Z. Zhou, and G. Li, "Equilibrium, kinetics and mechanism of Au^{3+}, Pd^{2+} and Ag^{+} ions adsorption from aqueous solutions by graphene oxide functionalized persimmon tannin," *Material Science and Engineering: C Materials for Biological Application,* vol. 79, pp. 227-236, 2017.

[119] Wang, Z., M. Gao, X. Li, J. Ning, Z. Zhou, and G. Li, "Efficient adsorption of methylene blue from aqueous solution by graphene oxide modified persimmon tannins," *Materials Science and Engineering: C,* vol. 108, p. 110196, 2020.

[120] Zhang, Y., X. Li, L. Gong, Z. Xing, Z. Lou, W. Shan, and Y. Xiong, "Persimmon tannin/graphene oxide composites: Fabrication and superior adsorption of germanium ions in aqueous solution," *Journal of the Taiwan Institute of Chemical Engineers*, vol. 104, pp. 310-317, 2019.

[121] Al-Kinani, A., M. Gheibi, and M. Eftekhari, "Graphene oxide–tannic acid nanocomposite as an efficient adsorbent for the removal of malachite green from water samples," *Modeling Earth Systems and Environment*, vol. 5, no. 4, pp. 1627-1633, 2019.

[122] Chang, Z., L. Yang, K. Zhang, W. Hu, C. Ni, P. Shao, H. Shi, K. Yu, and X. Luo, "Weak electric field enabling enhanced selectivity of tannic acid-graphene aerogels for Pb^{2+} harvesting from wastewater," *Chemical Engineering Journal*, p. 129144, 2021.

[123] Viswanathan, T., G. Gunawan, S. Bourdo, V. Saini, J. Moran, L. Pack, and S. Owen, "Evaluation of a renewable resource-based carbon-iron oxide nanocomposite for removal of arsenic from contaminated water," *Journal of Macromolecular Science, Part A*, vol. 48, no. 5, pp. 348-354, 2011.

[124] Gao, M., Z. Wang, C. Yang, J. Ning, Z. Zhou, and G. Li, "Novel magnetic graphene oxide decorated with persimmon tannins for efficient adsorption of malachite green from aqueous solutions," *Colloids and Surfaces A: Physicochemical and Engineering Aspects*, vol. 566, pp. 48-57, 2019.

[125] Gao, L., Z. Wang, C. Qin, Z. Chen, M. Gao, N. He, X. Qian, Z. Zhou, and G. Li, "Preparation and application of iron oxide/persimmon tannin/graphene oxide nanocomposites for efficient adsorption of erbium from aqueous solution," *Journal of Rare Earths*, vol. 38, no. 12, pp. 1344-1353, 2020.

[126] Fan, R., H. Min, X. Hong, Q. Yi, W. Liu, Q. Zhang, and Z. Luo, "Plant tannin immobilized Fe_3O_4@SiO_2 microspheres: A novel and green magnetic bio-sorbent with superior adsorption capacities for gold and palladium," *Journal of Hazardous Materials*, vol. 364, pp. 780-790, 2019.

[127] Luo, H., S. Zhang, X. Li, X. Liu, Q. Xu, J. Liu, and Z. Wang, "Tannic acid modified Fe_3O_4 core–shell nanoparticles for adsorption of Pb^{2+} and Hg^{2+}," *Journal of the Taiwan Institute of Chemical Engineers*, vol. 72, pp. 163-170, 2017.

[128] Wang, C., J. Zhao, S. Wang, L. Zhang, N. Liu, and B. Zhang, "Selective capture models and mechanisms of Pb(II) from wastewater using tannic-functionalized nickel-iron oxide Nanoparticles," *Colloids and Surfaces A: Physicochemical and Engineering Aspects*, vol. 570, pp. 265-273, 2019.

[129] Qian, Y., S. Chen, C. He, C. Ye, W. Zhao, S. Sun, Y. Xie, and C. Zhao, "Green Fabrication of Tannic Acid-Inspired Magnetic Composite Nanoparticles toward Cationic Dye Capture and Selective Degradation," *ACS Omega*, vol. 5, no. 12, pp. 6566-6575, 2020.

[130] Huang, L., Q. Shuai, and S. Hu, "Tannin-based magnetic porous organic polymers as robust scavengers for methylene blue and lead ions," *Journal of Cleaner Production*, vol. 215, pp. 280-289, 2019.

[131] Sánchez-Martín, J., J. Beltrán-Heredia, A. Delgado-Regaña, M.A. Rodríguez-González, and F. Rubio-Alonso, "Adsorbent tannin foams: New and complementary applications in wastewater treatment," *Chemical Engineering Journal*, vol. 228, pp. 575-582, 2013.

[132] Sánchez-Martín, J., J. Beltrán-Heredia, A. Delgado-Regaña, M.A. Rodríguez-González, and F. Rubio-Alonso, "Optimization of tannin rigid foam as adsorbents for wastewater treatment," *Industrial Crops and Products*, vol. 49, pp. 507-514, 2013.

[133] Lacoste, C., M.C. Basso, A. Pizzi, M.P. Laborie, A. Celzard, and V. Fierro, "Pine tannin-based rigid foams: Mechanical and thermal properties," *Industrial Crops and Products*, vol. 43, pp. 245-250, 2013.

[134] Lacoste, C., A. Pizzi, M.C. Basso, M.-P. Laborie, and A. Celzard, "*Pinus pinaster* tannin/furanic foams: PART I. Formulation," *Industrial Crops and Products*, vol. 52, pp. 450-456, 2014.

[135] Hamadi, Z., R. Chaid, M. Kebir, S. Amirou, H. Essawy, and A. Pizzi, "Adsorption of Cr(VI) from Aqueous Solutions Using Algerian Pinus Halepensis Tannin Foam," *Polymer(Korea)*, vol. 44, no. 4, pp. 425-435, 2020.

[136] Issaoui, H., F. Sallem, J. Lafaille, B. Grassl, and F. Charrier–El Bouhtoury, "Biosorption of Heavy Metals from Water onto Phenolic Foams Based on Tannins and Lignin Alkaline Liquor," *International Journal of Environmental Research*, pp. 1-13, 2021.

[137] Ungureanu, G., S. Santos, R. Boaventura, and C. Botelho, "Biosorption of Antimony by brown algae *S. muticum* and *A. nodosum*," *Environmental Engineering and Management Journal,* vol. 14, no. 2, pp. 455-463, 2015.

[138] *Water - Determination of True Colour. NP 627:1972*, 1972.

[139] Eaton, A.D., L.S. Clesceri, E.W. Rice, A.E. Greenberg, and M.A.H. Franson, "Standard methods for the examination of water and wastewater," *American Public Health Association,* vol. 1015, 2005.

[140] Koopmann, A.-K., C. Schuster, J. Torres-Rodríguez, S. Kain, H. Pertl-Obermeyer, A. Petutschnigg, and N. Hüsing, "Tannin-Based Hybrid Materials and Their Applications: A Review," *Molecules,* vol. 25, no. 21, p. 4910, 2020.

[141] Grasel, F.d.S., M.F. Ferrão, and C.R. Wolf, "Development of methodology for identification the nature of the polyphenolic extracts by FTIR associated with multivariate analysis," *Spectrochimica Acta Part A: Molecular and Biomolecular Spectroscopy,* vol. 153, pp. 94-101, 2016.

[142] Ricci, A., K.J. Olejar, G.P. Parpinello, P.A. Kilmartin, and A. Versari, "Application of Fourier Transform Infrared (FTIR) Spectroscopy in the Characterization of Tannins," *Applied Spectroscopy Reviews,* vol. 50, no. 5, pp. 407-442, 2015.

[143] Ping, L., A. Pizzi, Z.D. Guo, and N. Brosse, "Condensed tannins from grape pomace: characterization by FTIR and MALDI TOF and production of environment friendly wood adhesive," *Industrial Crops and Products,* vol. 40, pp. 13-20, 2012.

[144] Çakar, S. and M. Özacar, "Fe–tannic acid complex dye as photo sensitizer for different morphological ZnO based DSSCs," *Spectrochimica Acta Part A: Molecular and Biomolecular Spectroscopy,* vol. 163, pp. 79-88, 2016.

[145] Gust, J. and J. Suwalski, "Use of Mossbauer-Spectroscopy to Study Reaction-Products of Polyphenols and Iron Compounds," *Corrosion,* vol. 50, no. 5, pp. 355-365, 1994.

[146] Hao, B., F. Wang, H. Huang, Y. Wu, S. Jia, Y. Liao, and H. Mao, "Tannin foam immobilized with ferric ions for efficient removal of ciprofloxacin at low concentrations," *Journal of Hazardous Materials,* vol. 414, p. 125567, 2021.

[147] *Decreto-Lei n.º 152/2017*, Diário da República n.º 235/2017, Série I de 2017-12-07, Lisboa, Portugal, 2017.

[148] Cheng, K., Y.-n. Wu, B. Zhang, and F. Li, "New insights into the removal of antimony from water using an iron-based metal-organic framework: Adsorption behaviors and mechanisms," *Colloids and Surfaces A: Physicochemical and Engineering Aspects,* vol. 602, p. 125054, 2020.

[149] Antunes, E., M.V. Jacob, G. Brodie, and P.A. Schneider, "Isotherms, kinetics and mechanism analysis of phosphorus recovery from aqueous solution by calcium-rich biochar produced from biosolids via microwave pyrolysis," *Journal of Environmental Chemical Engineering,* vol. 6, no. 1, pp. 395-403, 2018.

[150] Dai, L., F. Tan, H. Li, N. Zhu, M. He, Q. Zhu, G. Hu, L. Wang, and J. Zhao, "Calcium-rich biochar from the pyrolysis of crab shell for phosphorus removal," *Journal of Environmental Management,* vol. 198, no. Pt 1, pp. 70-74, 2017.

[151] Jung, K.-W., T.-U. Jeong, H.-J. Kang, and K.-H. Ahn, "Characteristics of biochar derived from marine macroalgae and fabrication of granular biochar by entrapment in calcium-alginate beads for phosphate removal from aqueous solution," *Bioresource Technology,* vol. 211, pp. 108-116, 2016.

[152] Xu, N., Y. Li, L. Zheng, Y. Gao, H. Yin, J. Zhao, Z. Chen, J. Chen, and M. Chen, "Synthesis and application of magnesium amorphous calcium carbonate for removal of high concentration of phosphate," *Chemical Engineering Journal,* vol. 251, pp. 102-110, 2014.

[153] Suresh Kumar, P., T. Prot, L. Korving, K.J. Keesman, I. Dugulan, M.C.M. van Loosdrecht, and G.-J. Witkamp, "Effect of pore size distribution on iron oxide coated granular activated carbons for phosphate adsorption – Importance of mesopores.," *Chemical Engineering Journal,* vol. 326, pp. 231-239, 2017.

[154] Yang, Q., X.L. Wang, W. Luo, J. Sun, Q.X. Xu, F. Chen, J.W. Zhao, S.N. Wang, F.B. Yao, D.B. Wang, X.M. Li, and G.M. Zeng, "Effectiveness and mechanisms of phosphate adsorption on iron-modified biochars derived from waste activated sludge," *Bioresource Technology,* vol. 247, pp. 537-544, 2018.

CHAPTER IV

UPTAKE OF ARSENIC

1. Literature Review

Arsenic (As) is a metalloid ubiquitous in the environment and highly toxic to all life forms. It exists in four oxidation states: As(–III) (arsines), As (elemental arsenic), As(III) (arsenite), and As(V) (arsenate). In natural environment, arsenic appears more commonly in trivalent and pentavalent oxidation states, with As(V) being the most stable form [1, 2], and frequently combined with sulphur, oxygen and/or iron. As(V) is a thermodynamically stable state in aerobic water, while As(III) is predominant in reduced redox environments [3]. Moreover, arsenite is known to be more toxic than arsenate and inorganic As is more toxic than organic As [4]. Natural As species in aqueous solution include arsenious acids, arsenic acids, arsenites, arsenates, methylarsenic acid, dimethylarsinic acid, and arsine [5]. Arsenic speciation in aqueous solution depends on the redox potential and on solution pH and involves the presence of neutral species and oxyanions. Arsenic Eh-pH diagrams can be found in literature [6, 7]. Fig. IV.1 presents a simplified diagram of the distribution of As(V) and As(III) species as a function of pH. In typical aqueous conditions (pH 2-9), As(III) is more commonly present in neutral species while As(V) is expected to be found in the form of oxyanions at pH >2 and in neutral species below that value [8].

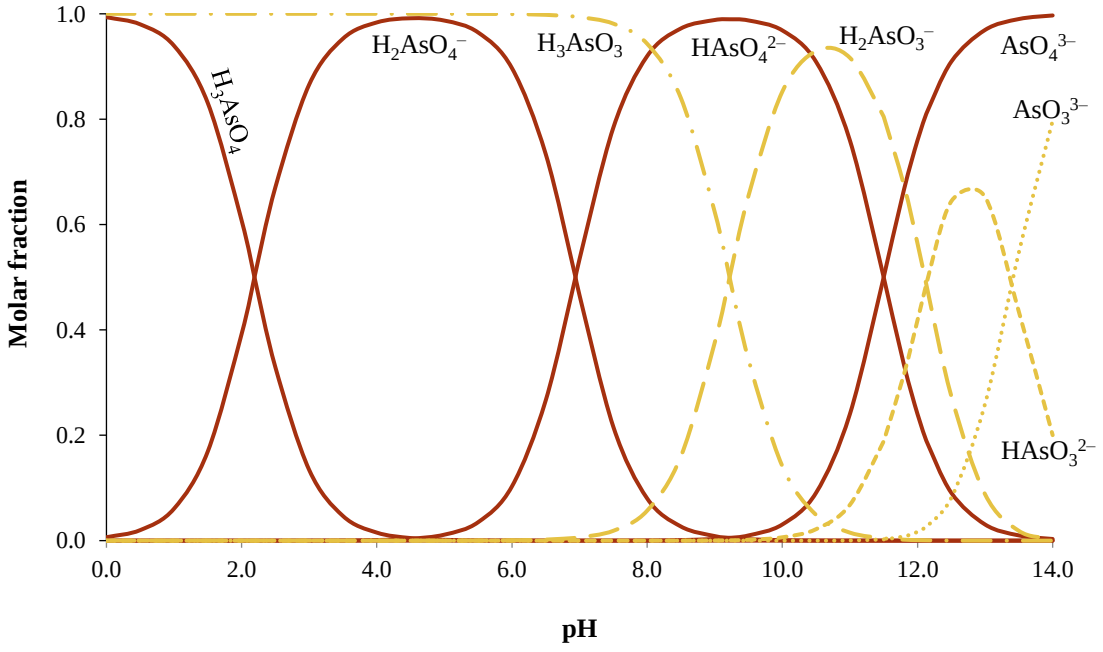

Fig. IV.1 Arsenate (orange solid lines) and arsenite (yellow dash lines) speciation as a function of pH.

Arsenic leaches into groundwater through natural weathering reactions, biological activity, geochemical reactions, volcanic emissions [5], and through human activities, such as mining, agriculture, fossil fuel combustion, and metal smelting [9, 10]. Long-term exposure to arsenic may contribute to the development of several types of cancer and non-carcinogenic diseases such as respiratory system dysfunction, injury to the central nervous system, and vascular diseases [11, 12]. The main reason for chronic arsenic poisoning worldwide is the consumption of As-contaminated water and food [13-15], with estimations suggesting that tens to hundreds of millions people may be currently at risk of long exposure to arsenic from water intake [15, 16]. Several countries have problems with arsenic-contaminated water, mainly in South Asia and South America [16-20] but also in Europe [21-23]. Moreover, there are also reports of contaminated surface and groundwaters in Portugal, mainly in the areas of abandoned mines, which are used either for human consumption or for irrigation of agricultural fields [24-26]. Arsenic-contaminated groundwaters have been reported as having concentration ranging from 0.5 mg L^{-1} to 5.0 g L^{-1} [27] while surface waters usually present lower levels (<8 mg L^{-1}) [9]. Wastewaters usually present concentrations within the range of 0.2-300 mg L^{-1} [28-32]. The legal standard for arsenic in drinking water in most countries ranges is below 50 μg L^{-1} [9]; the Portuguese legal standard is 10 μg L^{-1} [33]. For these reasons, the development of efficient and sustainable remediation techniques for arsenic-contaminated waters, either for drinking water production or for safe discharge of effluents, is of interest.

There are several methods for As removal from contaminated waters: coagulation/flocculation, membrane processes (micro-, ultra-, and nano-filtration, and reverse osmosis), electrochemical methods, phytoremediation, bioremediation, adsorption, and ion exchange [9, 34, 35]. Arsenate is easier to remove by precipitation, adsorption, or ion exchange than uncharged arsenite thus oxidation of As(III) is believed to be necessary to maximize the efficiency of the mentioned removal techniques [34, 36]. Adsorption processes are viewed as relatively simple methods, effective for the removal of various contaminants from aqueous solution. However, arsenic removal through adsorption is not easy because of its anionic nature in aqueous solution and difficult complexation with many functional groups, as shown by poor adsorption capacities of alginates beads [37] and chitosan [38]. Nevertheless, iron-based adsorbents (iron oxides, iron-impregnated materials, and bimetal oxides) have been identified as promising adsorbents presenting high removal efficiencies [39, 40]. One of the shortcomings of these adsorbents is related

to leaching (secondary pollution) or inadequate particle size for scale-up and for continuous systems (e.g., fixed-bed columns). Hence, some authors have been focusing in loading iron into supporting materials, such as activated carbons [41-44], activated alumina [45], cellulose [46], chitosan [47, 48], alginate beads [49], clays [50], poly(vinyl alcohol) nanofibers [51], seaweeds [52], and cork granulates [53-55]. Even though these adsorbents present properties adequate for scale-up and for solid:liquid separation, many of them cause iron leaching and are difficult to regenerate. Additionally, the chemical stability of the adsorbents is not always assessed, leading to inconclusive results on their applicability. Alternatively, the supporting material could be based on tannins since it presents several advantages: tannins can be extracted from natural source-materials, the cost of the procedure is potentially lower than conventional supporting materials (activated carbon and alumina), and the produced adsorbents can be obtained in different particle sizes. Table IV.1 presents maximum adsorption capacities of As(III) and As(V) by several adsorbents obtained in batch mode reported in recent years. Adsorption of arsenic in fixed-bed systems has been investigated with several adsorbents, mainly using biosorbents, usually treated with iron or, less frequently, with aluminium or zirconium [56].

As shown in Chapter III, tannin-adsorbents produced from different sources (tannic acid, persimmon, *Acacia*, bayberry) have been studied for the uptake of many adsorbates from water but scarcely for oxyanions, including arsenic. A few studies with tannin-adsorbents have been reported for arsenic uptake from water [57-60]. Tannin-formaldehyde and tannin-aniline-formaldehyde resins produced from commercial tannin powder in ammonia solutions were proven to be quite effective for As(III) (adsorption capacities of 140-300 mg g^{-1}) and for As(V) (5-25 mg g^{-1}) at a wide range of pH (2-10) [57, 58]. However, these resins presented very low particle sizes (<2 μm), making their application in fixed-bed systems or in continuous stirred adsorbers unfeasible. The remaining reports on arsenic uptake by tannin-adsorbents are based on materials prepared by procedures quite different from those reported here, namely a nanocomposite yielded after pyrolysis of precipitated iron-tannin complexes [59] and a Zr-based metal-organic framework with magnetic cores composed of Fe_3O_4 and tannic acid [60].

Besides preliminary studies carried out by the author [61], reports on arsenic-contaminated water remediation by pine bark tannin resins are not found in the literature. Hence, the potential of a pine tannin resin for arsenic uptake should be assessed. Unmodified tannin resins are not expected to be efficient whatsoever for arsenic [61]. However, the

iron-loading of tannin resins has been reported and the resulting adsorbent was shown to be efficient for phosphate uptake [62]. The predominant species of arsenic are neutral or negative (Fig. IV.1) and thus adsorption via electrostatic attraction is not expected to happen due to the negatively charged surface of tannin resin. Iron-loading of tannin resins could avoid this obstacle by creating specific adsorption sites since iron has a high affinity towards arsenic. Thus, the main goal of the work presented in this Chapter was the application of an iron-loaded tannin-adsorbent for arsenic uptake.

Table IV.1 Maximum adsorption capacities reported in literature for the uptake of As(III) and As(V) from aqueous solutions by various adsorbents.

Adsorbent	C_{in} (mg L^{-1})	pH	T (°C)	Q_m (mg g^{-1})	Ref.
As(III)					
Fe/Ca in-situ-impregnated activated carbons	0.05-1.0	7	4	3.385	[43]
Graphene oxide Fe_3O_4@CuO nanocomposite	3.75-75	7	25	72.36	[63]
Iron acetate coated activated alumina	0.40-0.52	7.4	28-38	0.09	[45]
Hydrous iron oxide-impregnated alginate beads	7-430	6	23	47.8	[49]
Iron-coated *S. muticum*	1-40	7	20	4	[52]
Iron-coated cork granulates	1-40	9	20	4.9	[53]
Zr-based MOF with Fe_3O_4@TA magnetic cores	0.5-40	7	20	97.8	[60]
Natural clay with iron, iron oxide and rice bran	0.5-100	7	25	19.06	[64]
Fe(III)-treated *Staphylococcus xylosus* biomass	0-250[a]	7	–	54.35	[65]
Iron oxides nanoparticles loaded bacterial EPS	0.25-20	7	–	12.4	[66]
Graphene oxide iron nanohybrid	0.1-550	7	22	306.10	[67]
As(V)					
Fe/Ca in-situ-impregnated activated carbons	0.05-1.0	7	4	3.385	[43]
Chitosan with magnetic nanoparticles	5-500	3	25	15.23	[48]
Hydrous iron oxide-impregnated alginate beads	10-550	6	23	55.1	[49]
Iron oxide nanoparticles dispersed on PVA nanofibers	0.25-1.5	3	25	52	[51]
Iron-coated *S. muticum*	1-40	7	20	7	[52]
Iron-coated cork granulates	1-40	3	20	4.3	[53]
Natural clay with iron, iron oxide and rice bran	0.5-100	7	25	13.33	[64]
Fe(III)-treated *Staphylococcus xylosus* biomass	0-200[a]	3	–	61.34	[65]
Iron oxides nanoparticles loaded bacterial EPS	0.25-20	7	–	31.8	[66]
Graphene oxide iron nanohybrid	0.1-550	7	22	431.41	[67]
Hybrid iron oxide silicates	0-100	7	–	300	[68]
Iron oxide modified clay-activated carbon	5-75	4.5	25	5.0	[69]
Unmodified iron-ore sludge	0-50	5.5	25	1.113	[70]
Graphene oxide Fe_3O_4@CuO nanocomposite	3.75-75	7	25	62.6	[63]
Fe_2O_3 nanocubes-impregnated graphene aerogel	5-70	5	35	217.34	[71]
Palm oil fuel ash	0-100	3	25	50.8	[72]
Modified saxaul tree ash	0.001-0.25	7	20-50	0.004	[73]
Acicular goethite nanoparticles	0-400[a]	6	25	20	[74]

a – Estimated range of equilibrium concentrations; MOF – metal organic frameworks; TA – tannic acid; PVA – poly(vinyl alcohol); EPS – exopolysaccharide.

2. Methodology

2.1. Adsorbent and Adsorbate

In every adsorption assay reported in this Chapter, the adsorbent used was the TRO-Fe (iron-loaded oxidized tannin resin, particle size <0.15 mm or 0.15-0.5 mm), which was obtained by the procedure described in Sections 2.2. and 3.2. of Chapter III.

As(III) and As(V) solutions were obtained by diluting lab-made standards prepared with As_2O_3 (1000±10 mg-As L^{-1}, 2-5 % HCl) and with $HAsNa_2O_4{\cdot}7H_2O$ (994±10 mg-As L^{-1}, 2 % HCl), respectively. As(III) standard solution was prepared by dissolution of the dried salt in 0.05 mol L^{-1} NaOH and posterior addition of concentrated HCl. As(V) standard solution was simply prepared by dissolution of $HAsNa_2O_4{\cdot}7H_2O$ in ultrapure water with addition of concentrated HCl.

2.2. Analytical Methods

Arsenic concentrations in solution were measured by atomic absorption spectrometry (AAS) with electrothermal atomization (*GBC* GF 3000 SenAA Dual spectrometer). After proper dilution, the concentrations were measured in the linear range of 3-50 µg L^{-1} (detection limit: 1.3 mg L^{-1}), adding nickel (5 µL of $NiNO_3$ solution, containing 150 mg-Ni L^{-1}, per 15 µL of sample injection) as chemical modifier, and using the following instrumental conditions: wavelength of 197.3 nm, with background correction, 1.0 nm slit width and 8 mA lamp current. Iron concentrations in solution were measured by AAS with air-acetylene flame (*GBC* 932 Plus spectrometer) at wavelength of 248.3 nm (linear range: 0.25-5 mg L^{-1}) or 386.0 nm (5-70 mg L^{-1}), slit width of 0.2 nm and using 5.0 mA lamp current.

Speciation of dissolved iron was assessed by the spectrometric method using phenanthroline (ISO 6332:1988) [75]: 1.0 mL of 1,10-phenanthroline 1 g L^{-1} and 1.0 mL of ammonium acetate buffer solution were added to 4.0 mL of sample. Colour intensity of the red-orange complex formed was measured by a double beam spectrophotometer (*VWR* UV-6300PC) at 510 nm before and after adding a spatula of ascorbic acid. The obtained values were respectively correlated with Fe(II) and total Fe levels, and Fe(III) was calculated by difference.

2.3. Adsorption Studies

Adsorption experiments were conducted in batch mode and were carried out by adding 0.2 g of TRO-Fe to an accurately measured volume of 20.0 mL of As(III) or As(V) solution, which makes up a solid:liquid ratio of 10 g L^{-1}, and suspensions were kept stirring for 20 h at constant temperature (20 ºC). Samples were then filtered using cellulose membrane filters (0.45 µm porosity) and the liquid phase analysed for total dissolved arsenic. The amount of As adsorbed per gram of adsorbent (q_t) was calculated by Eq. IV.1, where C_{in} is the initial As concentration, C_t is the As concentration at time t and S/L is the solid:liquid ratio.

$$q_t = \frac{C_{in} - C_t}{S/L} \qquad \textbf{Eq. IV.1}$$

For every sample, iron concentration in solution was determined by AAS to consider the iron leaching as a potential source for secondary pollution. Also, speciation of the iron present in the solution was analysed.

2.3.1. Effect of pH

The effect of pH on the adsorbed amount of As(III) and As(V) by TRO-Fe (<0.15 mm and 0.15-0.50 mm) was studied in the range 2-5. The pH range selected was based on the following reasons: (1) arsenic contaminated waters commonly present low pH; and (2) effective treatment techniques, other than adsorption (e.g., coagulation [52]), are available for high pH waters. The initial pH of the solutions was adjusted, using diluted HCl or NaOH solutions. Arsenic solutions (C_{in} = 5 mg L^{-1}) was continuously stirred with TRO-Fe particles. During the assays, pH was measured and, if necessary, readjusted to be approximately constant (maximum variations of 0.5). Samples were then filtered the liquid phase analysed for total dissolved arsenic.

2.3.2. Adsorption Kinetics

The effect of contact time on As(V) adsorption by TRO-Fe <0.15 mm was studied in batch mode with an adsorbent dosage of 10 g L^{-1} and at pH 3.0±0.5. Experiments were

conducted using different initial adsorbate concentrations (0.5 mg L^{-1}, 5 mg L^{-1}, and 10 mg L^{-1}). Arsenic solutions (10.0 mL) were continuously stirred with TRO-Fe particles (0.1 g) for different contact times. Solutions pH was initially adjusted to the desired value and remained constant throughout the assay. Suspensions were filtered and analysed for As concentration. Total iron dissolved in the solution was also measured.

Scanning electron microscopy (SEM) and energy dispersion spectroscopy (EDS) were used to observe the morphology and detect the chemical elemental composition in the TR surface after saturation with arsenic solution. The SEM/EDS exam was carried out following the procedure described in Section 2.4. of Chapter III.

Adsorption is a multistep process involving (1) the transport of the adsorbate from the bulk solution, (2) external diffusion of the solute (from the bulk phase to the external surface of the adsorbent), (3) intraparticle diffusion in pores and in the solid phase, and, finally, (4) adsorption on the sites. The rate at which the overall process takes place is defined by the slowest of these steps, which in well-stirred systems is usually the third step (intraparticle diffusion). However, the use of models based in the "reaction step" such as Lagergren's pseudo-first-order [76] and pseudo-second-order [77] to describe adsorption kinetics is a common practice. These models are generally very simple to use and usually provide high-quality fittings. The kinetic data obtained was only adjusted to those two kinetic models. Pseudo-first [76] (Eq. IV.2) and pseudo-second order [77, 78] (Eq. IV.3) models were fitted to the experimental data by non-linear regression using the software *CurveExpert 1.4*. In Eq. IV.2 and Eq. IV.3, q_t and q_{eq} denote adsorbed amounts per unit mass of adsorbent, at time t and at equilibrium, respectively; k_1 and k_2 are kinetic constants.

$$q_t = q_{eq}[1 - \exp(-k_1 t)] \qquad \textbf{Eq. IV.2}$$

$$q_t = q_{eq}\frac{k_2 q_{eq} t}{1 + k_2 q_{eq} t} \qquad \textbf{Eq. IV.3}$$

2.3.3. Equilibrium Studies

Adsorption equilibrium isotherms were determined for As(V) at pH 3 and pH 4 using TRO-Fe <0.15 mm and TRO-Fe 0.15-0.50 mm, respectively, with initial As concentrations ranging from 0.1 mg L^{-1} to 15 mg L^{-1}. Arsenic solutions were stirred with TRO-Fe particles for 20 h (more than enough to reach equilibrium). Samples were then filtered and analysed for As concentration. The amount of As adsorbed at equilibrium per gram of adsorbent (q_{eq}, mg g^{-1}) was calculated by Eq. IV.1, replacing C_t by C_{eq}, which represents the concentration of arsenic in equilibrium (mg L^{-1}).

Two well-known models were used to describe As(V) adsorption data: Langmuir and Freundlich models. The Langmuir model [79] was developed for monolayer adsorption and assumes the existence of free sites where biosorption occurs. In this model, each active site can only accommodate one adsorbate entity, being connected in fixed sites. Adsorption is assumed to be energetically equal in all active sites and does not depend on the presence of adsorbed species in the vicinity. The Langmuir model is described by Eq. IV.4, where Q_m is the maximum adsorption capacity (mg g^{-1}) and K_L is the Langmuir equilibrium constant (L mg^{-1}). The Freundlich model [80] is an empirical model based on the occurrence of heterogeneous adsorption along the surface with different active sites. This model is ruled by Eq. IV.5, where K_F is the Freundlich equilibrium constant (mg g^{-1} (mg $L^{-1})^{-1/n}$) and n is the adsorption intensity identification constant (if n >1 the isotherm if favourable, if n ≤1 the isotherm is unfavourable). Both models were adjusted to the experimental values and the isotherm parameters were determined by non-linear adjustment of the experimental data using the software *CurveExpert 1.4*.

$$q_{eq} = \frac{Q_m \cdot K_L \cdot C_{eq}}{1 + K_L C_{eq}} \qquad \textbf{Eq. IV.4}$$

$$q_{eq} = K_F \cdot C_{eq}^{\frac{1}{n}} \qquad \textbf{Eq. IV.5}$$

3. Results and Discussion

3.1. Effect of pH

The pH effect on adsorption of As(V) was evaluated using two granulometric samples of TRO-Fe, <0.15 mm and 0.15-0.50 mm, and in the pH range 2-5 and results are presented in Fig. IV.2. The resin sample with smaller particles achieved higher adsorption capacities. TRO-Fe <0.15 mm had twice as much iron content (≈30 mg-Fe g^{-1}) than TRO-Fe 0.15-0.50 mm (≈13 mg-Fe g^{-1}), presented a higher surface area and, probably for those reasons, adsorbed higher As(V) amounts (Fig. IV.2a). For TRO-Fe <0.15 mm, adsorption capacity is the lowest at pH 2 and it starts the decrease from the optimal value after pH 3. These results suggest that TRO-Fe has more affinity towards the anionic form $H_2AsO_4^-$, predominant at pH 3-6, than the neutral species H_3AsO_4, predominant for pH <2 (Fig. IV.1) Alternatively, the lower adsorption capacity at pH 2 may be explained by the higher loss of iron content since iron is an active site for arsenic adsorption. The further decrease of adsorption capacities above pH 3 may be due to the increasingly negatively charge surface of the adsorbent (see zeta potential, Fig. III.13). Since adsorption capacities of TRO-Fe 0.15-0.50 mm were very low, it is not possible to conclude on the optimal pH. The best adsorbed amount obtained here was 0.46±0.02 mg g^{-1} for TRO-Fe <0.15 mm at pH 3 (Fig. IV.2a), which represents a removal of 91±5 % from a 5 mg L^{-1} As(V) solution.

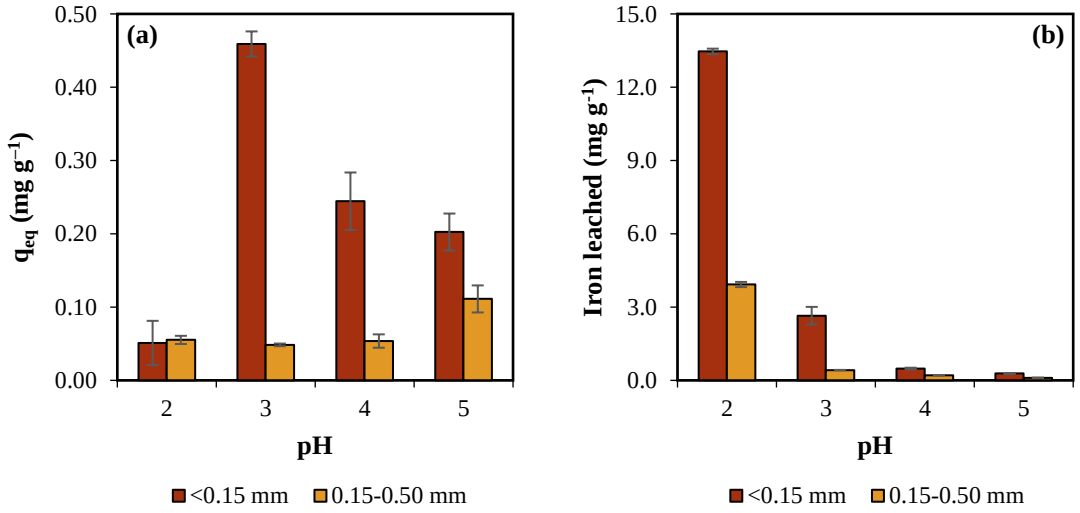

Fig. IV.2 Effect of pH on (a) adsorption capacity of As(V) by iron-loaded tannin resins (C_{in} = 5 mg L^{-1}, S/L = 10 g L^{-1}, 20 h, 20 °C) and (b) iron leaching, with iron concentrations determined by AAS and values expressed in mg of Fe per g of adsorbent. Every assay was done in duplicate and error bars represent absolute deviations.

Pintor et al. [53] reported a marked decline of As(V) adsorption by iron-coated cork granules with increasing pH, similar to what was observed here. The authors of that work also indicate pH 3 to be optimal, even though maximum adsorption was observed at pH 2. Such decision was explained as an attempt to minimise iron leaching. On the other hand, the iron-coated *S. muticum* adsorbent produced by Vieira et al. [52] was shown to have affinity towards As(V) at any pH between 2 and 7, indicating that adsorption did not occur only through electrostatic attraction.

The liquid phase was also analysed for total dissolved Fe, Fe(II) and Fe(III). As expected, due to its higher surface area and higher metal content (higher driving force for dissolution), the adsorbent fraction <0.15 mm leached more iron to the solution. The maximum value of 13.5±0.1 mg g^{-1} (corresponding to a dissolved iron concentration of 131±1 mg L^{-1}) was found at pH 2 (Fig. IV.2b). This means the tannin resin loses almost half of its iron content (44 %) at strong acidic conditions. However, at pH 3, optimal for adsorption, iron leaching was considerably lower (2.7±0.4 mg g^{-1}, 26±3 mg L^{-1}, 9 % of the initial resin iron content). Still, these values are high and should be considered when assessing the quality of the adsorbent.

For both fractions, the general tendency of iron leaching had a sharp decrease with increasing pH. At very low pH, H^+ ions in solution may compete with iron, by an ion-exchange process, promoting iron dissolution. On the other hand, metal solubility decreases with the increase of OH^- ions in solution. Vieira et al. [52] reported similar levels of dissolved iron, leached from an iron-coated seaweed, while Pintor et al. [53] managed to yield very low iron leaching (<5 mg L^{-1}) from iron-coated cork granulates. In this work, a high adsorbent dosage was applied and in a practical case iron leaching could be controlled by adjusting the S/L ratio and pH.

Iron speciation results indicate that for both particle sizes most of the iron leached to the solution (69-91 %) was Fe(II) (Table IV.2) suggesting that the Fe(III) loaded into the resin was reduced. Blank experiments (contact between distilled water at different pH and TRO-Fe) have been also performed and the same observation was made, with 64-91 % of total iron leached being Fe(II). These observations suggest that Fe(III) reduction was accompanied by the oxidation of –OH groups of the tannin resin (no involvement of As). This is possible because during the adsorbent preparation, TR was subjected only to a limited oxidation with HNO_3 to protect its stability, which left some non-oxidized –OH groups in TRO and TRO-Fe.

Table IV.2 Fe speciation in As(V) solution after contact with TRO-Fe (10 g L^{-1}) at different pH. Values represent average from duplicates ± absolute deviation.

Fraction		pH			
		2	3	4	5
<0.15 mm	Fe(II) (mg L^{-1})	106±5	20±4	3.5±0.3	1.9±0.2
	Fe(III) (mg L^{-1})	13.5±0.1	4.2±0.3	1.6±0.2	0.8±0.2
	Fe(II) (%)	89±6	83±22	69±8	70±11
0.15-0.50 mm	Fe(II) (mg L^{-1})	35.8±0.3	3.9±0.2	2.1±0.1	1.33±0.03
	Fe(III) (mg L^{-1})	4.9±0.1	1.5±0.1	0.34±0.01	0.13±0.03
	Fe(II) (%)	88±1	72±5	86±5	91±3

For As(III), adsorption was found to be negligible at every tested pH. This is probably explained by the higher affinity of iron for As(V). Literature has reported that the uptake of As(III) by iron-based adsorbents could be possible after a preliminary oxidation to As(V) that would be promoted by the reduction of Fe(III) into Fe(II) [52]. This does not happen here, because that reduction reaction is coupled with the oxidation of OH surface groups. The lack of ability to uptake As(III) of the iron-loaded tannin resin is clearly a drawback when compared to other adsorbents such as iron-coated *S. muticum* [52] and iron-coated cork granules [53], and limits the applicability of TRO-Fe to oxidizing media.

3.2. Adsorption Kinetics

The adsorption kinetics assays for As(V) were performed using 0.5 mg L^{-1}, 5 mg L^{-1}, and 10 mg L^{-1} initial concentrations, 10 g L^{-1} adsorbent (TRO-Fe <0.15 mm) dosage and pH 3. Kinetic models of pseudo-first (Eq. IV.2) and pseudo-second order (Eq. IV.3) were fitted to the experimental data and kinetic parameters were determined by non-linear adjustment.

The variation of the adsorption capacity through time is presented in Fig. IV.3 for As(V). The adsorption capacity achieved at equilibrium for higher initial concentration was 0.53 mg g^{-1} (61 % removal), while for the lowest initial concentration (500 μg L^{-1}) adsorption capacity did not surpass 22 μg g^{-1} (44 % removal). The time required to reach equilibrium is higher for higher initial concentrations: 1 hour was enough for the lowest initial concentration, however for the highest one a contact time of 4 h was required. Nonetheless, adsorption was somewhat fast for all initial concentrations used. Furthermore, the iron leached to the solution at equilibrium time was not higher than 10 mg L^{-1}: iron concen-

trations of 3.4 mg L^{-1}, 6.4 mg L^{-1}, and 3.6 mg L^{-1} were measured for initial arsenic concentrations of 0.5 mg L^{-1}, 5 mg L^{-1}, and 10 mg L^{-1}, respectively. This value is considerably lower than the one observed in the pH assay at pH 3 (26±3 mg L^{-1}, Fig. IV.2b), indicating that iron leaching could be controlled by limiting contact time without affecting adsorption results.

The obtained kinetic parameters are presented in Table IV.3. Both models adjust quite well the experimental data for initial concentrations of 0.5 mg L^{-1} and 10 mg L^{-1} since the coefficients of correlation (0.97 and 0.93-0.94, respectively) and the standard errors (0.002 mg g^{-1} and 0.05 mg g^{-1}, respectively) are similar for both models. For initial concentration of 5 mg L^{-1}, the pseudo-first order model fits slightly better to the experimental data since it presents higher R and lower SE. The equilibrium adsorbed amounts (q_{eq}) predicted by both models are in line with the experimental results (Table IV.3).

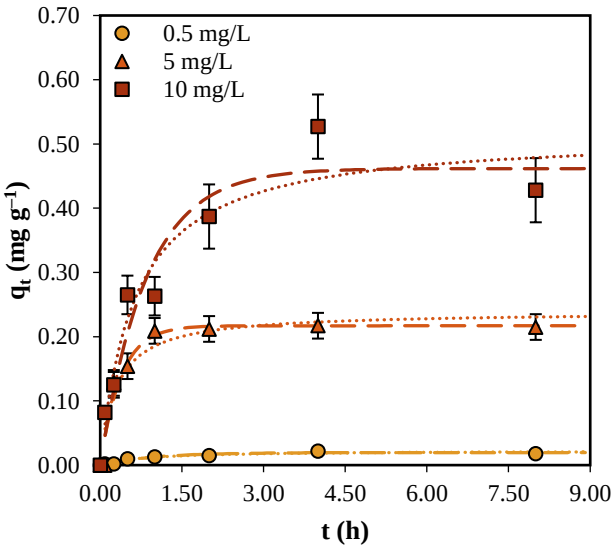

Fig. IV.3 Adsorption kinetics for As(V) uptake (20 ºC, S/L = 10 g L^{-1}, pH 3) with TRO-Fe <0.15 mm: experimental data and model curves (– – – pseudo-first order; ····· pseudo-second order fittings). Every assay was done in duplicate and error bars represent absolute deviations.

Table IV.3 Kinetic parameters for As(V) adsorption on the iron-loaded tannin resin (particle size <0.15 mm, 20 ºC, adsorbent dosage 10 g L^{-1}, pH 3): parameters (±standard error) and statistical data.

	Pseudo-first order model				Pseudo-second order model			
C_{in} (mg L^{-1})	k_1 (h^{-1})	q_{eq} (mg g^{-1})	R	SE (mg g^{-1})	k_2 (g mg^{-1} h^{-1})	q_{eq} (mg g^{-1})	R	SE (mg g^{-1})
0.5	1.0±0.2	0.020±0.001	0.97	0.002	53±25	0.023±0.003	0.97	0.002
5	2.7±0.5	0.22±0.01	0.96	0.020	14±6	0.24±0.02	0.94	0.025
10	1.2±0.3	0.46±0.03	0.93	0.051	3±1	0.52±0.05	0.94	0.049

SEM analysis revealed no morphological differences in TRO-Fe particles before and after contact with arsenic solutions (Fig. IV.4, confront with Fig. III.10). Arsenic presence was not detected in EDS spectra, probably due to the low adsorption capacities.

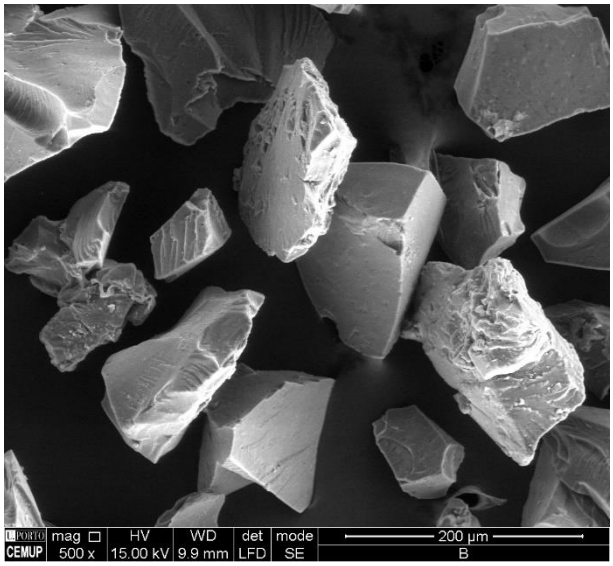

Fig. IV.4 SEM image of TRO-Fe particles after contact with arsenic solution.

3.3. Equilibrium Studies

Equilibrium assays were performed to determine the maximum adsorption capacity of the studied adsorbent, for different particle sizes (<0.15 mm and 0.15-0.50 mm), and define the equilibrium relation for As distribution between the solid and liquid phases. Langmuir (Eq. IV.4) and Freundlich (Eq. IV.5) models were adjusted to the experimental data (q_{eq} as a function of C_{eq}). The isotherm parameters were determined by non-linear adjustment of the experimental data. The results of the equilibrium assays are presented in Fig. IV.5.

Both models fitted equally well into experimental data obtained for TRO-Fe 0.15-0.50 mm, with similar values for correlation coefficient and standard error (R = 0.95 and SE = 0.017 mg g^{-1}). The calculated Freundlich equilibrium constant (K_F) was 0.034±0.009 mg g^{-1} (mg L^{-1})$^{-1/n}$, with n = 1.4±0.3, which indicated a favourable isotherm. The maximum adsorption capacity of As(V), predicted by the Langmuir model, for TRO-Fe 0.15-0.50 mm was found to be 0.3±0.1 mg g^{-1} (K_L = 0.12±0.07 L mg^{-1}). These results reveal a poor performance of the resin as an adsorbent with removal remaining lower than 25 %.

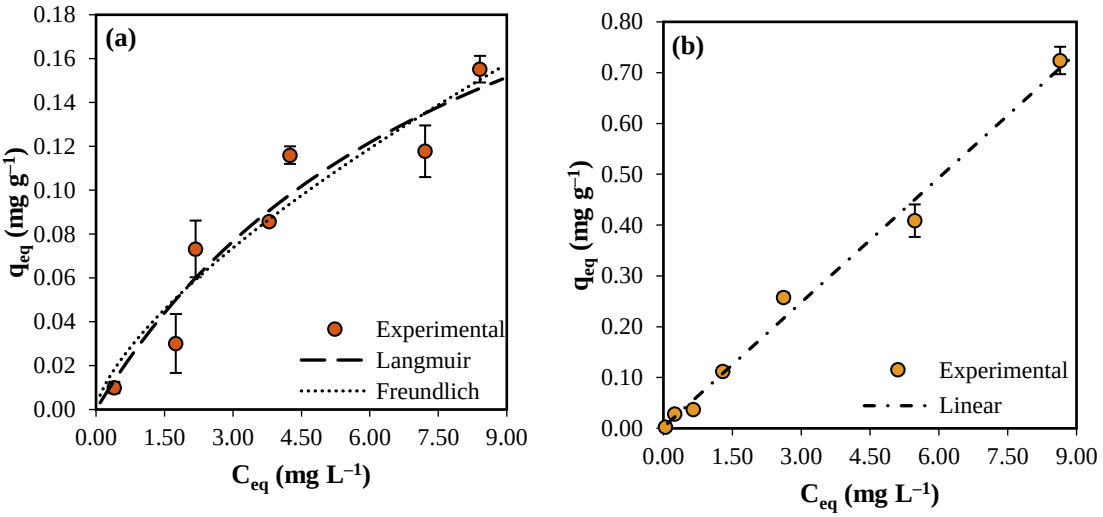

Fig. IV.5 Equilibrium isotherms for the adsorption of As(V) by TRO-Fe with a particle size of (a) 0.15-0.50 mm at pH 4 and (b) <0.15 mm, at pH 3 (20 h, 20 ºC, S/L = 10 g L^{-1}). Every assay was done in duplicate and error bars represent absolute deviations.

Equilibrium data obtained using TRO-Fe <0.15 mm revealed a more interesting performance and a linear behaviour within the range of concentrations used, which means that the saturation of the adsorbent was not reached. A linear fitting between the amount of As(V) adsorbed and the equilibrium concentration (R = 0.99, SE = 0.03) generated a proportionality constant of 0.082±0.004 L g^{-1}. Although the assay may be prolonged by the use of higher As concentrations, to ascertain that the saturation is reached, it would be pointless since contaminated waters rarely present As concentrations higher than 10 mg L^{-1}. Nevertheless, better results were achieved with this sample of the resin. Indeed, the maximum experimental adsorption capacity was 0.72±0.03 mg g^{-1}, with removals up to ≈50 %. This is explained by the higher surface area of the resin and higher iron content. Clearly, the studied adsorbent presents one of the lowest adsorption capacities reported in the literature (Table IV.1), which means that its potential for arsenic uptake is mostly not realized.

4. Conclusions

The potential of iron-loaded oxidized tannin resins to adsorb arsenic was assessed. Adsorption of As(V) was optimal using a resin sample with a particle size of <0.15 mm at pH 3 with a removal of ≈90 % (S/L = 10 g L^{-1} and C_{in} = 5 mg L^{-1}). The resin leached a considerable amount of iron to the solution, although it can be minimized by controlling the contact time. Most of it was found to be Fe(II). The results suggest that the reduction of Fe(III) into Fe(II) is possibly coupled with the oxidation of the –OH groups of the adsorbent, which blocked As(III) conversion into As(V) and explains the negligible adsorption of As(III) at every pH tested. Kinetics assays showed As(V) adsorption to be somewhat fast, with equilibrium being achieved in 1 to 4 hours. Equilibrium data obtained for As(V) adsorption showed maximum adsorption capacities of 0.3±0.1 mg g^{-1} (pH 4, particle size: 0.15-0.50 mm) and 0.72±0.03 mg g^{-1} (pH 3, <0.15 mm) within the conditions studied. Overall, TRO-Fe presented a limited performance, yielding very low adsorption capacities.

5. References

[1] Zhao, F.J., S.P. McGrath, and A.A. Meharg, "Arsenic as a food chain contaminant: mechanism of plant uptake and metabolism and mitigation strategies," *Annual Review of Plant Biology*, vol. 61, pp. 535-559, 2010.

[2] Gupta, D.K., S. Srivastava, H. Huang, M.C. Romero-Puertas, and L.M. Sandalio, "Arsenic Tolerance And Detoxification Mechanisms In Plants," in *Detoxification of Heavy Metals* (Soil Biology). Heidelberg: Springer, 2011, pp. 169–180.

[3] Singh, R., S. Singh, P. Parihar, V.P. Singh, and S.M. Prasad, "Arsenic contamination, consequences and remediation techniques: A review," *Ecotoxicology and Environmental Safety*, vol. 112, pp. 247-270, 2015.

[4] Petrick, J.S., F. Ayala-Fierro, W.R. Cullen, D.E. Carter, and H. Vasken Aposhian, "Monomethylarsonous Acid (MMA^{III}) Is More Toxic Than Arsenite in Chang Human Hepatocytes," *Toxicology Applied Pharmacology*, vol. 167, pp. 203-210, 2000.

[5] Mohan, D. and C.U. Pittman Jr, "Arsenic removal from water/wastewater using adsorbents - A critical review," *Journal of Hazardous Materials*, vol. 142, pp. 1-53, 2007.

[6] Takeno, N., "Atlas of Eh-pH diagrams: Intercomparison of thermodynamic databases," in "Geological Survey of Japan Open File Report No.419." National Institute of Advanced Industrial Science and Technology. 2005, vol. 419.

[7] Smedley, P.L. and D.G. Kinniburgh, "A review of the source, behaviour and distribution of arsenic in natural waters," *Applied Geochemistry*, vol. 17, no. 5, pp. 517-568, 2002.

[8] Flora, S.J.S., "Arsenic: Chemistry, Occurrence, And Exposure," in *Handbook Of Arsenic Toxicology*: Elsevier, 2015, pp. 1-49.

[9] Ungureanu, G., S. Santos, R. Boaventura, and C. Botelho, "Arsenic and antimony in water and wastewater: Overview of removal techniques with special reference to latest advances in adsorption," *Journal of Environmental Management*, vol. 151, pp. 326-342, 2015.

[10] Xie, Z.M. and C.Y. Huang, "Control of arsenic toxicity in rice plants grown on an arsenic-polluted paddy soil," *Communications in Soil Science & Plant Analysis*, vol. 29, pp. 2471-2477, 1998.

[11] Thomas, D.J., M. Styblo, and S. Lin, "The cellular metabolism and systemic toxicity of arsenic," *Toxicology and Applied Pharmacology*, vol. 176, pp. 127-144, 2001.

[12] Sun, G., G. Yu, L. Zhao, X. Li, Y. Xu, B. Li, and D. Sun, "Endemic Arsenic Poisoning," in *Endemic Disease in China*: Springer, 2019, pp. 97-123.

[13] Hughes, M.F., B.D. Beck, Y. Chen, A.S. Lewis, and D.J. Thomas, "Arsenic exposure and toxicology: a historical perspective," *Toxicology Science*, vol. 123, pp. 305-337, 2011.

[14] Rodríguez-Lado, L., G. Sun, M. Berg, Q. Zhang, H. Xue, and Q. Zheng, "Groundwater arsenic contamination throughout China," *Science*, vol. 341, pp. 866-872, 2013.

[15] Sharma, A.K., J.C. Tjell, J.J. Sloth, and P.E. Holm, "Review of arsenic contamination, exposure through water and food and low cost mitigation options for rural areas," *Applied Geochemistry*, vol. 41, pp. 11-33, 2014.

[16] Shaji, E., M. Santosh, K.V. Sarath, P. Prakash, V. Deepchand, and B.V. Divya, "Arsenic contamination of groundwater: A global synopsis with focus on the Indian Peninsula," *Geoscience Frontiers*, vol. 12, no. 3, p. 101079, 2021.

[17] Mukherjee, A., M.K. Sengupta, M.A. Hossain, S. Ahamed, B. Das, B. Nayak, D. Lodh, M.M. Rahman, and D. Chakraborti, "Arsenic Contamination In Groundwater: A Global Perspective With Emphasis On The Asian Scenario," *Journal of Health, Population and Nutrition*, pp. 142-163, 2006.

[18] Mandal, B.K. and K.T. Suzuki, "Arsenic round the world: a review," *Talanta*, vol. 58, no. 1, pp. 201-235, 2002.

[19] Sharma, V.K. and M. Sohn, "Aquatic arsenic: Toxicity, speciation, transformations, and remediation," *Environment International*, vol. 35, no. 4, pp. 743-759, 2009.

[20] Buschmann, J., M. Berg, C. Stengel, and M.L. Sampson, "Arsenic and Manganese Contamination of Drinking Water Resources in Cambodia: Coincidence of Risk Areas with Low Relief Topography," *Environmental Science & Technology*, vol. 41, no. 7, pp. 2146-2152, 2007.

[21] Katsoyiannis, I.A., M. Mitrakas, and A.I. Zouboulis, "Arsenic occurrence in Europe: emphasis in Greece and description of the applied full-scale treatment plants," *Desalination and Water Treatment*, vol. 54, no. 8, pp. 2100-2107, 2015.

[22] Rowland, H.A.L., E.O. Omoregie, R. Millot, C. Jimenez, J. Mertens, C. Baciu, S.J. Hug, and M. Berg, "Geochemistry and arsenic behaviour in groundwater resources of the Pannonian Basin (Hungary and Romania)," *Applied Geochemistry*, vol. 26, no. 1, pp. 1-17, 2011.

[23] Zuzolo, D., D. Cicchella, A. Demetriades, M. Birke, S. Albanese, E. Dinelli, A. Lima, P. Valera, and B. De Vivo, "Arsenic: Geochemical distribution and age-related health risk in Italy," *Environmental Research*, vol. 182, p. 109076, 2020.

[24] Antunes, I.M.H.R. and M.T.D. Albuquerque, "Using indicator kriging for the evaluation of arsenic potential contamination in an abandoned mining area (Portugal)," *Science of the Total Environment*, vol. 442, pp. 545-552, 2013.

[25] Neiva, A.M.R., I.M.H.R. Antunes, P.C.S. Carvalho, and A.C.T. Santos, "Uranium and arsenic contamination in the former Mondego Sul uranium mine area, Central Portugal," *Journal of Geochemical Exploration*, vol. 162, pp. 1-15, 2016.

[26] Antunes, I.M.H.R., A.M.R. Neiva, M.T.D. Albuquerque, P.C.S. Carvalho, A.C.T. Santos, and P.P. Cunha, "Potential toxic elements in stream sediments, soils and waters in an abandoned radium mine (central Portugal)," *Environmental Geochemistry and Health*, vol. 40, no. 1, pp. 521-542, 2018.

[27] Shankar, S., U. Shanker, and Shikha, "Arsenic Contamination of Groundwater: A Review of Sources, Prevalence, Health Risks, and Strategies for Mitigation," *The Scientific World Journal*, vol. 2014, p. 304524, 2014.

[28] Langsch, J.E., M. Costa, L. Moore, P. Morais, A. Bellezza, and S. Falcão, "New technology for arsenic removal from mining effluents," *Journal of Materials Research and Technology*, vol. 1, no. 3, pp. 178-181, 2012.

[29] Li, Y., X. Zhu, X. Qi, B. Shu, X. Zhang, K. Li, Y. Wei, and H. Wang, "Removal and immobilization of arsenic from copper smelting wastewater using copper slag by in situ encapsulation with silica gel," *Chemical Engineering Journal*, vol. 394, p. 124833, 2020.

[30] Liu, L., W. Tan, S.L. Suib, G. Qiu, L. Zheng, and S. Su, "Enhanced adsorption removal of arsenic from mining wastewater using birnessite under electrochemical redox reactions," *Chemical Engineering Journal*, vol. 375, p. 122051, 2019.

[31] Nguyen, H.T.H., B.Q. Nguyen, T.T. Duong, A.T.K. Bui, H.T.A. Nguyen, H.T. Cao, N.T. Mai, K.M. Nguyen, T.T. Pham, and K.-W. Kim, "Pilot-scale removal of arsenic and heavy metals from mining wastewater using adsorption combined with constructed wetland," *Minerals*, vol. 9, no. 6, p. 379, 2019.

[32] Barakan, S. and V. Aghazadeh, "Structural modification of nano bentonite by aluminum, iron pillarization and 3D growth of silica mesoporous framework for arsenic removal from gold mine wastewater," *Journal of Hazardous Materials*, vol. 378, p. 120779, 2019.

[33] *Decreto-Lei n.º 306/2007*, Diário da República n.º 164, Série I de 2007-08-27, Lisboa, Portugal, 2007.

[34] Nicomel, N.R., K. Leus, K. Folens, P. Van Der Voort, and G. Du Laing, "Technologies For Arsenic Removal From Water: Current Status And Future Perspectives," *International Journal Of Environmental Research And Public Health*, vol. 13, no. 1, p. 62, 2016.

[35] Baig, S.A., T. Sheng, Y. Hu, J. Xu, and X. Xu, "Arsenic Removal From Natural Water Using Low Cost Granulated Adsorbents: A Review," *CLEAN–Soil, Air, Water*, vol. 43, no. 1, pp. 13-26, 2015.

[36] Johnston, R., H. Heijnen, and P. Wurzel, "Safe Water Technology," in *United Nations Synthesis Report on Arsenic in Drinking Water*, 2001, pp. 1-98.

[37] Ociński, D., I. Jacukowicz-Sobala, and E. Kociołek-Balawejder, "Alginate beads containing water treatment residuals for arsenic removal from water—formation and adsorption studies," *Environmental Science and Pollution Research*, vol. 23, no. 24, pp. 24527-24539, 2016.

[38] Gérente, C., Y. Andrès, G. McKay, and P. Le Cloirec, "Removal of arsenic(V) onto chitosan: From sorption mechanism explanation to dynamic water treatment process," *Chemical Engineering Journal,* vol. 158, no. 3, pp. 593-598, 2010.

[39] Asere, T.G., C.V. Stevens, and G. Du Laing, "Use of (modified) natural adsorbents for arsenic remediation: A review," *Science of The Total Environment,* vol. 676, pp. 706-720, 2019.

[40] Giles, D.E., M. Mohapatra, T.B. Issa, S. Anand, and P. Singh, "Iron and aluminium based adsorption strategies for removing arsenic from water," *Journal of Environmental Management,* vol. 92, no. 12, pp. 3011-3022, 2011.

[41] Arcibar-Orozco, J.A., D.B. Josue, J.C. Rios-Hurtado, and J.R. Rangel-Mendez, "Influence of iron content, surface area and charge distribution in the arsenic removal by activated carbons," *Chemical Engineering Journal,* vol. 249, pp. 201-209, 2014.

[42] Chang, Q., W. Lin, and W.-c. Ying, "Preparation of iron-impregnated granular activated carbon for arsenic removal from drinking water," *Journal of Hazardous Materials,* vol. 184, no. 1, pp. 515-522, 2010.

[43] Gong, X.-J., Y.-S. Li, Y.-Q. Dong, and W.-G. Li, "Arsenic adsorption by innovative iron/calcium in-situ-impregnated mesoporous activated carbons from low-temperature water and effects of the presence of humic acids," *Chemosphere,* p. 126275, 2020.

[44] Rahman, H.L., H. Erdem, M. Sahin, and M. Erdem, "Iron-incorporated activated carbon synthesis from biomass mixture for enhanced arsenic adsorption," *Water, Air, & Soil Pollution,* vol. 231, no. 1, pp. 1-17, 2020.

[45] Das, B., R.R. Devi, I.M. Umlong, K. Borah, S. Banerjee, and A.K. Talukdar, "Arsenic(III) adsorption on iron acetate coated activated alumina: thermodynamic, kinetics and equilibrium approach," *Journal of Environmental Health Science and Engineering,* vol. 11, 2013.

[46] Xi, C., R. Wang, P. Rao, W. Zhang, L. Yan, G. Li, F. Chai, Y. Cai, T. Luo, and X. Zhou, "The fabrication and arsenic removal performance of cellulose nanocrystal-containing absorbents based on the “bridge joint” effect of iron ions," *Carbohydrate Polymers,* vol. 237, p. 116129, 2020.

[47] Gupta, A., V.S. Chauhan, and N. Sankararamakrishnan, "Preparation and evaluation of iron–chitosan composites for removal of As(III) and As(V) from arsenic contaminated real life groundwater," *Water Research,* vol. 43, no. 15, pp. 3862-3870, 2009.

[48] Kloster, G.A., M. Valiente, N.E. Marcovich, and M.A. Mosiewicki, "Adsorption of arsenic onto films based on chitosan and chitosan/nano-iron oxide," *International Journal of Biological Macromolecules,* vol. 165, pp. 1286-1295, 2020.

[49] Sigdel, A., J. Park, H. Kwak, and P.-K. Park, "Arsenic removal from aqueous solutions by adsorption onto hydrous iron oxide-impregnated alginate beads," *Journal of Industrial and Engineering Chemistry,* vol. 35, pp. 277-286, 2016.

[50] Mishra, T. and D.K. Mahato, "A comparative study on enhanced arsenic(V) and arsenic(III) removal by iron oxide and manganese oxide pillared clays from ground water," *Journal of Environmental Chemical Engineering,* vol. 4, no. 1, pp. 1224-1230, 2016.

[51] Torasso, N., A. Vergara-Rubio, P. Rivas-Rojas, C. Huck-Iriart, A. Larrañaga, A. Fernández-Cirelli, S. Cerveny, and S. Goyanes, "Enhancing arsenic adsorption via excellent dispersion of iron oxide nanoparticles inside poly(vinyl alcohol) nanofibers," *Journal of Environmental Chemical Engineering,* vol. 9, no. 1, p. 104664, 2021.

[52] Vieira, B.R.C., A.M.A. Pintor, R.A.R. Boaventura, C.M.S. Botelho, and S.C.R. Santos, "Arsenic removal from water using iron-coated seaweeds," *Journal of Environmental Management,* vol. 192, pp. 224-233, 2017.

[53] Pintor, A.M.A., B.R.C. Vieira, S.C.R. Santos, R.A.R. Boaventura, and C.M.S. Botelho, "Arsenate and arsenite adsorption onto iron-coated cork granulates," *Science of the Total Environment,* vol. 642, pp. 1075-1089, 2018.

[54] Pintor, A.M.A., B.R.C. Vieira, C.C. Brandão, R.A.R. Boaventura, and C.M.S. Botelho, "Complexation mechanisms in arsenic and phosphorus adsorption onto iron-coated cork granulates," *Journal of Environmental Chemical Engineering,* vol. 8, no. 5, p. 104184, 2020.

[55] Pintor, A.M.A., C.C. Brandão, R.A.R. Boaventura, and C.M.S. Botelho, "Multicomponent adsorption of pentavalent As, Sb and P onto iron-coated cork granulates," *Journal of Hazardous Materials*, p. 124339, 2020.

[56] Carneiro, M.A., A. Pintor, R.A.R. Boaventura, and C. Botelho, "Current Trends of Arsenic Adsorption in Continuous Mode: Literature Review and Future Perspectives," *Sustainability*, vol. 13, no. 3, p. 1186, 2021.

[57] Mulani, K., S. Daniels, K. Rajdeo, S. Tambe, and N. Chavan, "Tannin-aniline-formaldehyde resole resins for arsenic removal from contaminated water," *Canadian Chemical Transactions*, vol. 2, no. 4, p. 450, 2014.

[58] Patil-Shinde, V., K.B. Mulani, K. Donde, N.N. Chavan, S. Ponrathnam, and S.S. Tambe, "The Removal of arsenite [As(III)] and arsenate [As(V)] ions from wastewater using TFA and TAFA resins: Computational intelligence based reaction modeling and optimization," *Journal of Environmental Chemical Engineering*, vol. 4, no. 4, pp. 4275-4286, 2016.

[59] Viswanathan, T., G. Gunawan, S. Bourdo, V. Saini, J. Moran, L. Pack, and S. Owen, "Evaluation of a renewable resource-based carbon-iron oxide nanocomposite for removal of arsenic from contaminated water," *Journal of Macromolecular Science, Part A*, vol. 48, no. 5, pp. 348-354, 2011.

[60] Qi, P., R. Luo, T. Pichler, J. Zeng, Y. Wang, Y. Fan, and K. Sui, "Development of a magnetic core-shell Fe_3O_4@TA@UiO-66 microsphere for removal of arsenic(III) and antimony(III) from aqueous solution," *Journal of Hazardous Materials*, Article vol. 378, 2019, Art. no. 120721.

[61] Bacelo, H.A.M., "Tannin-based biomaterials: Production, Characterization and Application in Water and Wastewater Treatment," Master Thesis, Faculdade de Engenharia da Universidade do Porto, 2016.

[62] Ogata, T., S. Morisada, Y. Oinuma, Y. Seida, and Y. Nakano, "Preparation of adsorbent for phosphate recovery from aqueous solutions based on condensed tannin gel," *Journal of Hazardous Materials*, vol. 192, no. 2, pp. 698-703, 2011.

[63] Wu, K., C. Jing, J. Zhang, T. Liu, S. Yang, and W. Wang, "Magnetic Fe_3O_4@CuO nanocomposite assembled on graphene oxide sheets for the enhanced removal of arsenic(III/V) from water," *Applied Surface Science*, vol. 466, pp. 746-756, 2019.

[64] Te, B., B. Wichitsathian, C. Yossapol, and W. Wonglertarak, "Development of low-cost iron mixed porous pellet adsorbent by mixture design approach and its application for arsenate and arsenite adsorption from water," *Adsorption Science & Technology*, vol. 36, no. 1-2, pp. 372-392, 2018.

[65] Aryal, M., M. Ziagova, and M. Liakopoulou-Kyriakides, "Study on arsenic biosorption using Fe(III)-treated biomass of *Staphylococcus xylosus*," *Chemical Engineering Journal*, vol. 162, no. 1, pp. 178-185, 2010.

[66] Casentini, B., M. Gallo, and F. Baldi, "Arsenate and arsenite removal from contaminated water by iron oxides nanoparticles formed inside a bacterial exopolysaccharide," *Journal of Environmental Chemical Engineering*, vol. 7, no. 1, p. 102908, 2019.

[67] Das, T.K., T.S. Sakthivel, A. Jeyaranjan, S. Seal, and A.N. Bezbaruah, "Ultra-high arsenic adsorption by graphene oxide iron nanohybrid: Removal mechanisms and potential applications," *Chemosphere*, vol. 253, p. 126702, 2020.

[68] El-Moselhy, M.M., A. Ates, and A. Çelebi, "Synthesis and characterization of hybrid iron oxide silicates for selective removal of arsenic oxyanions from contaminated water," *Journal of Colloid and Interface Science*, vol. 488, pp. 335-347, 2017.

[69] Pawar, R.R., M. Kim, J.-G. Kim, S.-M. Hong, S.Y. Sawant, and S.M. Lee, "Efficient removal of hazardous lead, cadmium, and arsenic from aqueous environment by iron oxide modified clay-activated carbon composite beads," *Applied Clay Science*, vol. 162, pp. 339-350, 2018.

[70] Nguyen, K.M., B.Q. Nguyen, H.T. Nguyen, and H.T.H. Nguyen, "Adsorption of Arsenic and Heavy Metals from Solutions by Unmodified Iron-Ore Sludge," *Applied Sciences*, vol. 9, no. 4, p. 619 (14 pp.), 2019.

[71] Yu, X., Y. Wei, C. Liu, J. Ma, H. Liu, S. Wei, W. Deng, J. Xiang, and S. Luo, "Ultrafast and deep removal of arsenic in high-concentration wastewater: A superior bulk adsorbent of porous Fe_2O_3 nanocubes-impregnated graphene aerogel," *Chemosphere*, vol. 222, pp. 258-266, 2019.

[72] Yusof, M.S.M., M.H.D. Othman, R.A. Wahab, K. Jumbri, F.I.A. Razak, T.A. Kurniawan, R.A. Samah, A. Mustafa, M.A. Rahman, and J. Jaafar, "Arsenic adsorption mechanism on palm oil fuel ash (POFA) powder suspension," *Journal of Hazardous Materials*, vol. 383, p. 121214, 2020.

[73] Rahdar, S., M. Taghavi, R. Khaksefidi, and S. Ahmadi, "Adsorption of arsenic(V) from aqueous solution using modified saxaul ash: isotherm and thermodynamic study," *Applied Water Science*, vol. 9, no. 4, pp. 1-9, 2019.

[74] Moreira, R.F.P.M., S. Vandresen, D.B. Luiz, H.J. José, and G. Li Puma, "Adsorption of arsenate, phosphate and humic acids onto acicular goethite nanoparticles recovered from acid mine drainage," *Journal of Environmental Chemical Engineering*, vol. 5, no. 1, pp. 652-9, 2017.

[75] ISO 6332:1988, *Water quality — Determination of iron — Spectrometric method using 1,10-phenanthroline*, 1988.

[76] Lagergren, S.Y., "Zur theorie der sogenannten adsorption gelöster stoffe, Kungliga Svenska Vetenskapsakademiens," *Handlingar*, vol. 24, pp. 1-39, 1898.

[77] Blanchard, G., M. Maunaye, and G. Martin, "Removal of Heavy-Metals from Waters by Means of Natural Zeolites," *Water Research*, vol. 18, no. 12, pp. 1501-1507, 1984.

[78] Ho, Y.S., "Adsorption of heavy metals from waste streams by peat," The University of Birmingham, Birmingham, U.K., 1995.

[79] Langmuir, I., "The adsorption of gases on plane surfaces of glass, mica and platinum," *Journal of the American Chemical Society*, vol. 40, pp. 1361-1403, 1918.

[80] Freundlich, H.M.F., "Over the adsorption in solution," *Journal of Physical Chemistry*, vol. 57, pp. 385-471, 1906.

CHAPTER V

REMOVAL AND RECOVERY OF ANTIMONY

1. Literature Review

Antimony (Sb) is a natural occurring trace metalloid that has four oxidation states: Sb(V), Sb(III), Sb(0), and Sb(-III). In water, it is mostly under trivalent and pentavalent oxidation states in the form of antimony hydroxide ($Sb(OH)_3$) or antimonate ion ($Sb(OH)_6^-$) [1]. Redox conditions and pH determine which oxidation state is predominant in a particular water body. Antimony Eh-pH diagrams can be found in literature [2]. Fig. V.1 presents a simplified diagram of the antimony speciation as a function of pH. Both forms are subjected to strong hydrolysis forming neutral or negatively-charged species; the formation of positively-charged antimony species is rare, only occurring in strongly acidic conditions [3]. The strong antimony affinity to –OH groups in solution limits its complexing ability with other inorganic and organic ligands, making difficult its uptake from water in comparison to metals that exist as cations [3], such as heavy metals, well researched and addressed in literature. Antimony trioxide is classified as possibly carcinogenic to humans [4] and various health adverse effects are related to antimony exposure by oral route [5]. Generally, Sb(III) is known to be more toxic than Sb(V) [5, 6]. Moreover, antimony present a similar toxicity to that of arsenic: both metalloids have the ability to substitute phosphorous in biological processes leading to adverse effects in the organism [7].

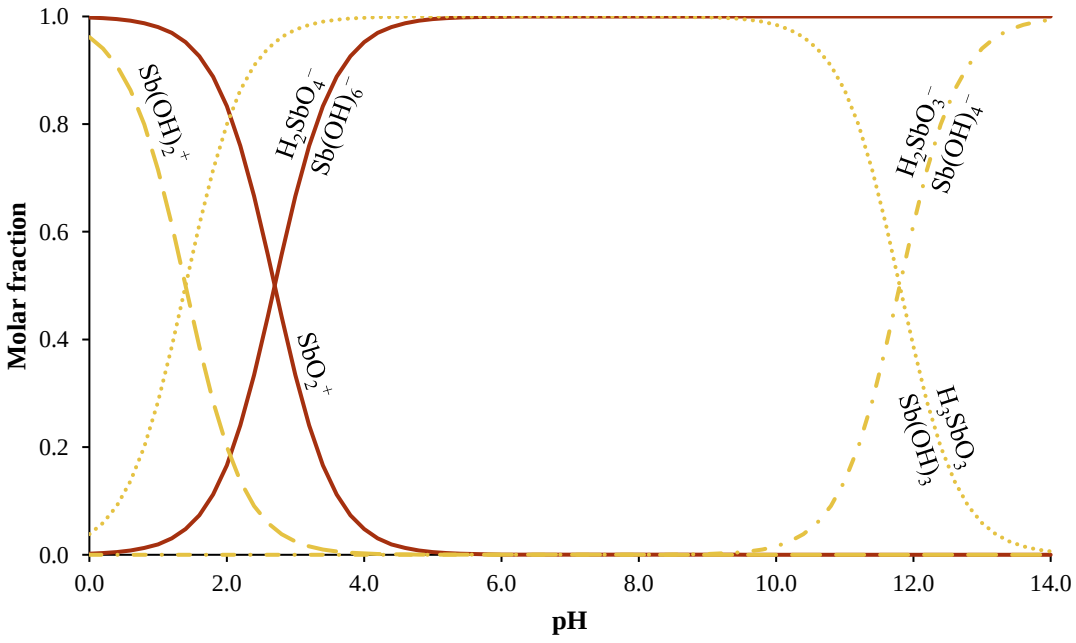

Fig. V.1 Antimonate (orange solid lines) and antimonite (yellow dash lines) speciation as a function of pH.

In one hand, antimony is present in the environment because of natural processes, such as, volcanic activity, rock weathering, biological activities, and soil runoff [1]. On the other, accumulation of this metalloid can also be contributed by anthropogenic activity: mining, industry, coal burning, smelting, military training, pharmaceuticals, and pesticides use [8-10]. According to the World Health Organization [11], the guideline value for antimony concentration in drinking water is 20 μg L^{-1} but many countries present lower legal limits: United States of America (6 μg L^{-1}) [9], European Union (5 μg L^{-1}) [12]. Guidelines set by different countries and organizations for surface water, groundwater, and other aqueous compartments have been summarized by Bagherifam et al. [13].

Non-polluted waters usually present concentrations below 1 μg L^{-1}; however, in many sites, especially the ones related to localized anthropogenic sources, antimony levels in surface and groundwaters can reach or even exceed 1 mg L^{-1} [9]. Hence, the production of drinking water from these waters should involve an effective technique to remove antimony. Moreover, mining industry, possibly the main anthropogenic source, generates process mine wastewater and acid mine drainage with high concentrations of antimony, commonly found in both oxidation states (Sb(III) and Sb(V)) [14]. Table V.1 presents several properties of mining-affected waters, such as pH and concentrations of cations (Ca, Mg, Mn) and anions (As, Sb). The development of techniques to handle antimony-contaminated waters prior to their discharge or use is then critically important.

Antimony is not only an element of concern regarding pollution but is also an important mineral commodity due to its wide array of industrial applications. One of the 30 critical raw materials of the 2020 European Union list [15] is antimony, considering its supply risk and economic importance. Considering the protection of the environment and the criticality of antimony, the removal of this contaminant from water and its further recovery is also worthy of investigation.

In mine water treatment practice, antimony removal is commonly achieved by coagulation/adsorption using ferric salts followed by filtration, which is more effective at pH 5 [14]. Several authors have reported successful antimony removal by coagulation, achieving removal rates close to 100 % in optimal conditions [16-22]. Nevertheless, coagulation may be environmentally disadvantageous due to the considerable doses of chemicals used and the formation of toxic sludge.

Table V.1 Characteristics of several mining-affected waters reported in the literature.

Water type	pH	SO_4	Ca	Mg	Mn	As	Sb	Ref.
		mg L^{-1}			µg L^{-1}			
Mine water	2.8-3	513-1054	—	—	300-1280	—	1431-7753	[23]
Mine drainage	—	—	—	—	—	—	<1-2200	[24]
Groundwater, surface waters and mine waters	6.3-8.2	2.7-259	5.4-141	5.8-66.8	—	—	<1-9300	[25]
Groundwater	3.4-8.4	5.3-267	5.4-70.7	1.2-40.6	6-1400	<5	<1-9300	[26]
Surface water	7.7-8.4	63-1267	25-430	7-43	—	—	0.33-11.4 [a]	[27]
River water	6.5-8.6	4.9-322	—	—	0.5-566	—	0.002-6.4	[28]
Creek water	6.6-8.4	4.6-10.5	—	—	—	21-84	1.6-32.2[a]	[29]
Drainage water	—	849-1125	—	—	—	21-42	159-366	[30]
Acid mining drainage	3.0-3.3	—	—	—	10000-27000	—	—	[31]
Acid mining drainage	2.3	2564	—	—	81800	—	—	[32]

a – Only Sb(V)

Adsorption or biosorption has been viewed as a valuable technology for toxic metal and metalloid removal from wastewater [33-38], and for the recovery of valuable compounds [39-42]. If a suitable adsorbent is found, the adsorption method could meet both targets for antimony: remediation and recovery. Commercial and hierarchical macro-/mesoporous alumina [43], zirconium dioxide fibres [44], granular TiO_2 [45], iron-based materials [46], such as Fe-Mn binary oxides [47], Mg-Al layered double hydroxides [48], and Fe- and Zr-based metal organic frameworks (MOF) [49, 50] have been presenting great adsorption capacities for antimony. In a context of sustainable management and efficient use of natural resources, the use of bio-derived materials to uptake contaminants from water and to recover elements [51] has been encouraged. However, few studies on biosorption of antimony are found in literature. These include marine algal species [52, 53], agri-food waste [54], and Fe(III)-treated biomaterials such as aerobic granules [55], cork-granulates [56], and saponified orange waste gel [57]. Some kind of pre-treatment of the precursor biomaterial is usually required, varying from a simple wash and dry procedures [52, 53] to more complex processing, such as saponification and metal loading. The pre-treatment increases the cost of the adsorbents, but the improvement of physical and chemical stability of the material is usually necessary to tailor physical and chemical characteristics and enhance adsorptive performance and handling properties. Table V.2 presents

an overview of maximum adsorbed amounts reported in literature for Sb(III) and Sb(V) by different adsorbents.

Similarly to what was observed for arsenic (Chapter IV), the literature review revealed reports on antimony uptake by tannin-adsorbents to be scarce. For example, Qi et al. [58] produced a composite based on Zr-based microspheres (UiO-66) with magnetic cores composed of Fe_3O_4 and tannic acid. The resulting material was evaluated as an adsorbent for Sb(III), which was shown to be effective across the pH range of 3-10 and in the individual presence of coexisting anions. However, to the best of the author's knowledge, there are no reports on antimony uptake by tannin resins, with or without a chemical modification. Hence, the work presented in this Chapter is an attempt the fill that void in the scientific literature by investigating the potential of tannin resins to uptake antimony from water.

Table V.2 Maximum adsorption capacities (Q_m) reported in literature for the uptake of antimony from water by different adsorbents.

Adsorbent	C_{eq} (mg L^{-1})	pH	T (ºC)	Q_m (mg g^{-1})	Ref.
Sb(III)					
Fe(III)-treated humus sludge adsorbent	0-300	2	20	9.4	[46]
Fe-based MOF (Fe-MIL-88B), 588.6 nm	0-23	6	25	566.1	[49]
Amino modified Zr MOF (UiO-66(NH_2)), 50 nm	0-550	4	25	64.89	[50]
Marine green macroalgae (*C. sericea*), 5 mm	0-30	7	22	1.8	[52]
Marine brown macroalgae (*S. muticum*), 5 mm	0-15	7	23	4	[53]
Green bean husk (*Vigna radiata*), 1-2 mm	0-70	4	25	20.14	[54]
Iron-coated cork granulates, 0.8-1.0 mm	0-4	6	20	5.8	[56]
Fe(III)-loaded saponified orange waste gel	0-30	10.5	30	136	[57]
Fe_3O_4-TA modified Zr MOF (UiO-66)	0-30	7	25	49.5	[58]
PVA-Fe^0 granules, 2.04±0.98 mm	0-7	7	25	6.99	[59]
Sb(V)					
Amorphous alumina AlOOH	0-17	5.0	25	35	[43]
Commercial activated alumina	≈0-20	5.0	25	5-53	[43]
Mesoporous alumina, fine powder	0-0.69	5.0	25	118	[43]
ZrO_2 fibers calcined at 500 ºC, 570-720 nm	0-20	6	–	8.6[b]	[44]
Calcined (400 ºC) Mg/Al LDH	0-75	7	25	303.3	[48]
Fe-based MOF (Fe-MIL-88B), 588.6 nm	0-28	6	–	318.9	[49]
Amino modified Zr MOF (UiO-66(NH_2)), 50 nm	0-550	4-5	25	110.86	[50]
Marine green macroalgae (*C. sericea*), 5 mm	0-30	2	22	3.1	[52]
Fe(III)-treated fungi aerobic granules	0-400	3.4	35	111	[55]
Iron-coated cork granulates, 0.8-1.0 mm	0-10	3	20	12±2	[56]
Fe(III)-loaded saponified orange waste gel	0-36	2.5	30	145	[57]
PVA-Fe^0 granules, 2.04±0.98 mm	0-14	7	25	1.65	[59]

[a] adsorbed amount at referred conditions; [b] maximum adsorbed amount obtained experimentally; MOF – metal-organic framework; TA – tannic acid; PVA - polyvinyl alcohol; LDH – layered double hydroxide.

2. Methodology

2.1. Adsorbent and Adsorbate

Given the results of the preliminary studies presented in Subsection 3.5.2 of Chapter III, antimony adsorption assays were initially carried out by further comparing the performance of the following adsorbents: TR, TRO, and TRO-Fe (tannin resin, oxidized tannin resin, and iron-loaded oxidized tannin resin, respectively, particle size 0.15-0.50 mm), obtained by the procedures described in Sections 2.1. and 2.2., and with properties presented in Sections 3.1. and 3.2. of Chapter III. The subsequent adsorption assays were carried out using a tannin resin either produced with a freeze-dried extract (TR) or a precipitated extract (TRp) with particle sizes of 0.15-0.50 mm, <0.15mm, or 1-2 mm.

Sb(III) and Sb(V) were studied as adsorbates. Sb(III) solutions were prepared by dilution of a commercial standard solution (*SCP Science*), containing 1000 mg-Sb L^{-1} in a tartaric acid matrix. Sb(V) solutions were prepared from dissolution of potassium hexahydroxoantimonate(V) salt (analytical grade). Antimony solutions with concentrations up to 30 mg L^{-1} were used in this work, considering maximum levels reported for Sb-contaminated waters in some surveys [10]. Unless otherwise stated, all Sb solutions were prepared in distilled water.

2.2. Analytical Methods

Antimony concentrations in the liquid phase were measured by AAS in air-acetylene flame (*GBC* 932 Plus spectrometer) or by electrothermal atomization in a graphite furnace (*GBC* GF 3000 SenAA Dual spectrometer), at a wavelength of 217.6 nm, using background correction, 0.2 nm slit width and lamp currents of 10 mA or 8 mA, respectively. Flame was used to measure concentrations in the range 2-30 mg L^{-1} (detection limit: 0.8 mg L^{-1}) and graphite furnace used to assess concentrations lower than 2.0 mg L^{-1} (detection limit: 3 µg L^{-1}), after proper dilution and adding nickel (5 µL of $NiNO_3$ solution, containing 50 mg-Ni L^{-1}, per 15 µL of sample injection) as chemical modifier. For both techniques, calibration curves were obtained and accepted for a determination coefficient (R^2) higher than 0.995.

Antimony speciation in solution was achieved by measuring Sb(III) and obtaining Sb(V) by difference from the total dissolved antimony. Sb(III) concentration was measured after liquid/liquid extraction, using ammonium pyrrolidinedithiocarbamate (APDC) as complexing reagent and methyl isobutyl ketone (MIBK) as solvent [60]. The procedure is based on the selective chelate formation of Sb(III) with APDC at pH 5-8 [61, 62], followed by its quantitative extraction in MIBK and direct measure of antimony in the organic phase by AAS. First, 0.6 mL of buffer solution, prepared with sodium acetate 0.1 mol L^{-1} and acetic acid 0.1 mol L^{-1} (9:1 v/v), were added to 15.0 mL of sample solution. Then, 3.0 mL of APDC 2 % solution was added, followed by the addition of 3.0 mL of MIBK. Each sample were vigorously shaken for 2 min and rested for 5 min. Then, antimony concentration in the organic phase was measured. Standard solutions were prepared following the same procedure with concentrations in the range of 0.25-5.0 mg L^{-1}.

Speciation of dissolved iron was assessed by the spectrometric method using phenanthroline [63], as described in Section 2.2. of Chapter IV. Values of dissolved organic carbon of some samples were measured by catalytic oxidation at 680 °C, in a *Shimadzu* TOC-L CSH analyser.

2.3. Batch Adsorption Studies

Adsorption experiments of Sb(III) and Sb(V) by tannin resin were conducted in batch mode. The amount of Sb adsorbed per gram of TR (at a certain contact time, q_t, or at the equilibrium, q_{eq}) was calculated by Eq. IV.1. Suspensions were kept stirring for 24 h (more than the required time to achieve equilibrium) or for the desired contact times (in the case of kinetic experiments, Subsection 2.3.4). Initial pH of solutions was adjusted to different values, using diluted HCl or NaOH solutions. During the contact time, pH was measured and, if necessary, readjusted to be approximately constant (maximum variations of 0.5 pH units). Samples were then taken, filtrated using mixed cellulose ester membrane filters (0.45 µm porosity) and the liquid phase analysed for total dissolved antimony.

2.3.1. Effect of Adsorbent Dosage

The effect of adsorbent dosage on the uptake of Sb(III) by TRp 0.15-0.50 mm was assessed. Adsorption experiments were carried out by adding 50 mL of solution (initial adsorbate concentration: 20 mg L^{-1}) at pH 6 to different adsorbent amounts (12.5-250 mg, corresponding to S/L values ranging from 0.25 g L^{-1} to 5.0 g L^{-1}).

2.3.2. Adsorbent Comparison and Effect of pH

A set of tests were conducted to compare the performance of TR, TRp, TRO, and TRO-Fe on Sb(III) and Sb(V) uptake. These assays were carried out using adsorbate concentrations of 20 mg L^{-1}, adsorbent dosage of 0.50 g L^{-1}, and at pH 2-5. Adsorption assays with TR or TRp were also performed at pH 6. Adsorption capacity of TRO and TRO-Fe was not evaluated for pH above 5 because it becomes unfeasible to keep the pH constant due to the persistent decrease of pH values. In the case of TRO-Fe, iron leaching was re-evaluated (AAS measurement in the liquid phase), and at pH 3 and pH 4, speciation of antimony (Sb(III)/Sb(V)) and iron (Fe(II)/Fe(III)) in solution was assessed.

2.3.3. Competitive Assays

The performance of an adsorbent towards a certain adsorbate may be considerably affected by the presence of other substances in the aqueous medium. Competitive effect of several (oxy)anions on the uptake of Sb(III) and Sb(V) by TRp 0.15-0.50 mm was studied individually. Anions and oxyanions (such as arsenic, chloride, nitrate, etc.) may present a similar chemical behaviour to antimony and compete for the same active sites. The initial Sb(III) and Sb(V) concentration was 20 mg L^{-1} and assays were carried out at 20 °C and at pH 6 (Sb(III)) or pH 2 (Sb(V)) with solid:liquid ratio of 0.50 g L^{-1}. Competitor concentrations used are listed in Table V.3.

Considering that adsorption studies on Sb uptake have mostly addressed the interference of oxyanions, and many works have reported little effect of these compounds [53, 64], additional studies were here conducted. The focus was given on sulphate, which appears in Sb-contaminated waters in levels much greater than other oxyanions (e.g., see [27]), and on metal cations, considering that their influence have been mostly ignored, although

some studies report a more significant effect compared to oxyanions [53]. Thus, competitive effect of several cations, arsenic, and sulphate on the uptake of Sb(III) by TR 0.15-0.50 mm was also studied. The initial Sb(III) was 12 mg L^{-1} or 25 mg L^{-1} and assays were carried out at 20 °C and at pH 6 with solid:liquid ratio of 0.50 g L^{-1}. The concentrations of competing compounds (Table V.3) were chosen based on literature for antimony contaminated mine water and samples collected in the vicinity of abandoned mines [23, 25, 27, 65, 66] (Table V.1).

Table V.3 Concentrations (mg L^{-1}) of coexisting compounds used in competitive assays (pH 6 for Sb(III), pH 2 for Sb(V), S/L = 0.50 g L^{-1}).

System	Sb	As(III)	As(V)	Cl^-	NO_3^-	SO_4^{2-}	PO_4^{3-}	Mg(II)	Mn(II)	Ca
TRp/Sb(III)	20	1.0	–	50	50	600	60	–	–	–
TRp/Sb(V)	20	–	1.0	50	50	600	60	–	–	–
TR/Sb(III)	12	0.5	0.5	–	–	500	–	5	1.0	25
TR/Sb(III)	25	0.5	0.5	–	–	500	–	5	1.0	25

2.3.4. Adsorption Kinetics

The effect of contact time on antimony adsorption by TRp 0.15-0.50 mm was studied in batch mode at constant temperature (25 ºC), adsorbent dosage (0.50 g L^{-1}) and pH (6.0±0.3 for Sb(III) and 2.0±0.2 for Sb(V)). Experiments were conducted using different initial adsorbate concentrations (1 mg L^{-1}, 5 mg L^{-1}, and 20 mg L^{-1}). A volume of 0.50 L of antimony solution was continuously stirred with TRp at 400 rpm. The pH of solutions was initially adjusted to the desired values, frequently checked, and readjusted when necessary. Samples (5 mL) were regularly withdrawn, filtrated, and analysed for Sb concentration. Adsorption kinetics were modelled following the methodology described in Subsection 2.3.2. of Chapter IV, fitting the pseudo-first [67] (Eq. IV.2) and pseudo-second order [68, 69] (Eq. IV.3) models onto the experimental data using the software *CurveExpert 1.4*.

Scanning electron microscopy (SEM) and energy dispersion spectroscopy (EDS) were used to observe the morphology and detect the chemical elemental composition in the TRp surface after saturation with antimony solution. The SEM/EDS exam was carried out following the procedure described in Section 2.4. of Chapter III.

2.3.5. Equilibrium Studies

Adsorption equilibrium isotherms were determined at 25 ºC, for different pH conditions (2, 4, and 6 for Sb(III), 2 and 4 for Sb(V)), using TRp 0.15-0.50 mm, with a dosage of 0.50 g L^{-1} and different initial Sb concentrations (1-30 mg L^{-1}). Equilibrium isotherms were also determined for the adsorption of Sb(III) at pH 6, and Sb(V) at pH 2, at 20 °C, using TR, the same solid:liquid ratio and initial concentrations, by different granulometric fractions: <0.15 mm, 0.15-0.50 mm, and 1-2 mm. To check whether conversion between the two oxidation states occurs, some samples were analysed to assess Sb(III)/Sb(V) distribution.

Moreover, to evaluate the influence of species typically coexisting in Sb-contaminated waters, adsorption isotherms were obtained using (1) a tailings water from a Portuguese mining site (ME) and TRp, and (2) a simulated mine effluent (SME) and TR. Because ME presented a low level of antimony (<10 µg L^{-1}), it was spiked with Sb(III) or Sb(V) to provide the required levels to measure the isotherms (C_{in} = 1-30 mg L^{-1}). Other properties measured in the effluent were: pH 4.2, <3 mg-P L^{-1}, 378 mg-Ca L^{-1}, 430 mg-Mg L^{-1}, <0.5 mg-Fe L^{-1}, 25 mg-Zn L^{-1}, 0.6 mg-Cu L^{-1}. SME was prepared to contain arsenic (0.5 mg-As(III) L^{-1} and 0.5 mg-As(V) L^{-1}), manganese(II) (1.0 mg L^{-1}), magnesium (5 mg L^{-1}), calcium (25 mg L^{-1}) and sulphate (500 mg L^{-1}) and was spiked with different amounts of Sb(III) (C_{in} = 1-30 mg L^{-1}). The concentrations in the SME of the possible interfering species were the same ones used individually in the competitive assays (Subsection 2.3.3.).

Adsorption isotherms were modelled following the methodology described in Subsection 2.3.3. of Chapter IV, fitting the Langmuir [70] (Eq. IV.4) and Freundlich [71] (Eq. IV.5) models onto the experimental data using the software *CurveExpert 1.4*.

2.3.6. Desorption

To study the possible antimony recovery, the regeneration of the adsorbent and an additional understanding of the mechanism involved in antimony uptake by tannin resin (TRp or TR), some desorption experiments were done. Six different eluents were tested: HNO_3 (0.1 mol L^{-1}), HCl (0.04 mol L^{-1}, 0.18 mol L^{-1} and 0.5 mol L^{-1}), NaOH (0.1 mol L^{-1} and 0.5 mol L^{-1}), NaCl (0.5 mol L^{-1}), Na_2HPO_4 (0.5 mol L^{-1}), and EDTA (0.1 mol L^{-1}). Using

a solid:liquid ratio of 2.5 g L^{-1}, suspensions of Sb(III)- or Sb(V)-saturated TR with each eluent were kept stirring for the desired time (20-24 h), were then filtered, and final solutions were analysed for antimony and DOC.

2.4. Column Experiments

Continuous adsorption studies using a fixed-bed column were carried out using TR 1-2 mm as adsorbent and Sb(III) as adsorbate. A glass column (1 cm internal diameter) equipped with two flow adapters to regulate the bed height (L), and polyethylene bed supports (20 µm porosity) at the top and bottom ends, was used. After filling the column with the desired amount of adsorbent (m), and before starting the experiment, distilled water was pumped for 4 h. Antimony solutions (inlet concentration denoted as C_i) were then pumped up through the column at varying flow rates (denoted as F) using a peristaltic pump (*Heidolph* Hei-FLOW Advantage 01). Sb(III) solutions prepared in distilled water or in the SME matrix, with pH adjusted to 6, percolated the bed in continuous upward mode and samples taken regularly from the outlet of the column were analysed for total antimony (outlet concentration denoted as C_e). The experiments were conducted at different operating conditions, to evaluate the effect of Sb concentration in the feed (C_i = 1 mg L^{-1} and 9 mg L^{-1}), the volumetric flow rate (F = 1.0 mL min^{-1}, 3.0 mL min^{-1}, and 6.0 mL min^{-1}), and the bed height (L = 6.5 cm and 10.5 cm).

Thomas, Bohart-Adams, and Yan models were fitted to experimental data. The simplified version of the Bohart-Adams (B-A) model [72] is presented in Eq. V.1, as derived in [73]. The parameters k_{BA} and N_0 are the rate coefficient and the adsorption capacity of the adsorbent per unit of bed volume, respectively.

$$ln\left(\frac{C_i}{C_e} - 1\right) = \frac{k_{BA}N_0L}{u} - k_{BA}C_it \qquad \textbf{Eq. V.1}$$

The simplified version of the Thomas model (originally derived in [74, 75]), presented in Eq. V.2, assumes Langmuir equilibrium relationship (valid to Sb(III)/TR adsorption data), although it can be used without regard to the adsorption equilibrium model [73], as k_{Th} (Thomas rate constant) and q_{Th} (maximum adsorption capacity) are determined empirically.

$$ln\left(\frac{C_i}{C_e} - 1\right) = \frac{k_{Th} q_{Th} m}{F} - k_{Th} C_i t \qquad \textbf{Eq. V.2}$$

The non-linear forms of Eq. V.1 and Eq. V.2 are mathematically equivalent and can be expressed in terms of the logistic growth function (Eq. V.3) with two general parameters, a and b [73]:

$$\frac{C_e}{C_i} = \frac{1}{1 + exp(a + bt)} \qquad \textbf{Eq. V.3}$$

The logistic function was fitted to breakthrough data, the two general parameters *a* and *b* were obtained, from which B-A and Thomas model parameters were computed.

The empirical Yan model [76] was also used to describe breakthrough curves, which is represented by Eq. V.4, where q_Y is the maximum adsorption capacity of the adsorbent and a_Y a model parameter.

$$\frac{C_e}{C_i} = \frac{1}{1 + \left(\frac{C_i F t}{q_Y m}\right)^{a_Y}} \qquad \textbf{Eq. V.4}$$

3. Results and Discussion

3.1. Batch Adsorption Studies

3.1.1. Effect of Adsorbent Dosage

Fig. V.2 shows the effect of the solid:liquid ratio on the amount of Sb(III) adsorbed per gram of TRp. As expected, the removal percentage of antimonite increased with the solid:liquid ratio, reaching 97 % at 5.0 g L^{-1}, while adsorption capacity decreased. The highest adsorption capacities, 19±2 mg g^{-1} and 20.4±0.9 mg g^{-1}, were respectively found for 0.25 g L^{-1} and 0.50 g L^{-1}, which are comparable values. The best use of the adsorptive capacity of the adsorbent was then obtained in these conditions. Subsequent adsorption studies using TR or TRp were conducted using 0.50 g L^{-1}, instead of 0.25 g L^{-1}, to decrease the error related to the use of very low adsorbent dosages and to provide higher removal percentages. Adsorption assays with TRO or TRO-Fe were also carried out with an adsorbent dosage of 0.50 g L^{-1}.

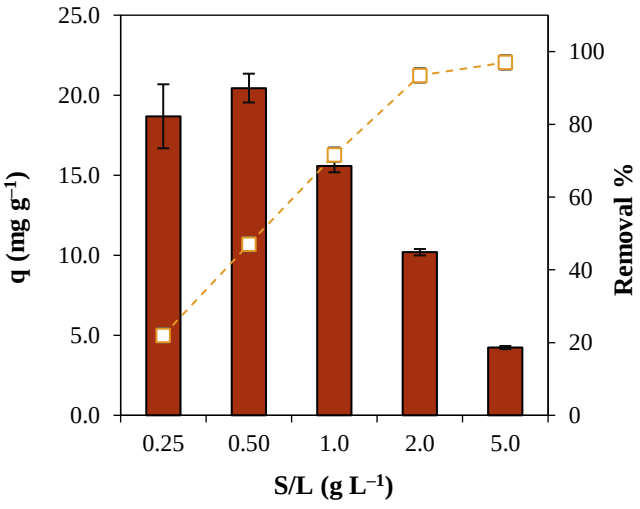

Fig. V.2 Influence of the solid:liquid ratio on equilibrium adsorbed amounts of antimonite (bars) and on the removal efficiency (points) (TRp 0.15-0.50 mm, C_{in} = 20 mg L^{-1}, pH 6).

3.1.2. Adsorbent Comparison and Effect of pH

Fig. V.3 presents antimony adsorbed amounts by TR, TRp, TRO and TRO-Fe at different pH. In general, the adsorptive ability for Sb(III) and Sb(V) of TR and TRp is higher than those of modified forms TRO and TRO-Fe. The uptake of Sb(III) by TR (Fig. V.3a) occurred in the whole pH range studied but is favoured at pH 2 and particularly at near-neutral conditions (pH 6), in which maximum adsorption was obtained (25.1 mg g^{-1}). A similar trend was observed for TRp, with Sb(III) uptake gradually increasing with the increase of pH until achieving a maximum adsorption capacity at pH 6 (19.8 mg g^{-1}). Further increasing the pH to 7 and 8 (data not shown) did not improved adsorption capacity of TRp. The same behaviour was observed on the uptake of Sb(III) by dead seaweeds, where biosorbed amounts increased with increasing pH [53, 77].

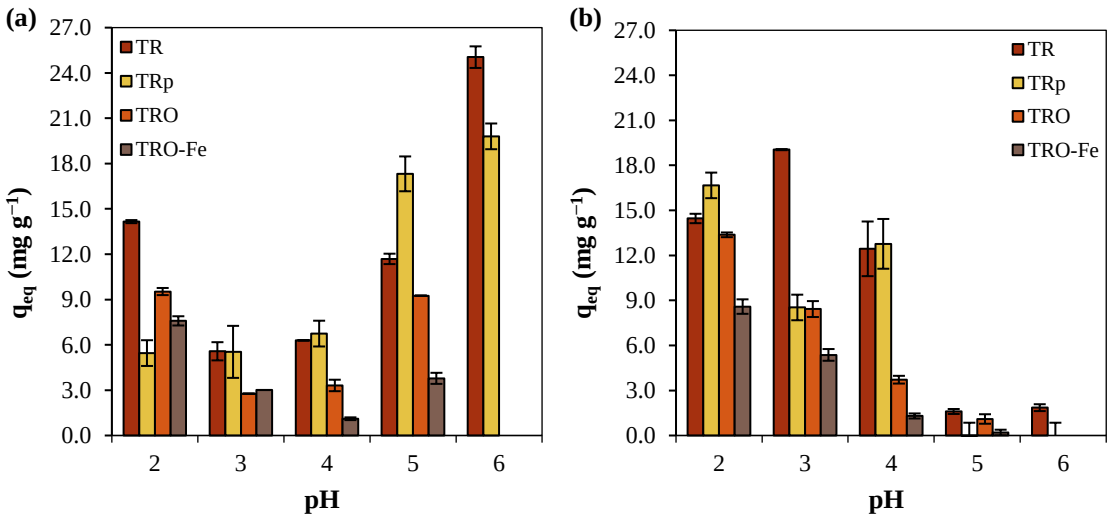

Fig. V.3 Effect of pH on adsorbed amounts of (a) antimonite and (b) antimonate by TR, TRp, TRO and TRO-Fe (C_{in} = 20 mg L^{-1}, S/L = 0.50 g L^{-1}, 20 °C).

According to the speciation diagram of antimony [78] (Fig. V.1), Sb(III) may occur in water under $Sb(OH)_2^+$, $Sb(OH)_3$, and $Sb(OH)_4^-$ species. The neutral species predominates virtually over the cationic and anionic ones in the whole pH range (pH 1.4-11.9). $Sb(OH)_2^+$ occurs at pH levels below 3, and $Sb(OH)_4^-$ at pH above 9. Sb(III) adsorption by TR is attributed to the complexation of $Sb(OH)_3$ with catecholic groups of tannins. At acidic conditions, catechol will be protonated and a 1:1 complex is expected to be formed, whereas for basic conditions, 1:2 complexes are predicted with monodeprotonated catechol [3]. The significant increase in Sb(III) adsorbed amounts from pH 3 to pH 6 is probably due to the increase in $Sb(OH)_3$ predominance in solution to form these complexes.

Considering the IEP of TR (below 2), electrostatic attraction will be not possible between the negatively charged adsorbent and the predominant Sb(III) neutral species. The only opportunity for electrostatic attraction may occur at pH slightly higher than 2, where some surface groups become negatively charged and some Sb(III) remain in solution as $Sb(OH)_2^+$. This may explain the slightly higher adsorbed amount by TR recorded at pH 2, compared to pH 3-4.

Tella and Pokrovski [3] studied the stability of Sb(III) complexes formed with organic ligands in aqueous solution. They reported the establishment of Sb(III) complexes via Sb-O–C bonds with ligands having two or more adjacent carboxyl and/or hydroxyl functional groups (Fig. V.4b). In the case of di-hydroxy-phenol (catechol), which serves for comparison purposes with the present work, two types of complexes are expected to be formed with $Sb(OH)_3$ at acidic conditions (where catechol is protonated) and at basic conditions (monodeprotonated catechol). This observation suggests an adsorption mechanism based on Sb(III) complexation with the di-hydroxy-phenol surface groups, present in B-rings of tannin-materials (Fig. V.4) and explains why Sb(III) is reasonably adsorbed in the whole pH range studied. The infrared spectrum of Sb(III)-loaded adsorbent (not shown) seems to be in line with the proposed mechanism as a decrease in the intensity of the –OH stretching vibration bands and a change in the peak frequency were observed.

Concerning Sb(V), Fig. V.3b indicates maximum removal at pH 2 (TRp, 16.7 mg g^{-1}) and pH 3 (TR, 19.0 mg g^{-1}), although considerable values were also recorded at pH 4. Noticeably, the increase in pH beyond 4 suppressed Sb(V) uptake by both tannin resins, with negligible removals observed. Antimonate is expected to be present in solution as $Sb(OH)_5$ or $Sb(OH)_6^-$ [2, 78]. The anionic species is expected to prevail over the uncharged one for pH levels above 2.5, as per speciation diagrams (Fig. V.1). Considering the IEP of tannin resin, there is no way to uptake Sb(V) by electrostatic attraction at pH above 2.5. However, literature [78] reports the formation of stable complexes between Sb(V) and catechol under a 1:3 stoichiometry (Fig. V.4c). The formation of these type of complexes in aqueous solution and in the pH range 2-4 was demonstrated [78] and is in line with the pH effect observed here, including the uptake inhibition for pH higher than 4. With the increase in pH, the decrease in the affinity between the dominant anionic Sb(V) species and the catecholic groups, which also become deprotonated, explains the negligible uptake recorded at pH 5-6. The main differences between the infrared spectrum

of the tannin-resin before and after Sb(V) uptake (data not shown) are also observed in the –OH stretching region.

Other authors also reported acidic conditions as the most suitable for Sb(V) uptake: for commercial activated alumina, the optimal pH range was identified as 2.8-4.3 and a dramatically decrease was also reported for higher pH values [79]; optimal pH of 2-3 were observed for untreated and modified aerobic granules [80], and for freshwater cyanobacteria *Microcystis* biomass [81].

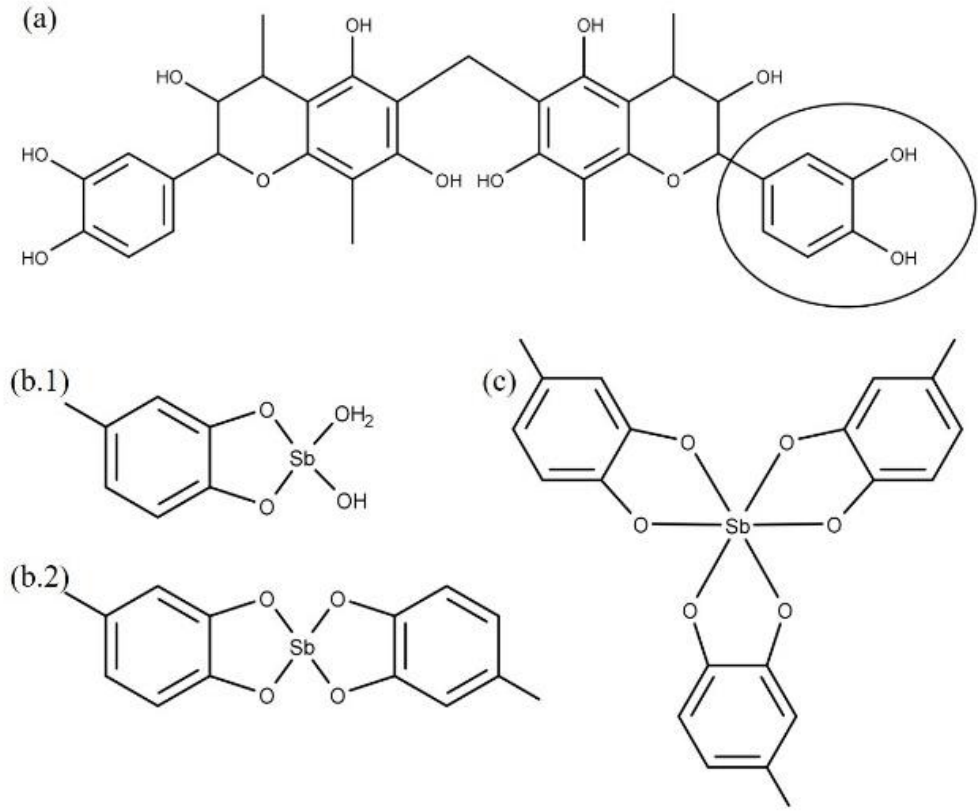

Fig. V.4 Possible structure of the (a) tannin-resin (adapted from [82]), and (b) Sb(III) and (c) Sb(V) complexes formed during adsorption.

Compared to the original TR, TRO presented a lower performance on the uptake of both adsorbates, Sb(III) and Sb(V). This was expected considering that the oxidation was only conducted as an intermediate step to obtain the iron-loaded adsorbent, and that TR partial oxidation causes loss of hydroxyl groups, decreasing the available sites for complexation. Fig. V.3 also shows that TRO-Fe performed worse than TR. The zeta potential results (Section 3.4., Chapter III) made this observation somewhat expected, as the desired improvement in the surface chemistry (decrease in the magnitude of the negative surface charge) was not achieved. A wide variety of materials have been modified with iron,

bearing in mind the specific affinity between Fe-O bonds and Sb [49]. In this case, however, iron-loading did not enhance adsorptive properties of TR, which indicate a higher affinity of Sb to the polyol groups of TR, than to the iron complexes in TRO-Fe.

Total dissolved iron values were most significant at pH 2 (≈3 mg L^{-1}, data not shown), corresponding to approximately 50 % of the loaded metal in TRO-Fe. A possible use of this adsorbent will be limited to pH values above 3 (desirably 4), in which the expected leaching is below 20 % (or 7 %) and generates acceptable dissolved iron concentrations in the liquid phase. Iron leaching here observed was lower than in the stability assays (Section 3.4. of Chapter III) due to lower solid:liquid ratio used (0.5 g L^{-1} vs. 2.0 g L^{-1}).

An additional observation can be made: 50-100 % of the leached iron is under Fe(II) redox state, which indicates that iron(III) was reduced. Blank experiments, conducted using TRO-Fe and distilled water (in replacement of Sb solutions at different pH) showed similar conversions (64-91 % of the total leached iron is under Fe(II), data not shown). Iron(III) reduction is then attributed to the oxidation of some of the remaining hydroxyl groups in TRO-Fe. Indeed, standard reduction potential for Fe^{3+}/Fe^{2+} is 0.77 V, whereas for plant polyphenols ranges from 0.3 V to 0.8 V [83, 84]. These values show that reduction of Fe(III) to Fe(II) in solution via polyphenols oxidation is possible. Sb(III) and Sb(V) were also assessed in solution, but no redox state conversions were observed. The standard reduction potential of $Sb(OH)_6^-/Sb(OH)_3$ is 0.76 V [7, 85], but Sb(V) reduction required high acidity and may not occur at the conditions studied.

In conclusion, tannin resin obtained using a freeze-dried extract and without further treatment (TR) was found to be more suitable to adsorb antimony in both oxidation states, than the oxidized and iron-loaded forms. TR was hence selected to be used in the subsequent experiments. From an operation and environmental point of view, TR is advantageous over TRO-Fe, considering its simpler preparation, easier pH control and absence of secondary pollution generated by iron leaching.

3.1.3. Competitive Assays

The competitive effect of As(III) or As(V), Cl^-, NO_3^-, SO_4^{2-}, and PO_4^{3-} anions on the uptake of Sb(III) and Sb(V) by TRp 0.15-0.50 mm was studied individually and the results on the influence of coexisting compounds are depicted in Fig. V.5. Antimonite uptake by TRp seems to be not affected by the presence of the studied anions. The observed differences between the adsorbed amounts in the control experiment (absence of possible interfering components) and in the presence of the referred competitors was also statistically insignificant for Sb(V), although a minor influence seems to exist due to sulphate and phosphate. The results here obtained indicate that under typical conditions the TRp presents a good selectivity towards Sb(III) and Sb(V) against anions. Literature also reports negligible or minor effects of the studied anions on the uptake of Sb(III) by seaweeds and ferric hydroxide [53, 86]. A little effect (≈16 % decrease) was reported for the performance of a green seaweed on Sb(V) uptake due to sulphate and phosphate [52].

Considering these results, it was decided to assess the impact of some metallic cations, arsenic, and sulphate (species present in the simulated mining effluent) on Sb(III) uptake by TR at for two Sb(III) initial concentrations, 12 mg L^{-1} and 25 mg L^{-1} and results are presented in Fig. V.6. Arsenic and sulphate did not affect antimony uptake by TR, corroborating the results obtained using TRp. Only Mg and Ca ions (metal cations at higher levels) influenced adsorbent performance. Calcium is responsible for 16 % and 19 % reductions of Sb(III) adsorbed amounts from 12 mg-Sb L^{-1} and 25 mg-Sb L^{-1} solutions, respectively. Metal concentrations were measured in solution, before and after contact with TR, and results indicated coadsorption of Mn, Mg and Ca ions together with Sb(III). Adsorbed amounts of 5 mg g^{-1} and 4 mg g^{-1} for magnesium, and 17 mg g^{-1} and 13 mg g^{-1} for calcium, were respectively recorded for initial Sb(III) concentrations of 12 mg L^{-1} and 25 mg L^{-1}. Mn(II) showed no significant effect, possibly due to its low concentration, but Mn dissolved concentration measured in solution has also confirmed its uptake by TR. Despite the high sulphate level tested, this compound did not affect TR performance. These results are not surprising, considering the known ability of polyhydroxy groups in tannins for metal complexation [87] and consequent competition between Sb(III), calcium, magnesium and manganese ions for the same sites.

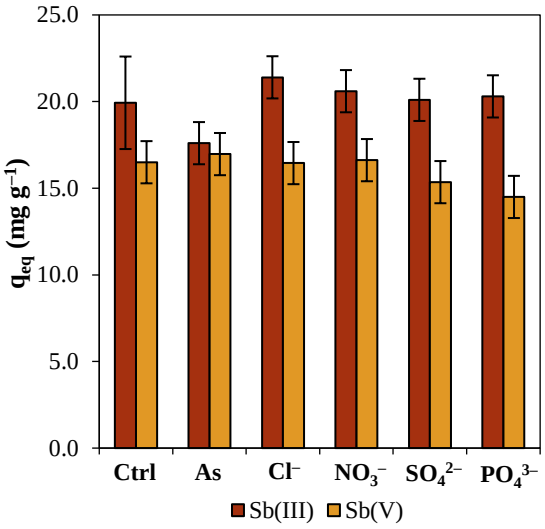

Fig. V.5 Influence of possible coexisting compounds in solution on equilibrium adsorbed amounts of antimony by TRp (C_{in} = 20 mg L^{-1}; S/L = 0.50 g L^{-1}; pH 6 for Sb(III); pH 2 for Sb(V)).

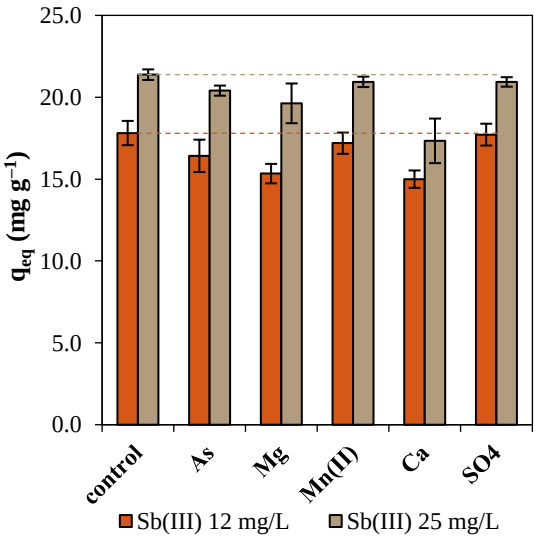

Fig. V.6 Effect of different species on Sb(III) adsorbed amounts by TR, at two different initial adsorbate concentrations (C_{in} = 12 mg L^{-1} and 25 mg L^{-1}, pH 6 and S/L = 0.50 g L^{-1}).

3.1.4. Adsorption Kinetics

Contact time influence on Sb(III) and Sb(V) uptake by TRp was studied for different initial adsorbate concentrations at constant pH, temperature and solid:liquid ratio. The kinetic parameters obtained are presented in Table V.4 and the experimental data alongside with the modelled curves (pseudo-first and pseudo-second order models) depicted in Fig. V.7.

Both models describe adsorption dynamics considerably well, although pseudo-second order regressions provided slightly lower standard errors and the pseudo-first order predicted q_{eq} values are closer to the experimental ones. Adsorption of Sb(III) is evidently faster than Sb(V), suggesting that different kinds of complexes are formed for each oxidation state.

Table V.4 Kinetic models for Sb adsorption on TRp 0.15-0.50 mm (25 ºC, adsorbent dosage 0.50 g L^{-1}, pH 6 for Sb(III) and pH 2 for Sb(V)): parameters (±standard error) and statistical data.

		Pseudo-first order model				Pseudo-second order model			
	C_{in} (mg L^{-1})	$k_1 \cdot 10^2$ (min^{-1})	q_{eq} (mg g^{-1})	R	SE (mg g^{-1})	$k_2 \cdot 10^4$ (g mg^{-1} min^{-1})	q_{eq} (mg g^{-1})	R	SE (mg g^{-1})
Sb(III)	1	2.2±0.1	1.96±0.03	1.00	0.05	122±9	2.22±0.03	1.00	0.04
	5	1.3±0.2	10.0±0.4	0.99	0.57	12±1	11.8±0.3	1.00	0.25
	20	0.58±0.03	23.6±0.6	1.00	4.38	1.5±0.1	32±1	1.00	0.37
Sb(V)	1	0.6±0.1	1.7±0.2	0.98	0.11	21±8	2.3±0.1	0.99	0.11
	5	0.4±0.1	5.2±0.6	0.99	0.31	5±2	7±1	0.99	0.29
	20	0.14±0.05	21±2	1.00	0.46	0.4±0.2	33±6	1.00	0.52

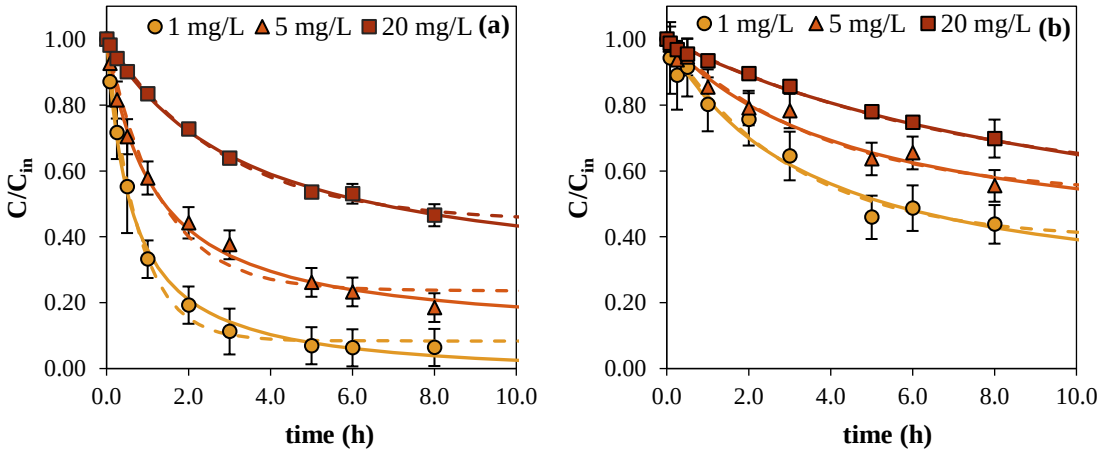

Fig. V.7 Adsorption kinetics of TRp 0.15-0.50 mm for uptake of (a) Sb(III) at pH 6 and (b) Sb(V) at pH 2 (25 ºC, S/L = 0.50 g L^{-1}): experimental data and model curves (- - - pseudo-first order; — pseudo-second order fittings).

Complexation of Sb with catechol is established with Sb/ligand reaction stoichiometries of 1:1 and 1:2 for Sb(III) and 1:3 for Sb(V) [3, 78]. The conjugation with more hydroxyl groups may explain the lower Sb(V) uptake kinetics comparing with Sb(III). Initial adsorption rates (dq/dt for t = 0) were calculated using pseudo-first order parameters. For initial Sb concentrations of 1 mg L^{-1}, 5 mg L^{-1}, and 20 mg L^{-1}, the values respectively obtained were 0.060±0.005 mg g^{-1} min^{-1}, 0.17±0.02 mg g^{-1} min^{-1}, and 0.16±0.02 mg g^{-1} min^{-1} for Sb(III) and 0.011±0.005 mg g^{-1} min^{-1}, 0.03±0.01 mg g^{-1} min^{-1}, and 0.05±0.02

mg g^{-1} min^{-1} for Sb(V). For both adsorbates, initial adsorption rates increased when the initial Sb concentration was changed from 1 mg L^{-1} to 5 mg L^{-1}, due to the increase of the driving force for mass transfer but remained almost constant between initial concentrations of 5 mg L^{-1} and 20 mg L^{-1}.

For Sb(III), time required to reach equilibrium varied between 5 h (C_{in} = 1 mg L^{-1}) and 10 h (C_{in} = 20 mg L^{-1}), although after 5 h of contact time ≈90 % of the maximum adsorbed amount was already attained in the experiment conducted with C_{in} = 20 mg L^{-1}. Times required to reach equilibrium in Sb(V) uptake were estimated to be longer: 11 h for C_{in} = 1 mg L^{-1}, and 20 h for C_{in} = 20 mg L^{-1}. Of note, kinetic studies were only carried out using TRp. In the equilibrium studies, the adsorbent (TRp or TR) was kept in contact with antimony solutions for longer times than those obtained here to assure equilibrium was reached.

Adsorbent samples saturated with Sb(III) and Sb(V), obtained at the end of kinetic assays using initial concentrations of 5 mg L^{-1} and 20 mg L^{-1}, were analysed by SEM and EDS. The antimony did not cause any visible alteration of the adsorbent (Fig. V.8a, confront with Fig. III.10c), although EDS analysis (Fig. V.8b) confirmed antimony presence in the solids, suggesting a homogeneous distribution of the adsorbate on the adsorbent surface.

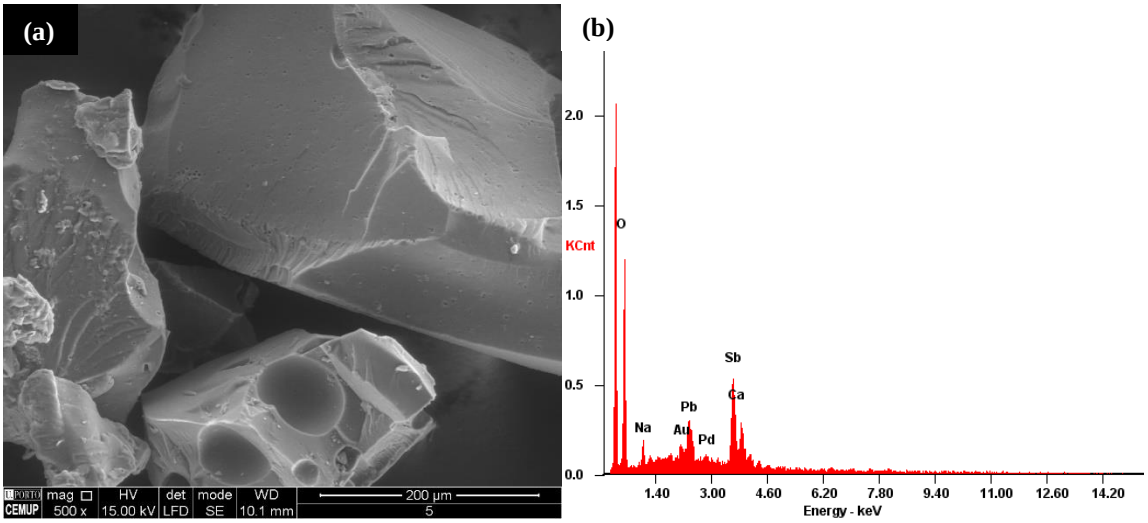

Fig. V.8 SEM image of Sb(III)-saturated TRp (a) and EDS spectrum obtained in a specific particle observed in the image (b).

3.1.5. Equilibrium Studies

Equilibrium isotherms for the adsorption of Sb(III) and Sb(V) by TRp 0.15-0.50 mm at different pH are presented in Fig. V.9. As previously explained, pH 6-8 is the optimal pH range to bind Sb(III) to the TRp. The isotherm was measured at pH 6 considering that most of the Sb-polluted waters present an acidic or slightly acidic pH. Fig. V.9a corroborates previous observations and shows that a significant effect of pH is observed in almost the entire concentration range. In the selected operating conditions (pH 6, S/L = 0.50 g L^{-1}), antimonite removal efficiencies varied between 38±2 % (C_{in} = 30 mg L^{-1}) and 90±1 % (C_{in} = 1 mg L^{-1}). These values clearly illustrate the considerable ability to uptake this toxic metalloid from water in typical soluble concentrations.

Regarding Sb(V) (Fig. V.9b), considerable adsorbed amounts were also recorded, reaching 21.0±0.9 mg g^{-1} and 16.0±0.9 mg g^{-1} at pH 2 and 4, respectively. A slightly better performance of the adsorbent was observed at pH 2 with efficiencies between 33±2 % (C_{in} = 30 mg L^{-1}) and 69±4 % (C_{in} = 1 mg L^{-1}).

Final solutions from adsorption experiments with 20 mg L^{-1} initial Sb(III) and Sb(V) concentrations were subjected to speciation analysis. Final trivalent and pentavalent concentrations were found to be the same as total dissolved Sb, which means that no significant oxidation or reduction reactions involving antimony occurred in solution. Ungureanu et al. [53] also did not observe Sb(III)/Sb(V) conversions in solution during antimony adsorption by seaweeds, and Wu et al. [88] reported up to 6.9 % of Sb(V) in final solutions resultant from Sb(III) adsorption experiments using *Microcystis* biomass.

Langmuir and Freundlich parameters are presented in Table V.5 and model curves plotted in Fig. V.9. Both models described quite well the experimental data, with most of the correlation coefficients (R) being close to 1. Except for the Sb(V) isotherm measured at pH 2, Langmuir fitting provided lower regression standard errors (SE).

Limited adsorption capacities were obtained for Sb(III) at pH 2 and 4 but at pH 6 a very considerable value was achieved (24±3 mg g^{-1}). Similar values were also obtained for Sb(V) at pH 2 and 4 (27±7 mg g^{-1} and 25±10 mg g^{-1}). Observed results show the ability of TRp to uptake both forms of antimony at selected pH values, according to the antimony predominant oxidation state in solution. From the thermodynamic point of view, the pentavalent form is the most stable in oxygenated waters and the trivalent one in reduc-

ing/middle reducing conditions. However, the occurrence of both oxidation forms in thermodynamically unforeseen situations has been reported, which has been attributed to slow kinetics of conversion or biological activity [1], and reinforces the importance to study the uptake of both forms.

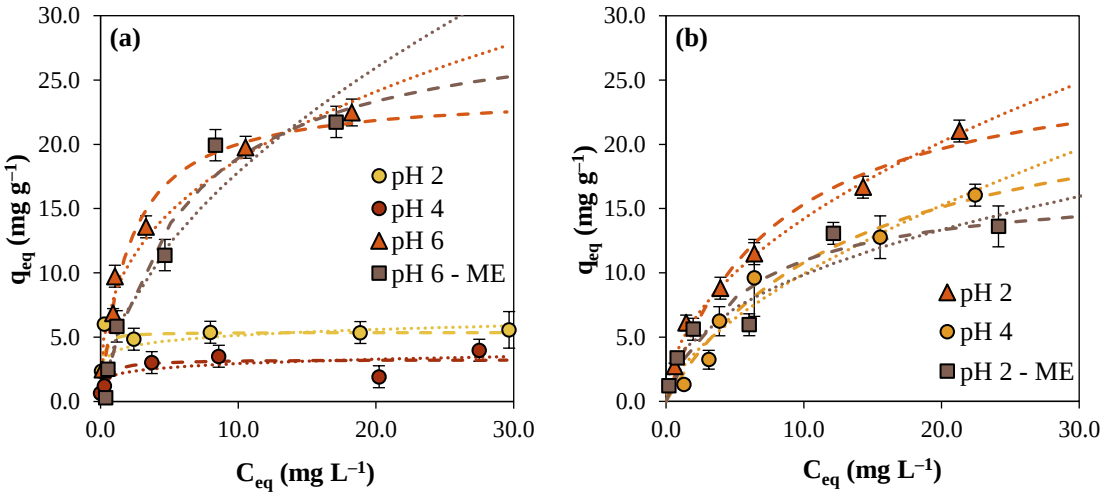

Fig. V.9 Equilibrium isotherms for the adsorption of (a) Sb(III) and (b) Sb(V) by TRp at different pH conditions (25 ºC, S/L = 0.50 g L^{-1}), using Sb distilled water solution and a mine tailings water (ME): experimental data and model curves (– – – Langmuir; ····· Freundlich).

Table V.5 Equilibrium models for Sb adsorption on the TRp 0.15-0.50 mm at different pH and from different aqueous matrices (S/L = 0.5 g L^{-1}, C_{in} = 1-30 mg L^{-1}, 25 ºC): parameters (±standard error) and statistical data.

pH	Langmuir				Freundlich			
	K_L (L mg^{-1})	Q_m (mg g^{-1})	R	SE (mg g^{-1})	K_F (mg$^{1-1/n}$g^{-1}L$^{1/n}$)	n	R	SE (mg g^{-1})
DW – Sb(III)								
pH 2	10±2	5.4±0.1	0.99	0.23	3.88±0.01	8±2	0.95	0.50
pH 4	<6	3.3±0.5	0.84	0.83	2.06±0.01	6±5	0.80	0.92
pH 6	0.5±0.1	24±2	0.99	1.2	8.26±0.04	2.8±0.3	0.99	1.4
ME – Sb(III)								
pH 6	0.16±0.06	30±5	0.99	1.7	5±2	1.9±0.4	0.97	2.6
DW – Sb(V)								
pH 2	0.13±0.04	27±3	0.99	1.3	4.42±0.03	2.0±0.1	1.00	0.57
pH 4	0.07±0.03	25±5	0.96	1.2	2.4±0.2	1.5±0.3	0.95	1.5
ME – Sb(V)								
pH 2	0.2±0.1	17±4	0.95	1.8	3.6±0.8	2.3±0.5	0.96	1.7

Antimony needs to be removed from heavy-contaminated solutions, e.g., mine drainage and mine flotation wastewaters and/or from much more diluted solutions, such as surface or groundwaters, where levels are typically lower than 1 mg L^{-1}. In the latter case, the affinity of the adsorbent to the target adsorbates is also an important parameter. It is a measure of the adsorbent ability to uptake contaminants from very dilute solutions and can be calculated from the slope of the isotherm when equilibrium concentration tends to zero, i.e., the product of K_L and Q_m from the Langmuir model. The following conclusions were obtained from calculated values for TRp: (i) a much higher affinity for Sb(III) than for Sb(V); (ii) similar affinities for Sb(III) at pH 4 and 6; and (iii) similar affinities for Sb(V) at pH 2 and 4. Last observations indicate that pH does not significantly affect the adsorption from low-Sb levels waters.

Fig. V.9 also presents equilibrium adsorption isotherms measured using a mine tailings water (ME) as aqueous matrix and TRp as adsorbent (modelling parameters in Table V.5). In the case of antimonite (Fig. V.9a), there seems to be a small effect of the aqueous matrix for low adsorbate concentrations, which ceases for C_{eq} higher than ≈7 mg L^{-1} as the adsorbed amounts are comparable to the ones obtained in the distilled water matrix. These results were unexpected since ME presented high levels of Ca and Mg (378 mg-Ca L^{-1} and 430 mg-Mg L^{-1}) which are two cations that competitive assays (Subsection 3.1.3.) revealed to be somewhat adsorbed by TR, competing with Sb(III). Nevertheless, metals concentrations in the ME represent the dissolved and particulate contents combined and, if a significant portion of metal was precipitated, it would not substantially exert an influence on Sb adsorption. On the other hand, regarding antimonate (Fig. V.9b), a moderate matrix effect was observed in the mining effluent, with a decrease of up to 38 % in the ability of the TR to uptake Sb(V).

The influence of TR particles size on equilibrium isotherms was assessed at the optimal pH for each oxidation state and results are presented in Fig. V.10. Table V.6 presents the parameters obtained for both equilibrium models and the respective coefficients of correlation (R) and standard errors of the regressions (SE), as quality measures of the fittings. Both models described quite well the adsorption data, considering that R values are in all cases equal or higher than 0.95. In general, Langmuir model fits better the adsorptive behaviour, considering it generates higher R and lower SE values in almost all conditions.

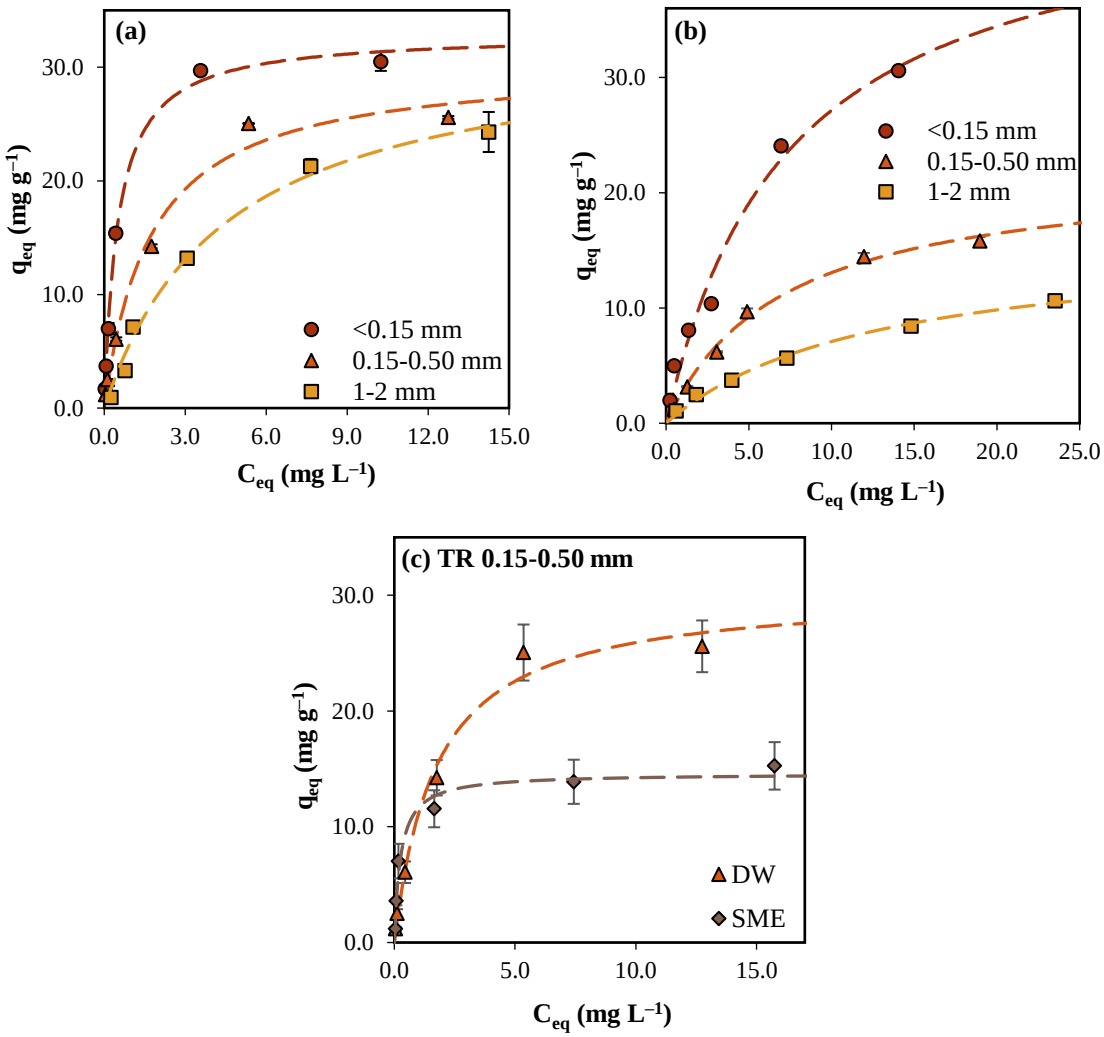

Fig. V.10 Equilibrium isotherms for the adsorption of antimony from (a) Sb(III) solutions (pH 6) and (b) Sb(V) solutions (pH 2) by different granulometric fractions of TR, and from (c) Sb(III) solutions (pH 6) prepared in distilled water (DW) and in the simulated mine effluent (SME) by TR 0.15-0.50 mm (C_{in} = 1-30 mg L^{-1}, S/L = 0.50 g L^{-1}, 20 °C). Points: experimental data; dotted lines: Langmuir model curves.

Table V.6 Langmuir and Freundlich modelling for the adsorption of antimony using TR of different particle sizes, and from different aqueous matrices (S/L: 0.5 g L^{-1}, C_{in} = 1-30 mg L^{-1}, 20 °C): parameters (± standard error) and statistical data.

Particle size	Langmuir				Freundlich			
	K_L (L mg^{-1})	Q_m (mg g^{-1})	R	SE (mg g^{-1})	K_F (mg$^{1-1/n}$ g^{-1} L$^{1/n}$)	n	R	SE (mg g^{-1})
DW – Sb(III) – pH 6								
<0.15 mm	1.9±0.2	32.9±0.8	1.00	0.88	16±2	3.1±0.7	0.95	4.53
0.15-0.50 mm	0.6±0.1	30±2	0.99	1.36	10±2	2.5±0.5	0.96	3.30
1-2 mm	0.22±0.04	33±2	1.00	1.05	6±1	1.9±0.3	0.98	2.35
SME – Sb(III) – pH 6								
0.15-0.50 mm	4±1	14.6±0.8	0.99	1.10	8±1	4.1±0.9	0.95	2.08
DW – Sb(V) – pH 2								
<0.15 mm	0.14±0.04	47±7	0.99	1.78	7±1	1.7±0.2	0.99	1.92
0.15-0.50 0m	0.14±0.02	22±1	1.00	0.53	3.6±0.7	1.9±0.3	0.98	1.32
1-2 mm	0.08±0.01	16±1	1.00	0.66	1.75±0.09	1.73±0.06	1.00	0.19

Equilibrium data shows an effect of the particle size on the uptake of antimony. Higher adsorbed amounts were obtained with finer particles, which is explained by the higher specific surface area and availability of surface groups for the adsorption. The adsorption of Sb(V) was found to be more impacted by TR particle size than of Sb(III). The maximum predicted adsorbed amount calculated for Sb(V) using the coarser particles (16±1 mg g^{-1}) is about one third of the value for smaller particles (47±7 mg g^{-1}). The coarser particles (1-2 mm) have however applicability in fixed-bed adsorption.

Furthermore, maximum adsorption capacities achieved by TR were comparable to the ones achieved by TRp. For the same particle size fraction (0.15-0.50 mm), TR presented a slightly better adsorption capacity for Sb(III) at pH 6 (30±2 mg g^{-1} vs. 24±2 mg g^{-1}) and slightly worse for Sb(V) at pH 2 (22±1 mg g^{-1} vs. 27±3 mg g^{-1}), while both resins presented equivalent K_L values for each oxidation state (Sb(III): 0.5±0.1 L mg^{-1} vs. 0.6±0.1 L mg^{-1}; Sb(V): 0.13±0.04 L mg^{-1} vs. 0.14±0.02 L mg^{-1}) indicating that there is little difference in terms of affinity.

Fig. V.10c presents a comparison of Sb(III) adsorption isotherms measured in distilled water and in the simulated mining effluent (SME) using TR as adsorbent (modelling parameters in Table V.6). For initial Sb concentrations up to 7.5 mg L^{-1} ($C_{eq} \approx 2$ mg L^{-1}), which covers typical levels found in contaminated groundwaters or mine effluents, isotherms measured in distilled water and in SME are practically coincident. This means that the effect of coexisting species was negligible. Nevertheless, with the rise of adsorbate concentration, the adsorbent performance is increasingly affected by the SME matrix. Such results suggest that competition only occurs for lower affinity sites, as shown by the higher value of K_L obtained for SME when compared to the one obtained for DW (Table V.6). The maximum adsorption capacity predicted in SME aqueous media (14.6±0.8 mg g^{-1}) is half the value found in distilled water (30±2 mg g^{-1}). The undermining of Sb(III) adsorption from SME at higher antimony concentrations may be due to the presence of Ca which was the cation that most affected antimony adsorption in the competitive assays (Fig. V.6). These results do not match the ones obtained with ME and, consequently, further studies, particularly with real waters and wastewaters, are required.

The maximum adsorption capacities found for tannin resin indicate a quite effective material. Tannin resin presented a very good performance when compared to other biosorbents, and a comparable uptake to amorphous and commercial alumina (Table V.2).

MOFs present remarkably higher uptake capacities, but also require a considerable processing in their synthesis and present particle sizes not amenable for continuous and large-scale applications. There are not many studies on the use of activated carbon as adsorbent for antimony, but it is known that an additional treatment (usually modification by $FeCl_3$) is required to make it effective [9]. Even so, the performance of the TR seems to be slightly higher, considering that for a modified iron-activated carbon adsorbed amounts of ≈3 mg g^{-1} were obtained under Sb(III) equilibrium concentration of approximately 1 mg L^{-1} (pH 7), while TR uptake was ≈8 mg g^{-1} (pH 6).

3.1.6. Desorption

The desorption percentages of antimony from Sb(III)- and Sb(V)-saturated adsorbents are presented in Table V.7. Results obtained with TRp and TR will be analysed together, due to the similarities between the two adsorbents. Quite limited desorption efficiencies were obtained for adsorbents saturated with Sb(III) and Sb(V), and for all eluents tested. Low desorbed amounts were observed in saline solutions, which is in line with the competitive adsorption studies. Cl^- and PO_4^{3-} did not affect Sb uptake, hence a very low degree of reversibility of the adsorption was expected with chloride and phosphate salts. Furthermore, EDTA has also showed low complexing ability for antimony. Acid solutions were tested with different concentrations and a slight increase in desorption rates with the increase of acid concentration was observed. However, even increasing acid concentration above 0.1 mol L^{-1} did not solve the insufficient desorption efficiency problems, with desorbed amounts remaining low (<17 %), suggesting the involvement of strong and stable chemical bonds between antimony and the tannin resin.

Table V.7 Desorption percentages of antimony from saturated TR with different eluents (S/L = 2.5 g L^{-1}).

Adsorbent	Eluent	Desorption (%)	
		Sb(III)-loaded adsorbent	Sb(V)-loaded adsorbent
TRp	**HNO_3 0.1 mol L^{-1}**	5.4±0.9	13±2
TR	**HCl 0.04 mol L^{-1}**	3±1	8±4
TR	**HCl 0.18 mol L^{-1}**	9±2	11±4
TR	**HCl 0.5 mol L^{-1}**	13±1	17±4
TRp	**NaOH 0.1 mol L^{-1}**	42±6	45±8
TR	**NaOH 0.5 mol L^{-1}**	75±8	69±10
TRp	**NaCl 0.5 mol L^{-1}**	1.9±0.9	2±1
TR	**Na_2HPO_4 0.5 mol L^{-1}**	<3	<3
TRp	**EDTA 0.1 mol L^{-1}**	8±1	2±1

The regeneration of the exhausted material was only found to be feasible using alkaline solutions, with best results observed for NaOH 0.5 mol L^{-1} (desorption efficiencies of 69-75 %). Nevertheless, the use of strong alkaline eluents raised concerns on the stability of the regenerated tannin resin and feasibility of the process. DOC was measured in the eluted solution (NaOH 0.5 mol L^{-1}) and values around 0.2 g-C L^{-1} were observed. This indicates that desorption and regeneration of antimony-saturated tannin resin may not be feasible, not only because the regenerated adsorbent would have a significant drop in its adsorption capacity, but also because the recovery of antimony from a strong alkaline and organic contaminated solution would be impracticable. Indeed, the reusability of other adsorbents on antimony uptake has been frequently described as difficult and raising problems of adsorbent stability [52, 64], although some studies report successful elution with still stronger alkaline solutions: NaOH 1 mol L^{-1} [47, 49] and 0.5 mol L^{-1} [89]. Limited Sb desorption efficiencies were also reported in literature for different biosorbents. Ungureanu et al. [52] indicated desorption efficiencies in the range 12-23 % from Sb(III)-saturated seaweeds and using different saline (0.5 mol L^{-1}), alkaline, and acid solutions (0.5 mol L^{-1}). Wu et al. [88] obtained values (≈63 %) closer to the ones here found, from exhausted *Microcystis* biomass but using HCl 4 mol L^{-1} as eluent.

NaOH 0.5 mol L^{-1} was then selected to be used in regeneration experiments, which were carried out through two adsorption/desorption cycles, using 20 mg L^{-1} Sb(V) solution at pH 2 to load the adsorbent. The second adsorption step took place with no loss on the adsorption capacity (16±2 mg g^{-1} and 18±2 mg g^{-1} were the Sb(V) adsorbed amounts recorded in the first and second adsorption steps, respectively), which show the ability of the alkaline solution to regenerate the adsorbent. However, a strong decrease on the desorption efficiency was observed in the second desorption step, reaching only 28 %. In addition, some colour leaching was observed in these conditions.

As results on TR elution obtained here have demonstrated nonviable regeneration, in the actual context of circular economy, an alternative recovery of antimony through the application of Sb-loaded TR in catalysis or functional materials [51] is suggested to be explored in the future.

3.2. Column Experiments

Continuous adsorption studies using a fixed-bed column were carried out to evaluate the effect of Sb concentration in the feed, the volumetric flow rate, and the bed height. The breakthrough curves (normalized concentrations, C_e/C_i, versus elapsed time, t) are presented in Fig. V.11. Table V.8 presents the model parameters and the quality measures of fittings. The three models represented quite well the breakthrough curves, with most correlation coefficients above 0.97. A slight better adjustment was found for Yan model (lower standard errors) and a more accurate curve for short times.

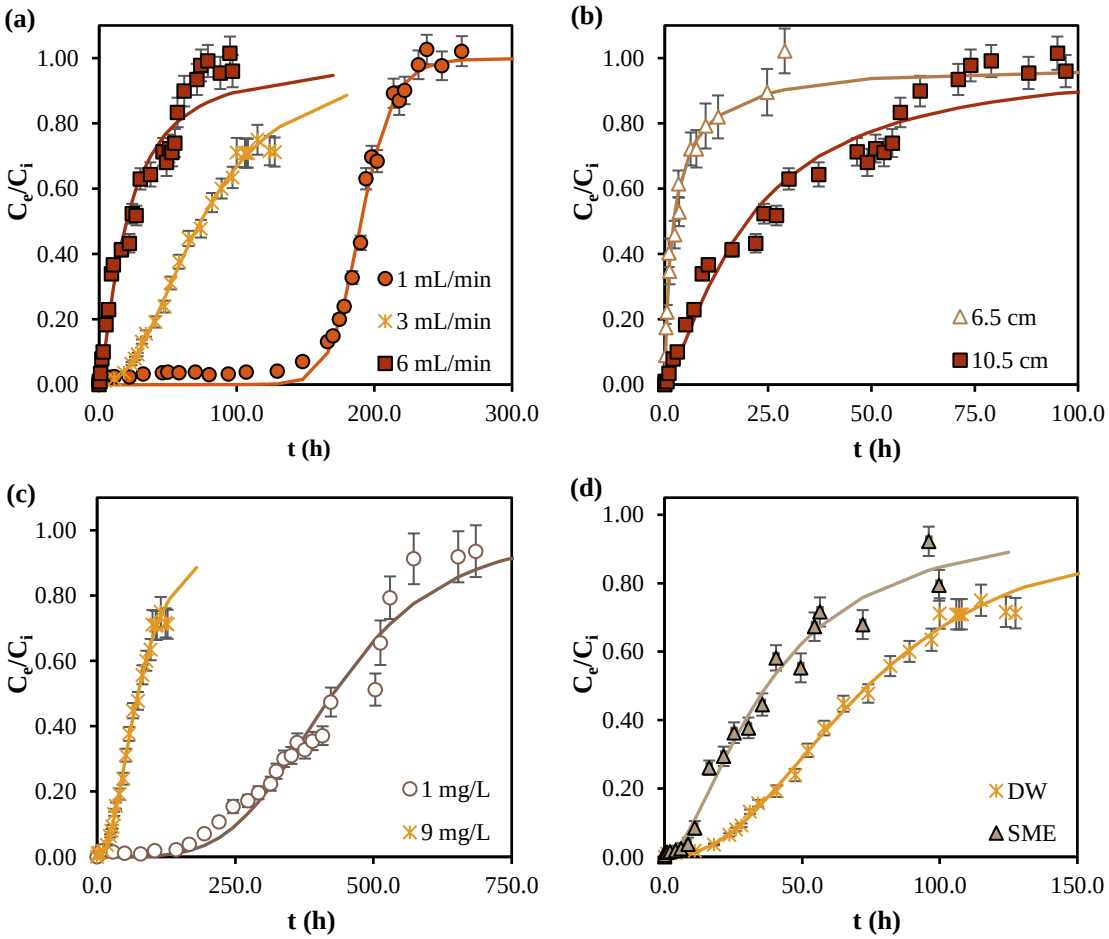

Fig. V.11 Breakthrough curves obtained for the adsorption of Sb(III) by TR (1.0-2.0 mm) in fixed-bed experiments conducted at different: (a) flow rates (C_i = 9 mg L^{-1}, L = 10.5 cm), (b) packed-bed heights (C_i = 9 mg L^{-1}, F = 6 mL min^{-1}), (c) antimony concentrations (L = 10.5 cm, F = 3 mL min^{-1}), and (d) aqueous matrix (C_i = 9 mg L^{-1}, F = 3 mL min^{-1}, L = 10.5 cm). Points represent experimental data and lines Yan model curve.

Table V.8 Bohart-Adams, Thomas, and Yan model parameters for the adsorption of Sb(III) by TR in fixed-bed columns (experimental conditions defined in Table V.9).

Operating condition	**Aqueous matrix**	DW	DW	DW	DW	DW	SME
	C_i (mg L^{-1})	9	9	9	9	1	9
	F (mL min^{-1})	10.5	10.5	10.5	6.5	10.5	10.5
	L (cm)	1.0	3.0	6.0	6.0	3.0	3.0
B-A model	**k_{BA} (mL mg^{-1} h^{-1})**	9.4±0.7	4.6±0.3	6.5±0.6	50±9	11.8±0.9	6.7±0.8
	N_o (mg cm^{-1})	12±1	14±1	12±2	2.0±0.5	8.2±0.8	8±1
Thomas	**k_T (mL mg^{-1} h^{-1})**	9.4±0.7	4.6±0.3	6.5±0.6	50±9	11.8±0.9	6.7±0.8
	q_T (mg g^{-1})	25±2	33±3	25±3	4±1	17±2	17±5
B-A / Thomas	**R**	1.00	0.99	0.97	0.94	0.99	0.97
	SE	0.03	0.05	0.08	0.11	0.05	0.08
Yan model	**a_Y**	16.1±0.9	2.30±0.06	1.3±0.1	0.86±0.06	4.2±0.3	1.7±0.1
	q_Y (mg g^{-1})	25±1	31±2	17±2	2.7±0.2	17±1	15±4
	R	1.00	1.00	0.98	0.99	0.98	0.99
	SE	0.04	0.02	0.07	0.04	0.06	0.04

Table V.9 summarizes the experimental conditions used in each column experiment and presents some results obtained from the analysis of the experimental data. The empty bed contact time (EBCT) was calculated by the ratio between the packed bed height and the superficial velocity of the liquid and represents the average time the feed is in contact with the adsorbent. BV_b denotes the number of the bed volumes until breakthrough (considered as the point where C_e reaches 10 % of C_i). The adsorbent usage rate (AUR) denotes the amount of adsorbent that is necessary to treat a unit volume of water and was calculated by the ratio between the adsorbent mass used in the packed bed and the water volume treated until the breakthrough. The total amount of antimony adsorbed by TR expressed per mass unit of adsorbent (Q) was calculated based on experimental data using Eq. V.5, where t_s symbolize the saturation time:

$$Q = \frac{F}{m} \cdot \int_0^{t_s} (C_i - C_e)\, dt \qquad \textbf{Eq. V.5}$$

Table V.9 Experimental conditions used in fixed-bed column adsorption experiments and performance indicators obtained from experimental data.

Aqueous media	C_i (mg L^{-1})	L (cm)	F (mL min^{-1})	EBCT (min)	Q (mg g^{-1})	BV_b	AUR (kg m^{-3})
DW	9	10.5	1.0	8.4	24.1	1119	0.44
DW	9	10.5	3.0	2.7	30.5	655	0.65
DW	9	10.5	6.0	1.4	25.4	133	3.65
DW	9	6.5	6.0	0.8	8.1	12.4	15.6
DW	1	10.5	3.0	2.7	18.1	4669	0.11
SME	9	10.5	3.0	2.7	19.6	249	1.95

3.2.1. Effect of Flow Rate

Fig. V.11a shows the breakthrough curves obtained at different flow rates (1 mL min^{-1}, 3 mL min^{-1}, and 6 mL min^{-1}), for constant inlet concentration (9 mg L^{-1}) and bed height (10.5 cm). The breakthrough time and the volume of water treated efficiently until the breakthrough decreased with the increase in the flow rate. The effect of flow rate is particularly visible when it increases from 3 mL min^{-1} to 6 mL min^{-1}, where the amount of TR necessary to treat water efficiently has a six-fold increase (AUR, Table V.9). Under these conditions, the operation of the column is then recommended at flow rates lower than 3 mL min^{-1}. The decrease in the bed efficiency with the increase in the flow rate, as a consequence of a lower contact time, is the typical observed pattern in literature [90]. Some authors report that the total adsorption capacity of the adsorbent in a fixed-bed operation could decrease with the increase in the flow rate and explained this by insufficient solute residence time and diffusional limitations [53]. In the present study, however, the results did not show an evident variation of the adsorption capacity of the packed bed with the flow rate. Adsorption capacities (Q, Table V.9) calculated with experimental data varied between 25 mg g^{-1} and 30 mg g^{-1}, which are close to the adsorption capacities estimated by Thomas (q_T) and Yan models (q_Y), and to the maximum adsorption capacity predicted by batch mode adsorption (Q_m = 33±2 mg g^{-1}).

3.2.2. Effect of Bed Height

The effect of the bed height was examined for constant inlet concentration (9 mg L^{-1}) and flow rate (6 mL min^{-1}) with two different bed heights (6.5 cm and 10.5 cm). As it can be seen in Fig. V.11b, the breakthrough curves did not show the typical S-shape with a clear initial phase where the outlet solution should be completely free of antimony. This is justified by the low EBCT (0.8 min and 1.3 min). As expected, and as commonly observed in literature [90], the breakthrough time and the volume efficiently treated increased significantly with the bed height. The breakthrough point obtained for the 6.5 cm bed occurred almost immediately after the experiment start (12.4 BV, Table V.9), which reflected in an extreme inefficiency of the adsorbent usage (AUR = 15.6 kg m^{-3}) and in the maximum adsorbed amount, which was reduced to one-third of the value recorded for 10.5 cm.

3.2.3. Effect of Inlet Concentration

The effect of the inlet concentration was investigated using solutions containing 1 mg L^{-1} and 9 mg L^{-1}, simulating low and heavy-Sb(III) contaminated waters (Fig. V.11c). As expected, feeding the column with a lower Sb(III) concentration led to a slower breakthrough (4669 BV vs. 665 BV) and a decrease in the TR usage (AUR decreased from 0.65 kg m^{-3} to 0.11 kg m^{-3}). The calculated adsorption capacity of the packed bed (in line with capacities predicted by Thomas and Yan models) was lower when 1 mg L^{-1} Sb(III) concentration was used (Q = 18.1 mg g^{-1} vs. 30.5 mg g^{-1}). This is a result of the reduced driving force for adsorption [90] and has been observed in literature [53, 90, 91].

3.2.4. Effect of the Water Matrix

Fig. V.11d compares breakthrough curves obtained for the adsorption of Sb(III) from distilled water (DW) and simulated mine effluent (SME), at constant flow rate (3 mL min^{-1}), bed height (10.5 cm) and inlet Sb(III) concentration (9 mg L^{-1}). The breakthrough point was reached faster in the presence of coexisting compounds in solution (249 BV vs. 655 BV), which led to a lower TR usage efficiency and a decrease in the adsorption capacity (Q reduced from 30.5 mg g^{-1} to 19.6 mg g^{-1}). The explanation lies in the competitive effect of calcium and magnesium, observed in batch mode assays and here corroborated. Outlet solutions obtained at the breakthrough point were analysed for calcium, magnesium, manganese, and arsenic. Results indicated negligible As uptake, whereas 61 %, 100 %, and 83 % removals were recorded for Ca, Mn, and Mg ions, respectively. Despite the reduction in the performance indicators, under a complex aqueous matrix, TR still acted very efficiently on the uptake of antimony, even when the adsorption capacity found in SME (19.6 mg g^{-1}) is compared to literature results obtained in fixed-bed operations using simple Sb(III)/distilled water solutions: 1.1-3.8 mg g^{-1} (*S. muticum* brown alga) [53], 2.83-6.09 mg g^{-1} (composite of quartz sand coated with Fe_3O_4 and graphene oxide) [90] and 20 mg g^{-1} (green bean husk) [54].

4. Conclusions

The performance of the tannin resin on Sb(III) and Sb(V) uptake was compared to a chemical modified form, obtained by its partial oxidation followed by iron-loading. The iron-loaded resin showed a lower adsorptive capacity for both adsorbates, in addition to a significant chemical instability at strong acidic conditions. Further studies proceeded with the unmodified tannin resin, which adsorbed Sb(III) efficiently in the whole acidic pH range, particularly at circum-neutral pH conditions, and Sb(V) at more acidic conditions. The adsorptive ability of the tannin resin is higher for lower particle sizes. The adsorption of Sb(III) and Sb(V) is not significantly affected by the presence of arsenic, chloride, nitrate, sulphate or phosphate, at typical levels, but it is affected by the presence of cations. The time required to reach equilibrium depends on the adsorbate (higher time for Sb(V)) and its initial concentration and varied between 5 and 20 h. Equilibrium results showed that tannin resins present a strong affinity to antimony species, particularly to the trivalent species, which is advantageous since this is the most toxic Sb form. Maximum adsorption capacities of 30-33 mg g^{-1} (Sb(III), pH 6) and 16-47 mg g^{-1} (Sb(V), pH 2) were obtained by Langmuir fittings. A similar value (30±5 mg g^{-1}) was obtained for Sb(III) when a tailings water from a mining site was used as aqueous matrix, while for Sb(V) adsorption capacity was significantly lower (17±4 mg g^{-1}). Furthermore, adsorption of Sb(III) from a complex aqueous media (simulated mine effluent, containing high levels of sulphate, calcium, magnesium, arsenic and manganese) was studied, and a significant effect of the metals was only recorded for high Sb(III) levels (above 7.5 mg L^{-1}). Desorption of Sb(III) and Sb(V) was assessed using different eluents. Strong alkaline solutions were found to be the most effective desorbing agent, although with still limited efficiency (75 % and 69 % desorption of Sb(III) and Sb(V), respectively) and leading to high levels of organic matter in solution. Tannin resin was successfully applied in packed bed adsorption columns run at different flow rates, bed heights and inlet Sb(III) concentrations. The results show that with the right choice of the operating conditions, the maximum adsorption capacities found in batch mode are practically attained in this adsorber configuration. The adsorptive capacity of the tannin resin was practically maintained and adsorbent usage rates as low as 0.11 kg m^{-3} were determined to treat efficiently (90 % removal) 1 mg-Sb(III) L^{-1} contaminated water.

5. References

[1] Filella, M., N. Belzile, and Y.W. Chen, "Antimony in the environment: a review focused on natural waters I. Occurrence," *Earth-Science Reviews*, vol. 57, no. 1-2, pp. 125-176, 2002.

[2] Takeno, N., "Atlas of Eh-pH diagrams: Intercomparison of thermodynamic databases," in "Geological Survey of Japan Open File Report No.419." National Institute of Advanced Industrial Science and Technology. 2005, vol. 419.

[3] Tella, M. and G.S. Pokrovski, "Antimony(III) complexing with O-bearing organic ligands in aqueous solution: An X-ray absorption fine structure spectroscopy and solubility study," *Geochimica Et Cosmochimica Acta*, vol. 73, no. 2, pp. 268-290, 2009.

[4] IARC, *Antimony Trioxide and Antimony Trisulfide. IARC Monographs, Volume 47*. International Agency for Research on Cancer, 1989, pp. 291-305.

[5] WHO, "Antimony in Drinking-water," in "Background document for development of WHO Guidelines for Drinking-water Quality," World Health Organization. 2003.

[6] Stemmer, K.L., "Pharmacology and toxicology of heavy-metals: antimony," *Pharmacology and Therapeutics Part A*, vol. 1, no. 2, pp. 157-160, 1976.

[7] Wilson, S.C., P.V. Lockwood, P.M. Ashley, and M. Tighe, "The chemistry and behaviour of antimony in the soil environment with comparisons to arsenic: A critical review," *Environmental Pollution*, vol. 158, no. 5, pp. 1169-1181, 2010.

[8] Herath, I., M. Vithanage, and J. Bundschuh, "Antimony as a global dilemma: Geochemistry, mobility, fate and transport," *Environmental Pollution*, vol. 223, pp. 545-559, 2017.

[9] Ungureanu, G., S. Santos, R. Boaventura, and C. Botelho, "Arsenic and antimony in water and wastewater: Overview of removal techniques with special reference to latest advances in adsorption," *Journal of Environmental Management*, vol. 151, pp. 326-342, 2015.

[10] Long, X., X. Wang, X. Guo, and M. He, "A review of removal technology for antimony in aqueous solution," *Journal of Environmental Sciences*, vol. 90, pp. 189-204, 2020.

[11] WHO, "Guidelines For Drinking-Water Quality," World Health Organization. Geneva. 2011.

[12] *Council Directive 98/83/EC of 3 November 1998 on the quality of water intended for human consumption*, 1998.

[13] Bagherifam, S., T.C. Brown, C.M. Fellows, and R. Naidu, "Derivation methods of soils, water and sediments toxicity guidelines: A brief review with a focus on antimony," *Journal of Geochemical Exploration*, vol. 205, p. 106348, 2019.

[14] Liang, H.C., "Trends in mine water treatment," *Mining Magazine*, vol. 66, pp. 83-85, 2014.

[15] EU, "Communication from the commission to the European Parliament, the Council, the European Economic and Social Committee of the Regions. Critical Raw Materials Resilience: Charting a Path towards greater Security and Sustainability. European Comission," in "COM(2020) 474 final, 3.9.2020." Brussels. 2020.

[16] Guo, X.J., Z.J. Wu, and M.C. He, "Removal of antimony(V) and antimony(III) from drinking water by coagulation-flocculation-sedimentation (CFS)," *Water Research*, vol. 43, no. 17, pp. 4327-4335, 2009.

[17] Wu, Z., M. He, X. Guo, and R. Zhou, "Removal of antimony (III) and antimony (V) from drinking water by ferric chloride coagulation: Competing ion effect and the mechanism analysis," *Separation and Purification Technology*, vol. 76, no. 2, pp. 184-190, 2010.

[18] Du, X., F. Qu, H. Liang, K. Li, H. Yu, L. Bai, and G. Li, "Removal of antimony (III) from polluted surface water using a hybrid coagulation–flocculation–ultrafiltration (CF–UF) process," *Chemical Engineering Journal*, vol. 254, pp. 293-301, 2014.

[19] Inam, M.A., R. Khan, D.R. Park, B.A. Ali, A. Uddin, and I.T. Yeom, "Influence of pH and contaminant redox form on the competitive removal of arsenic and antimony from aqueous media by coagulation," *Minerals*, vol. 8, no. 12, p. 574, 2018.

[20] Inam, M.A., R. Khan, D.R. Park, S. Khan, A. Uddin, and I.T. Yeom, "Complexation of antimony with natural organic matter: Performance evaluation during coagulation-flocculation process," *International Journal of Environmental Research and Public Health,* vol. 16, no. 7, p. 1092, 2019.

[21] Inam, M.A., R. Khan, M.W. Inam, and I.T. Yeom, "Kinetic and isothermal sorption of antimony oxyanions onto iron hydroxide during water treatment by coagulation process," *Journal of Water Process Engineering,* vol. 41, p. 102050, 2021.

[22] Liu, Y., C. Zhou, Z. Lou, C. Li, K. Yang, and X. Xu, "Antimony removal from textile wastewater by combining PFS&PAC coagulation: Enhanced Sb(V) removal with presence of dispersive dye," *Separation and Purification Technology,* p. 119037, 2021.

[23] Sun, W., E. Xiao, M. Kalin, V. Krumins, Y. Dong, Z. Ning, T. Liu, M. Sun, Y. Zhao, S. Wu, J. Mao, and T. Xiao, "Remediation of antimony-rich mine waters: Assessment of antimony removal and shifts in the microbial community of an onsite field-scale bioreactor," *Environmental Pollution,* vol. 215, pp. 213-222, 2016.

[24] Filella, M., S. Philippo, N. Belzile, Y. Chen, and F. Quentel, "Natural attenuation processes applying to antimony: a study in the abandoned antimony mine in Goesdorf, Luxembourg," *Science of Total Environment,* vol. 407, no. 24, pp. 6205-16, 2009.

[25] Hiller, E., B. Lalinská, M. Chovan, Ľ. Jurkovič, T. Klimko, M. Jankulár, R. Hovorič, P. Šottník, R. Fľaková, and Z. Ženišová, "Arsenic and antimony contamination of waters, stream sediments and soils in the vicinity of abandoned antimony mines in the Western Carpathians, Slovakia," *Applied Geochemistry,* vol. 27, no. 3, pp. 598-614, 2012.

[26] Ondrejková, I., Z. Ženišová, R. Fľaková, D. Krčmář, and O. Sracek, "The distribution of antimony and arsenic in waters of the Dúbrava abandoned mine site, Slovak Republic," *Mine Water and the Environment,* vol. 32, no. 3, pp. 207-221, 2013.

[27] Liu, F., X.C. Le, A. McKnight-Whitford, Y. Xia, F. Wu, E. Elswick, C.C. Johnson, and C. Zhu, "Antimony speciation and contamination of waters in the Xikuangshan antimony mining and smelting area, China," *Environmental Geochemistry and Health,* vol. 32, no. 5, pp. 401-413, 2010.

[28] Wang, X., M. He, J. Xi, and X. Lu, "Antimony distribution and mobility in rivers around the world's largest antimony mine of Xikuangshan, Hunan Province, China," *Microchemical Journal,* vol. 97, no. 1, pp. 4-11, 2011.

[29] Casiot, C., M. Ujevic, M. Munoz, J.L. Seidel, and F. Elbaz-Poulichet, "Antimony and arsenic mobility in a creek draining an antimony mine abandoned 85 years ago (upper Orb basin, France)," *Applied Geochemistry,* vol. 22, no. 4, pp. 788-798, 2007.

[30] Khan, U.A., K. Kujala, S.P. Nieminen, M.L. Raisanen, and A.K. Ronkanen, "Arsenic, antimony, and nickel leaching from northern peatlands treating mining influenced water in cold climate," *Science of Total Environment,* vol. 657, pp. 1161-1172, 2019.

[31] Carvalho, D.L., "Monitorização de áreas mineiras abandonadas: Metodologias de amostragem e análise," 2011.

[32] Masukume, M., M.S. Onyango, and J.P. Maree, "Sea shell derived adsorbent and its potential for treating acid mine drainage," *International Journal of Mineral Processing,* vol. 133, pp. 52-59, 2014.

[33] Farooq, U., J.A. Kozinski, M.A. Khan, and M. Athar, "Biosorption of heavy metal ions using wheat based biosorbents–a review of the recent literature," *Bioresource technology,* vol. 101, no. 14, pp. 5043-5053, 2010.

[34] Fomina, M. and G.M. Gadd, "Biosorption: current perspectives on concept, definition and application," *Bioresource Technology,* vol. 160, pp. 3-14, 2014.

[35] He, J.S. and J.P. Chen, "A comprehensive review on biosorption of heavy metals by algal biomass: Materials, performances, chemistry, and modeling simulation tools," *Bioresource Technology,* vol. 160, pp. 67-78, 2014.

[36] Ighalo, J.O. and A.G. Adeniyi, "Adsorption of pollutants by plant bark derived adsorbents: An empirical review," *Journal of Water Process Engineering,* vol. 35, p. 101228, 2020.

[37] Xu, X., B. Gao, B. Jin, and Q. Yue, "Removal of anionic pollutants from liquids by biomass materials: A review," *Journal of Molecular Liquids,* vol. 215, pp. 565-595, 2016.

[38] Zubair, M., M. Daud, G. McKay, F. Shehzad, and M.A. Al-Harthi, "Recent progress in layered double hydroxides (LDH)-containing hybrids as adsorbents for water remediation.," *Applied Clay Science*, vol. 143, pp. 279-292, 2017.

[39] Anastopoulos, I., A. Bhatnagar, and E.C. Lima, "Adsorption of rare earth metals: A review of recent literature," *Journal of Molecular Liquids*, vol. 221, pp. 954-962, 2016.

[40] Ampiaw, R.E. and W. Lee, "Persimmon tannins as biosorbents for precious and heavy metal adsorption in wastewater: a review," *International Journal of Environmental Science and Technology*, 2020.

[41] Loganathan, P., S. Vigneswaran, J. Kandasamy, and N.S. Bolan, "Removal and Recovery of Phosphate From Water Using Sorption," *Critical Reviews in Environmental Science and Technology*, vol. 44, no. 8, pp. 847-907, 2014.

[42] Mack, C., B. Wilhelmi, J.R. Duncan, and J.E. Burgess, "Biosorption of precious metals," *Biotechnology Advances*, vol. 25, no. 3, pp. 264-271, 2007.

[43] Dou, X., D. Mohan, X. Zhao, and C.U. Pittman Jr., "Antimonate removal from water using hierarchical macro-/mesoporous amorphous alumina," *Chemical Engineering Journal*, vol. 264, pp. 617-624, 2015.

[44] Paajanen, J., S. Lönnrot, M. Heikkilä, K. Meinander, M. Kemell, T. Hatanpää, K. Ainassaari, M. Ritala, and R. Koivula, "Novel electroblowing synthesis of submicron zirconium dioxide fibers: effect of fiber structure on antimony(V) adsorption," *Nanoscale Advances*, vol. 1, no. 11, pp. 4373-4383, 2019.

[45] Qiu, S., L. Yan, and C. Jing, "Simultaneous removal of arsenic and antimony from mining wastewater using granular TiO_2: Batch and field column studies," *Journal of Environmental Sciences*, vol. 75, pp. 269-276, 2019.

[46] Deng, R.-J., C.-S. Jin, B.-Z. Ren, B.-L. Hou, and A.S. Hursthouse, "The Potential For The Treatment Of Antimony-Containing Wastewater By Iron-Based Adsorbents," *Water*, vol. 9, no. 10, p. 794, 2017.

[47] Yang, K., J. Zhou, Z. Lou, X. Zhou, Y. Liu, Y. Li, S.A. Baig, and X. Xu, "Removal of Sb(V) from aqueous solutions using Fe-Mn binary oxides: the influence of iron oxides forms and the role of manganese oxides," *Chemical Engineering Journal*, vol. 354, pp. 577-588, 2018.

[48] Lee, S.-H., M. Tanaka, Y. Takahashi, and K.-W. Kim, "Enhanced adsorption of arsenate and antimonate by calcined Mg/Al layered double hydroxide: Investigation of comparative adsorption mechanism by surface characterization," *Chemosphere*, vol. 211, pp. 903-911, 2018.

[49] Cheng, K., Y.-n. Wu, B. Zhang, and F. Li, "New insights into the removal of antimony from water using an iron-based metal-organic framework: Adsorption behaviors and mechanisms," *Colloids and Surfaces A: Physicochemical and Engineering Aspects*, vol. 602, p. 125054, 2020.

[50] He, X., X. Min, and X. Luo, "Efficient removal of antimony (III, V) from contaminated water by amino modification of a zirconium metal–organic framework with mechanism study," *Journal of Chemical & Engineering Data*, vol. 62, no. 4, pp. 1519-1529, 2017.

[51] Dodson, J.R., H.L. Parker, A.M. Garcia, A. Hicken, K. Asemave, T.J. Farmer, H. He, J.H. Clark, and A.J. Hunt, "Bio-derived materials as a green route for precious & critical metal recovery and re-use," *Green Chemistry*, vol. 17, no. 4, pp. 1951-1965, 2015.

[52] Ungureanu, G., C. Filote, S.C.R. Santos, R.A.R. Boaventura, I. Volf, and C.M.S. Botelho, "Antimony oxyanions uptake by green marine macroalgae," *Journal of Environmental Chemical Engineering*, vol. 4, no. 3, pp. 3441-3450, 2016.

[53] Ungureanu, G., S.C.R. Santos, I. Volf, R.A.R. Boaventura, and C.M.S. Botelho, "Biosorption of antimony oxyanions by brown seaweeds: Batch and column studies," *Journal of Environmental Chemical Engineering*, vol. 5, no. 4, pp. 3463-3471, 2017.

[54] Iqbal, M., A. Saeed, and R.G.J. Edyvean, "Bioremoval of antimony(III) from contaminated water using several plant wastes: Optimization of batch and dynamic flow conditions for sorption by green bean husk (*Vigna radiata*)," *Chemical Engineering Journal*, vol. 225, pp. 192-201, 2013.

[55] Wan, C., L. Wang, D.-J. Lee, Q. Zhang, J. Li, and X. Liu, "Fungi aerobic granules and use of Fe(III)-treated granules for biosorption of antimony(V)," *Journal of the Taiwan Institute of Chemical Engineers*, vol. 45, no. 5, pp. 2610-2614, 2014.

[56] Pintor, A.M.A., B.R.C. Vieira, R.A.R. Boaventura, and C.M.S. Botelho, "Removal of antimony from water by iron-coated cork granulates," *Separation and Purification Technology*, vol. 233, p. 116020, 2020.

[57] Biswas, B.K., J.-i. Inoue, H. Kawakita, K. Ohto, and K. Inoue, "Effective removal and recovery of antimony using metal-loaded saponified orange waste," *Journal of Hazardous Materials*, vol. 172, no. 2-3, pp. 721-728, 2009.

[58] Qi, P., R. Luo, T. Pichler, J. Zeng, Y. Wang, Y. Fan, and K. Sui, "Development of a magnetic core-shell Fe_3O_4@TA@UiO-66 microsphere for removal of arsenic(III) and antimony(III) from aqueous solution," *Journal of Hazardous Materials*, Article vol. 378, 2019, Art. no. 120721.

[59] Zhao, X.Q., X.M. Dou, D. Mohan, C.U. Pittman, Y.S. Ok, and X. Jin, "Antimonate and antimonite adsorption by a polyvinyl alcohol-stabilized granular adsorbent containing nanoscale zero-valent iron," *Chemical Engineering Journal*, vol. 247, pp. 250-257, 2014.

[60] Smichowski, P., Y. Madrid, and C. Camara, "Analytical methods for antimony speciation in waters at trace and ultratrace levels. A review," *Fresenius Journal of Analytical Chemistry*, vol. 360, no. 6, pp. 623-629, 1998.

[61] Castillo, J.R., C. Martínez, P. Chamorro, and J.M. Mir, "Speciation Of Antimony By Differential Generation Of Its Volatile Covalent Hydride In Aqueous And Organic Phase," *Microchimica Acta*, vol. 90, no. 1-2, pp. 95-103, 1986.

[62] Serafimovska, J.M., S. Arpadjan, and T. Stafilov, "Speciation of dissolved inorganic antimony in natural waters using liquid phase semi-microextraction combined with electrothermal atomic absorption spectrometry," *Microchemical Journal*, vol. 99, no. 1, pp. 46-50, 2011.

[63] ISO 6332:1988, *Water quality — Determination of iron — Spectrometric method using 1,10-phenanthroline*, 1988.

[64] Yan, R., Z. Qiu, X. Bian, J. Yang, S. Lyu, and A. Zhou, "Effective adsorption of antimony from aqueous solution by cerium hydroxide loaded on Y-tape molecular sieve adsorbent: Performance and mechanism," *Colloids and Surfaces A: Physicochemical and Engineering Aspects*, vol. 604, p. 125317, 2020.

[65] Neiva, A.M.R., P.C.S. Carvalho, I.M.H.R. Antunes, M.M.V.G. Silva, A.C.T. Santos, M.M.S. Cabral Pinto, and P.P. Cunha, "Contaminated water, stream sediments and soils close to the abandoned Pinhal do Souto uranium mine, central Portugal," *Journal of Geochemical Exploration*, vol. 136, pp. 102-117, 2014.

[66] Gomes, M.E.P. and P.J.C. Favas, "Mineralogical controls on mine drainage of the abandoned Ervedosa tin mine in north-eastern Portugal," *Applied Geochemistry*, vol. 21, no. 8, pp. 1322-1334, 2006.

[67] Lagergren, S.Y., "Zur theorie der sogenannten adsorption gelöster stoffe, Kungliga Svenska Vetenskapsakademiens," *Handlingar*, vol. 24, pp. 1-39, 1898.

[68] Blanchard, G., M. Maunaye, and G. Martin, "Removal of Heavy-Metals from Waters by Means of Natural Zeolites," *Water Research*, vol. 18, no. 12, pp. 1501-1507, 1984.

[69] Ho, Y.S., "Adsorption of heavy metals from waste streams by peat," The University of Birmingham, Birmingham, U.K., 1995.

[70] Langmuir, I., "The adsorption of gases on plane surfaces of glass, mica and platinum," *Journal of the American Chemical Society*, vol. 40, pp. 1361-1403, 1918.

[71] Freundlich, H.M.F., "Over the adsorption in solution," *Journal of Physical Chemistry*, vol. 57, pp. 385-471, 1906.

[72] Bohart, G.S. and E.Q. Adams, "Some aspects of the behavior of charcoal with respect to chlorine," *Journal of the American Chemical Society*, vol. 42, no. 3, pp. 523-544, 1920.

[73] Chu, K.H., "Breakthrough curve analysis by simplistic models of fixed bed adsorption: In defense of the century-old Bohart-Adams model," *Chemical Engineering Journal*, vol. 380, p. 122513, 2020.

[74] Thomas, H.C., "Heterogeneous ion exchange in a flowing system," *Journal of the American Chemical Society*, vol. 66, no. 10, pp. 1664-1666, 1944.

[75] Thomas, H.C., "Chromatography: a problem in kinetics," *Annals of the New York Academy of Sciences*, vol. 49, no. 2, pp. 161-182, 1948.

[76] Yan, G., T. Viraraghavan, and M. Chen, "A new model for heavy metal removal in a biosorption column," *Adsorption Science & Technology*, vol. 19, no. 1, pp. 25-43, 2001.

[77] Vijayaraghavan, K. and R. Balasubramanian, "Antimonite Removal Using Marine Algal Species," *Industrial & Engineering Chemistry Research*, vol. 50, no. 17, pp. 9864-9869, 2011.

[78] Tella, M. and G.S. Pokrovski, "Stability and structure of pentavalent antimony complexes with aqueous organic ligands," *Chemical Geology*, vol. 292, pp. 57-68, 2012.

[79] Xu, Y.H., A. Ohki, and S. Maeda, "Adsorption and removal of antimony from aqueous solution by an activated Alumina," *Toxicological & Environmental Chemistry*, vol. 80, no. 3-4, pp. 133-144, 2001.

[80] Wang, L., C. Wan, D.J. Lee, X. Liu, Y. Zhang, X.F. Chen, and J.H. Tay, "Biosorption of antimony(V) onto Fe(III)-treated aerobic granules," *Bioresource Technology*, vol. 158, pp. 351-354, 2014.

[81] Sun, F.H., F.C. Wu, H.Q. Liao, and B.S. Xing, "Biosorption of antimony(V) by freshwater cyanobacteria *Microcystis* biomass: Chemical modification and biosorption mechanisms," *Chemical Engineering Journal*, vol. 171, no. 3, pp. 1082-1090, 2011.

[82] García, D.E., W.G. Glasser, A. Pizzi, C. Lacoste, and M.-P. Laborie, "Polyphenolic resins prepared with maritime pine bark tannin and bulky-aldehydes," *Industrial Crops and Products*, vol. 62, pp. 84-93, 2014.

[83] Eslami, S., M.A. Ebrahimzadeh, and P. Biparva, "Green synthesis of safe zero valent iron nanoparticles by *Myrtus communis* leaf extract as an effective agent for reducing excessive iron in iron-overloaded mice, a thalassemia model," *RSC advances*, vol. 8, no. 46, pp. 26144-26155, 2018.

[84] Nadagouda, M.N., A.B. Castle, R.C. Murdock, S.M. Hussain, and R.S. Varma, "*In vitro* biocompatibility of nanoscale zerovalent iron particles (NZVI) synthesized using tea polyphenols," *Green Chemistry*, vol. 12, no. 1, pp. 114-122, 2010.

[85] Dorjee, P., D. Amarasiriwardena, and B. Xing, "Antimony adsorption by zero-valent iron nanoparticles (nZVI): Ion chromatography–inductively coupled plasma mass spectrometry (IC–ICP-MS) study," *Microchemical Journal*, vol. 116, pp. 15-23, 2014.

[86] He, Z., R.P. Liu, H.J. Liu, and J.H. Qu, "Adsorption of Sb(III) and Sb(V) on Freshly Prepared Ferric Hydroxide (FeOxHy)," *Environmental Engineering Science*, vol. 32, no. 2, pp. 95-102, 2015.

[87] Koopmann, A.-K., C. Schuster, J. Torres-Rodríguez, S. Kain, H. Pertl-Obermeyer, A. Petutschnigg, and N. Hüsing, "Tannin-Based Hybrid Materials and Their Applications: A Review," *Molecules*, vol. 25, no. 21, p. 4910, 2020.

[88] Wu, F.C., F.H. Sun, S. Wu, Y.B. Yan, and B.S. Xing, "Removal of antimony(III) from aqueous solution by freshwater cyanobacteria *Microcystis* biomass," *Chemical Engineering Journal*, vol. 183, pp. 172-179, 2012.

[89] Zhao, T., Z. Tang, X. Zhao, H. Zhang, J. Wang, F. Wu, J.P. Giesy, and J. Shi, "Efficient removal of both antimonite (Sb(III)) and antimonate (Sb(V)) from environmental water using titanate nanotubes and nanoparticles," *Environmental Science: Nano*, vol. 6, no. 3, pp. 834-850, 2019.

[90] Yang, X., Z. Shi, and L. Liu, "Adsorption of Sb(III) from aqueous solution by QFGO particles in batch and fixed-bed systems," *Chemical Engineering Journal*, vol. 260, pp. 444-453, 2015.

[91] Bulgariu, D. and L. Bulgariu, "Potential use of alkaline treated algae waste biomass as sustainable biosorbent for clean recovery of cadmium(II) from aqueous media: batch and column studies," *Journal of Cleaner Production*, vol. 112, pp. 4525-4533, 2016.

CHAPTER VI

UPTAKE AND RECOVERY OF GOLD

1. Literature Review

Gold (Au) is a precious metal commonly used in jewellery and electronics [1], but also in medicine and as a catalyst in various chemical processes [2]. The wide use of gold in electric and electronic devices is explained by its chemical stability, fine ductility, and high conductivity [3]. For that reason, waste electrical and electronic equipment (WEEE), or e-waste, is known to present high levels of gold, among other precious metals, which could be recovered and reused. The recovery of gold from wastes is crucial for the construction of a sustainable circular economy.

WEEE is a fast-growing waste stream: in 2019, 53.6 Mt of e-waste were generated in the world, corresponding to an average of 7.3 kg per capita [4]. Globally, however, only 17.4 % of that waste was documented to be formally collected and recycled [4]. In Europe, the management of WEEE is regulated by the Directive 2012/19/EU [5], which states that, from 2019, member states should achieve an annual collection rate of WEEE of 65 % of the average weight of EEE placed on the market in the three preceding years. Although Europe was the continent presenting the highest rate (42.5 %), collection and recycling must increase even further to meet the target [4]. WEEE contains bulky metals, along with plastics and toxic elements, but also technology metals which, in the frame of a circular economy, should be recovered. The content of precious/critical metals in WEEE vary considerably, but in certain types of WEEE can even exceed those found in primary sources [6-8]. For instance, levels of 250-2050 ppm of gold have been reported in waste printed circuit boards [9] while actual and chief natural ores present averages concentrations ranging from 1 ppm to 30 ppm [10]. However, greener and more economically competitive routes are necessary to extract metals from WEEE and achieve sustainable processes.

The recovery of precious metals from e-waste usually involves dismantling, comminution, and separation [9, 11, 12], chemical pre-treatments to dissolve base metals [12, 13], followed by pyrometallurgical and/or hydrometallurgical processes. Despite the challenges related to the use of strong acids in leaching processes, and the need to minimise the loss of chemicals, hydrometallurgical processes have been considered a cleaner option to be integrated at the back end of a recycling scheme for the recovery and production of high purity metals [7, 8, 14]. Hydrometallurgical processes also have lower capital costs

and benefit from easier implementation at the small scale. Cyanide has been the dominating leaching reagent of Au from primary resources [15] and is possibly the most reliable and economic for WEEE [12]. However, the toxicity of cyanide makes its use prohibitive in modern processes. Alternative leaching reagents have been proposed to dissolve Au from WEEE, including chloride, aqua regia, thiourea and thiosulfate [15]. The subsequent stage of a typical flowsheet is the extraction of gold from leaching liquors.

Many techniques for recovery of gold from aqueous solutions have been reported to be effective, such as precipitation, solvent extraction, reverse osmosis, electrodialysis, and adsorption. Among them, adsorption has been the dominant one, especially in cyanide liquors, and due to a favourable cost-effectiveness [16], in which activated carbon has been for decades the adsorbent of choice [17, 18]. Adsorption also has the advantage of being effective in concentrating adsorbates from very low concentration solutions. The current interest in moving forward to a more benign recovery has been motivating the search for alternative adsorbents, at more competitive prices and able to sequester gold from non-cyanide leach liquors, more commonly HCl and aqua regia solutions. The use of bio-derived adsorbents has been regarded as a key technology [19], offering advantages related to the ready availability of the biomass, to the simple synthesis and chemical functionality, which usually make them good sequestrants of metals. Important criteria to be met by biosorbents for gold recovery include: (i) high uptake capacity of the metal from actual matrices; (ii) selectivity, i.e., adsorbents should be able to uptake gold to the detriment of other base metals and noble metals coexisting in solution; (iii) fast adsorption kinetics; and (iv) feasible subsequent recovery of the adsorbed metal. In addition, the adsorbents should have particle sizes suitable for use in fixed bed systems, avoiding pressure drop and column clogging, and should also have good chemical stability in strong acidic solutions, considering this is the condition of typical gold-bearing liquors [20]. Various adsorbents have been investigated for gold recovery, including commercial resins [21, 22], crosslinked polyethyleneimine resin [21], and a wide range of natural-derived adsorbents such as polyethyleneimine modified Ca-alginate fibres [20], polyethyleneimine modified *Lagerstroemia speciosa* leaves [23], banana peel derivatives [24], and raw date pits [25]. The successful uptake of gold has been explained by electrostatic interaction between the gold complexes in solution and the adsorbent surface, followed by a reduction mechanism, involving amine, hydroxyl, and aldehyde groups of the adsorbents [20, 23, 26, 27].

Uptake of gold from leach liquors by tannin-adsorbents has also been widely reported in the literature, as discussed in Chapter III. Outstanding uptake capacities of gold have been reported for different tannin-adsorbents [3, 7, 26, 28-39], explained by the oxidation of polyhydroxyl groups and the reduction of the metal to its elemental form [27, 29, 37, 40, 41]. Tannin resins have shown a selective uptake of gold, against negligible or weakly uptakes of other metals present in the solution (Fe^{3+}, Pb^{2+}, Cu^{2+}, Zn^{2+}, Ni^{2+}, Pd^{2+}, Pt^{4+}) [3, 29, 30, 38]. Table VI.1 presents maximum adsorption capacities of gold(III) reported in the literature for different adsorbents. Maximum adsorbed amounts obtained experimentally ($q_{e,m}$) and from Langmuir modelling (Q_m) are presented, together with the most relevant operating conditions, to allow a suitable comparison.

In general, literature has been mostly focused on batch adsorption studies, with few studies reporting results in continuous mode fixed-bed columns [3, 40]. The column studies carried out by Xie et al. [3] suggested that the resin was effective for the uptake of Au(III) from aqueous solutions, but during the adsorption step, and even after 8,000 bed volumes, adsorption equilibrium (saturation) was not achieved. Based on the observations, the researchers suggested that the loaded Au(III) was being aggregated at the upper surface layer of the bed as nanoscale gold particles form, and the separation of the reduced gold particles from the biosorbent was generating new active sites in the persimmon powder-formaldehyde resin. Results presented by Fan et al. [38] also show that during adsorption in a packed-bed column, the outlet gold concentration has never reached the inlet value, which corroborates the previous observations.

The elution of the gold from the loaded-biosorbent has been successfully carried out more commonly using acidic thiourea solutions (1.0 mol L^{-1} at pH 2 [3] or 1.0 mol L^{-1} combined with 1.0 mol L^{-1} HCl [32, 34, 39]) but also using a HCl 50 % solution [42]. In contrast, Fan et al. [38] proposed incineration to recover gold from the loaded adsorbent. The authors reported an amount of 50.6 mg of gold (99.9 % purity), obtained by incineration of 100 mg of saturated tannin resin.

Chemical modified resins with amine compounds (BTU, AG, TEPA, DMA) have been also synthesized and evaluated for gold recovery [32-35]. Even though these treatments seem to have little impact on adsorption capacity when compared to unmodified resins [7, 30], Gurung et al. [33] reported an outstanding selectivity of an AG-modified persimmon tannin resin, stating that the amine treatment creates positively charged sites due to

amine protonation in acidic medium. Gold concentration in these amine-modified adsorbents has been reported as a result of anion exchange coupled electrostatic interaction, with simultaneous reduction of adsorbed Au(III) to elemental form [32-34], similarly to unmodified tannin resins.

Table VI.1 Maximum adsorption capacities reported in literature for the adsorption of gold from chloride media by different adsorbents.

Adsorbent	T (°C)	pH or [H^+]	C_e (mg L^{-1})	$q_{e,m}$ (mg g^{-1})	Q_m (mg g^{-1})	Ref.
Persimmon resin	30	pH 2	150-351	≈965	1905	[3]
TEPA-persimmon tannin gel	30	0.1 mol L^{-1}	0-1.2 × 10^3	—	1168	[7]
PEI-alginate fibres	25	0.1 mol L^{-1}	0-2000	1240	1404	[20]
GA-PEI-alginate fibres	25	0.1 mol L^{-1}	0-1500	2325	2182	[20]
Commercial resin IRA400	—	pH 2	0-215	—	902.3	[21]
Crosslinked PEI resins	—	pH 2	0-210	—	943.5	[21]
Commercial resin Lewatit TP214	25	pH 6.1	35-225	—	108.7	[22]
Activated rice husk	25	pH 6.1	50-260	—	93.46	[22]
PEI-modified *L. speciosa* leaves	25	pH 1	0-200	282	286	[23]
Banana peel	25	pH 1	0-1200	370.18	377.2	[24]
Banana peel (lipid extraction)	25	pH 1	0-1000	475.48	448.4	[24]
Raw date pits	25	0.5 mol L^{-1}	0-35	78	61	[25]
Sericin and alginate particles chemically crosslinked by proanthocyanidins	25	pH 2.5-3	0-140	196.1	188.4	[26]
Persimmon tannin functionalized viscose fibre	25	pH 2	0-120	528	536	[27]
Persimmon peel gel	30	0.1 mol L^{-1}	0-11 × 10^3	1.8 × 10^3	—	[29]
Crosslinked persimmon tannin gel	30	0.1 mol L^{-1}	0-2.4 × 10^3	1517	—	[30]
Persimmon tannin onto Fe_3O_4@SiO_2 microspheres	25	pH 5	(0.2-1.8) × 10^3	860	917.4	[37]
EDA-modified persimmon tannin	30	0.1 mol L^{-1}	0-1.5 × 10^3	—	1550.4	[39]
Oil palm trunk (dewaxed)	30	pH 2	0-120	91.47	95.16	[43]
Polyaniline modified by TMP	25	pH 4	0-300	881	883	[44]
NIPA gel	50	1 mol L^{-1}	0-790	—	125.5	[45]
Cellulose acetate fibres	25	2 mol L^{-1}	0-800	110	—	[46]
PAR-modified Zr MOF (PAR-UiO-66)	25	pH 4	288-988	—	662.6	[47]

a – Aqua regia (HCl/HNO_3). EDA – ethylenediamine; GA – glutaraldehyde; NIPA – *N*-isopropylacrylamide; PEI – polyethyleneimine; TEPA – tetraethylenepentamine; TMP – trimethyl phosphate; PAR – 4-(2-pyridylazo)resorcinol; MOF – metal organic framework.

Moreover, immobilized bayberry tannins onto collagen fibres were also able to uptake gold extensively from an acidic solution [36]. However, desorption was proven to be impossible; many eluents were tested (sodium bicarbonate, sodium carbonate, hydrochloric acid, urea, and thiourea) and all failed. This is a drawback for this adsorbent, limiting the subsequent recovery to burning, as suggested by the authors. Another possible way but limited to specific applications (catalysis, for instance) is the direct reuse of gold loaded in the adsorbent.

Even though literature on the recovery of gold by tannin-adsorbents has yielded many reports, it has been limited almost exclusively to persimmon tannins [7, 21, 27, 30, 32, 37, 38, 42, 48-52], with a few reports using tannic acid [53, 54] or bayberry [31] as tannin source-materials. No studies were found in the literature evaluating the uptake of precious metals by pine bark tannin-adsorbents and subsequent recovery. More research is also needed to obtain results in aqua regia solutions and stronger chloride and acidic media. Consequently, the work presented in this Chapter focused on the study of gold(III) adsorption by a tannin resin prepared from the bark of maritime pine (*Pinus pinaster*). Chloride and aqua regia solutions were used, and the uptake of gold was investigated from single and multi-metal systems, simulating actual hydrometallurgical liquors. The final recovery of the metal was achieved by elution.

2. Methodology

2.1. Adsorbent and Adsorbate

In every adsorption assay reported in this Chapter, the adsorbent used was the TR (tannin resin, particle size 0.15-0.50 mm), which was obtained by the procedure described in Sections 2.1. and 3.1. of Chapter III.

Au(III) solutions, with concentrations ranging from 10 mg-Au L^{-1} to 550 mg-Au L^{-1}, were prepared by dilution of a commercial standard 1000 mg-Au L^{-1} containing 2.0 mol L^{-1} HCl (*Merck*). To evaluate the uptake of Au(III) from chloride and aqua regia liquors, two types of strong acidic solutions containing different levels of H^+ were used as aqueous matrices: hydrochloric acid (HCl) and a mixture of hydrochloric acid and nitric acid (HCl/HNO_3 in a ratio of 3:1 (v/v), molar ratio of 2.6:1.0). The desired HCl and HNO_3 concentrations were obtained by the addition of analytical grade commercial acid solutions (HCl 37 % w/w, density 1.19 g mL^{-1}; HNO_3 65 % w/w, density 1.39 g mL^{-1}) and taking into account the pre-existing HCl concentration in the gold standard solution.

2.2. Analytical Methods

The analysis of dissolved metals (Au and, in multi-metal experiments, Cu, Fe, Ni, Pd and Zn) in aqueous solutions was performed by atomic absorption spectroscopy (AAS) with flame atomization (*GBC* 932 Plus spectrometer). The calibration plots were taken daily and accepted for coefficients of determination (R^2) higher than 0.995. In particular, the dissolved gold was measured by air-acetylene flame, using a hollow-cathode lamp operating at 242.8 nm, intensity of 4.0 mA and in the range 3-14 mg L^{-1} (detection limit: 2.7 mg L^{-1}). Potassium nitrate (analytical grade) was added to the standards and samples at final concentrations of 2000 mg-K L^{-1}, to suppress ionization.

2.3. Adsorption Studies

Adsorption studies were conducted in batch mode. Accurately measured volumes of Au solutions (15.0 mL) were put in contact with the required amount of adsorbent (depending

on the desired solid-liquid ratio) in Erlenmeyer closed flasks. Suspensions were stirred in an orbital shaker, operating at 280 rpm. Samples taken from the suspensions were filtered using cellulose acetate membranes (0.45 µm porosity), the liquid phase was diluted when necessary and analysed for gold concentration. All the experiments were made in duplicate, and results are presented as the average values with corresponding uncertainties (absolute deviations or propagated errors). The amount of Au adsorbed per gram of adsorbent (q_t) was calculated by Eq. IV.1.

2.3.1. Effect of Leaching Reagent

Aqueous solutions of 100 mg-Au L^{-1} were prepared in HCl, using acid concentrations varying from 0.2 mol L^{-1} to 3.7 mol L^{-1}, and in aqua regia (HCl/HNO_3), with total H^+ varying from 0.3 mol L^{-1} to 4.2 mol L^{-1}. These solutions were mixed with the tannin resin (adsorbent dosage of 2.0 g L^{-1}) and stirred for two days. The uptake percentages of gold from the initial solution were calculated by Eq. VI.1, where C_{in} and C_f denote gold concentrations (mg L^{-1}) in the initial and the final solutions, respectively.

$$\text{Uptake (\%)} = \frac{C_{in} - C_f}{C_{in}} \times 100 \qquad \textbf{Eq. VI.1}$$

2.3.2. Adsorption Kinetics

The contact time effect on the amount of adsorbed Au was studied using 1.0 mol L^{-1} HCl solution and aqua regia at the same HCl level (total H^+ concentration of 1.4 mol L^{-1}), adsorbent dosages of 0.5 g L^{-1}, 1.0 g L^{-1}, and 2.0 g L^{-1}, and different initial Au concentrations (100 mg L^{-1} and 300 mg L^{-1}). The liquid solutions were stirred with the tannin resin for different periods of time, at room temperature (20±2 °C). Control assays (with no adsorbent) were conducted in parallel. After designated times, suspensions were immediately filtered, and the liquid phase analysed for Au concentration. The amount of Au adsorbed per gram of adsorbent (q_t) was calculated by the mass balance expressed by Eq. IV.1.

Scanning electron microscopy (SEM) and energy dispersion spectroscopy (EDS) were used to observe the morphology and detect the chemical elemental composition in the TR surface after saturation with gold solution. The SEM/EDS exam was carried out following the procedure described in Section 2.4. of Chapter III.

Lagergren's pseudo-first order and pseudo-second order reaction-based models have been widely applied in numerous adsorption systems, due to their simplicity and the commonly good fittings generated and were also employed here. Adsorption kinetics were modelled following the methodology described in Subsection 2.3.2. of Chapter IV, fitting the pseudo-first [55] (Eq. IV.2) and pseudo-second order [56, 57] (Eq. IV.3) models onto the experimental data using the software *CurveExpert 1.4*.

In addition, an intraparticle diffusion model was also used. Linear Driving Force (LDF) approximation (Eq. VI.2) [58] assumes that the uptake rate of an adsorbate is proportional to the difference between the adsorbed phase concentration at the solid/fluid interface (q*, given by Langmuir model) and the average adsorbed phase concentration in the particle (q). The calculation of the LDF constant (k_{LDF}) was done using the explicit equation Eq. VI.7 that results from Eq. VI.2, combined with the use of the variables expressed in Eq. VI.3 to Eq. VI.6 [59]. The *solver* tool in Excel was used to obtain k_{LDF} constants, by minimizing the sum of squared residuals. The calculation of D_h, based on Eq. VI.7 [60], assumes spherical adsorbent particles (r_p denotes the average particle radius) and a parabolic profile of metal concentration inside the particle.

$$\frac{\partial q}{\partial t} = k_{LDF} \times (q^* - q) \qquad \textbf{Eq. VI.2}$$

$$\xi = \frac{Q_m}{C_0} \times S/L \qquad \textbf{Eq. VI.3}$$

$$y = \frac{C}{C_0} \qquad \textbf{Eq. VI.4}$$

$$a = \xi - 1 + \frac{1}{K_L \cdot C_0};\ b = \frac{1}{K_L \cdot C_0};\ \alpha = \frac{-a+\sqrt{a^2+4b}}{2};\ \beta = \frac{-a-\sqrt{a^2+4b}}{2} \qquad \textbf{Eq. VI.5}$$

$$t = -\frac{1}{k_{LDF}}\left\{\frac{1}{2b} \times ln\left[\frac{y^2 + ay - b}{a - b + 1}\right] + \left(1 - \frac{a}{2b}\right)\left(\frac{1}{\alpha - \beta}\right) \times ln\left[\frac{(1-\beta)(y-\alpha)}{(1-\alpha)(y-\beta)}\right]\right\} \quad \text{Eq. VI.6}$$

$$k_{LDF} = \frac{15 D_h}{{r_p}^2} \quad \text{Eq. VI.7}$$

2.3.3. Equilibrium Studies

Adsorption equilibrium data allow for the design and optimization of the adsorption systems and provide information on the capacity of an adsorbent to accumulate the adsorbate on its surface. Equilibrium isotherms were obtained for the adsorption of Au(III) by the tannin resin at 20 °C and for different aqueous matrices: HCl (1.0 mol L^{-1} and 2.0 mol L^{-1}) and aqua regia (3:1 v/v HCl/HNO_3, $[H^+]$ = 1.0 mol L^{-1}, 1.4 mol L^{-1}, and 2.0 mol L^{-1}). The experimental data was obtained using solutions with initial concentrations of Au in the range 10-550 mg L^{-1} (range reported in literature as possible concentrations in leach liquors) and a constant solid-to-liquid ratio (S/L = 1.0 g L^{-1}). Adsorbent dosages in the range 0.3-3.0 g L^{-1} have been reported in literature [3, 30, 43] for gold uptake. Usually, a higher adsorbent dosage provides a higher uptake efficiency, but a lower usage capacity of the solid. Considering the results obtained with 2.0 g L^{-1} in the assay on the effect of leaching reagent (Subsection 2.3.1), it was decided to use a lower solid-to-liquid ratio (1.0 g L^{-1}) to ensure that final measurable gold concentrations (significantly different from zero) would be obtained to plot the isotherm. Suspensions were stirred for 72 h (enough to attain the steady state). The amount of Au adsorbed per gram of adsorbent in the equilibrium was calculated by the mass balance expressed by Eq. IV.1.

Adsorption isotherms were modelled following the methodology described in Subsection 2.3.3. of Chapter IV, fitting the Langmuir [61] (Eq. IV.4) and Freundlich [62] (Eq. IV.5) models onto the experimental data using the software *CurveExpert 1.4*.

2.3.4. Competitive Assays

The dissolution of precious metals from WEEE is usually preceded by chemical pre-treatments to dissolve base metals (e.g., copper, lead) [12]. However, certain amounts of these metals remain in the residue, together with the precious metals, and are leached out with gold in the subsequent steps. The presence of these metals in solution may affect the adsorption capacity of the adsorbent, due to possible competition. In addition, if an adsorbent sequesters significant amounts of other metals, besides gold, the generation of a final high purity recovered product may be compromised. Assessing the performance of an adsorbent in a multi-metal solution simulating an actual hydrometallurgical liquor is therefore important. Multi-metal solutions containing Au(III) (200 mg L^{-1}), Cu(II) (200 mg L^{-1}), Fe(III) (150 mg L^{-1}), Ni(II) (80 mg L^{-1}), Zn(II) (10 mg L^{-1}) and Pd(II) (40 mg L^{-1}) were prepared in aqua regia at different acidity levels ($[H^+]$ = 0.75 mol L^{-1}, 1.3 mol L^{-1}, and 2.0 mol L^{-1}). The desired concentration of each metal was obtained by the dilution of commercial metal standards (1000 mg L^{-1}) or, in the case of Cu(II), by the dissolution of the $CuCl_2 \cdot 2H_2O$ salt. The metal composition of the simulated solutions was based on the levels reported in literature for aqua regia liquors of WEEE [38, 39]. Simulated leaching solutions were then mixed with the tannin resin at an adsorbent dosage of 1.0 g L^{-1}. After 72 h of stirring, the concentration of each metal was analysed in the liquid and adsorbed amounts and uptake percentages were calculated (Eq. IV.1 and Eq. VI.1). Control assays were conducted in parallel, in similar conditions, but using single-metal solutions (200 mg-Au L^{-1}).

2.4. Desorption and Regeneration

Desorption and regeneration studies were conducted to evaluate the recovery of gold by elution from exhausted adsorbents and the possibility to reuse the regenerated material. A sample of Au-loaded adsorbent was prepared by stirring the tannin resin (1.0 g L^{-1}) with 500 mg L^{-1} Au solution, prepared in HCl 1.0 mol L^{-1} H^+. After the saturation with gold, the adsorbent was separated from the remaining liquid by vacuum filtration, washed with distilled water and dried at 50 °C overnight. The first desorption stage was conducted using a solid-to-liquid ratio of 2.5 g L^{-1} and two different eluents: acid thiourea solution (0.5 mol L^{-1} thiourea and 0.5 mol L^{-1} HCl) and HCl 50 % (v/v). After 3 days stirring, the

liquid phase was analysed for Au and the desorbed percentage calculated. Adsorption and desorption steps were repeated for 3 cycles, using the acid thiourea solution as eluent.

3. Results and Discussion

3.1. Effect of Leaching Reagent

Fig. VI.1 presents the results on gold(III) uptake from aqueous matrices containing different levels of HCl and HCl/HNO_3. In both aqueous systems, the acidity of the medium affected the amount of gold adsorbed by tannin resin.

Total removal of gold from HCl solutions was achieved up to 1.2 mol L^{-1} H^+. Above 2.0 mol L^{-1} HCl the uptake of the metal was seriously affected, and for 3.7 mol L^{-1} HCl it was practically suppressed. Results can be explained considering the effect of H^+, but also the presence of Cl^- ligands, and their effect on the adsorbate species (gold complexes) and on the adsorbent surface. The adsorption mechanism that has been proposed for the uptake of gold by tannin materials is based on an electrostatic attraction followed by the reduction of Au(III) and the oxidation of hydroxyl groups [21, 37]. The redox reaction is expressed by Eq. VI.8, where the reduction of the chlorogold complex is accompanied by the oxidation of hydroxyl to carbonyl groups [41].

$$AuCl_4^- + 3\ R\text{-}OH \rightarrow Au^0 + 3\ R=O + 3\ H^+ + 4\ Cl^- \qquad \textbf{Eq. VI.8}$$

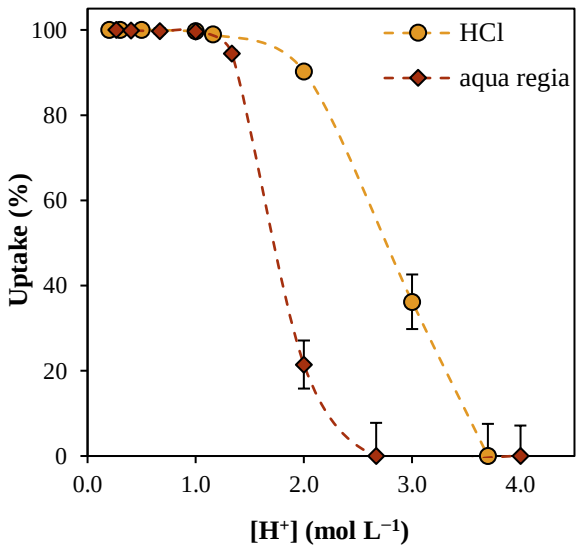

Fig. VI.1 Effect of hydrogen ion concentration ([H^+]) on the uptake of gold by the pine bark tannin resin from HCl and HCl/HNO_3 (aqua regia) aqueous solutions (Cin = 100 mg-Au L^{-1}, S/L = 2.0 g L^{-1}).

Under the HCl concentrations used in this study, Au should be present in solution as tetrachloroaurate(III) complex ($AuCl_4^-$) (speciation diagram presented in [63]), and the resin surface should present a high positive charge. These conditions favour the uptake of Au complexes by electrostatic attraction, which explains the good results observed up to 1.2 mol L^{-1} HCl. However, an excessive increase in HCl concentration (and, consequently, in H^+ and Cl^- levels) impairs the reduction of gold (Eq. VI.8), and chloride ions, abundantly present in solution, may also compete with $AuCl_4^-$ to the active sites of the adsorbent [21, 37]. This explains the marked reduction in the gold uptake observed for HCl levels above 2.0 mol L^{-1}.

With regards to the aqua regia, Fig. VI.1 shows that 100 % of gold in HCl/HNO_3 solutions is sequestered by the tannin resin for acidic levels below 1.0 mol-H^+ L^{-1}. The adsorptive ability sharply decreased for higher acid concentrations and ceases at 2.7 mol L^{-1} H^+ (corresponding to 2.0 mol L^{-1} HCl and 0.7 mol L^{-1} HNO_3). These results can be explained in the same way as for the HCl solutions. For acidity levels higher than 1.2 mol-H^+ L^{-1}, the tannin resin exhibits a higher performance for the uptake of Au(III) from HCl solutions than from aqua regia, and it is much more affected by the acid concentration in the latter system than in the former. This means that the presence of nitric acid in solution impairs the uptake of Au by the adsorbent, being a result of the strong oxidizing capacity of aqua regia which hinders the reduction of Au(III) [38].

The results here obtained are generally in line with those reported in literature. Fan et al. [38] studied the adsorption of Au(III) by a persimmon tannin resin in HCl and HNO_3 media. Under the studied conditions, the adsorbent performance was only significantly reduced for HCl and HNO_3 concentrations higher than 3.74 mol L^{-1} and 3 mol L^{-1}, respectively. The adsorbent performed better in HCl than in HNO_3 aqueous medium. Yi et al. [39] studied the effect of HCl concentration on the adsorption of gold(III) by ethylenediamine modified persimmon tannin-adsorbent and reported a gradual decrease in the Au uptake when the H^+ concentration rose from 0.1 mol L^{-1} to 5.82 mol L^{-1}. Al-Saidi [25] reported an increase in Au(III) removal by raw date pits for HCl concentrations up to 0.5 mol L^{-1}, but a decrease in the uptake efficiency above this level. Most of literature studies were conducted using HCl aqueous matrices. However, aqua regia is also employed as leaching reagent for WEEE, being superior to chloride leaching in some criteria [12, 15], thus the study of gold uptake from aqua regia is important.

Several works have evaluated the uptake of gold under HCl levels equal and lower than 0.1 mol L^{-1}, corresponding to pH values between 1 and 5-6 [20, 23, 24], which are weaker acidic conditions than those used here. In fact, our experiments were carried out by using 1.0-2.0 mol H^+ L^{-1} (HCl and HCl/HNO_3 solutions), closer to the H^+ concentration in actual leach liquors of WEEE, even though a greater adsorbent performance would be assured by using acid levels below 1.0 mol L^{-1}.

3.2. Adsorption Kinetics

The effect of contact time on the uptake of gold was studied at 20 °C, for different adsorbate concentrations, solid-to-liquid ratios, and acidic aqueous matrices. The kinetic profiles are presented in Fig. VI.2 and show a relatively slow adsorptive process, with equilibrium times of two or three days. Similar contact times were found by Gurung et al. [30], with persimmon tannin resins, although other authors report considerably lower values (8 h) [3]. The slow kinetics on the gold uptake appears to be a shortcoming of many biosorbents, but this has been explained by the reductive process of gold, which is essential for high uptake capacities.

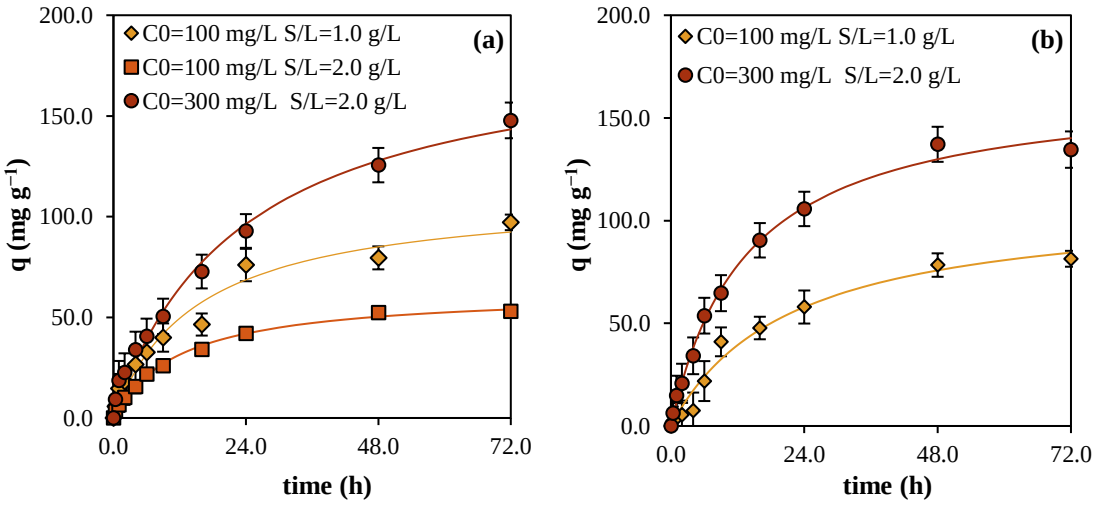

Fig. VI.2 Effect of contact time on the uptake of gold by the pine bark tannin resin at 20 °C, using different initial gold concentrations and adsorbent dosages, and using aqueous solutions of (a) 1.0 mol L^{-1} HCl and (b) aqua regia 1.0 mol L^{-1} H^+: experimental data and pseudo-second order modelling.

Table VI.2 presents kinetic parameters for Lagergren's pseudo-first and pseudo-second order models. Both models describe very well the experimental data, with all coefficients of correlation equal or higher than 0.98. Even though the pseudo-second order model (Fig. VI.2) has mostly provided the lowest SE values, the pseudo-first order predicted equilibrium adsorbed amounts (q_{eq}) closest to the experimental values.

Table VI.2 Kinetic parameters of reaction-based models (k, kinetic constants; q_{eq}, equilibrium adsorbed amounts) for the adsorption of gold from HCl and aqua regia solutions by the pine bark tannin resin, at 20 °C and for different initial Au(III) concentrations (C_{in}) and adsorbent dosages (S/L).

		Pseudo-first order model				Pseudo-second order model			
C_{in} (mg L^{-1})	S/L (g L^{-1})	$k_1 \cdot 10^2$ (h^{-1})	q_{eq} (mg g^{-1})	R	SE (mg g^{-1})	$k_2 \cdot 10^4$ (g mg^{-1} h^{-1})	q_{eq} (mg g^{-1})	R	SE (mg g^{-1})
1.0 mol L^{-1} HCl									
100	1.0	6±1	91±6	0.98	7.2	6±2	112±9	0.98	6.2
100	2.0	7.7±0.6	52±2	0.99	2.2	1.3±0.1	63±2	1.00	1.4
300	2.0	4.7±0.6	147±8	0.99	7.5	2.3±0.5	190±12	0.99	6.0
1.4 mol L^{-1} H^+ aqua regia									
100	1.0	5.3±0.7	84±4	0.99	4.5	4±1	109±9	0.99	4.8
300	2.0	7.2±0.5	136±3	1.0	4.2	4.4±0.5	167±5	1.0	3.8

The kinetics of gold uptake by the tannin resin was also analysed considering an intra-particle diffusion-controlled process. Assuming a negligible mass transfer resistance in the outer layer and considering that intraparticle resistance is governed by surface diffusion (as this adsorbent is essentially a non-porous material), homogeneous solid diffusion model (HSDM) combined with Linear Driving Force (LDF) approximation were used to model kinetic data and to calculate the average values of the homogeneous diffusion coefficients (D_h) (equations in Subsection 2.3.2).

Table VI.3 presents k_{LDF} and D_h estimated values. The quality of the LDF fitting onto the experimental data (coefficients of correlation equal or higher than 0.98) shows that this model can also successfully describe the adsorption of gold by the tannin resin. The homogeneous solid diffusivity coefficients calculated were in the range 10^{-14}-10^{-13} m^2 s^{-1}. Similar values are found in the literature. For example, Saman et al. [43] reported values in the order of magnitude of 10^{-13} m^2 s^{-1} for the adsorption of Au(III) by oil palm trunk biosorbents. For the same adsorbent dosage, the results show an increase in D_h with the initial adsorbate concentration, which has been reported in various adsorptive systems [59, 64], including on the uptake of gold cyanide by activated carbon [18]. For the same

initial adsorbate concentrations and adsorbent dosages, lower k_{LDF} and D_h values were obtained for the aqua regia solutions, in comparison to HCl, which indicates slower adsorption kinetics.

Table VI.3 Kinetic constant (k_{LDF}) of LDF approximation and solid diffusivity coefficients (D_h) calculated by HSDM model for the adsorption of gold from HCl and aqua regia solutions by the pine bark tannin resin at 20 °C.

C_{in} (mg L^{-1})	S/L (g L^{-1})	R	k_{LDF} (h^{-1})	D_h (m^2 s^{-1})
1.0 mol L^{-1} HCl				
100	1.0	0.98	0.076	3.6×10^{-14}
100	2.0	0.98	0.051	2.5×10^{-14}
300	2.0	0.99	0.215	1.1×10^{-13}
1.4 mol L^{-1} H^+ aqua regia				
100	1.0	1.00	0.021	1.0×10^{-14}
300	2.0	0.99	0.087	4.3×10^{-14}

Fig. VI.3 presents the SEM images of the tannin resin adsorbent after gold uptake. After adsorbing gold from HCl (Fig. VI.3a) and aqua regia solutions (Fig. VI.3b and Fig. VI.3c), the adsorbent surface presented an accumulation of metal particles, identified as gold through the EDS spectra (Fig. VI.4). These images are in line with the quantitative adsorption results previously obtained, considering that Fig. VI.3a and Fig. VI.3b (Au-loaded adsorbents in HCl and aqua regia solutions 1.0 mol L^{-1} H^+, respectively) show high amounts of gold particles, whereas Fig. VI.3c shows a much scarce distribution. The EDS spectra obtained in areas not covered by gold particles (not illustrated) showed an abundance of carbon and oxygen (also observed before adsorption), but the additional presence of chlorine. This confirms the competition between chloride and gold to the adsorbent surface.

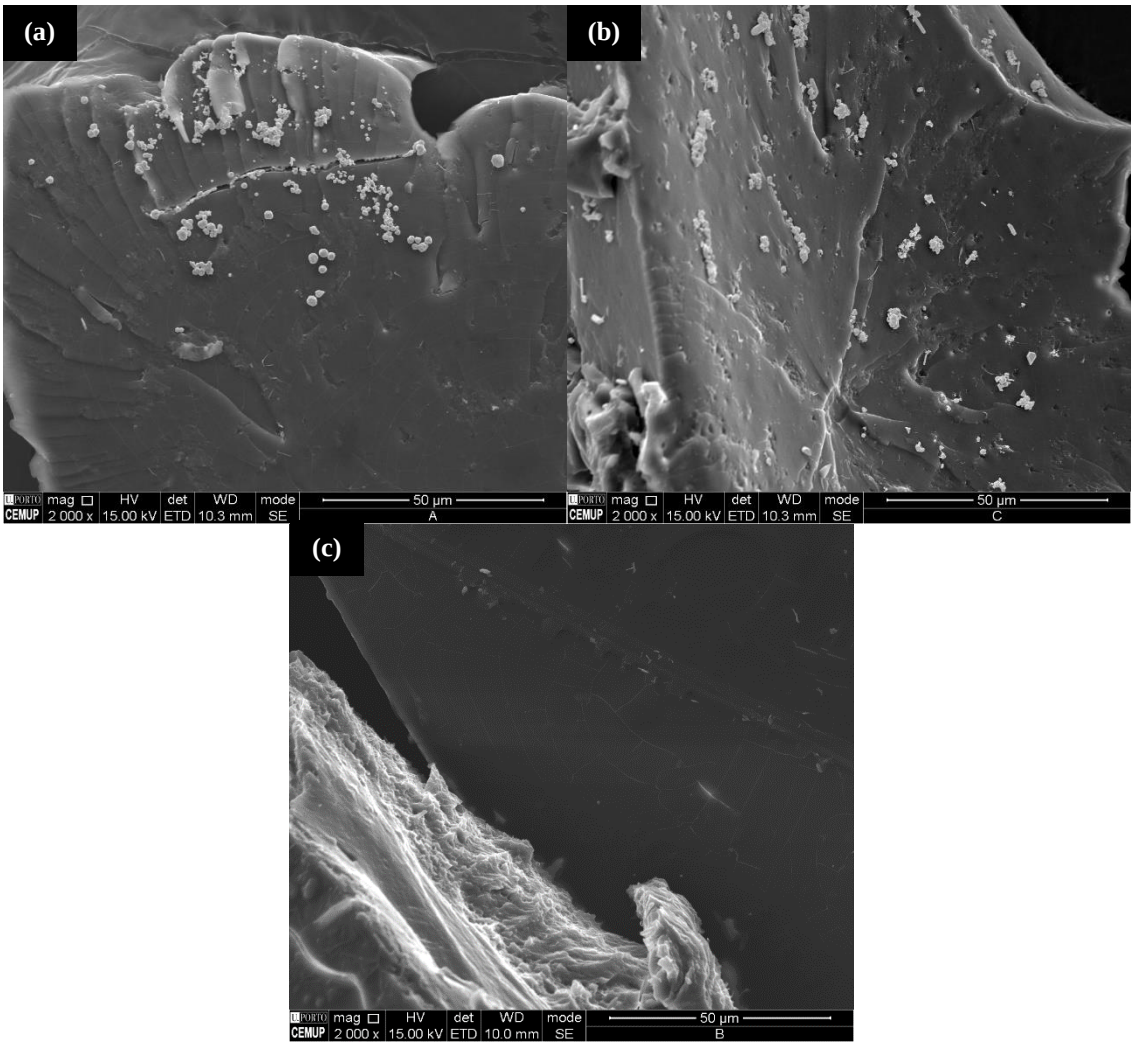

Fig. VI.3 SEM images obtained for the tannin resin after adsorption of gold (a) from 1.0 mol L^{-1} HCl, and from aqua regia solutions (b) 1.0 mol L^{-1} H^+ and (c) 2.0 mol L^{-1} H^+.

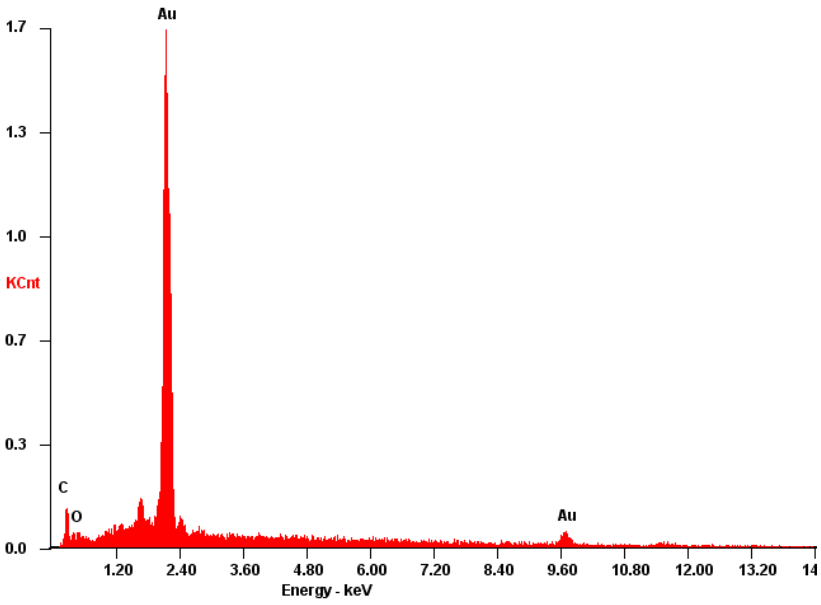

Fig. VI.4 EDS spectra obtained for tannin resin loaded with Au in HCl 1.0 mol L^{-1} H^+ from one of the particles observed in Fig. VI.3a.

3.3. Equilibrium Studies

Fig. VI.5 shows adsorption isotherms obtained for the uptake of gold by the tannin resin, in different acidic systems (HCl and aqua regia). In line with previous results, Fig. VI.5a and Fig. VI.5b show a negative effect of increasing the solution acidity. The slope of the isotherms for low equilibrium concentrations gives indication about the affinity adsorbent/adsorbate, and in both charts (Fig. VI.5a, Fig. VI.5b), the decrease of adsorption is evident for higher H^+ concentrations. Nonetheless, the results show that the negative influence of acid concentrations tends to cease as the Au concentration increases. The adsorbed amounts of Au from 1.0 mol L^{-1} HCl solution are significantly higher than the ones recorded at 2.0 mol L^{-1} only for equilibrium gold concentrations below 100 mg L^{-1} but are practically the same for higher adsorbate levels (Fig. VI.5a). The same happens when it comes to aqua regia (Fig. VI.5b), as the isotherms measured at 1.0 mol L^{-1} and 1.4 mol L^{-1} H^+ get closer for Au concentrations of ≈200 mg L^{-1}. This is reflected by the similarity of the maximum adsorbed amounts obtained experimentally ($q_{e,m}$, Table VI.4) between HCl 1.0 mol L^{-1} and HCl 2.0 mol L^{-1} HCl, and between aqua regia 1.0 mol L^{-1} H^+ and aqua regia 1.4 mol L^{-1} H^+. The use of 2.0 mol L^{-1} of H^+, however, impaired more dramatically the uptake ability, as even for higher Au levels the adsorbed amounts remained significantly below the values obtained at lower acidity.

Fig. VI.5c and Fig. VI.5d compare isotherms measured from HCl and aqua regia matrices, under the same total H^+ concentrations. For 1.0 mol L^{-1} H^+, the two isotherms are quite similar, mainly for low gold concentrations. For 2.0 mol L^{-1} H^+, the performance of the tannin resin is unquestionably worse under aqua regia solutions (Fig. VI.5d). In this case, the maximum adsorbed amounts, recorded within the experimental conditions were 289 mg g^{-1} in HCl solution and 136 mg g^{-1} in aqua regia solution (Table VI.4). Such behaviour should be related to the strong oxidizing power of aqua regia that inhibits the reduction of Au and limits the sequestering ability of the adsorbent. Therefore, the use of HCl as a leaching agent for gold in hydrometallurgical processes has proven to create more favourable conditions than aqua regia, considering its subsequent uptake and recovery.

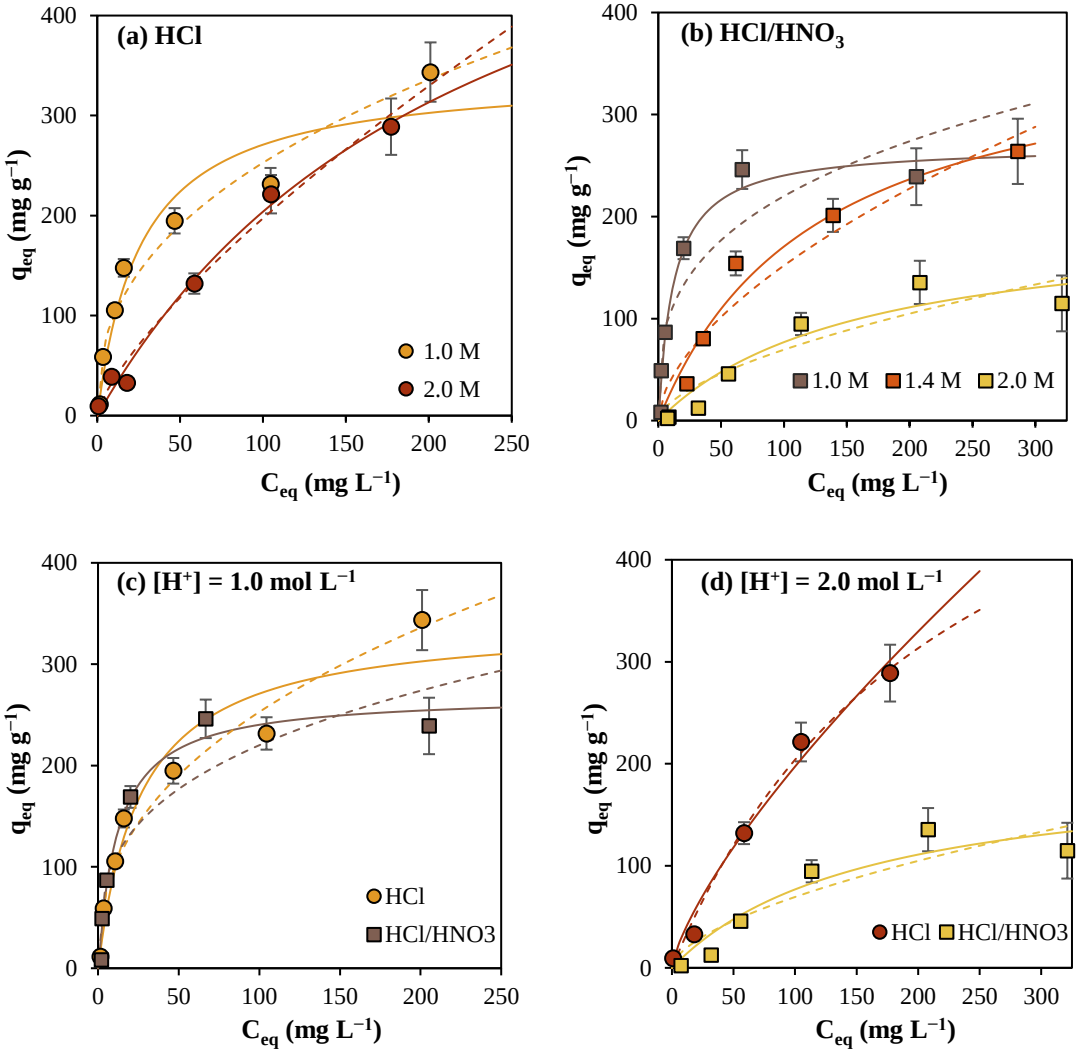

Fig. VI.5 Equilibrium isotherms for the adsorption of gold by the pine bark tannin resin from different acidic matrices (20 °C, S/L = 1.0 g L^{-1}): effect of H^+ concentration in (a) HCl and (b) aqua regia solutions; effect of the leaching reagent for a total H^+ concentration of (c) 1.0 mol L^{-1} and (d) 2.0 mol L^{-1}. Langmuir and Freundlich models are represented by solid and dashed lines, respectively.

Table VI.4 Parameters of Langmuir and Freundlich isotherms for the adsorption of gold from HCl and aqua regia solutions using pine bark tannin resin, at 20 °C.

[H+] (mol L^{-1})	Exp.	Langmuir				Freundlich			
	$q_{e,m}$ (mg g^{-1})	$K_L \times 10^3$ (L mg^{-1})	Q_m (mg g^{-1})	R	SE (mg g^{-1})	K_F ($mg^{1-1/n} g^{-1} L^{1/n}$)	n	R	SE (mg g^{-1})
HCl Solution									
1.0	344 ± 30	38 ± 13	343 ± 38	0.97	31.0	38 ± 7	2.4 ± 0.3	0.98	23.7
2.0	289 ± 28	4 ± 2	675 ± 152	1.00	12.6	7 ± 2	1.4 ± 0.1	0.99	15.7
Aqua Regia Solution									
1.0	246 ± 19	81 ± 21	270 ± 19	0.99	19.3	51 ± 21	3 ± 2	0.91	47.2
1.4	264 ± 32	8 ± 3	386 ± 62	0.98	20.9	10 ± 6	1.7 ± 0.3	0.96	31.5
2.0	136 ± 21	6 ± 4	200 ± 65	0.95	19.3	5 ± 4	1.7 ± 0.5	0.92	24.8

The parameters of Langmuir and Freundlich models are shown in Table VI.4. The coefficients of correlation (R) and the standard error of the regressions (SE) are also presented, as quality measures of the fittings. Modelled curves are illustrated in Fig. VI.5. Both equilibrium models described quite well the experimental data. Considering the higher correlation coefficients and the lower standard errors, the Langmuir model provided better fittings (with the sole exception being the isotherm measured at 1.0 mol L^{-1} HCl). Despite this, in the experimental range of concentrations studied and in certain conditions (e.g., 2.0 mol L^{-1} HCl; 1.4 mol L^{-1} and 2.0 mol L^{-1} HNO_3/HCl), the maximum experimental adsorbed amounts (denoted as $q_{e,m}$, in Table VI.4) are lower than the Q_m values predicted by Langmuir model. This is an indication that the monolayer capacity was not attained, which means that the adsorbent still has capacity to sequester more gold ions from solution. Indeed, other studies present similar observations. A continuous rise of the isotherm curve, even for Au equilibrium concentrations of 1500-2000 mg L^{-1}, has been reported for the adsorption of gold by crosslinked polyethylenimine/calcium-alginate fibres, and attributed to a continuous reduction process of Au(III) [20].

In a general way, and despite the negative effect of H^+ and aqua regia, pine bark tannin resin showed an excellent ability to sequester and accumulate gold on its surface in all the conditions tested. The pine bark tannin resin presents adsorbed amounts in the range of the reported values for other biosorbents (Table VI.1). Looking only at the uptake capacities of gold, its performance seems to be comparable to the banana peel derived adsorbent and PEI-modified *L. speciosa* leaves, superior to some other biosorbents or synthetic polymers (e.g., commercial resin Lewatit TP214, raw date pits, activated rice husk), but worse than other tannin-adsorbents. However, the adsorption capacity of the pine bark tannin resin was evaluated here under more harsh acidic conditions (1.0 mol L^{-1} acid solutions) than most of the data collected from literature and referred in Table VI.1. Although strong acidic conditions impair gold uptake (Fig. VI.1; [38, 39]), they are more representative of the actual conditions found industrially, making the results obtained in such conditions more meaningful. On this basis, pine bark tannin resin has been proven to be a promising material for gold uptake.

3.4. Competitive Assays

The tannin resin was tested in multi-metal solutions containing Cu(II), Fe(III), Ni(II), Zn(II), Pd(II) and Au(III). The results are depicted in Fig. VI.6. The ability of the tannin resin to uptake gold from the simulated liquors is practically the same as that found in single-metal solutions (Fig. VI.6a). The uptake percentages of gold obtained in multi-metal systems (Fig. VI.6b) were noticeably higher than those of the other metals (which has never surpassed 11 %), particularly for total acidities of 1.0 and 1.4 mol L^{-1}. For instance, at acidic level of 0.75 mol L^{-1} H^+, almost 100 % of the gold in solution was adsorbed by the tannin resin, whereas Ni and Pd were very weakly extracted (11±4 % and 10±3 %, respectively), and other metals remained practically solubilized (uptake percentages <3 %).

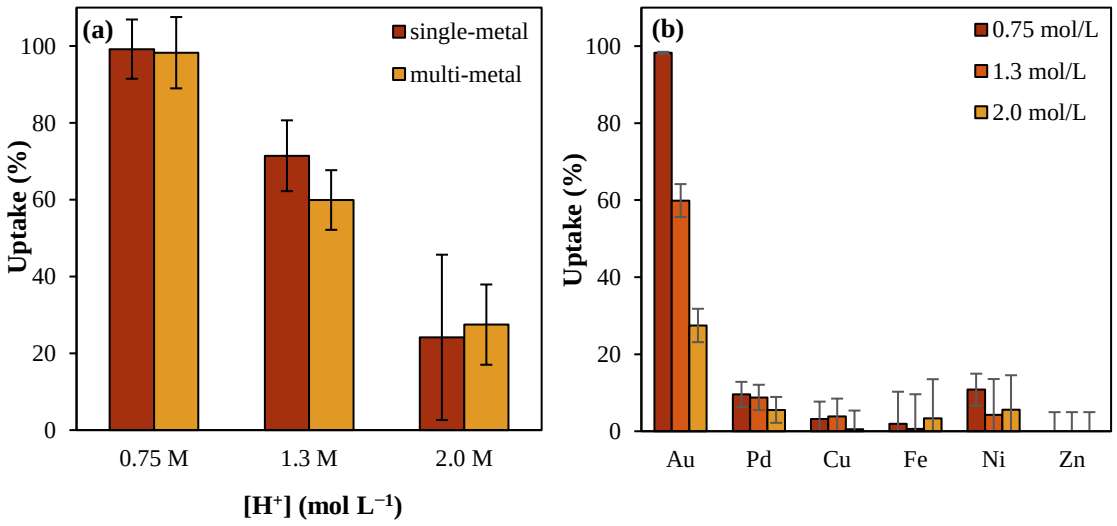

Fig. VI.6 Percentages of metals extracted from simulated liquors containing aqua regia in different H^+ concentrations by the pine bark tannin resin from (20 °C, S/L 1.0 g L^{-1}, initial Au concentration 200 mg L^{-1}): (a) comparison of Au uptake from single and multi-metal solutions; (b) uptake of metals from the multi-metal solution.

In the presence of high chloride concentrations and low pH, gold and platinum group metals are present as anionic chloro-complexes, which favour their uptake by the positively charged adsorbent surface. Palladium has similar properties and behaviour as Au, namely a low reduction potential. It has been reported that $PdCl_4^-$ can be also adsorbed by tannin-adsorbents through the oxidation of the functional groups of tannins and reduction to Pd(0) [37], which justify its co-adsorption. Base metals, on the other hand, are present in solution as cationic species and are electrostatically repelled. Indeed, in bio-

sorption processes, anions are typically adsorbed at low pH (1.0-3.0), whereas metal cations are typically adsorbed under optimum conditions of pH 5.0-5.5 [65]. This explains the reduced competition observed between gold and base metals. The present results are generally in line with results published in literature, which have shown very good selectivity for gold over other metals for different HCl and HNO_3 media [38].

3.5. Desorption and Regeneration

The final recovery of gold from the loaded adsorbent and the regeneration of the adsorbent are important for industrial applications. A first desorption test of gold(III) was conducted using HCl 50 % (v/v) and 0.5 mol L^{-1} acidic thiourea as eluents. Negligible desorption percentage (<1 %) was obtained in HCl eluent, whereas 57 % was registered using the acidic thiourea solution. In fact, formulations of thiourea with HCl have been identified in literature as the most effective desorbing solutions for gold [20, 24, 26, 66]. The desorption mechanism of the process is based on the displacement of the electrostatically adsorbed Au(III), that complexes with chloride in the HCl eluent, and on the oxidation of the elemental gold forming the gold(I)-thiourea $Au(CS[NH_2]_2)_2^+$ [20, 66]. Details about the reactions of gold dissolution using acid thiourea solution can be found in literature [67, 68].

Adsorption-desorption assays were then conducted for three cycles, using the acidic thiourea solution and the results are presented in Fig. VI.7. The desorption efficiency observed in the first cycle (57 %) decreased to 38 % and 39 % in the two subsequent desorption steps. Nevertheless, the regeneration ability of the tannin resin was quite good, as the adsorbed amount remained practically constant in two cycles and reduced moderately (19 %) in the third one, indicating that the regenerated tannin resin still has capacity to accumulate gold on its surface. These results are promising, but the necessity of more research is evident to find an improved solution (e.g., increasing HCl concentration) to desorb gold more efficiently from tannin resins. Even though the desorption and regeneration seem to be the most interesting options in terms of environmental benignity and of cost-effectiveness to recover gold, incineration could be considered in future as it is a direct way to obtain metallic gold.

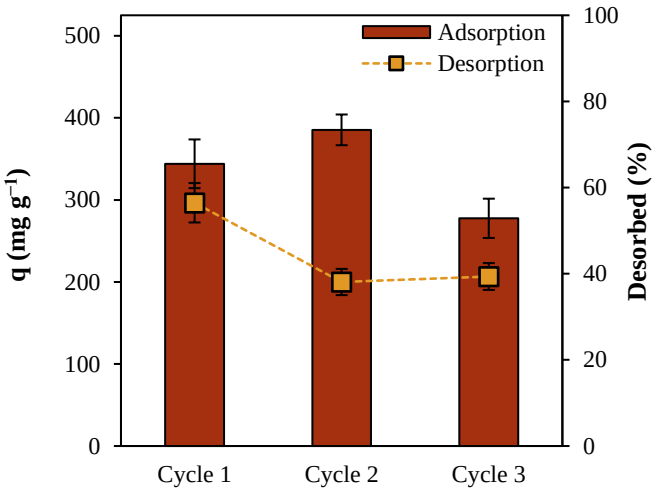

Fig. VI.7 Results obtained in the adsorption (C_{in} = 500 mg L^{-1}, S/L = 1.0 g L^{-1}, 20 °C) and desorption cycles (eluent: 0.5 mol L^{-1} thiourea and 0.5 mol L^{-1} HCl solution, S/L = 2.5 g L^{-1}, 20 °C).

4. Conclusions

Tannin resins were evaluated for the uptake and recovery of gold from simulated e-waste hydrometallurgical liquors. Higher extraction efficiencies of gold were obtained from HCl solutions, in comparison to aqua regia, but excessive levels of HCl caused a severe impact in the metal uptake from both aqueous systems. Even though, at strong acidic levels and in both acidic systems, the pine bark tannin resin presented a good performance, with maximum adsorption capacities ranging from 200 mg g^{-1} (2.0 mol L^{-1} H^{+}) to 343 mg g^{-1} (1.0 mol L^{-1} H^{+}). The adsorption process was found to be a rather slow process (2-3 days to be completed) and successfully described by the homogeneous solid diffusion model and Linear Driving Force approximation. The selectivity of the adsorbent towards gold was evaluated using simulated hydrometallurgical liquors. The amount of gold extracted by the tannin resin from multi-metal solutions was similar to the values registered in the single-metal solutions and the co-adsorption of Pd(II), Cu(II), Fe(II), Ni(II) and Zn(II) was in general low. Desorption and regeneration studies conducted in through three adsorption-desorption cycles, using a solution of 0.5 mol L^{-1} thiourea and 0.5 mol L^{-1} HCl as eluent, indicate desorption percentages of 38-57 %, although with only a mild loss of the adsorption capacity of the regenerated adsorbent. Considering the harsher conditions at which the pine bark tannin resin was evaluated, it can be said that it presents analogous or even better performance when compared to other biosorbents or synthetic resins.

5. References

[1] Perez, J.P.H., K. Folens, K. Leus, F. Vanhaecke, P. Van der Voort, and G. Du Laing, "Progress in hydrometallurgical technologies to recover critical raw materials and precious metals from low-concentrated streams," *Resources Conservation and Recycling*, vol. 142, pp. 177-188, 2019.

[2] Falahati, M., F. Attar, M. Sharifi, A.A. Saboury, A. Salihi, F.M. Aziz, I. Kostova, C. Burda, P. Priecel, J.A. Lopez-Sanchez, S. Laurent, N. Hooshmand, and M.A. El-Sayed, "Gold nanomaterials as key suppliers in biological and chemical sensing, catalysis, and medicine," *Biochimica et Biophysica Acta (BBA) - General Subjects*, vol. 1864, no. 1, p. 129435, 2020.

[3] Xie, F., Z.J. Fan, Q.L. Zhang, and Z.R. Luo, "Selective Adsorption of Au^{3+} from Aqueous Solutions Using Persimmon Powder-Formaldehyde Resin," *Journal of Applied Polymer Science*, vol. 130, no. 6, pp. 3937-3946, 2013.

[4] Forti, V., C.P. Balde, R. Kuehr, and G. Bel, "The Global E-waste Monitor 2020: Quantities, flows and the circular economy potential," 2020.

[5] *Directive 2012/19/EU of the European Parliament and of the Council of 4 July 2012 on waste electrical and electronic equipment (WEEE)*, 2012.

[6] Akcil, A., C. Erust, C.S. Gahan, M. Ozgun, M. Sahin, and A. Tuncuk, "Precious metal recovery from waste printed circuit boards using cyanide and non-cyanide lixiviants - A review," *Waste Management*, vol. 45, pp. 258-271, 2015.

[7] Gurung, M., B.B. Adhikari, H. Kawakita, K. Ohto, K. Inoue, and S. Alam, "Recovery of gold and silver from spent mobile phones by means of acidothiourea leaching followed by adsorption using biosorbent prepared from persimmon tannin," *Hydrometallurgy*, vol. 133, pp. 84-93, 2013.

[8] Rao, M.D., K.K. Singh, C.A. Morrison, and J.B. Love, "Challenges and opportunities in the recovery of gold from electronic waste," *RSC Advances*, vol. 10, no. 8, pp. 4300-4309, 2020.

[9] Kaya, M., "Recovery of metals and nonmetals from electronic waste by physical and chemical recycling processes," *Waste Management*, vol. 57, pp. 64-90, 2016.

[10] Aghaei, E., R.D. Alorro, A.N. Encila, and K. Yoo, "Magnetic Adsorbents for the Recovery of Precious Metals from Leach Solutions and Wastewater," *Metals*, vol. 7, no. 12, p. 529, 2017.

[11] Ventura, E., A. Futuro, S.C. Pinho, M.F. Almeida, and J.M. Dias, "Physical and thermal processing of Waste Printed Circuit Boards aiming for the recovery of gold and copper," *Journal of Environmental Management*, vol. 223, pp. 297-305, 2018.

[12] Zhang, Y.H., S.L. Liu, H.H. Xie, X.L. Zeng, and J.H. Li, "Current status on leaching precious metals from waste printed circuit boards," *Procedia Environmental Sciences*, vol. 16, pp. 560-568, 2012.

[13] Camelino, S., J. Rao, R.L. Padilla, and R. Lucci, "Initial studies about gold leaching from printed circuit boards (PCB's) of waste cell phones," *International Congress of Science and Technology of Metallurgy and Materials, Sam - Conamet 2014*, vol. 9, pp. 105-112, 2015.

[14] Diaz, L.A. and T.E. Lister, "Economic evaluation of an electrochemical process for the recovery of metals from electronic waste," *Waste Management*, vol. 74, pp. 384-392, 2018.

[15] Birich, A., S.R. Mohamed, and B. Friedrich, "Screening of Non-cyanide Leaching Reagents for Gold Recovery from Waste Electric and Electronic Equipment," *Journal of Sustainable Metallurgy*, vol. 4, no. 2, pp. 265-275, 2018.

[16] Korolev, I., E. Kolehmainen, M. Haapalainen, K. Yliniemi, and M. Lundström, "Gold Recovery from Chloride Leaching Solutions by Electrodeposition-Redox Replacement Method," presented at the 10th European Metallurgical Conference (EMC 2019), Düsseldorf, Germany, 2019.

[17] Sayiner, B. and N. Acarkan, "Effect of Silver, Nickel and Copper Cyanides on Gold Adsorption on Activated Carbon in Cyanide Leach Solutions," *Physicochemical Problems of Mineral Processing*, vol. 50, no. 1, pp. 277-287, 2014.

[18] Leroux, J.D., A.W. Bryson, and B.D. Young, "A Comparison of Several Kinetic-Models for the Adsorption of Gold Cyanide onto Activated Carbon," *Journal of the South African Institute of Mining and Metallurgy*, vol. 91, no. 3, pp. 95-103, 1991.

[19] Dodson, J.R., H.L. Parker, A.M. Garcia, A. Hicken, K. Asemave, T.J. Farmer, H. He, J.H. Clark, and A.J. Hunt, "Bio-derived materials as a green route for precious & critical metal recovery and re-use," *Green Chemistry*, vol. 17, no. 4, pp. 1951-1965, 2015.

[20] Bediako, J.K., S. Lin, A.K. Sarkar, Y.F. Zhao, J.W. Choi, M.H. Song, W. Wei, D.H.K. Reddy, C.W. Cho, and Y.S. Yun, "Benignly-fabricated crosslinked polyethylenimine/calcium-alginate fibers as high-performance adsorbents for effective recovery of gold," *Journal of Cleaner Production*, vol. 252, 2020.

[21] Liu, F.L., L. Zhou, W.J. Wang, G. Yu, and S.B. Deng, "Adsorptive recovery of Au(III) from aqueous solution using crosslinked polyethyleneimine resins," *Chemosphere*, vol. 241, 2020.

[22] Morcali, M.H., B. Zeytuncu, E. Ozlem, and S. Aktas, "Studies of Gold Adsorption from Chloride Media," *Materials Research-Ibero-American Journal of Materials*, vol. 18, no. 3, pp. 660-667, 2015.

[23] Choudhary, B.C., D. Paul, A.U. Borse, and D.J. Garole, "Surface functionalized biomass for adsorption and recovery of gold from electronic scrap and refinery wastewater," *Separation and Purification Technology*, vol. 195, pp. 260-270, 2018.

[24] Bediako, J.K., J.W. Choi, M.H. Song, Y.F. Zhao, S. Lin, A.K. Sarkar, C.W. Cho, and Y.S. Yun, "Recovery of gold via adsorption-incineration techniques using banana peel and its derivatives: Selectivity and mechanisms," *Waste Management*, vol. 113, pp. 225-235, 2020.

[25] Al-Saidi, H.M., "The fast recovery of gold(III) ions from aqueous solutions using raw date pits: Kinetic, thermodynamic and equilibrium studies," *Journal of Saudi Chemical Society*, vol. 20, no. 6, pp. 615-624, 2016.

[26] Santos, N.T.D., L.F. Moraes, M.G.C. da Silva, and M.G.A. Vieira, "Recovery of gold through adsorption onto sericin and alginate particles chemically crosslinked by proanthocyanidins," *Journal of Cleaner Production*, vol. 253, 2020.

[27] Liu, F.L., S.Y. Wang, and S.X. Chen, "Adsorption behavior of Au(III) and Pd(II) on persimmon tannin functionalized viscose fiber and the mechanism," *International Journal of Biological Macromolecules*, vol. 152, pp. 1242-1251, 2020.

[28] Nakajima, A. and T. Sakaguchi, "Uptake and Recovery of Gold by Immobilized Persimmon Tannin," *Journal of Chemical Technology and Biotechnology*, vol. 57, no. 4, pp. 321-326, 1993.

[29] Parajuli, D., H. Kawakita, K. Inoue, K. Ohto, and K. Kajiyama, "Persimmon peel gel for the selective recovery of gold," *Hydrometallurgy*, vol. 87, no. 3-4, pp. 133-139, 2007.

[30] Gurung, M., B.B. Adhikari, H. Kawakita, K. Ohto, K. Inoue, and S. Alam, "Recovery of Au(III) by using low cost adsorbent prepared from persimmon tannin extract," *Chemical Engineering Journal*, vol. 174, no. 2-3, pp. 556-563, 2011.

[31] Huang, X., Y.P. Wang, X.P. Liao, and B. Shi, "Adsorptive recovery of Au^{3+} from aqueous solutions using bayberry tannin-immobilized mesoporous silica," *Journal of Hazardous Materials*, vol. 183, no. 1-3, pp. 793-798, 2010.

[32] Gurung, M., B.B. Adhikari, H. Kawakita, K. Ohto, K. Inoue, and S. Alam, "Selective Recovery of Precious Metals from Acidic Leach Liquor of Circuit Boards of Spent Mobile Phones Using Chemically Modified Persimmon Tannin Gel," *Industrial & Engineering Chemistry Research*, vol. 51, no. 37, pp. 11901-11913, 2012.

[33] Gurung, M., B.B. Adhikari, S. Morisada, H. Kawakita, K. Ohto, K. Inoue, and S. Alam, "*N*-aminoguanidine modified persimmon tannin: A new sustainable material for selective adsorption, preconcentration and recovery of precious metals from acidic chloride solution," *Bioresource Technology*, vol. 129, pp. 108-117, 2013.

[34] Gurung, M., B.B. Adhikari, S. Alam, H. Kawakita, K. Ohto, and K. Inoue, "Persimmon tannin-based new sorption material for resource recycling and recovery of precious metals," *Chemical Engineering Journal*, vol. 228, pp. 405-414, 2013.

[35] Xiong, Y., C.R. Adhikari, H. Kawakita, K. Ohto, K. Inoue, and H. Harada, "Selective recovery of precious metals by persimmon waste chemically modified with dimethylamine," *Bioresource Technology*, vol. 100, no. 18, pp. 4083-4089, 2009.

[36] Liao, X., M. Zhang, and B. Shi, "Collagen-fiber-immobilized tannins and their adsorption of Au(III)," *Industrial & Engineering Chemistry Research*, vol. 43, pp. 2222-2227, 2004.

[37] Fan, R., H. Min, X. Hong, Q. Yi, W. Liu, Q. Zhang, and Z. Luo, "Plant tannin immobilized Fe_3O_4@SiO_2 microspheres: A novel and green magnetic bio-sorbent with superior adsorption capacities for gold and palladium," *Journal of Hazardous Materials*, vol. 364, pp. 780-790, 2019.

[38] Fan, R.Y., F. Xie, X.L. Guan, Q.L. Zhang, and Z.R. Luo, "Selective adsorption and recovery of Au(III) from three kinds of acidic systems by persimmon residual based bio-sorbent: A method for gold recycling from e-wastes," *Bioresource Technology*, vol. 163, pp. 167-171, 2014.

[39] Yi, Q., R. Fan, F. Xie, H. Min, Q. Zhang, and Z. Luo, "Selective Recovery of Au(III) and Pd(II) from Waste PCBs Using Ethylenediamine Modified Persimmon Tannin Adsorbent," *Procedia Environmental Sciences*, vol. 31, pp. 185-194, 2016.

[40] Nakajima, A., K. Ohe, Y. Baba, and T. Kijima, "Mechanism of gold adsorption by persimmon tannin gel," *Analytical Sciences*, vol. 19, no. 7, pp. 1075-1077, 2003.

[41] Ogata, T. and Y. Nakano, "Mechanisms of gold recovery from aqueous solutions using a novel tannin gel adsorbent synthesized from natural condensed tannin," *Water Research*, vol. 39, no. 18, pp. 4281-4286, 2005.

[42] Wang, Z., X. Li, H. Liang, J. Ning, Z. Zhou, and G. Li, "Equilibrium, kinetics and mechanism of Au^{3+}, Pd^{2+} and Ag^{+} ions adsorption from aqueous solutions by graphene oxide functionalized persimmon tannin," *Material Science and Engineering: C Materials for Biological Application*, vol. 79, pp. 227-236, 2017.

[43] Saman, N., J.W. Tan, S.S. Mohtar, H. Kong, J.W.P. Lye, K. Johari, H. Hassan, and H. Mat, "Selective biosorption of aurum(III) from aqueous solution using oil palm trunk (OPT) biosorbents: Equilibrium, kinetic and mechanism analyses," *Biochemical Engineering Journal*, vol. 136, pp. 78-87, 2018.

[44] Wang, C., J.L. Zhao, S.X. Wang, L.B. Zhang, and B. Zhang, "Efficient and Selective Adsorption of Gold Ions from Wastewater with Polyaniline Modified by Trimethyl Phosphate: Adsorption Mechanism and Application," *Polymers*, vol. 11, no. 4, 2019.

[45] Tokuyama, H. and A. Kanehara, "Temperature swing adsorption of gold(III) ions on poly(*N*-isopropylacrylamide) gel," *Reactive & Functional Polymers*, vol. 67, no. 2, pp. 136-143, 2007.

[46] Yang, J., F. Kubota, Y. Baba, N. Kamiya, and M. Goto, "Application of cellulose acetate to the selective adsorption and recovery of Au(III)," *Carbohydrate Polymers*, vol. 111, pp. 768-774, 2014.

[47] Tang, J., Y. Chen, S. Wang, and L. Zhang, "Engineering of UiO-66-NH_2 as selective and reusable adsorbent to enhance the removal of Au(III) from water: Kinetics, isotherm and thermodynamics," *Journal of Colloid and Interface Science*, 2021.

[48] Gurung, M., B.B. Adhikari, K. Khunathai, H. Kawakita, K. Ohto, H. Harada, and K. Inoue, "Quaternary Amine Modified Persimmon Tannin Gel: An Efficient Adsorbent for the Recovery of Precious Metals from Hydrochloric Acid Media," *Separation Science and Technology*, vol. 46, no. 14, pp. 2250-2259, 2011.

[49] Inoue, K., M. Gurung, Y. Xiong, H. Kawakita, K. Oht, and S. Alam, "Hydrometallurgical recovery of precious metals and removal of hazardous metals using persimmon tannin and persimmon wastes," *Metals*, Review vol. 5, no. 4, pp. 1921-1956, 2015, Art. no. A13.

[50] Fana, R., X. Hongb, H. Minb, Q. Yic, Q. Zhangb, and Z. Luob, "Preparation of formaldehyde-free persimmon tannin-based rigid foam as an adsorbent for selective recovery of Au(III) ions," *Desalination and Water Treatment*, vol. 151, pp. 219-229, 2019.

[51] Zhang, S., Y. Ji, F. Ao, Y. Wang, J. Zhao, and S. Chen, "Selective adsorption of Au^{III} from aqueous solution using 2,5-Dimercapto-1,3,4-thiadiazole modified persimmon tannin," *Journal of the Brazilian Chemical Society*, vol. 29, no. 7, pp. 1487-1498, 2018.

[52] Liu, F., Z. Zhou, and G. Li, "Persimmon tannin functionalized polyacrylonitrile fiber for highly efficient and selective recovery of Au(III) from aqueous solution," *Chemosphere*, vol. 264, p. 128469, 2021.

[53] Liu, F., G. Peng, T. Li, G. Yu, and S. Deng, "Au(III) adsorption and reduction to gold particles on cost-effective tannin acid immobilized dialdehyde corn starch," *Chemical Engineering Journal*, vol. 370, pp. 228-236, 2019.

[54] Kim, J., K.R. Kim, Y. Hong, S. Choi, C.T. Yavuz, J.W. Kim, and Y.S. Nam, "Photochemically enhanced selective adsorption of gold ions on tannin-coated porous polymer microspheres," *ACS Applied Materials & Interfaces*, vol. 11, no. 24, pp. 21915-21925, 2019.

[55] Lagergren, S.Y., "Zur theorie der sogenannten adsorption gelöster stoffe, Kungliga Svenska Vetenskapsakademiens," *Handlingar*, vol. 24, pp. 1-39, 1898.

[56] Blanchard, G., M. Maunaye, and G. Martin, "Removal of Heavy-Metals from Waters by Means of Natural Zeolites," *Water Research*, vol. 18, no. 12, pp. 1501-1507, 1984.

[57] Ho, Y.S., "Adsorption of heavy metals from waste streams by peat," The University of Birmingham, Birmingham, U.K., 1995.

[58] Glueckauf, E., "Theory of chromatography. Part 10. Formulae for diffusion into spheres and their application to chromatography," *Tansactions of the Faraday Society*, vol. 51, pp. 1540-1554, 1955.

[59] Santos, S.C.R. and R.A.R. Boaventura, "Adsorption of cationic and anionic azo dyes on sepiolite clay: Equilibrium and kinetic studies in batch mode," *Journal of Environmental Chemical Engineering*, vol. 4, no. 2, pp. 1473-1483, 2016.

[60] Tien, C., "Chapter 4 - Adsorbate Uptake and Equations Describing Adsorption Processes," in *Introduction to Adsorption*, C. Tien, Ed.: Elsevier, 2019, pp. 87-118.

[61] Langmuir, I., "The adsorption of gases on plane surfaces of glass, mica and platinum," *Journal of the American Chemical Society*, vol. 40, pp. 1361-1403, 1918.

[62] Freundlich, H.M.F., "Over the adsorption in solution," *Journal of Physical Chemistry*, vol. 57, pp. 385-471, 1906.

[63] Bergamini, M.F., D.P. Santos, and M.V.B. Zanoni, "Screen-Printed Carbon Electrode Modified with Poly-L-histidine Applied to Gold(III) Determination," *Journal of the Brazilian Chemical Society*, vol. 20, no. 1, pp. 100-106, 2009.

[64] da Silva, J.S., M.P. da Rosa, P.H. Beck, E.C. Peres, G.L. Dotto, F. Kessler, and F.S. Grasel, "Preparation of an alternative adsorbent from *Acacia Mearnsii* wastes through acetosolv method and its application for dye removal," *Journal of Cleaner Production*, vol. 180, pp. 386-394, 2018.

[65] Mack, C., B. Wilhelmi, J.R. Duncan, and J.E. Burgess, "Biosorption of precious metals," *Biotechnology Advances*, vol. 25, no. 3, pp. 264-271, 2007.

[66] Wei, W., D.H.K. Reddy, J.K. Bediako, and Y.-S. Yun, "Aliquat-336-impregnated alginate capsule as a green sorbent for selective recovery of gold from metal mixtures," *Chemical Engineering Journal*, vol. 289, pp. 413-422, 2016.

[67] Li, J. and J.D. Miller, "Reaction kinetics for gold dissolution in acid thiourea solution using formamidine disulfide as oxidant," *Hydrometallurgy*, vol. 63, no. 3, pp. 215-223, 2002.

[68] Durovic, M.D., R. Puchta, Z.D. Bugarcic, and R. van Eldik, "Studies on the reactions of $[AuCl4]^-$ with different nucleophiles in aqueous solution," *Dalton Transactions*, vol. 43, no. 23, pp. 8620-8632, 2014.

CHAPTER VII

FINAL REMARKS

1. General Conclusions

Adsorption is an important technique for wastewater treatment due to its high selectivity, particularly of highly toxic species given its efficacy in low concentrations. Moreover, adsorption can also be applied for the recovery of valuable substances, contributing thus to the sustainability of materials which are essential in several industries. In addition, forest residues, such as bark of the widely distributed species in Portugal *Pinus pinaster*, have often their chemical richness, namely phenolic content, ignored. Hence, finding a way to salvage those residues taking advantage of their chemical richness is of great importance. Furthermore, arsenic, a toxic metalloid, is found at high concentrations in multiple places, creating an imperative need to develop techniques to remediate such incidents. On the other hand, elements like phosphorous and antimony are both water pollutants and critical materials with several applications. Considering the depletion of the natural reserves of phosphorous and the antimony supply risk in the European Union, these elements should be removed from contaminated waters and recovered for reuse. Finally, precious metals such as gold should be recovered from acid liquors yielded from obsolete electronic devices. This thesis aimed at producing a pine-tannin adsorbent to have its applicability to uptake arsenic, antimony, phosphate, and gold from aqueous solutions assessed. Tannin-adsorbents have been rarely applied to anionic species and using pine as a source for tannins is uncommon. In this way, this thesis may have helped improve the literature by addressing those limitations.

Summarizing the strengths and weaknesses:

(i) The tannin resin used here was a biosorbent, prepared through a relatively simple process from a readily locally available resource, a forest/industrial waste (pine bark);

(ii) Tannins were extracted from pine bark in alkaline solutions (NaOH 7.5 % of bark mass) at high temperature (90 °C) after one hour of contact (optimal conditions) and the extracts obtained presented a phenolic content of 631±30 mg of gallic acid equivalents per g of extract, granting the production of 166±2 mg of polymerized material per g of bark used in the extraction;

(iii) Tannins were polymerized in NaOH 0.25 mol L^{-1} solution (4.0 mL per g of extract) and using formaldehyde as a cross-linking reagent (0.20 mL per g of extract) with an optimal expected yield of tannin resin of 80 %;

(iv) Tannin resins can be prepared at different particle sizes, including larger particles with convenient handling and adsorptive properties for continuous and full-scale operation, are stable in strongly acidic, neutral and slightly alkaline conditions, present isoelectric points close to pH 2, and were successfully loaded with iron or calcium yielding metal contents of 22±2 mg g^{-1} and 32±1 mg g^{-1}, respectively;

(v) Iron-loaded oxidized tannin resin was the only adsorbent assessed able to uptake arsenic with a removal of ≈90 % using high dosages (S/L = 10 g L^{-1}), nevertheless it granted very low adsorption capacities (0.72±0.03 mg g^{-1}, pH 3, 20 °C);

(vi) Tannin resin has good uptake capacities for both antimony redox states and for most actual conditions, e.g., adsorption capacities of 30-33 mg g^{-1} (Sb(III), pH 6, 20 °C) and 16-47 mg g^{-1} (Sb(V), pH 2, 20 °C), and with no drastic effect of typical coexisting species; however, adsorbent regeneration was found to be challenging;

(vii) Several adsorbents produced were screened for phosphate removal from water and none was found to be sufficiently effective to proceed with further adsorption assays;

(viii) Tannin resin performed well for gold uptake even at very acidic conditions, with maximum adsorption capacities ranging from 200 mg g^{-1} (2.0 mol L^{-1} H^{+}) to 343 mg g^{-1} (1.0 mol L^{-1} H^{+}), it presented selectivity for gold comparatively to base metals and other precious metals (e.g., palladium), and, thus, this adsorbent seems to be applicable to the recovery of precious metals in urban mining.

2. Suggestions for Future Work

In terms of tannin extraction, an economic analysis should be undertaken to guarantee that the conditions chosen are indeed optimal. For instance, an increase in contact time and temperature may have led to an increase on extraction yield but the additional energy spent may not compensate that improvement. Furthermore, the feedstock used in the extraction should be submitted to analysis to help validate the extraction method chosen. Tannin polymerization should be evaluated using aldehydes other than formaldehyde or even in the absence of cross-linking reagents (through self-condensation) to further increase the environmental benignity of the procedure. Additionally, modifications on the polymerization procedure should be explored to improve iron and calcium uptake and to strengthen bonding stability between the metals and resins, and, if better results are achieved, the potential of the resulting materials for arsenic and phosphate removal should be reassessed.

On the other hand, antimony adsorption by the unmodified tannin resin should be further evaluated in real Sb-contaminated waters and wastewaters, given the considerable variability of their characteristics as the result of different geographic locations, soils with different geochemical properties, the presence or absence of mining activity, etc. Future work should involve adsorption assays with solutions that contain simultaneously Sb(III) and Sb(V), with speciation analysis to check if competition between oxidation states occurs and to reassessed possible conversions. Moreover, column experiments with tannin resin and antimonate should also be carried out to complement the fixed-bed results here obtained for antimonite. The regeneration of the Sb-loaded tannin resin by elution was not feasible, but alternative ways to reintroduce antimony (a critical raw material) in the industrial chain (e.g., as catalysts) are proposed and can be explored in the future.

Regarding gold, a deeper analysis on the final recovery of gold from the exhausted adsorbents, either by elution or incineration, should be considered in forthcoming work. More research is needed in this field to improve the circularity in e-waste, particularly by the promotion of benign practices. Furthermore, adsorption assays using real or simulated e-waste leaching liquors should be done, as well as experiments in continuous mode.